Global Methane Budget 2000-2020

Marielle Saunois[1], Adrien Martinez[1], Benjamin Poulter[2], Zhen Zhang[3,4], Peter A. Raymond[5], Pierre Regnier[6], Josep G. Canadell[7], Robert B. Jackson[8], Prabir K. Patra[9,10], Philippe Bousquet[1], Philippe Ciais[1], Edward J. Dlugokencky[11], Xin Lan[11,12], George H. Allen[13], David Bastviken[14], David J. Beerling[15], Dmitry A. Belikov[16], Donald R. Blake[17], Simona Castaldi[18], Monica Crippa[19], Bridget R. Deemer[20], Fraser Dennison[21], Giuseppe Etiope[22,23], Nicola Gedney[24], Lena Höglund-Isaksson[25], Meredith A. Holgerson[26], Peter O. Hopcroft[27], Gustaf Hugelius[28], Akihiko Ito[29], Atul K. Jain[30], Rajesh Janardanan[31], Matthew S. Johnson[32], Thomas Kleinen[33], Paul B. Krummel[21], Ronny Lauerwald[34], Tingting Li[35], Xiangyu Liu[36], Kyle C. McDonald[37], Joe R. Melton[38], Jens Mühle[39], Jurek Müller[40], Fabiola Murguia-Flores[41], Yosuke Niwa[31,42], Sergio Noce[43], Shufen Pan[44], Robert J. Parker[45], Changhui Peng[46,47], Michel Ramonet[1], William J. Riley[48], Gerard Rocher-Ros[49], Judith A. Rosentreter[50], Motoki Sasakawa[31], Arjo Segers[51], Steven J. Smith[52,53], Emily H. Stanley[54], Joël Thanwerdas[55,*], Hanqin Tian[56], Aki Tsuruta[57], Francesco N. Tubiello[58], Thomas S. Weber[59], Guido R. van der Werf[60], Douglas E. J. Worthy[61], Yi Xi[1], Yukio Yoshida[31], Wenxin Zhang[62], Bo Zheng[63,64], Qing Zhu[48], Qiuan Zhu[65], and Qianlai Zhuang[36]

[1]Laboratoire des Sciences du Climat et de l'Environnement, LSCE-IPSL (CEA-CNRS-UVSQ), Université Paris-Saclay 91191 Gif-sur-Yvette, France
[2]NASA Goddard Space Flight Center, Biospheric Science Laboratory, Greenbelt, MD 20771, USA
[3]National Tibetan Plateau Data Center (TPDC), State Key Laboratory of Tibetan Plateau Earth System, Environment and Resource (TPESER), Institute of Tibetan Plateau Research, Chinese Academy of Sciences, Beijing, 100101, China
[4]Earth System Science Interdisciplinary Center, University of Maryland, College Park, MD 20740, USA
[5]Yale School of the Environment, Yale University, New Haven, CT 06511, USA
[6]Department Geoscience, Environment & Society (BGEOSYS), Université Libre de Bruxelles, 1050 Bruxelles, Belgium
[7]Global Carbon Project, CSIRO Environment, Canberra, ACT 2601, Australia
[8]Department of Earth System Science, Woods Institute for the Environment, and Precourt Institute for Energy, Stanford University, Stanford, CA 94305-2210, USA
[9]Research Institute for Global Change, JAMSTEC, 3173-25 Showa-machi, Kanazawa, Yokohama, 236-0001, Japan
[10]Research Institute for Humanity and Nature, Kyoto 6038047, Japan
[11]NOAA Global Monitoring Laboratory, 325 Broadway, Boulder, CO 80305, USA
[12]Cooperative Institute for Research in Environmental Sciences, University of Colorado Boulder, CO 80303, USA
[13]Department of Geosciences, Virginia Polytechnic Institute and State University, Blacksburg, VA, USA
[14]Department of Thematic Studies – Environmental Change, Linköping University, 581 83 Linköping, Sweden
[15]School of Biosciences, University of Sheffield, UK
[16]Center for Environmental Remote Sensing, Chiba University, Chiba, 263-8522, Japan
[17]Department of Chemistry, University of California Irvine, 570 Rowland Hall, Irivine, CA 92697, USA
[18]Dipartimento di Scienze Ambientali, Biologiche e Farmaceutiche, Università degli Studi della Campania Luigi

42   Vanvitelli, via Vivaldi 43, 81100 Caserta, Italy

43   [19]European Commission, Joint Research Centre (JRC), Ispra, Italy

45   [20]U.S. Geological Survey, Southwest Biological Science Center, Flagstaff, AZ, USA

46   [21]CSIRO Environment, Aspendale, Victoria 3195, Australia

47   [22]Istituto Nazionale di Geofisica e Vulcanologia, Sezione Roma 2, via V. Murata 605 00143 Rome, Italy

48   [23]Faculty of Environmental Science and Engineering, Babes Bolyai University, Cluj-Napoca, Romania

49   [24] Met Office Hadley Centre, Joint Centre for Hydrometeorological Research, Maclean Building, Wallingford

50   OX10 8BB, UK

51   [25]Pollution Management Group (PM), International Institute for Applied Systems Analysis (IIASA), 2361

52   Laxenburg, Austria

53   [26] Department of Ecology & Evolutionary Biology, Cornell University, Ithaca, NY, USA

54   [27] School of Geography, Earth & Environmental Sciences, University of Birmingham, UK

55   [28] Department of Physical Geography and Bolin Centre for Climate Research, Stockholm University, 106 91

56   Stockholm, Sweden

57   [29] Graduate School of Agricultural and Life Sciences, The University of Tokyo, Tokyo, Japan

58   [30] Department of Atmospheric Sciences, University of Illinois, Urbana, IL 61821, USA

59   [31] Earth System Division, National Institute for Environmental Studies (NIES), Onogawa 16-2, Tsukuba, Ibaraki

60   305-8506, Japan

61   [32]Earth Science Division, NASA Ames Research Center, Moffett Field, CA USA.

62   [33]Max Planck Institute for Meteorology, Bundesstraße 53, 20146 Hamburg, Germany

63   [34] Université Paris-Saclay, INRAE, AgroParisTech, UMR EcoSys, Palaiseau, France

64   [35] LAPC, Institute of Atmospheric Physics, Chinese Academy of Sciences, Beijing, 100029, China

65   [36]Department of Earth, Atmospheric, and Planetary Sciences, Purdue University, West Lafayette, IN, USA

66   [37]Department of Earth and Atmospheric Sciences, City College of New York, City University of New York, NY,

67   USA

68   [38]Climate Research Division, Environment and Climate Change Canada, Victoria, BC, V8W 2Y2, Canada

69   [39]Scripps Institution of Oceanography, University of California San Diego, La Jolla, CA, 92037, USA

70   [40]Climate and Environmental Physics, Physics Institute and Oeschger Centre for Climate Change Research,

71   University of Bern, Sidlerstr. 5, 3012 Bern, Switzerland

72   [41]Instituto de Investigaciones en Ecología y Sustentabilidad, Universidad Nacional Autónoma de México,

73   Morelia, Mexico

74   [42]Department of Climate and Geochemistry Research, Meteorological Research Institute (MRI), Nagamine 1-1, Tsukuba,

75   Ibaraki 305-0052, Japan

76   [43]CMCC Foundation - Euro-Mediterranean Center on Climate Change, Italy

77   [44]Department of Engineering and Environmental Studies Program, Boston College, Chestnut Hill, MA 02467,

78   USA

79   [45]National Centre for Earth Observation, School of Physics and Astronomy, University of Leicester, Leicester,

80   LE1 7RH, UK

81   [46]Department of Biology Sciences, Institute of Environment Science, University of Quebec at Montreal,

82   Montreal, QC H3C 3P8, Canada

83   [47] School of Geographic Sciences, Hunan Normal University, Changsha 410081, China

84   [48] Climate and Ecosystem Sciences Division, Lawrence Berkeley National Lab, 1 Cyclotron Road, Berkeley, CA

85   94720, US

86   [49] Department of Forest Ecology and Management, Swedish University of Agricultural Sciences, 90183 Umeå,

87   Sweden

88   [50] Faculty of Science and Engineering, Southern Cross University, Lismore, NSW 2480, Australia

89   [51]TNO, dep. of Climate Air & Sustainability, P.O. Box 80015, NL-3508-TA, Utrecht, The Netherlands

90   [52]Joint Global Change Research Institute, Pacific Northwest National Lab, College Park, MD, USA

91   [53]Center for Global Sustainability, University of Maryland, College Park, MD, USA
92   [54]Center for Limnology, University of Wisconsin-Madison, Madison, WI, USA
93   [55]Empa, Swiss Federal Laboratories for Materials Science and Technology, Dübendorf, Switzerland
94   [56]Center for Earth System Science and Global Sustainability, Schiller Institute for Integrated Science and
95   Society, Department of Earth and Environmental Sciences, Boston College, Chestnut Hill, MA 02467, USA
96   [57]Finnish Meteorological Institute, P.O. Box 503, FI-00101, Helsinki, Finland
97   [58]Statistics Division, Food and Agriculture Organization of the United Nations (FAO), Viale delle
98   Terme di Caracalla, Rome 00153, Italy
99   [59]Department of Earth and Environmental Sciences, University of Rochester, Rochester, NY 14627,
100   USA
101   [60]Meteorology and Air Quality Group, Wageningen University and Research, Wageningen, the Netherlands
102   [61]Environment and Climate Change Canada, 4905, Dufferin Street, Toronto, Canada
103   [62]Department of Physical Geography and Ecosystem Science, Lund University, Sölvegatan 12, 223 62, Lund, Sweden
104   [63]Institute of Environment and Ecology, Tsinghua Shenzhen International Graduate School, Tsinghua University,
105   Shenzhen 518055, China
106   [64]State Environmental Protection Key Laboratory of Sources and Control of Air Pollution Complex, Beijing 100084,
107   China
108   [65]College of Geography and Remote Sensing, Hohai University, Nanjing, 210098, China
109
110   *formerly at LSCE [1]

112   *Correspondence to*: Marielle Saunois (marielle.saunois@lsce.ipsl.fr)

113   **Abstract.** Understanding and quantifying the global methane (CH_4) budget is important for assessing realistic pathways to

114   mitigate climate change. CH_4 is the second most important human-influenced greenhouse gas in terms of climate forcing

115   after carbon dioxide (CO_2) and both emissions and atmospheric concentrations of CH_4 continue to increase since 2007 after

116   a temporary pause. The relative importance of CH_4 emissions compared to those of CO_2 for temperature change is related

117   to its shorter atmospheric lifetime, stronger radiative effect, and acceleration in atmospheric growth rate over the past decade,

118   the causes of which are still debated. Two major challenges in quantifying the factors responsible for the observed

119   atmospheric growth rate arise from diverse, geographically overlapping CH_4 sources and from the uncertain magnitude and

120   temporal change in the destruction of CH_4 by short-lived and highly variable hydroxyl radicals (OH). To address these

121   challenges, we have established a consortium of multi-disciplinary scientists under the umbrella of the Global Carbon Project

122   to improve, synthesise and update the global CH_4 budget regularly and to stimulate new research on the methane cycle.

123   Following Saunois et al. (2016, 2020), we present here the third version of the living review paper dedicated to the decadal

124   CH_4 budget, integrating results of top-down CH_4 emission estimates (based on in-situ and greenhouse gas observing satellite

125   (GOSAT) atmospheric observations and an ensemble of atmospheric inverse-model results) and bottom-up estimates (based

126   on process-based models for estimating land-surface emissions and atmospheric chemistry, inventories of anthropogenic

127   emissions, and data-driven extrapolations). We present a budget for the most recent 2010-2019 calendar decade (the latest

128   period for which full datasets are available), for the previous decade of 2000-2009 and for the year 2020.

The revision of the bottom-up budget in this 2024 edition benefits from important progress in estimating inland freshwater emissions, with better accounting of emissions from lakes and ponds, reservoirs, and streams and rivers. This budget also reduces double accounting across freshwater and wetland emissions and, for the first time, includes an estimate of the potential double accounting that may exist (average of 23 Tg CH_4 yr^{-1}). Bottom-up approaches show that the combined wetland and inland freshwater emissions average 248 [159-369] Tg CH_4 yr^{-1} for the 2010-2019 decade. Natural fluxes are perturbed by human activities through climate, eutrophication, and land use. In this budget, we also estimate, for the first time, this anthropogenic component contributing to wetland and inland freshwater emissions. Newly available gridded products also allowed us to derive an almost complete latitudinal and regional budget based on bottom-up approaches.

For the 2010-2019 decade, global CH_4 emissions are estimated by atmospheric inversions (top-down) to be 575 Tg CH_4 yr^{-1} (range 553-586, corresponding to the minimum and maximum estimates of the model ensemble). Of this amount, 369 Tg CH_4 yr^{-1} or ~65% are attributed to direct anthropogenic sources in the fossil, agriculture and waste and anthropogenic biomass burning (range 350-391 Tg CH_4 yr^{-1} or 63-68%). For the 2000-2009 period, the atmospheric inversions give a slightly lower total emission than for 2010-2019, by 32 Tg CH_4 yr^{-1} (range 9-40). The 2020 emission rate is the highest of the period and reaches 608 Tg CH_4 yr^{-1} (range 581-627), which is 12% higher than the average emissions in the 2000s. Since 2012, global direct anthropogenic CH_4 emission trends have been tracking scenarios that assume no or minimal climate mitigation policies proposed by the Intergovernmental Panel on Climate Change (shared socio-economic pathways SSP5 and SSP3). Bottom-up methods suggest 16% (94 Tg CH_4 yr^{-1}) larger global emissions (669 Tg CH_4 yr^{-1}, range 512-849) than top-down inversion methods for the 2010-2019 period. The discrepancy between the bottom-up and the top-down budgets has been greatly reduced compared to the previous differences (167 and 156 Tg CH_4 yr^{-1} in Saunois et al. (2016, 2020), respectively), and for the first time uncertainty in bottom-up and top-down budgets overlap. Although differences have been reduced between inversions and bottom-up, the most important source of uncertainty in the global CH_4 budget is still attributable to natural emissions, especially those from wetlands and inland freshwaters.

The tropospheric loss of methane, as the main contributor to methane lifetime, has been estimated at 563 [510-663] Tg CH_4 yr^{-1} based on chemistry climate models. These values are slightly larger than for 2000-2009 due to the impact of the rise in atmospheric methane, and remaining large uncertainty (~25%). The total sink of CH4 is estimated at 633 [507-796] Tg CH4 yr-1 by the bottom-up approaches and at 554 [550-567] Tg CH4 yr-1 by top-down approaches. Though, most of the top-down models use the same OH distribution, which introduces less uncertainty to the global budget than is likely justified.

For 2010-2019, agriculture and waste contributed an estimated 228 [213-242] Tg CH_4 yr^{-1} in the top-down budget and 211 [195-231] Tg CH_4 yr^{-1} in the bottom-up budget. Fossil fuel emissions contributed 115 [100-124] Tg CH_4 yr^{-1} in the top-down budget and 120 [117-125] Tg CH_4 yr^{-1} in the bottom-up budget. Biomass and biofuel burning contributed 27 [26-27] Tg CH_4 yr^{-1} in the top-down budget and 28 [21-39] Tg CH_4 yr^{-1} in the bottom-up budget.

We identify five major priorities for improving the CH$_4$ budget: i) producing a global, high-resolution map of water-saturated soils and inundated areas emitting CH$_4$ based on a robust classification of different types of emitting ecosystems; ii) further development of process-based models for inland-water emissions; iii) intensification of CH$_4$ observations at local (e.g., FLUXNET-CH$_4$ measurements, urban-scale monitoring, satellite imagery with pointing capabilities) to regional scales (surface networks and global remote sensing measurements from satellites) to constrain both bottom-up models and atmospheric inversions; iv) improvements of transport models and the representation of photochemical sinks in top-down inversions, and v) integration of 3D variational inversion systems using isotopic and/or co-emitted species such as ethane as well as information in the bottom-up inventories on anthropogenic super-emitters detected by remote sensing (mainly oil and gas sector but also coal, agriculture and landfills) to improve source partitioning.

The data presented here can be downloaded from https://doi.org/10.18160/GKQ9-2RHT(Martinez et al., 2024).

1 Introduction

The average surface dry air mole fraction of atmospheric methane (CH$_4$) reached 1912 ppb in 2022 (Fig. 1; Lan et al., 2024), 2.6 times greater than its estimated pre-industrial value in 1750. This increase is attributable in large part to increased anthropogenic emissions arising primarily from agriculture (e.g., livestock production, rice cultivation, biomass burning), fossil fuel production and use, waste disposal, and alterations to natural CH$_4$ fluxes due to increased atmospheric CO$_2$ concentrations, land use (Woodward et al., 2010, Fluet-Chouinard et al., 2023) and climate change (Ciais et al., 2013; Canadell et al., 2021). An equal mass of CH$_4$ emissions have a stronger impact on climate than carbon dioxide (CO$_2$), which is reflected by its global warming potential (GWP) relative to CO$_2$ on a given time horizon. For a 100-yr time horizon the GWP of CH$_4$ emitted by fossil sources is 29.8 (GWP of CH$_4$ emitted by microbial sources is 27), whereas the values reach 82.5 over a 20-year horizon for CH$_4$ emitted by fossil sources and 79.7 for CH$_4$ emitted by microbial sources (Forster et al., 2021). Although global anthropogenic emissions of CH$_4$ are estimated at around 359 Tg CH$_4$ yr^{-1} (Saunois et al., 2020), representing around 2.5% of the global CO$_2$ anthropogenic emissions when converted to units of carbon mass flux for the recent decade, the emissions-based effective radiative forcing of CH$_4$ concentrations has contributed ~31% (1.19 W m^{-2}) to the additional radiative forcing from anthropogenic emissions of greenhouse gases and their precursors (3.84 W m^{-2}) over the industrial era (1750-2019) (Forster et al., 2021). Changes in other chemical compounds such as nitrogen oxides (NO$_x$) or carbon monoxide (CO) also influence atmospheric CH$_4$ through changes to its atmospheric lifetime. Emissions of CH$_4$ contribute to the production of ozone, stratospheric water vapour, and CO$_2$, and most importantly affect its own lifetime (Myhre et al., 2013; Shindell et al., 2012). CH$_4$ has a short lifetime in the atmosphere (about 9 years for the year 2010, Prather et al., 2012; Szopa et al., 2021). Hence a stabilisation or reduction of CH$_4$ emissions leads to the stabilisation or reduction of its atmospheric concentration (assuming no change in the chemical oxidants), and therefore its radiative forcing, in only a few decades. While reducing CO$_2$ emissions is necessary to stabilise long-term warming, reducing CH$_4$ emissions

192   is recognized as an effective option to limit climate warming in the near-term (Shindell et al., 2012; Jackson et al., 2020;

193   Ocko et al., 2021; UNEP, 2021), because of its shorter lifetime compared to CO_2.

194   The momentum around the potential of CH_4 to limit near-term warming has led to the launch of the Global Methane

195   Pledge at the November 2021 Conference of the Parties (COP 26). Signed by 158 countries (update on October 2024), this

196   collective effort aims at reducing global CH_4 anthropogenic emissions at least 30 percent from 2020 levels by 2030 (Global

197   Methane Pledge, 2023). Given that global baseline CH_4 emissions are expected to grow through 2030 (by an additional 20-

198   50 Million tons (Mt) of CH_4, UNEP 2022), the CH_4 emission reductions currently needed to reach the Global Methane

199   Pledge objective (UNEP, 2022) correspond to 36% of the projected baseline emissions in 2030 (ie. if no further emission

200   reductions were implemented). This implies that large reductions of CH_4 emissions are needed to meet the Global Methane

201   Pledge that is consistent also with the 1.5-2°C target of the Paris Agreement (UNEP, 2022). Moreover, because CH_4 is a

202   precursor of important air pollutants such as ozone, CH_4 emissions reductions are required by two international conventions:

203   the United Nations Framework Convention on Climate Change (UNFCCC) and the Convention on Long Range Transport

204   of Air Pollution (CLRTAP), making this global CH_4 budget assessment all the more critical.

205   Changes in the magnitude and temporal variation (annual to interannual) of CH_4 sources and sinks over the past

206   decades are characterised by large uncertainties (e.g., Kirschke et al., 2013; Saunois et al., 2017; Turner et al., 2019). Also,

207   the decadal budget suggests relative uncertainties (hereafter reported as min-max ranges) of 20-35% for inventories of

208   anthropogenic emissions in specific sectors (e.g., agriculture, waste, fossil fuels (Tibrewal et al., 2024)), 50% for biomass

209   burning and natural wetland emissions, and up to 100% for other natural sources (e.g., inland waters, geological sources).

210   The uncertainty in the chemical loss of CH_4 by OH, the predominant sink of atmospheric CH_4, has been estimated using

211   Prather et al. (2012) and Rigby et al. (2017). The former study estimated this uncertainty at ~10% from the uncertainty in

212   the reaction rate between CH_4 and OH, and the latter study was based on methyl-chloroform measurements. Bottom-up

213   approaches (chemistry transport models) estimate the uncertainty of the chemical loss by OH at around 15-20% (Saunois et

214   al., 2016, 2020). This uncertainty on the OH induced loss translates, in the top-down methods, into the minimum relative

215   uncertainty associated with global CH_4 emissions, as other CH_4 sinks (atomic oxygen and chlorine oxidations, soil uptake)

216   are much smaller and the atmospheric growth rate is well-defined (Dlugokencky et al., 2009). Globally, the contribution of

217   natural CH_4 emissions to total emissions can be quantified by combining lifetime estimates with reconstructed pre-industrial

218   atmospheric CH_4 concentrations from ice cores (assuming natural emissions have not been perturbed during the

219   anthropocene) (e.g., Ehhalt et al., 2001). Regionally or nationally, uncertainties in emissions may reach 40-60% (e.g., for

220   South America, Africa, China, and India; see Saunois et al., 2016). Another difficulty of the CH_4 budget lies in the necessity

221   to also match the isotopic signal and in particular reflect the decreasing methane isotopic signal [13]C (Nisbet et al., 2016;

222   2019). The previous budgets were tested against the isotopic observations (Saunois et al., 2017) and follow an exhaustive

223   assessment (Zhang et al., 2021b). To date only a couple of atmospheric inverse systems are able to assimilate both CH4

224   mixing ratios and stable isotopic signal to retrieve fluxes at the global scale (Thanwerdas et al., 2024; Basu et al., 2022), but

these systems still need improvements in terms of configuration set-up and computing time resources, in addition to characterisation of source signatures and chemical kinetic effect (Chandra et al., 2024). We hope to be able to report isotopic constrained budgets in the coming years, or at least test the budget against the isotopic balance.

To monitor emission reductions, for example to help conduct the Paris Agreement's stocktake, sustained and long-term monitoring of anthropogenic emissions per sector is needed in particular for hotspots of emissions that may be missed in inventories (Bergamaschi et al., 2018a; Pacala, 2010; Lauvaux et al., 2022). At the same time, reducing uncertainties in all individual CH_4 sources, and thus in the overall CH_4 budget remains challenging for at least four reasons. First, CH_4 is emitted by multiple processes, including natural and anthropogenic sources, point and diffuse sources, and sources associated with at least three different production origins (i.e., microbial, thermogenic, and pyrogenic). These multiple sources and processes require the integration of data from diverse scientific communities and across multiple temporal and spatial scales. The production of accurate bottom-up estimates is complicated by the fact that anthropogenic emissions result from leakage from fossil fuel production with large differences between countries depending on technologies and practices, the fact that many large leak events are sporadic, and the location of many emissions hotspots is not well known, and from uncertain emission factors used to summarise complex microbial processes in the agriculture and waste sectors. For the latter, examples include difficulties in upscaling methane emissions from livestock without considering the variety of animal weight, diet and environment, and difficulties in assessing emissions from landfills depending on waste type and waste management technology. Second, atmospheric CH_4 is removed mainly by chemical reactions in the atmosphere involving OH and other radicals that have very short lifetimes (typically ~1s). Due to the short lifetime of OH, the spatial and temporal distributions of OH are highly variable. While OH can be measured locally, calculating global CH_4 loss through OH measurements requires high-resolution global OH measurements (typically half an hour to integrate cloud cover, and 1 km spatially to consider OH high reactivity and heterogeneity) which is impossible from direct OH observations. As a result, OH can only be calculated through large scale atmospheric chemistry modelling. Those simulated OH concentrations from transport-chemistry models prescribed with emissions of precursor species affecting OH still show uncertain spatio-temporal distribution from regional to global scales (Zhao et al., 2019). Third, only the net CH_4 budget (sources minus sinks) is well constrained by precise observations of atmospheric growth rates (Dlugokencky et al., 2009), leaving the sum of sources and the sum of sinks uncertain. One distinctive feature of CH_4 sources compared to CO_2 fluxes is that the oceanic contribution to the global CH_4 budget is small (~1-3%), making CH4 source estimation predominantly a terrestrial endeavour (USEPA, 2010b). Finally, we lack comprehensive observations to constrain 1) the areal extent of different types of wetlands and inland freshwater (Kleinen et al., 2012, 2020, 2021, 2023; Stocker et al., 2014; Zhang et al., 2021), 2) models of wetland and inland freshwater emission rates (Melton et al., 2013; Poulter et al., 2017; Wania et al., 2013; Bastviken et al., 2011; Wik et al., 2016a; Rosentreter et al., 2021; Bansal et al., 2023; Lauerwald et al., 2023a; Stanley et al. 2023), 3) inventories of anthropogenic emissions (Höglund-Isaksson et al., 2020; Crippa et al., 2023; USEPA, 2019), and 4) atmospheric inversions, which aim to estimate CH_4 emissions from global to regional scales (Houweling et al., 2017; Jacob et al., 2022).

The global CH$_4$ budget inferred from atmospheric observations by atmospheric inversions relies on regional constraints from atmospheric sampling networks, which are relatively dense for northern mid-latitudes, with various high-precision and high-accuracy surface stations, but are sparser at tropical latitudes and in the Southern Hemisphere (Dlugokencky et al., 2011). Recently, the density of atmospheric observations has increased in the tropics due to satellite-based platforms that provide column-average CH$_4$ mixing ratios. Despite continuous improvements in the precision and accuracy of space-based measurements (e.g., Buchwitz et al., 2016), systematic errors greater than several ppb on total column observations can still limit the usage of such data to constrain surface emissions (e.g., Jacob et al., 2022). The development of robust bias corrections on existing data can help overcome this issue (e.g., Inoue et al., 2016, Lorente et al., 2023; Balasu et al., 2023) and satellite data are now widely used in atmospheric inversions where they provide more global information on the distribution of fluxes and highly complement the surface networks (e.g., Lu et al., 2021).

In this context, the Global Carbon Project (GCP) seeks to develop a complete picture of the carbon cycle by establishing common, consistent scientific knowledge to support policy development and actions to mitigate greenhouse gas emissions to the atmosphere (www.globalcarbonproject.org). The objective of this paper is to analyse and synthesise the current knowledge of the global CH$_4$ budget, by gathering results of observations and models to better understand and quantify the main robust features of this budget, its remaining uncertainties, and to make recommendations for improvement. We combine results from a large ensemble of bottom-up approaches (e.g., process-based models for natural wetlands, data-driven approaches for other natural sources, inventories of anthropogenic emissions and biomass burning, and atmospheric chemistry models), and top-down approaches (including CH$_4$ atmospheric observing networks, atmospheric inversions inferring emissions and sinks from the assimilation of atmospheric observations into models of atmospheric transport and chemistry). The focus of this work is to update the previous assessment made for the period 2000-2017 (Saunois et al., 2020) to the more recent 2000-2020 period. More in-depth analyses of trends and year-to-year changes are left to future publications. Our current paper is a living review, published at about four-year intervals, to provide an update and new synthesis of available observational, statistical, and model data for the overall CH$_4$ budget and its individual components.

Kirschke et al. (2013) was the first CH$_4$ budget synthesis followed by Saunois et al. (2016) and Saunois et al. (2020), with companion papers by Stavert et al. (2021) on regional CH$_4$ budgets and Jackson et al. (2020) focusing on the last year of the budget (2017). Saunois et al. (2020) covered 2000-2017 and reported CH$_4$ emissions and sinks for three time periods: 1) the latest calendar decade at that time (2000-2009), 2) data for the latest available decade (2008-2017), and 3) the latest available year (2017) at the time. Here, the Global Methane Budget (GMB) covers 2000-2020 split into the 2000-2009 decade, the 2010-2019 decade (where data are available), the year 2020 affected by COVID induced changes in human activity, and briefly for 2021-2023 as per data availability (Section 6). The CH$_4$ budget is presented at global, latitudinal, and regional scales and data can be downloaded from https://doi.org/10.18160/GKQ9-2RHT (Martinez et al., 2024). A global, regional and sectoral assessment of methane emission changes over the last two decades is discussed in Jackson et al. (2024) based on the data of Martinez et al. (2024).

Six sections follow this introduction. Section 2 presents the methodology used in the budget: units, definitions of source categories, regions, data analysis; and discusses the delay between the period of study of the budget and the release date. Section 3 presents the current knowledge about CH_4 sources and sinks based on the ensemble of bottom-up approaches reported here (models, inventories, data-driven approaches). Section 4 reports atmospheric observations and top-down atmospheric inversions gathered for this paper. Section 5, based on Sections 3 and 4, provides the updated analysis of the global CH_4 budget by comparing bottom-up and top-down estimates and highlighting differences. Section 6 discusses the recent changes in atmospheric CH_4 in relation with changes in CH_4 sources and sinks. Finally, Section 7 discusses future developments, missing components, and the most critical remaining uncertainties based on our update to the global CH_4 budget. For easier reading, the list of Contents of this manuscript is presented in the first section of the Supplementary Material.

2 Methodology

2.1 Units used

Unless specified, fluxes are expressed in teragrams of CH_4 per year (1 Tg CH_4 yr^{-1} = 10^{12} g CH_4 yr^{-1}), while atmospheric mixing ratios are expressed as dry air mole fractions, in parts per billion (ppb), with atmospheric CH_4 annual increases, G_{ATM}, expressed in ppb yr^{-1}. In the tables, we present mean values and ranges for the two decades 2000-2009 and 2010-2019, together with results for the most recent available year (2020). Results obtained from previous syntheses (i.e., Saunois et al., 2020 and Saunois et al., 2016) are also given for the decade 2000-2009. Following Saunois et al. (2016) and considering that the number of studies is often relatively small for many individual source and sink estimates, uncertainties are reported as minimum and maximum values of the available studies, given in brackets. In doing so, we acknowledge that we do not consider the uncertainty of the individual estimates, and we express uncertainty as the range of available mean estimates, i.e., differences across measurements/methodologies considered. These minimum and maximum values are those presented in Section 2.5 and exclude identified outliers.

The CH_4 emission estimates are provided with up to three significant digits, for consistency across all budget flux components and to ensure the accuracy of aggregated fluxes. Nonetheless, given the values of the uncertainties in the CH_4 budget, we encourage the reader to consider not more than two digits as significant for the global total budget.

2.2 Period of the budget and availability of data

The bottom-up estimates rely on global anthropogenic emission inventories, an ensemble of process-based models for wetlands emissions, and published estimates in the literature for other natural sources. The global gridded anthropogenic inventories (see Section (3.1.1)) are updated irregularly, generally every 3 to 5 years. The last reported years of available inventories were 2018 or 2019 when we started the top-down modelling activity. In order to cover the period 2000-2020, it

was necessary to extrapolate the anthropogenic inventory EDGARv6 (Crippa et al., 2021) to 2020 to use it as prior information for the anthropogenic emissions in the atmospheric inversion systems as explained in the supplementary material. Though EDGARv7 (EDGAR, 2022; Crippa et al., 2023) spanning until 2021 was then released, and was used for the bottom-up budget. EDGARv8 (EDGAR, 2023 ; Crippa et al., 2023) spanning until 2022 and released in 2024, was used in Section 6 to discuss the post 2020 methane budget. The land surface (wetland) models were run over the full period 2000-2020 using dynamical wetland areas, derived by remote sensing data or other models of flooded area variability (Sect. 3.2.1). The atmospheric inversions run until mid-2021, but the last year of reported inversion results is 2020, which represents a three-year lag with the present. This is due to the long time period it takes to acquire atmospheric in-situ data and integrate models. Even though satellite observations are processed operationally and are generally available with a latency of days to weeks, by contrast surface observations can lag from months to years because of the time for flask analyses and data quality checks in (mostly) non-operational chains. In addition, the final six months of inversions must be generally ignored because the estimated fluxes are not constrained by as many observations as the previous periods. Lastly, this budget presents an extended synthesis of the most recent development regarding inland water emissions (Sect. 3.2.2) and corrections associated with double counting with wetlands.

2.3 Definition of regions

Geographically, emissions are reported globally and for three latitudinal bands (90°S-30°N, 30-60°N, 60-90°N, only for gridded products). When extrapolating emission estimates forward in time (see Sect. 3.1.1), and for the regional budget presented by Stavert et al. (2021), a set of 19 regions (oceans and 18 continental regions, see supplementary Fig. S3) were used. As anthropogenic emissions are often reported by country, we define these regions based on a country list (Table S1). This approach was compatible with all top-down and bottom-up approaches considered. The number of regions was chosen to be close to the widely used TransCom inter-comparison map (Gurney et al., 2004) but with subdivisions to separate the contribution from important countries or regions for the CH_4 cycle (China, South Asia, Tropical America, Tropical Africa, United States of America, and Russia). The resulting region definition is the same as that used for the Global Carbon Project (GCP) N_2O budget (Tian et al., 2020). Compared to Saunois et al. (2020), the Oceania region has been replaced by Australasia including only Australia and New Zealand. Other territories formerly in Oceania were included in Southeast Asia.

2.4 Definition of source and sink categories

CH_4 is emitted by different processes (i.e., biogenic, thermogenic, or pyrogenic) and can be of anthropogenic or natural origin. Biogenic CH_4 is the final product of the decomposition of organic matter by methanogenic *Archaea* in anaerobic environments, such as water-saturated soils, swamps, rice paddies, marine and freshwater sediments, landfills, sewage and wastewater treatment facilities, or inside animal digestive systems. Thermogenic methane is formed on geological time

scales by the breakdown of buried organic matter due to heat and pressure deep in the Earth's crust. Thermogenic CH_4 reaches the atmosphere through marine and land geological gas seeps. These CH_4 emissions are increased by human activities, for instance, the exploitation and distribution of fossil fuels. Pyrogenic CH_4 is produced by the incomplete combustion of biomass and other organic materials. Peat fires, biomass burning in deforested or degraded areas, wildfires, and biofuel burning are the largest sources of pyrogenic CH_4. CH_4 hydrates, ice-like cages of frozen CH_4 found in continental shelves and slopes and below sub-sea and land permafrost, can be of either biogenic or thermogenic origin. Each of these three process categories has both anthropogenic and natural components.

In the following, we present the different CH_4 sources depending on their anthropogenic or natural origin, which is relevant to climate policy. Compared to the previous budgets, marginal changes have been made regarding source categories (naming and grouping), to reflect the improved estimates for inland water sources and their indirect anthropogenic component. In the previous Global Methane Budgets (Saunois et al., 2016, 2020), natural and anthropogenic emissions were split in a way that did not correspond exactly to the definition used by the UNFCCC following the IPCC guidelines (IPCC, 2006), where, for pragmatic reasons, all emissions from managed land are typically reported as anthropogenic. For instance, we considered all wetlands as natural emissions, despite some wetlands being on managed land and their emissions being partly reported as anthropogenic in UNFCCC national communications. Separating natural from anthropogenic sources could be quite challenging, especially over regions where sources overlap, as over heavily human-dominated floodplain deltas for example. The human induced perturbation of climate, atmospheric CO_2, and nitrogen and sulfur deposition may also cause changes in wetland sources we classified as natural. Following our previous definition, emissions from wetlands, inland freshwaters, thawing permafrost, or geological leaks are accountable for "natural" emissions, even though we acknowledge that climate change and other human perturbations (e.g., eutrophication) may cause changes in those emissions. CH_4 emissions from reservoirs were also considered as natural even though reservoirs are human-made. Indeed, since the 2019 refinement to the IPCC guidelines (IPCC, 2019) emissions from reservoirs and other flooded lands are considered to be anthropogenic by the UNFCCC and should be reported as such. However, these estimates are not provided by inventories and not systematically reported by all countries (especially non Annex-I countries). In this budget we rename "natural sources" to "natural and indirect anthropogenic sources" to acknowledge that CH_4 emissions from reservoirs, as well as from water bodies that were perturbed by agricultural activities (drainage, eutrophication, land use change) are indirect anthropogenic emissions. As a result, here, "natural and indirect anthropogenic sources" refer to "emissions that do not directly originate from fossil, agricultural, waste, and biomass burning sources" even if they are perturbed by anthropogenic activities and climate change. Natural and indirect anthropogenic emissions are split between "Wetlands and Inland Freshwaters" and "Other natural" emissions (e.g., wild animals, termites, land geological sources, oceanic geological and biogenic sources, and terrestrial permafrost). "Anthropogenic direct sources" are caused by direct human activities since pre-industrial/pre-agricultural time (3000-2000 BC, Nakazawa et al., 1993) including agriculture, waste management, fossil fuel-related activities and biofuel and biomass burning (yet we acknowledge that a small fraction of wildfires are naturally ignited). Direct anthropogenic

emissions are split between: "Agriculture and waste emissions", "Fossil fuel emissions", and "Biomass and biofuel burning emissions", assuming that all types of fires are caused by anthropogenic activities. To conclude, this budget reports "direct anthropogenic", and "natural and indirect anthropogenic" methane emissions for the five main source categories explained above for both bottom-up and top-down approaches.

The sinks of methane are split into the soil uptake that can be derived from land-surface models in the bottom-up budget, and the chemical sinks. The chemical sinks are estimated by either chemistry climate or chemistry transport models in the bottom-up budget, and are further detailed in terms of vertical distribution (troposphere and stratosphere) and oxidants.

Bottom-up estimates of CH_4 emissions for some processes are derived from process-oriented models (e.g., biogeochemical models for wetlands, models for termites), inventory models (agriculture and waste emissions, fossil fuel emissions, biomass and biofuel burning emissions), satellite-based models (large scale biomass burning), or observation-based upscaling models for other sources (e.g., inland water, geological sources). From these bottom-up approaches, it is possible to provide estimates for more detailed source subcategories inside each main category described above (see budget in Table 3). However, the total CH_4 emission derived from the sum of independent bottom-up estimates remains unconstrained.

For atmospheric inversions (top-down approach), atmospheric methane concentration observations provide a constraint on the global methane total source if we assume the global sink is known (OH and other oxidant prescribed), or inversions are optimising also for the chemical sink. OH estimates are constrained by methyl chloroform-inversion (Montzka et al., 2011; Rigby et al., 2017; Patra et al., 2021). The inversions reported in this work solve for the total net CH_4 flux at the surface (sum of sources minus soil uptake) (e.g., Pison et al., 2013), or a limited number of source categories (e.g., Bergamaschi et al., 2013). In most of the inverse systems the atmospheric oxidant concentrations were prescribed with pre-optimized or scaled OH fields, and thus the atmospheric sink is not optimised. The assimilation of CH_4 observations alone, as reported in this synthesis, can help to separate sources with different locations or temporal variations but cannot fully separate individual sources where they overlap in space and time in some regions. Top-down global and regional CH_4 emissions per source category were nevertheless obtained from gridded optimised fluxes, for the inversions that separated emissions into the five main GCP categories. Alternatively, for the inversion that only solved for total emissions (or for other categories other than the five described above), the prior contribution of each source category at the spatial resolution of the inversion was scaled by the ratio of the total (or embedding category) optimised flux divided by the total (or embedding category) prior flux (Kirschke et al., 2013). In other words, the prior relative mix of sources at model resolution is kept in each grid cell while total emissions are given by the atmospheric inversions. The soil uptake was provided separately to report total gross surface emissions instead of net fluxes (sources minus soil uptake).

In summary, bottom-up models and inventories emissions are presented for all relevant source processes and grouped if needed into the five main categories defined above. Top-down inversion emissions are reported globally and for the five main emission categories.

2.5 Processing of emission maps and box-plot representation of emission budgets

Common data analysis procedures have been applied to the different bottom-up models, inventories and atmospheric inversions whenever gridded products exist. Gridded emissions from atmospheric inversions, land-surface models for wetland or biomass burning were provided at the monthly scale. Emissions from anthropogenic inventories are usually available as yearly estimates. These monthly or yearly fluxes were provided on a 1°x1° grid or re-gridded to 1°x1°, then converted into units of Tg CH_4 per grid cell. Inversions with a resolution coarser than 1° were downscaled to 1° by each modelling group. Land fluxes in coastal pixels were reallocated to the neighbouring land pixel according to our 1° land-sea mask, and vice-versa for ocean fluxes. Annual and decadal means used for this study were computed from the monthly or yearly gridded 1°x1° maps.

Budgets are presented as boxplots with quartiles (25%, median, 75%), outliers, and minimum and maximum values without outliers. Outliers were determined as values below the first quartile minus three times the interquartile range, or values above the third quartile plus three times the interquartile range. Mean values reported in the tables are represented as "+" symbols in the corresponding figures.

3 Methane sources and sinks: bottom-up estimates

For each source category, a short description of the relevant processes, original data sets (measurements, models) and related methodology are given. More detailed information can be found in original publication references, in Annex A2 where the sources of data used to estimate the different sources and sinks are summarised and compared with those used in Saunois et al. (2020) and in the Supplementary Material of this study when specified in the text. The emission estimates for each source category are compared with Saunois et al. (2020) in Table 3 and with Saunois et al. (2016) in Table S12 for the decade 2000-2009.

3.1 Anthropogenic direct sources

3.1.1 Global inventories

The main bottom-up global inventory datasets covering direct anthropogenic emissions from all sectors (Table 1) are from the United States Environmental Protection Agency (USEPA, 2019), the Greenhouse gas and Air pollutant Interactions and Synergies (GAINS) model developed by the International Institute for Applied Systems Analysis (IIASA) (Höglund-Isaksson et al., 2020) and the Emissions Database for Global Atmospheric Research (EDGARv6 and v7, Crippa et al., 2021, 2023) compiled by the European Commission Joint Research Centre (EC-JRC) and Netherlands Environmental Assessment Agency (PBL). We also used the Community Emissions Data System for historical emissions (CEDS) (Hoesly et al., 2018) developed for climate modelling and the Food and Agriculture Organization (FAO) FAOSTAT emission database (Tubiello

et al., 2022), which covers emissions from agriculture and land use (including peatland fires and biomass fires). These inventories are not independent as they may use the same activity data or emission factors, as discussed below.

These inventory datasets report emissions from fossil fuel production, transmission, and distribution; livestock enteric fermentation; manure management and application; rice cultivation; solid waste and wastewater. Since the level of detail provided by country and by sector varies among inventories, the data were reconciled into common categories according to Table S2. For example, agricultural waste-burning emissions treated as a separate category in EDGAR, GAINS and FAO, are included in the biofuel sector in the USEPA inventory and in the agricultural sector in CEDS. The GAINS, EDGAR and FAO estimates of agricultural waste burning were excluded from this analysis (these amounted to 1-3 Tg CH_4 yr^{-1} in recent decades) to prevent any potential overlap with separate estimates of biomass burning emissions (e.g., GFEDv4.1s; Giglio et al. (2013); van der Werf et al (2017)). In the inventories used here, emissions for a given region/country and a given sector are usually calculated following IPCC methodology (IPCC, 2006), as the product of an activity factor and its associated emission factor. An abatement coefficient may also be used, to account for any regulations implemented to control emissions (see e.g., Höglund-Isaksson et al., 2015). These datasets differ in their assumptions and data used for the calculation; however, they are not completely independent because they often use the same activity data and some of them follow the same IPCC guidelines (IPCC, 2006). While the USEPA inventory adopts emissions reported by the countries to the UNFCCC, other inventories (FAOSTAT, EDGAR and the GAINS model) produce their own estimates using a consistent approach for all countries, typically IPCC Tier 1 methods or deriving IPCC Tier 2 emission factors from country-specific information using a consistent methodology. These other inventories compile country-specific activity data and emission factor information or, if not available, adopt IPCC default factors (Tibrewal et al., 2024; Oreggioni et al., 2021; Höglund-Isaksson et al., 2020; Tubiello, 2019). CEDS takes a different approach (Hoesly et al., 2018) and combines data from GAINS, EDGAR and FAO depending on the sector. Then their first estimates are scaled to match other individual or region-specific inventory values when available. This process maintains the spatial information in the default emission inventories while preserving consistency with country level data. The FAOSTAT dataset (hereafter FAO-CH_4) provides estimates at the country level and is limited to agriculture (CH_4 emissions from enteric fermentation, manure management, rice cultivation, energy usage, burning of crop residues, and prescribed burning of savannahs) and land-use (peatland fires and biomass burning). FAO-CH_4 uses activity data mainly from the FAOSTAT crop and livestock production database, as reported by countries to FAO (Tubiello et al., 2013), and applies mostly the Tier 1 IPCC methodology for emissions factors (IPCC, 2006), which depends on geographic location and development status of the country. For manure, the country-scale temperature was obtained from the FAO global agro-ecological zone database (GAEZv3.0, 2012). Although country emissions are reported annually to the UNFCCC by annex I countries, and episodically by non-annex I countries, data gaps of those national inventories do not allow the inclusion of these estimates in this analysis.

In this budget, we use the following versions of these inventories that were available at the start and during the analysis (see Table 1):

- EDGARv6 which provides yearly gridded emissions by sectors from 1970 to 2018 (Crippa et al., 2021; Oreggioni et al., 2021; EDGARv6 website https://edgar.jrc.ec.europa.eu/dataset_ghg60; Monforti Ferrario et al., 2021),
- EDGARv7, which provides yearly gridded emissions by sectors from 1970 to 2020 (monthly for some sectors), but emissions from fossil fuel energy are not separated (oil and gas, and coal are lumped together - see Table S2) (EDGARv7 website https://edgar.jrc.ec.europa.eu/dataset_ghg70; Crippa et al., 2023).
- GAINS model scenario version 4.0 (Höglund-Isaksson et al., 2020) which provides an annual sectorial gridded product from 1990 to 2020 both by country and gridded. USEPA (USEPA, 2019), which provides 5-year sectorial totals by country from 1990 to 2020 (estimates from 2015 onward are a projection), with no gridded distribution available. The USEPA dataset was linearly interpolated to provide yearly values from 1990-2020.
- CEDS version v_2021_04_21 which provides gridded monthly and annual country-based emissions by sectors from 1970 to 2019 (Hoesly et al., 2018; O'Rourke et al., 2021). Fossil fuel emissions for 2020 have been updated using the methodology described for CO in Zheng et al. (2023).
- FAO-CH$_4$ (database accessed in December 2022, FAO, 2022) containing annual country level data for the period 1961-2020, for rice, manure, and enteric fermentation; and 1990-2020 for burning savannah, crop residue and non-agricultural biomass burning.

3.1.2 Total anthropogenic direct emissions

We calculated separately the total anthropogenic emissions for each inventory by adding its values for "Agriculture and waste", "Fossil fuels" and "Biofuels" with additional large-scale biomass burning emissions data (Sect. 3.1.5). This method avoids double counting and ensures consistency within each inventory. This approach was used for the EDGARv6 and v7, CEDS and GAINS inventories, but we kept the USEPA inventory as originally reported because it includes its own estimates of biomass burning emissions. FAO-CH$_4$ was only included in the range reported for the "Agriculture and waste" category. For the latter, we calculated the range and mean value as the sum of the mean and range of the three anthropogenic subcategory estimates "Enteric fermentation and Manure", "Rice", and "Landfills and Waste". The values reported for the upper-level anthropogenic categories ("Agriculture and waste", "Fossil fuels" and "Biomass burning & biofuels") are therefore consistent with the sum of their subcategories, although there might be small percentage differences between the reported total anthropogenic emissions and the sum of the three upper-level categories. This approach provides a more accurate representation of the range of emission estimates, avoiding an artificial expansion of the uncertainty attributable to subtle differences in the definition of sub-sector categorisations between inventories.

Based on the ensemble of databases detailed above, total direct anthropogenic emissions were 358 [329-387] Tg CH$_4$ yr^{-1} for the decade 2010-2019 (Table 3, including biomass and biofuel burning) and 331 [305-365] Tg CH$_4$ yr^{-1} for the decade 2000-2009. Our estimate for the 2000-2009 decade is within the range of Saunois et al. (2020) (334 [321-358]), Saunois et al. (2016) (338 Tg CH4 yr-1 [329-342]) and Kirschke et al. (2013) (331 Tg CH$_4$ yr^{-1} [304-368]) for the same period. The

511 slightly larger range reported herein with respect to previous estimates is due to the USEPA lower estimate for agriculture,

512 waste and fossil emissions associated with the lowest estimate of biomass burning.

513 Figure 2 (left) summarises or projects global CH_4 emissions of anthropogenic sources (including biomass and biofuel

514 burning) by different datasets between 2000 and 2050. The datasets consistently estimate total anthropogenic emissions of

515 ~300 Tg CH_4 yr^{-1} in 2000. For the Sixth Assessment Report of the IPCC, seven main Shared Socioeconomic Pathways

516 (SSPs) were defined for future climate projections in the Coupled Model Intercomparison Project 6 (CMIP6) (Gidden et al.,

517 2019; O'Neill et al., 2016) ranging from 1.9 to 8.5 W m^{-2} radiative forcing by the year 2100 (as shown by the number in the

518 SSP names). For the 1970-2015 period, historical emissions used in CMIP6 (Feng et al., 2019) combine anthropogenic

519 emissions from CEDS (Hoesly et al., 2018) and a climatological value from the GFEDv4.1s biomass burning inventory (van

520 Marle et al., 2017). The harmonised scenarios used for CMIP6 activities start in 2015 at 388 Tg CH_4 yr^{-1}, which corresponds

521 to the higher range of our estimates. Since CH_4 emissions continue to track scenarios that assume no or minimal climate

522 policies (SSP5 and SSP3), it may indicate that climate policies, when present, have not yet produced sufficient results to

523 change the emissions trajectory substantially (Nisbet et al., 2019). After 2015, the SSPs span a range of possible outcomes,

524 but current emissions appear likely to follow the higher-emission trajectories, given that over the past decade their trend has

525 followed such trajectories, and because the peak emission year has not yet been reached. High or medium emission reduction

526 rates as suggested by scenarios SSP1 and SSP2 have not yet happened. This illustrates the challenge of methane mitigation

527 that lies ahead to help reach the goals of the Paris Agreement (Nisbet et al., 2020; Shindell et al., 2024). In addition, estimates

528 of methane atmospheric concentrations (Meinshausen et al., 2017, 2020) from the harmonised scenarios (Riahi et al., 2017)

529 indicate that observations of global CH_4 concentrations fall well within the range of scenarios in absolute values but their

530 trend over the past few years is closest to those of scenario SSP5-8.5 (Fig. 2 right). The CH_4 concentrations are estimated

531 using a simple exponential decay with inferred natural emissions (Meinshausen et al., 2011), and the emergence of any trend

532 between observations and scenarios needs to be confirmed in the following years. However, the current observed

533 concentrations and emissions estimates lie in the upper range of the former RCPs scenarios starting in 2005 (Fig. S1). In the

534 future, it will be important to monitor the trends from 2015 (the Paris Agreement) and from 2020 (Global Methane Pledge)

535 estimated in inventories and from atmospheric observations, and compare them to various scenarios.

3.1.3 Fossil fuel production and use

537 Most anthropogenic CH_4 emissions related to fossil fuels come from the exploitation, transportation, and usage of coal, oil,

538 and natural gas. Additional emissions reported in this category include small industrial contributions such as the production

539 of chemicals and metals, fossil fuel fires (e.g., underground coal mine fires and the Kuwait oil and gas fires), and transport

540 (road and non-road transport). CH_4 emissions from the oil processing industry (e.g., refining) and production of charcoal

541 are estimated to be a few Tg CH_4 yr^{-1} only and are included in the transformation industry sector in the inventory. Fossil

542 fuel fires are included in the subcategory "Oil & Gas". Emissions from industries, road and, non-road transport are reported

543 apart from the two main subcategories "Oil & Gas" and "Coal", as in Saunois et al. (2020) and contrary to Saunois et al.

544 (2016); each of these amounts to about 2 to 5 Tg CH_4 yr^{-1} (Table 3). The large range (1-9 Tg CH_4 yr^{-1}) is attributable to

545 difficulties in allocating some sectors to these sub-sectors consistently among the different inventories (See Table S2). The

546 spatial distribution of CH_4 emissions from fossil fuels is presented in Fig. 3 based on the mean gridded maps provided by

547 CEDS, EDGARv6, and GAINS for the 2010-2019 decade; USEPA lacks a gridded product.

548 Global mean emissions from fossil fuel-related activities, other industries and transport are estimated from the four global

549 inventories (Table 1) to be of 120 [117-125] Tg CH_4 yr^{-1} for the 2010-2019 decade (Table 3), but with large differences in

550 the rate of change during this period across inventories. The sector accounts on average for 34% (range 31-42%) of total

551 global anthropogenic emissions in 2010-2019. This contribution has slightly increased from 32% on average in 2000-2009.

552

553 **Coal mining.**

554 During mining, CH_4 is emitted primarily from ventilation shafts, where large volumes of air are pumped in and out of the

555 mine to keep the CH_4 mixing ratio below 0.5% to avoid accidental ignition, and from dewatering operations. In countries of

556 the Organization for Economic Co-operation and Development (OECD), coalbed CH_4 is often extracted as fuel up to ten

557 years before the coal mine starts operation, thereby reducing the CH_4 channelled through ventilation shafts during mining.

558 In many countries, large quantities of ventilation air CH_4 are still released to the atmosphere or flared, despite efforts to

559 extend coal mine gas recovery under the UNFCCC Clean Development Mechanisms (http://cdm.unfccc.int). CH_4 leaks also

560 occur during post-mining handling, processing, and transportation. Some CH_4 is released from coal waste piles and

561 abandoned mines; while emissions from these sources were believed to be low (IPCC, 2000), recent work has estimated

562 these at 22 billion m^3 (compared to 103 billion m^3 from functioning coal mines) in 2010 with emissions projected to increase

563 into the future (Kholod et al., 2020).

564 In 2020, more than 35% (IEA, 2023a) of the world's electricity is still produced from coal. This contribution grew in the

565 2000s at the rate of several percent per year, driven by Asian economic growth where large reserves exist, but global coal

566 consumption declined between 2014 and 2020. In 2020, the top ten largest coal producing nations accounted for ~90% of

567 total world CH_4 emissions from coal mining; among them, the top three producers (China, United States of America, and

568 India) produced almost two-thirds (66%) of the world's coal (IEA, 2021).

569 Global estimates of CH_4 emissions from coal mining show a reduced range of 37-44 Tg CH_4 yr^{-1} for 2010-2019 (Table 3),

570 compared to the previous estimate for 2008-2017 in Saunois et al. (2020) reporting a range of 29-61 Tg CH_4 yr^{-1} for 2008-

571 2017. This reduced range probably results from using similar activity data (mostly from IEA statistics) in the different

572 inventories. The highest value of the range in Saunois et al. (2020) came from the CEDS inventory while the lowest came

573 from USEPA. CEDS seems to have revised downward their estimate compared to the previous version used in Saunois et

574 al. (2020). There were previously large discrepancies in Chinese coal emissions, with a large overestimation from

575 EDGARv4.2 on which CEDS was based. As highlighted by Liu et al. (2021a), a county-based inventory of Chinese methane

576   emissions also confirms the overestimation of previous EDGAR inventories and estimated total anthropogenic Chinese
577   emissions at 38.2±5.5 Tg CH_4 yr^{-1} for 2000-2008 (Liu et al., 2021a). Coal mining emission factors depend strongly on the
578   type of coal extraction (underground mining emits up to 10 times more than surface mining), the geological underground
579   structure (region-specific), history (basin uplift), and the quality of the coal (brown coal (lignite) emits less than hard coal
580   (anthracite)). Finally, the different emission factors derived for coal mining is the main reason for the differences between
581   inventories globally (Fig. 2).

582   For the 2010-2019 decade, methane emissions from coal mining represent 33% of total fossil fuel-related emissions of CH_4
583   (40 [37-44] Tg CH_4 yr^{-1}, Table 3). An additional assumed very small source corresponds to fossil fuel fires, which are
584   mostly underground coal fires. This source is estimated at around 0.15 Tg yr^{-1} in EDGARv7, though this value remains the
585   same across EDGAR versions and for all years despite the changes in coal production, which could influence this estimate.
586   However, to date, insufficient data is available to better estimate this largely unknown source.   .

587

Oil and natural gas systems.

589   This sub-category includes emissions from both conventional and shale oil and gas exploitation. Natural gas is composed
590   primarily of CH_4, so both fugitive and planned emissions during the drilling of wells in gas fields, extraction, transportation,
591   storage, gas distribution, end use, and incomplete combustion in gas flares emit CH_4 (Lamb et al., 2015; Shorter et al., 1996).
592   Persistent fugitive emissions (e.g., due to leaky valves and compressors) should be distinguished from intermittent emissions
593   due to maintenance (e.g., purging and draining of pipes) or incidents. During transportation, fugitive emissions can occur in
594   oil tankers, fuel trucks and gas transmission pipelines, attributable to corrosion, manufacturing, and welding faults.
595   According to Lelieveld et al. (2005), CH_4 fugitive emissions from gas pipelines should be relatively low, however, old
596   distribution networks in some cities may have higher rates, especially those with cast-iron and unprotected steel pipelines
597   (Phillips et al., 2013). Measurement campaigns in cities within the USA (e.g., McKain et al., 2015) and Europe (e.g.,
598   Defratyka et al., 2021) revealed that significant emissions occur in specific locations (e.g., storage facilities, city natural gas
599   fueling stations, well and pipeline pressurisation/depressurisation points, sewage systems, and furnaces of buildings) along
600   the distribution networks (e.g., Jackson et al., 2014a; McKain et al., 2015; Wunch et al., 2016). However, CH_4 emissions
601   vary significantly from one city to another depending, in part, on the age of city infrastructure and the quality of its
602   maintenance, making urban emissions difficult to scale-up from measurement campaigns, although attempts have been made
603   (e.g., Defratyka et al., 2021). In many facilities, such as gas and oil fields, refineries, and offshore platforms, most of the
604   associated and other waste gas generated will be flared for security reasons with almost complete conversion to CO_2,
605   however, due to the large quantities of waste gas generated, small fractions of gas still being vented make up relatively large
606   quantities of methane. These two processes are usually considered together in inventories of oil and gas industries. In
607   addition, single-point failure of natural gas infrastructure can leak CH_4 at high rate for months, such as at the Aliso Canyon
608   blowout in the Los Angeles, CA (Conley et al., 2016) or the shale gas well blowout in Ohio (Pandey et al., 2019), thus

hampering emission control strategies. Production of natural gas from the exploitation of hitherto unproductive rock formations, especially shale, began in the 1970s in the US on an experimental or small-scale basis, and then, from the early 2000s, exploitation started at a large commercial scale. The shale gas contribution to total dry natural gas production in the United States reached 82% in 2023, growing rapidly from 48% in 2013 (IEA, 2023b). The possibly larger emission factors from shale gas compared to conventional gas, have been widely debated (e.g., Cathles et al., 2012; Howarth, 2019; Lewan, 2020). The latest studies tend to infer emission factors from the oil gas production chain of about 1% to 6% (e.g., Schneising et al., 2020; Varon et al., 2023; Zhang et al., 2020), but loss rate could be has high as more than 10% in low producing well sites (e.g., Omara et al., 2022, Williams et al., 2024).

CH_4 emissions from oil and natural gas systems vary greatly in different global inventories (67 to 80 Tg yr^{-1} in 2020, Table 3). The inventories generally rely on the same sources and magnitudes for activity data, with the derived differences therefore resulting primarily from different methodologies and parameters used, including emission factors. Those factors are country- or even site-specific and the few field measurements available often combine oil and gas activities (Brandt et al., 2014), resulting in high uncertainty in emission estimates for many major oil and gas producing countries. Depending on the region, the IPCC 2006 default emission factors may vary by two orders of magnitude for oil production and one order for gas production. For instance, the GAINSv4.0 estimate of CH_4 emissions from US oil and gas systems in 2015 is 16 Tg, which is almost twice as high as EDGARv8.0 (EDGAR, 2024) at 8.4 Tg and USEPA (UNFCCC, 2023) at 9.5 Tg. The difference can partly be explained by GAINS using a bottom-up methodology to derive country- and year-specific flows of associated petroleum gas and attributing these to recovery/reinjection, flaring or venting (Höglund-Isaksson, 2017), and partly to GAINS using a higher emission factor for unconventional gas production (Höglund-Isaksson et al., 2020). Recent quantifications using satellite observations and inversion estimate a relatively stable trend for US oil and gas systems emissions since 2010, with Lu et al. (2023) estimating 14.6 Tg for 2010, 15.9 Tg for 2014 and 15.6 Tg for 2019, Shen et al. (2022) estimating a mean of 12.6 Tg for 2018-2020, and Maasakkers et al (2021) a mean of 11.1 Tg for 2010 to 2015. The stable top-down trend for the US appears not well captured in the bottom-up inventories from GAINS and EDGAR, which tend to show an increasing trend driven by increase in production volumes.

Most recent studies (e.g., Zhang et al., 2020; Shen et al., 2023; Li et al., 2024, Tibrewal et al., 2024; Sherwin et al., 2024) still suggest that the methane emissions from oil and gas industry are underestimated by inventories, industries, and agencies, including the USEPA and UNFCCC reporting. Lauvaux et al.   (2022) showed that emissions from a few high-emitting facilities, i.e., super-emitters (> 20 t hr^{-1}), which are usually sporadic in nature, and not accounted for in the inventories, could represent 8-12% of global oil & gas emissions, or around 8 Tg CH_4 yr^{-1}. These high emitting points, located on the conventional part of the facilities, could be avoided through better operating conditions and repair of malfunctions. Over the last decade, absolute CH_4 emissions almost certainly increased, since USA crude oil production doubled and natural gas production rose by about 50% (IEA, 2023a). However, global implications of the rapidly growing shale gas activity in the US remain to be determined precisely.

For the 2010-2019 decade, CH_4 emissions from upstream and downstream oil and natural gas sectors are estimated to represent about 56% of total fossil CH_4 emissions (67 [57-74] Tg CH_4 yr^{-1}, Table 3) based on global inventories, with a lower uncertainty range than for coal emissions for most countries. However, it is worth noting that 8 Tg CH_4 yr^{-1} should be added on top of this estimate to acknowledge the ultra-emitters contribution, as done in Tibrewal et al (2024).

3.1.4 Agriculture and waste sectors

This main category includes CH_4 emissions related to livestock production (i.e., enteric fermentation in ruminant animals and manure management), rice cultivation, landfills, and wastewater handling. Of these activities, globally and in most countries, livestock is by far the largest source of CH_4, followed by waste handling and rice cultivation. Conversely, field burning of agricultural residues is a minor source of CH_4 reported in emission inventories (a few Tg at the global scale). The spatial distribution of CH_4 emissions from agriculture and waste handling is presented in Fig. 3 based on the mean gridded maps provided by CEDS, EDGARv6 and GAINS over the 2010-2019 decade.

Global emissions from agriculture and waste for the period 2010-2019 are estimated to be 211 [195-231] Tg CH_4 yr^{-1} (Table 3), representing 60% of total direct anthropogenic emissions. Agriculture emissions amount to 144 Tg CH_4 yr^{-1}, 40% of the direct anthropogenic emissions, with the rest coming from the fossil fuel sector (34%), waste (19%) and biomass (5%) and biofuel (3%) burning .

Livestock: Enteric fermentation and manure management. Domestic ruminants such as cattle, buffalo, sheep, goats, and camels emit CH_4 as a by-product of the anaerobic microbial activity in their digestive systems (Johnson et al., 2002). The very stable temperatures (about 39°C) and pH (6.5-6.8) within the rumen of domestic ruminants, along with a constant plant matter flow from grazing (cattle graze many hours per day), allow methanogenic *Archaea* residing within the rumen to produce CH_4. CH_4 is released from the rumen mainly through the mouth of multi-stomached ruminants (eructation, ~90% of emissions) or absorbed in the blood system. The CH_4 produced in the intestines and partially transmitted through the rectum is only ~10% (Hill et al. 2016).

The total number of livestock continues to grow steadily. There are currently (2020) about 1.5 billion cattle globally, almost 1.3 billion sheep, and nearly as many goats (http://www.fao.org/faostat/en/#data/GE). Livestock numbers are linearly related to CH_4 emissions in inventories using the Tier 1 IPCC approach such as FAOSTAT. In practice, some non-linearity may arise due to dependencies of emissions on the total weight of the animals and their diet, which are better captured by Tier 2 and higher approaches. Cattle, due to their large population, large individual size, and particular digestive characteristics, account for the majority of enteric fermentation CH_4 emissions from livestock worldwide (Tubiello, 2019; FAO, 2022), particularly in intensive agricultural systems in wealthier and emerging economies, including the United States (USEPA, 2016). CH_4 emissions from enteric fermentation also vary from one country to another as cattle may experience diverse living conditions that vary spatially and temporally, especially in the tropics (Chang et al., 2019).

673   Anaerobic conditions often characterise manure decomposition in a variety of manure management systems globally (e.g.,
674   liquid/slurry treated in lagoons, ponds, tanks, or pits), with the volatile solids in manure producing CH_4. In contrast, when
675   manure is handled as a solid (e.g., in stacks or dry-lots) or deposited on pasture, range, or paddock lands, it tends to
676   decompose aerobically and to produce little or no CH_4. However aerobic decomposition of manure tends to produce nitrous
677   oxide (N_2O), which has a larger global warming impact than CH_4. Ambient temperature, moisture, energy contents of the
678   feed, manure composition, and manure storage or residency time affect the amount of CH_4 produced. Despite these
679   complexities, most global datasets used herein apply a simplified IPCC Tier 1 approach, where amounts of manure treated
680   depend on animal numbers and simplified climatic conditions by country.

681   Global CH_4 emissions from enteric fermentation and manure management are estimated in the range of 114-124 Tg CH_4 yr^{-1},
682   for the year 2020, in the GAINS model and CEDS, USEPA, FAO-CH_4 and EDGARv7 inventories (Table 3). Using the
683   Tier 2 method adopted from the 2019 Refinement to 2006 IPCC guidelines, a recent study (Zhang et al., 2022) estimated
684   that global CH_4 emissions from livestock increased from 31.8 [26.5–37.1] (mean [minimum−maximum of 95% confidence
685   interval) Tg CH_4 yr^{-1} in 1890 to 131.7 [109.6–153.7] Tg CH_4 yr^{-1} in 2019, a fourfold increase in the past 130 years. Chang
686   et al. (2021) estimates enteric fermentation and manure management emissions based on mixed Tier 1&2 and Tier1
687   approaches and calculate livestock emissions being 120±13 and 136±15 Tg CH_4 yr^{-1} respectively for 2018. Chang et al.
688   (2021) and Zhang et al. (2022) estimates for 2018 or 2019 are on average a bit higher than the inventories estimates but in
689   agreement considering the uncertainties. It is worth recalling here that the ranges provided in this study correspond to the
690   minimum-maximum of the existing estimates and do not include the uncertainty of the individual estimate; these
691   uncertainties could be larger than the range proposed here.

692   For the period 2010-2019, we estimated total emissions of 112 [107-118] Tg CH_4 yr^{-1} for enteric fermentation and manure
693   management, about one third of total global anthropogenic emissions (Table 3).

694   **Rice cultivation.** Most of the world's rice is grown in flooded paddy fields (Baicich, 2013). The water management systems,
695   particularly flooding, used to cultivate rice are one of the most important factors influencing CH_4 emissions and one of the
696   most promising approaches for CH_4 emission mitigation: periodic drainage and aeration not only cause existing soil CH_4 to
697   oxidise, but also inhibit further CH_4 production in soils (Simpson et al., 1995; USEPA, 2016; Zhang, 2016). Upland rice
698   fields are not typically flooded, and therefore are not a significant source of CH_4. Other factors that influence CH_4 emissions
699   from flooded rice fields include fertilisation practices (i.e., the use of urea and organic fertilisers), soil temperature, soil type
700   (texture and aggregated size), rice variety and cultivation practices (e.g., tillage, seeding, and weeding practices) (Conrad et
701   al., 2000; Kai et al., 2011; USEPA, 2011; Yan et al., 2009). For instance, CH_4 emissions from rice paddies increase with
702   organic amendments (Cai et al., 1997) but can be mitigated by applying other types of fertilisers (mineral, composts, biogas
703   residues) or using wet seeding (Wassmann et al., 2000).

704   The geographical distribution of rice emissions has been assessed by global (e.g., Janssens-Maenhout et al., 2019; Tubiello,
705   2019; USEPA, 2012) and regional (e.g., Castelán-Ortega et al., 2014; Chen et al., 2013; Chen and Prinn, 2006; Peng et al.,

706   2016; Yan et al., 2009; Zhang and Chen, 2014) inventories and land surface models (Li et al., 2005; Pathak et al., 2005; Ren

707   et al., 2011; Spahni et al., 2011; Tian et al., 2010, 2011; Zhang, 2016). The emissions show a seasonal cycle, peaking in the

708   summer months in the extra-tropics associated with monsoons and land management. Emissions from rice paddies are

709   influenced not only by the extent of rice field area, but also by changes in the productivity of plants (Jiang et al., 2017) as

710   these alter the CH_4 emission factor used in inventories. However, the inventories considered herein are largely based on

711   IPCC Tier 1 methods, which mainly scale with cultivated areas and include regional specific emission factors but do not

712   account for changes in plant productivity and detailed cultivation practices.

713   The largest emissions from rice cultivation are found in Asia accounting for 30 to 50% of global emissions (Fig. 3). The

714   decrease of CH_4 emissions from rice cultivation over recent decades is confirmed in most inventories, because of the

715   decrease in rice cultivation area, changes in agricultural practices, and a northward shift of rice cultivation since the 1970s,

716   as in China (e.g., Chen et al., 2013).

717   Based on the global inventories considered in this study, global CH_4 emissions from rice paddies are estimated to be 32 [25-

718   37] Tg CH_4 yr^{-1} for the 2010-2019 decade (Table 3), or about 9% of total global anthropogenic emissions of CH_4. These

719   estimates are consistent with the 29 Tg CH_4 yr^{-1} estimated for the year 2000 by Carlson et al. (2017).

720   **Waste management.** This sector includes emissions from managed and non-managed landfills (solid waste disposal on

721   land), and wastewater handling, where all kinds of waste are deposited. CH_4 production from waste depends on the pH,

722   moisture, and temperature of the material. The optimum pH for CH_4 emission is between 6.8 and 7.4 (Thorneloe et al.,

723   2000). The development of carboxylic acids leads to low pH, which limits methane emissions. Food or organic waste, such

724   as leaves and grass clippings, ferment quite easily, while wood and wood products generally ferment slowly, and cellulose

725   and lignin even more slowly (USEPA, 2010a).

726   Waste management was responsible for about 11% of total global direct anthropogenic CH_4 emissions in 2000 (Kirschke et

727   al., 2013). A recent assessment of CH_4 emissions in the USA found landfills to account for almost 26% of total USA

728   anthropogenic CH_4 emissions in 2014, the largest contribution of any single CH_4 source in the United States of America

729   (USEPA, 2016). In Europe, gas control has been mandatory on all landfills since 2009, and more importantly for CH_4

730   emissions, the EU Landfill Directive (1999) with subsequent amendments, has diverted most biodegradable waste away

731   from landfills towards source separation, recycling, composting and energy recovery, and with a legally binding target not

732   to landfill more than 10% of municipal solid waste by 2035.

733   Wastewater from domestic and industrial sources is treated in municipal sewage treatment facilities and private effluent

734   treatment plants. The principal factor in determining the CH_4 generation potential of wastewater is the amount of degradable

735   organic material in the wastewater. Wastewater with high organic content is treated anaerobically, which leads to increased

736   emissions (André et al., 2014). Excessive and rapid urban development worldwide, especially in Asia and Africa, could

737   enhance methane emissions from waste unless adequate mitigation policies are designed and implemented rapidly.

738 The GAINS model and CEDS and EDGAR inventories give robust emission estimates from solid waste in the range of 37-

739 42 Tg CH_4 yr^{-1} for the year 2019, and more uncertain wastewater emissions in the range 20-45 Tg CH_4 yr^{-1}[1].

740 In our study, the global emission of CH_4 from waste management is estimated in the range of 56-80 Tg CH_4 yr^{-1} for the

741 2010-2019 period with a mean value of 69 Tg CH_4 yr^{-1}, about 19% of total global anthropogenic emissions (Table 3).

3.1.5 Biomass and biofuel burning

743 This category includes CH_4 emissions from biomass burning in forests, savannahs, grasslands, peats, agricultural residues,

744 as well as, from the burning of biofuels in the residential sector (stoves, boilers, fireplaces). Biomass and biofuel burning

745 emit CH_4 under incomplete combustion conditions (i.e., when oxygen availability is insufficient for complete combustion),

746 for example in charcoal manufacturing and smouldering fires. The amount of CH_4 emitted during the burning of biomass

747 depends primarily on the amount of biomass, burning conditions, fuel moisture and the specific material burned.

748 In this study, we use large-scale biomass burning (forest, savannah, grassland, and peat fires) from five biomass burning

749 inventories (described below) and the biofuel burning contribution from anthropogenic emission inventories (EDGARv6

750 and v7, CEDS, GAINS and USEPA). The spatial distribution of emissions from the burning of biomass and biofuel over

751 the 2010-2019 decade is presented in Fig. 3 based on data listed in Table 1.

752 At the global scale, during the period of 2010-2019, biomass and biofuel burning generated CH_4 emissions of 28 [21-39] Tg

753 CH_4 yr^{-1} (Table 3), of which 30-50% is from biofuel burning.

754

755 **Biomass burning.** Fire is an important disturbance event in terrestrial ecosystems globally (van der Werf et al., 2010), and

756 can be of either natural (typically ~10% of fires, ignited by lightning strikes or started accidentally) or anthropogenic origin

757 (~90%, human initiated fires) (USEPA, 2010b, chapter 9.1). As previously noted all fires are accounted as anthropogenic in

758 Table 3. Anthropogenic fires are concentrated in the tropics and subtropics, where forests, savannahs and grasslands may

759 be burned to clear land for agricultural purposes or to maintain pastures and rangelands. Small fires associated with

760 agricultural activity, such as field burning and agricultural waste burning, are often not detected by moderate resolution

761 remote sensing methods and are instead estimated based on cultivated area or through in-situ measurements such as

762 dedicated airborne campaigns (e.g., Barker et al., 2023).

763 Emission rates of biomass burning vary with biomass loading (depending on the biomes) at the location of the fire, the

764 efficiency of the fire (depending on the vegetation type), the fire type (smouldering or flaming) and emission factor (mass

765 of the considered species / mass of biomass burned). Depending on the approach, these parameters can be derived using

766 satellite data and/or biogeochemical model, or through simpler IPCC default approaches.

767 In this study, we use five products to estimate biomass burning emissions. The Global Fire Emission Database (GFED) is

768 the most widely used global biomass burning emission dataset and provides estimates from 1997 onwards. Here, we use

769 GFEDv4.1s (van der Werf et al., 2017), based on the Carnegie-Ames-Stanford-Approach (CASA) biogeochemical model

770 (van der Werf et al., 2010) driven by satellite derived vegetation characteristics and burned area mostly from the MODerate

771 resolution Imaging Sensor, MODIS (Giglio et al., 2013). GFEDv4.1s (with small fires) is available at a 0.25° resolution and

772 on a daily basis from 1997 to 2020. One characteristic of the GFEDv4.1s burned area is that small fires are better accounted

773 for compared to GFEDv4.1 (Randerson et al., 2012), increasing carbon emissions by approximately 35% at the global scale.

774 The latest version GFEDv5 (Chen et al., 2023) suggest 61% higher burned area than GFEDv4.1s, in closer agreement with

775 burned area products from higher resolution satellite sensors. The next budget would benefit from GFEDv5 to revisit the

776 estimates of biomass burning emissions (which would likely go up) based on more specific comparison studies.

777 The Quick Fire Emissions Dataset (QFED) is calculated using the fire radiative power (FRP) approach, in which the thermal

778 energy emitted by active fires (detected by MODIS) is converted to an estimate of CH_4 flux using biome specific emissions

779 factors and a unique method of accounting for cloud cover. Further information related to this method and the derivation of

780 the biome specific emission factors can be found in Darmenov and da Silva (2015). Here we use the historical QFEDv2.5

781 product available daily on a 0.1x0.1 grid for 2000 to 2020.

782 The Fire INventory from the National Center for Atmospheric Research (FINNv2.5, Wiedinmyer et al., 2023) provides

783 daily, 1 km resolution estimates of gas and particle emissions from open burning of biomass (including wildfire, agricultural

784 fires and prescribed burning) over the globe for the period 2002-2020. FINNv2.5 uses MODIS and VIIRS satellite

785 observations for active fires, land cover and vegetation density.

786 We use v1.3 of the Global Fire Assimilation System (GFAS, Kaiser et al., 2012), which calculates emissions of biomass

787 burning by assimilating Fire Radiative Power (FRP) observations from MODIS at a daily frequency and 0.5° resolution and

788 is available for 2000-2020.

789 The FAO-CH_4 yearly biomass burning emissions are based on the most recent MODIS 6 burned area products (Prosperi et

790 al., 2020), coupled with a pixel level (500 m) implementation of the IPCC Tier 1 approach, and are available from 1990 to

791 2020 (Table 1).

792 The differences in emission estimates for biomass burning arise from specific geographical and meteorological conditions

793 and fuel composition, which strongly impact combustion completeness and emission factors. The latter vary greatly

794 according to fire type, ranging from 2.2 g CH_4 kg^{-1} dry matter burned for savannah and grassland fires up to 21 g CH_4 kg^{-1}

795 dry matter burned for peat fires (van der Werf et al., 2010). Biomass burning emissions encountered large inter   annual

796 variability related to meteorological conditions, with generally higher emissions during El-Nino periods as in 2019 (20 [14-

797 28] Tg CH_4 yr^{-1}), 2015 (22 [15-28] Tg CH_4 yr^{-1}) and 2010 to a lesser extent (18 [15-29] Tg CH_4 yr^{-1}).

798 In this study, based on the five aforementioned products, biomass burning emissions are estimated at 17 Tg CH_4 yr^{-1} [12-

799 24] for 2010-2019, representing about 5% of total global anthropogenic CH_4 emissions (Table 3).

800

801 **Biofuel burning.** Burning of biomass to produce energy for domestic, industrial, commercial, or transportation purposes is

802 hereafter called biofuel burning. A largely dominant fraction of CH_4 emissions from biofuel burning comes from domestic

803 cooking or heating in stoves, boilers, and fireplaces, mostly in open cooking fires where wood, charcoal, agricultural
804 residues, or animal dung are burned. It is estimated that more than two billion people, mostly in developing countries, use
805 solid biofuels to cook and heat their homes daily (André et al., 2014), and yet CH_4 emissions from biofuel combustion have
806 received relatively little attention. Biofuel burning estimates are gathered from the CEDS, USEPA, GAINS and EDGAR
807 inventories. Due to the sectoral breakdown of the EDGAR and CEDS inventories the biofuel component of the budget has
808 been estimated as equivalent to the "RCO - Energy for buildings" sector as defined in Worden et al. (2017) and Hoesly et
809 al. (2018) (Table S2). This is equivalent to the sum of the IPCC 1A4a_Commercial-institutional, 1A4b_Residential,
810 1A4c_Agriculture-forestry-fishing and 1A5_Other-unspecified reporting categories. This definition is consistent with that
811 used in Saunois et al. (2016) and Kirschke et al. (2013). While this sector incorporates biofuel use, it also includes the use
812 of other combustible materials (e.g., coal or gas) for small-scale heat and electricity generation within residential and
813 commercial premises. Data provided by the GAINS inventory suggests that this approach may overestimate biofuels
814 emissions by between 5 and 50%. Further study into this category would be needed to better disentangle biofuels from fossil
815 combustibles.

816 In our study, biofuel burning is estimated to contribute 11 [8-14] Tg CH_4 yr^{-1} to the global CH_4 budget, about 3% of total
817 global anthropogenic CH_4 emissions for 2010-2019 (Table3).

818 **3.1.6 Other anthropogenic sources (not explicitly included in this study)**

819 Other anthropogenic sources not included in this study are related to agriculture and land-use management. In particular,
820 increases in agricultural areas (such as global palm oil production) have led to the clearing of natural peat forests, reducing
821 natural peatland area and associated natural CH_4 emissions. Peatlands planted to forests (like in Northern Europe) also lead
822 to reduced CH_4 emissions. While studies have long suggested that CH_4 emissions from peatland drainage ditches are likely
823 to be significant (e.g., Minkkinen and Laine, 2006, Peacock et al., 2021), CH_4 emissions related to palm oil plantations have
824 yet to be properly quantified (e.g., Manning et al, 2019). Taylor et al. (2014) have quantified global palm oil wastewater
825 treatment fluxes to be 4 ± 32 Tg CH_4 yr^{-1} for 2010-2013. This currently represents a small and highly uncertain source of
826 methane but one potentially growing in the future.

827 **3.2 Natural and indirect anthropogenic sources**

828 As introduced in section 2.4, natural and indirect anthropogenic sources refer to pre-agricultural CH_4 emissions even if they
829 are perturbed by anthropogenic climate change or other global change factors (e.g., eutrophication), and indirect emissions
830 resulting from anthropogenic perturbation of the landscape (reservoirs) and the biogeochemical characteristics of soil. They
831 include vegetated wetland emissions and inland freshwater systems (lakes, small ponds, reservoirs, and rivers), land
832 geological sources (gas-oil seeps, mud volcanoes, microseepage, geothermal manifestations, and volcanoes), wild animals,
833 wildfires, termites, thawing terrestrial and marine permafrost, and coastal and oceanic sources (biogenic, geological and

hydrate). In water-saturated or flooded ecosystems, the decomposition of organic matter gradually depletes most of the oxygen in the soil or the sediment zone, resulting in anaerobic conditions and CH_4 production. Once produced, CH_4 can reach the atmosphere through a combination of three processes: (1) diffusive loss of dissolved CH_4 across the air-water boundary; (2) ebullition flux from sediments; and (3) flux mediated by emergent aquatic macrophytes and terrestrial plants (plant transport). On its way to the atmosphere, in the soil or water columns, CH_4 can be partly or completely oxidised by microorganisms, which use CH_4 as a source of energy and carbon (USEPA, 2010b). Concurrently, methane from the atmosphere can diffuse into the soil column and be oxidised (See Sect. 3.3.4 on soil uptake).

3.2.1 Wetlands

Wetlands are generally defined as ecosystems in which mineral or peat soils are water-saturated at some depth or where surface inundation (permanent or not) has a dominating influence on the soil biogeochemistry and determines the ecosystem species composition (USEPA, 2010b). To refine such an overly broad definition for CH_4 emissions, we define wetlands as ecosystems with inundated or saturated soils or peats where anaerobic conditions below the water table lead to CH_4 production (Matthews and Fung, 1987; USEPA, 2010b). Brackish water emissions are discussed separately in Sect. 3.2.6. Our definition of wetlands includes ombrotrophic and minerotrophic peatlands (i.e., bogs and fens), mineral soil wetlands (swamps and marshes), and seasonal or permanent floodplains. It excludes exposed water surfaces without emergent macrophytes, such as lakes, rivers, estuaries, ponds, and reservoirs (addressed in the next section), as well as rice agriculture (see Sect. 3.1.4, rice cultivation paragraph), and wastewater ponds. It also excludes coastal vegetated ecosystems (mangroves, seagrasses, salt marshes) with salinities usually >0.5 (See Sect. 3.2.6). Even with this definition, some wetlands could be considered as anthropogenic systems, being affected by human land-use changes such as impoundments, drainage, or restoration (Woodward et al., 2012). In the following, we retain the generic denomination "wetlands" for natural and human-influenced wetlands, as discussed in Sect. 2.2.

The three most important factors influencing CH_4 production in wetlands are the spatial and temporal extent of anoxia (linked to water saturation), temperature, and substrate availability (Valentine et al., 1994; Wania et al., 2010; Whalen, 2005; Delwiche et al., 2021; Knox et al., 2021).

Land surface models estimate CH_4 emissions through a series of processes, including CH_4 production, oxidation, and transport. The models are then forced with inputs accounting for changing environmental factors (Melton et al., 2013; Poulter et al., 2017; Tian et al., 2010; Wania et al., 2013; Xu et al., 2010). CH_4 emissions from wetlands are computed as the product of an emission flux density and a CH_4 producing area or surface extent (see Supplementary Material; Bohn et al., 2015; Melton et al., 2013). The areal extent of different wetland types (having large differences in areal CH_4 emission rates) appears to be a primary contributor to uncertainties in the absolute flux of CH_4 emissions from wetlands, with meteorological response being the main source of uncertainty for seasonal and interannual variability (Poulter et al., 2017; Kuhn et al., 2021; Parker et al., 2022; McNicol et al., 2023; Karlson and Bastviken 2023). However, large uncertainty

remains in both spatial and temporal emission distributions, especially over tropical wetlands where data are lacking to evaluate the models but are nevertheless a key region for climate feedbacks (Nisbet, 2023; Zhang et al., 2023). Direct measurement campaigns and remote sensing are providing key insights where to improve the land surface models (e.g., France et al., 2022; Shaw et al., 2022).

In this work, sixteen land surface models computing net CH_4 emissions (Table 2) were run under a common protocol with a spin-up using repeated climate data from 1901-1920 to pre-industrial conditions followed by a transient simulation through the end of 2020. Of the 16 models, 13 previously contributed to Saunois et al. (2020), and three models were new to this release (CH4MOD$_{wetland}$ (Li et al., 2010), ISAM (Shu et al., 2020; Xu et al., 2021), and SDGVM (Beerling and Woodward, 2001; Hopcroft et al., 2011; Hopcroft et al., 2020)) (Table 2, see also in the Supplementary Material Table S3 for a history of the contributing models). Climatic forcing uncertainties are considered in the ensemble estimate by using two climate datasets, CRU/CRU-JRA55 (Harris, 2014) and GSWP3-W5E5 (Dirmeyer et al., 2006; Kim 2017; Lange, 2019; Cucchi et al., 2020). Atmospheric CO_2 was also prescribed in the models. For all models, two wetland area dynamic schemes were applied: a diagnostic scheme using a remote sensing-based wetland area and dynamics dataset called WAD2M (Wetland Area Dynamics for Methane Modeling; Zhang et al., 2021a; 2021b) available at 0.25 degree of horizontal resolution, as in Saunois et al. (2020), and a prognostic scheme using internal model-specific hydrologic models.

The diagnostic wetland extent product WAD2Mv1.0 (Zhang et al., 2021a) has been updated since Saunois et al. (2020) to WAD2Mv2.0 (Zhang et al., 2021b) and extended to 2020. It uses the same Surface Water Microwave Product Series (SWAMPSv3.2) for capturing inundation dynamics (Jenson and McDonald, 2019), which was extended to 2020. To reduce potential double-counting with the freshwater budget, the surface areas of rivers/streams and lakes/ponds are excluded by using the products Global River Widths from Landsat (GRWL) database v01.01 (Allen and Pavelsky, 2018) and HydroLakes v1.0 (Messenger et al., 2016), instead of the Global Surface Water (GSW) product (Pekel et al., 2016) used in WAD2Mv1.0. The GRWL and Hydrolakes are also the datasets used separately in the upscaling of the freshwater budget allowing for a more consistent approach between the wetland and freshwater CH_4 budgets (Sect. 3.2.2). This update in WAD2M leads to a downward revised annual average wetland extent by 0.5 Mkm^2 for the mid-high latitudes (mainly due to larger lake extent in HydroLakes than in the GSW dataset) with small impacts in other regions. However, since HydroLakes includes only vectorized lakes larger than 0.1 km², smaller lakes/ponds under 0.1 km² are implicitly still included as wetlands in WAD2Mv2.0. For the high-latitude region, the recent peatland extent product from Hugelius et al. (2020) is applied, which indicates a slightly higher peatland area by 0.2 Mkm^2 primarily in regions above 60°N, compared to the Northern Circumpolar Soil Carbon Database (NCSCD) product (Hugelius et al., 2013) used in WAD2Mv1.0. Rice agriculture was removed using the Monthly Irrigated and Rainfed Crop Areas (MIRCA2000, Portmann et al. (2010)) dataset from circa 2000, as a fixed distribution.

The combined remote-sensing and inventory WAD2Mv2.0 product leads to a maximum wetland area of 13.6 Mkm^2 during the peak season (7.9 Mkm^2 on annual average, with a range of 7.5 to 8.4 Mkm^2 from 2000-2020, about 5.2% of the global

899 land surface). The largest wetland areas in WAD2Mv2.0 are in Amazonia, the Congo Basin, and the Western Siberian

900 Lowlands, which in previous studies were underestimated by inventories (Bohn et al., 2015). However, the SWAMPS v3.2

901 dataset which serves as a proxy of temporal variations of wetland extent, has discontinuity issues over a few tropical hotspots

902 since 2015 and hence affects the temporal variations of WAD2M. Consequently, this affects CH_4 emissions estimates for a

903 subset of land surface models that are particularly sensitive to inundation in these hotspots. Meanwhile, prognostic estimates

904 show moderate consistency in capturing the spatial distribution of wetland area with WAD2M, with an annual average

905 wetland area of 8.0±2.0 Mkm^2 during the peak season for 2000-2020. The ensemble mean of annual wetland area anomaly

906 by the prognostic models show reasonable agreement with satellite-based estimates in capturing the response of wetland

907 area to climate variations (Zhang et al., in review), with higher agreement over temperate and boreal regions than in the

908 tropics.

909 For the wetland methane emissions estimate, we use the decadal mean from the prognostic runs and adjust these flux

910 estimates for double counting from inland waters (described in next section) given the reliance of the prognostic models on

911 satellite flooded area data like WAD2Mv2 to parameterize maximum wetland extent (Zhang et al., in review). The average

912 emission from wetlands for 2010-2019 for the 16 models is plotted in Fig. 3. The zones with the largest emissions are the

913 Amazon basin, equatorial Africa and Asia, Canada, western Siberia, eastern India, and Bangladesh. Regions where CH_4

914 emissions have high inter-model agreement (defined as regions where mean flux is larger than the standard deviation of the

915 models, on a decadal mean) represent 72% of the total CH_4 flux due to natural wetlands. The different sensitivities of the

916 models to temperature, vapour pressure, precipitation, and radiation can generate substantially different patterns, such as in

917 India. Emission estimates over regions with lower emissions (in total) are also consistently inferred between models (e.g.,

918 Scandinavia, Continental Europe, Eastern Siberia, Central United States of America, and Southern Africa).

919 The resulting global flux range for vegetated wetland emissions from the prognostic runs is 117-195 Tg CH_4 yr^{-1} for the

920 2000-2020 period, with an average of 157 Tg CH_4 yr^{-1} and a one-sigma standard deviation of 24 Tg CH_4 yr^{-1}. Using the

921 prognostic set of simulations, the average ensemble emissions were 159 [119-203] Tg CH_4 yr^{-1} for the 2010-2019 period

922 (Table 3). The estimated average ensemble annual total from the two sets of simulations by CRU/CRU-JRA55 and GSWP3-

923 W5E5 are 158 [126-193] and 158 [118-203] for 2010-2019, respectively. Generally, the magnitude and interannual

924 variability agree between these two sets of simulations (Zhang et al., 2024). Wetland emissions represent about 25% of the

925 total (natural plus anthropogenic) CH_4 sources estimated by bottom-up approaches. The large range in the estimates of

926 wetland CH_4 emissions results from difficulties in defining wetland CH_4 producing areas as well as in parameterizing

927 terrestrial anaerobic conditions that drive sources and the oxidative conditions leading to sinks (Melton et al., 2013; Poulter

928 et al., 2017; Wania et al., 2013). The ensemble mean emission using the same simulation setup (i.e., diagnostic wetland

929 extent and CRU/CRU-JRA55) in the models is 163 [117-195] Tg CH_4 yr^{-1}, higher by ~22 Tg CH_4 yr^{-1} than the one previously

930 reported (see Table 3, for 2000-2009 with comparison to Saunois et al., 2020). This difference is mainly due to the updated

931 model structure and parameterizations in the wetland CH_4 models compared to the versions in the previous budget and the
932 inclusion of three new land surface models.

933 For the last decade 2010-2019, we report in this budget an average ensemble estimate of 159 Tg CH_4 yr^{-1} with a range of
934 119-203 (based on prognostic wetland extent runs, Table 3)   .

3.2.2 Inland freshwater ecosystems (lakes, ponds, reservoirs, streams, rivers)

936 This category includes CH_4 emissions from freshwater systems (lakes, ponds, reservoirs, streams, and rivers). Numerous
937 advances have been made in the freshwater greenhouse gases knowledge base in the last few years (Lauerwald et al., 2023a).
938 These advances include improvements in the underlying databases used to estimate inland water surface areas and model
939 their dynamics, a rapidly growing number of direct measurements of methane fluxes, and improvements in our process-
940 based understanding of methane biogeochemistry. Despite this, aspects of global freshwater methane estimates remain rather
941 crude and continue to have large uncertainties. This includes the overall temperature dependency of methane emissions, the
942 relative role of ebullition (i.e., bubble flux, which may represent the most important, but most difficult-to-capture emission
943 path in many standing water bodies), fluxes from the smallest standing water bodies (sometimes referred to as ponds) having
944 large emissions per m^2 but uncertain area extent, and the magnitude of anthropogenic influence on emissions, all which are
945 discussed below.

946

947 **Streams and rivers.** The last global CH_4 budget used an estimate of 27 Tg CH_4 yr^{-1} for global streams and rivers based
948 largely on a data compilation by Stanley et al. (2016). This estimate was scaled from a simple data compilation without a
949 spatial component or an estimate of ebullition. More recently, Rosentreter et al. (2021) performed a new data compilation
950 of 652 flux estimates, including diffusive and ebullitive fluxes, coupled to an ice corrected surface area estimate of ~625,000
951 km^2 that was aggregated to 5 latitudinal bands to come up with a global estimate of 6 and 31± 17 Tg CH_4 yr^{-1} (respectively
952 for the median and mean ± c.i. 95%). We believe, due to better data representation in underlying datasets, that the mean
953 estimate of Rosentreter et al. (2021) is more representative statistically because the median does not capture hotspots and
954 hot moments of intense ebullitive fluxes. Finally, Rocher-Ros et al. (2023) used a new Global River Methane (GRiMeDB)
955 database (Stanley et al., 2023) with > 24,000 observations of CH_4 concentrations to predict ~28±17 Tg CH_4 yr^{-1} (±c.i. 95%)
956 river emissions globally. This approach used machine learning methods coupled to the latest spatially and temporally explicit
957 mapping of monthly stream surface area (the smallest streams are still extrapolated) which incorporates drying and freezing
958 effects (yearly average 672,000 km^2, Liu et al., 2022) and includes an ebullitive flux estimated from a correlation between
959 measured diffusive and ebullitive emissions in the GRiMeDB database (Stanley et al., 2023). Thus, for this study we use an
960 estimate of 29±17 (±c.i. 95%) Tg CH_4 yr^{-1} for streams and rivers (Figure 4), which averages the mean estimate of Rosentreter
961 et al. (2021) and Rocher-Ros et al. (2023). Currently, ebullitive fluxes remain a major unknown quantity in streams and
962 rivers but appear to be coarsely linearly correlated in a log-space to diffusive fluxes and of similar magnitude (Rocher-Ros

et al., 2023). Methodologically, the high-water velocity of many streams and rivers make measurement of ebullitive fluxes challenging (Robison et al., 2021). Effluxes are also linked to hydrology (Aho et al., 2021) although very few studies have sampled over a representative hydrograph. Plant-mediated effluxes of CH_4 in running waters also remain difficult to constrain, with a recent compilation highlighting very few measurements (Bodmer et al. 2024). Connected adjacent wetlands is a common source of CH_4 to streams and rivers (Borges et al., 2019) which may be important for the regulation of running water emissions but is currently difficult to assess at the global scale. Overall, the poor representation of sites and deficient mechanistic understanding make it difficult to model and predict methane evasion from streams and rivers using process-based models.

Lakes and ponds. The previous global CH_4 budget used an estimate of 71 Tg CH_4 yr^{-1} for lakes and 18 Tg CH_4 yr^{-1} for reservoirs. These estimates were based on an early study by Bastviken et al. (2011) coupled with a newer estimate for lakes north of 50°N (Wik et al., 2016b). There have been three new lake studies that have published their data with global estimates of 56 and 151± 73 (Rosentreter et al. , 2021; respectively for the median and mean ± c.i. 95% , 22±8 (Zhuang et al., 2023; ±lake-area-weighted normalised RMSE for all parameterized lake types), process-based model), and 41±36 Tg CH_4 yr^{-1} (Johnson et al., 2022, mean ±c.i. 95%). This large range in estimated emissions can be attributed to the differences in the datasets and methods used to calculate the surface area of small waterbodies, as well as the differences between how the flux data were analyzed and extrapolated between studies. For instance, total surface areas of all lakes and ponds of 3712-5688 × 10^3 km^2 (Rosentreter et al., 2021) and 2806 × 10^3 km^2 (Johnson et al., 2022) were used along with measurement data from 198 and 575 individual lake systems, respectively. In contrast, Zhuang et al. (2023) generated estimates using higher temporal resolution data from just 54 lakes to build a process-based model, which generated much lower flux estimates from tropical lakes than previously implemented statistical approaches, but in line with the most recent assessments by Borges et al. (2022). For this study, we explicitly excluded lakes <0.1 km^2 which are treated separately (see below). If we re-assess these three studies for only lakes greater than 0.1 km^2, we obtain global effluxes of 17 and 42.9±20.8 Tg CH_4 yr^{-1} (Rosentreter et al. (2021); median and mean ± c.i. 95% of global flux), 21.9±8.0. (Zhuang et al., 2023, ±lake-area-weighted normalised RMSE for all parameterized lake types), and 35.3±31.0 Tg CH_4 yr^{-1} (Johnson et al. 2022, ±95% C.I.) (with areas of 2556-3468 x10^3, 2640x10^3, and 2676x10^3 km^2 respectively). Thus, for lakes >0.1 km^2, we propose an efflux of 33±26 Tg CH_4 yr^{-1} (an average of the mean from Rosentreter et al., 2021 Zhuang et al., 2023, and Johnson et al., 2022, with the average c.i. 95% from Rosentreter et al., 2021 and Johnson et al. 2022) as represented in Figure 4.

Small waterbody emissions, hereafter small lakes and ponds<0.1 km^2, remain difficult to assess. Evidence is emerging that there is a lower limit to the power scaling laws that early studies used to extrapolate the surface area of these small systems (Bastviken et al., 2023; Kyzivat et al., 2022). Thus, for small lakes and ponds < 0.1 km^2 (and >0.001 km^2), we disregard the higher end surface area used in Rosentreter et al., 2021 which relied on these earlier estimates and scale their numbers to the evasion estimates to the lower end surface area of 1,002x10^3 to obtain a mean flux of 33 Tg CH_4 yr^{-1} (Rosentreter et al.,

2021). Johnson et al. (2022) estimated a surface area of only 166x103 km^2 for this size class to obtain an efflux of 6.3

Tg CH$_4$ yr^{-1}, which we acknowledge as a lower limit. Averaging these two values provide a conservative estimate of 20

[6-33] Tg CH$_4$ yr^{-1}, which is close to the number proposed by Holgerson and Raymond (2016) for diffusion effluxes only

for this size class. The experts involved in this assessment have low confidence in this estimate. This estimate also does not

include artificial ponds, which we discuss below. As a result, combined CH$_4$ emissions from large lakes (>0.1 km^2) and

small lakes and ponds (<0.1km^2) are estimated at 53 [19-86] Tg CH$_4$ yr^{-1} (Figure 4), which is lower than the 71 Tg estimated

in the previous budget.

Reservoirs. New mean estimates of diffusive + ebullitive CH$_4$ emissions from reservoirs include 15 and 24±8 (the median

and mean± c.i. 95% from Rosentreter et al., 2021), 10±4 (Johnson et al., 2021, mean±95% C.I.), 10 (Harrison et al., 2021,

low and high c.i. 95% 7 and 22, respectively), and 2.1 Tg CH$_4$ yr^{-1} (Zhuang et al., 2023). We compile the first three estimates

to a direct efflux of ~14 Tg CH$_4$ yr^{-1} (with ± c.i. 95% of 9 and 23). We note the fourth estimate as a lower bound, but exclude

it from this budget given that it was generated via a model that only included data from six reservoir systems (Zhuang et al.,

2023). We also add in an additional 12 Tg CH$_4$ yr^{-1} (c.i. 95% 7 and 37) that is estimated to degas in dam turbines (Harrison

et al., 2021), which was not addressed in the studies by Rosentreter et al. (2021), Zhuang et al. (2023), or Johnson et al.

(2021). Rocher-Ros et al. (2023) also excluded river observations below dams when executing their statistical model, and

so did not capture downstream dam emissions. Thus, we use a direct reservoir emission here of ~13 [6-28] Tg CH$_4$ yr^{-1} and

estimate an additional ~12 [7-37] Tg CH$_4$ yr^{-1} from dam turbine degassing fluxes, giving a total of 25 [13-65] Tg CH$_4$ yr^{-1}

from reservoirs (Figure 4).

Uncertainties and confidence levels. The emission estimates of lakes, reservoirs and ponds described above are limited by

several uncertainties. First, a major unknown for lakes remains the size cut off and the representation of small lakes and

ponds (Deemer and Holgerson, 2021), which are also more variable than larger water bodies in their CH$_4$ concentrations

and fluxes (Rosentreter et al. 2021, Ray et al., 2023). Interestingly, there is also a lack of methane data representation from

large lakes that are a large component of global lake surface area (Deemer and Holgerson, 2021; Messager et al., 2016).

There is also a growing knowledge base on the importance of high CH$_4$ fluxes from lake littoral zones that is not yet well

incorporated into global scaling efforts (e.g., Grinham et al., 2011; Natchimuthu et al., 2016), and emergent vegetation

(Bastviken et al., 2023; Kyzivat et al., 2022). Ebullition is more constrained in lakes/reservoirs compared to streams/rivers

but is still difficult to measure and model accurately. Finally, for all inland water systems a greater scrutiny for the limiting

factors (including the impact of ice-cover and seasonality, stratification of the water column) of different CH$_4$ production,

consumption and transport pathways is needed. In addition, a better understanding of the climatic, environmental and

geomorphological controls on key CH$_4$ processes (e.g., sedimentary diffusive and ebullitive production, bubble dissolution,

CH$_4$ oxidation) on the large-scale remains critically needed. For instance, the consistently lower global emissions determined

1029 by the process-based model of Zhuang et al. (2023) compared to observations, suggest that current datasets are too limited

1030 to fully capture the spatio-temporal variability in CH_4 dynamics and their key control factors, possibly leading to biased-

1031 high estimates.

1032 The majority of the inland water CH_4 estimates are from a limited number of studies, some without spatial representation or

1033 reported statistical uncertainties. Furthermore, as mentioned above the knowledge base of the surface area of these

1034 ecosystems is new and rapidly expanding, but not standardised between studies leading to uncertainty (but see Lauerwald

1035 et al. 2023b), particularly for ponds. For this study, we are able to provide confidence intervals from the original studies for

1036 all fluxes except the smallest lake/pond size class.

1037

1038 **The Surface Area of Inland Freshwaters.** For all of these ecosystems, determining their surface area remains a central

1039 challenge. Since the last GMB, several methodological advances have reduced the uncertainty associated with the surface

1040 area estimates of rivers, streams, lakes, and reservoirs. Using a single geospatial dataset that includes both lakes and

1041 reservoirs (Messager et al., 2016) has decreased double counting of lakes and reservoirs (Johnson et al., 2022; Rosentreter

1042 et al., 2021). For rivers and streams, high-resolution global streamflow simulations, informed by satellite observations,

1043 enabled a much finer scale estimate of surface areas for rivers with a new temporal component (Allen and Pavelsky, 2018;

1044 Lin et al., 2019; Liu et al., 2022), although the surface for the smaller streams are still estimated indirectly, and mapping of

1045 human-created drainage ditches and canals is lacking. Seasonal ice cover and melt turnover corrections also have been newly

1046 incorporated into rivers, streams, lakes, and reservoirs (Harrison et al., 2021; Johnson et al., 2022; Lauerwald et al., 2023b;

1047 Rocher-Ros et al., 2023; Rosentreter et al., 2021; Zhuang et al., 2023). Finally, removing open water body surface areas

1048 from wetland surface areas based on geographic location has reduced double counting between these two land cover types,

1049 as described in the wetlands section of the GMB. Yet, the surface area of small lakes and ponds (<0.1 km2) is still highly

1050 uncertain, and new techniques for counting these systems and determining the overlap with wetland data bases is paramount.

1051

1052 **Anthropogenic Contributions to Inland Freshwater Emissions.** We argue that all reservoirs should be categorised as a

1053 direct anthropogenic source of emissions. Most of the surface area of reservoirs are human-made and reservoir construction

1054 leads to anoxic sediments and/or bottom waters with labile organic matter sourced from the watershed and to in-situ nutrient

1055 augmented phytoplankton production (Deemer et al., 2016; Maavara et al., 2017; Prairie et al., 2018). It is also clear that the

1056 cultural eutrophication of natural lakes driven by run-off of agricultural nitrogen fertilizer and manure is augmenting

1057 CH_4 emissions (DelSontro et al., 2018; Li et al., 2021), with shallow lakes particularly likely to experience eutrophication

1058 (Qin et al., 2020). For instance, Beaulieu et al. (2019) modelled a 15% reduction in lake CH_4 with a 25% reduction in lake

1059 phosphorus concentrations. Several recent studies have estimated that anywhere between 30 and 50% of lakes are eutrophic

1060 (Cael et al., 2022; Qin et al., 2020; Sayers et al., 2015; Wu et al., 2022). These studies estimate numerical percentages (one

1061 by depth class: Qin et al., 2020), but none have estimated the percent of lake surface area that is eutrophic nor have any

determined the extent of anthropogenic vs. natural eutrophication. Still, numerous studies have noted widespread increases in eutrophication indicators across lakes due to nutrient loading and warming (Griffiths et al., 2022; Ho et al., 2019; Taranu et al., 2015), thus we estimate that ⅓, or 11 Tg CH_4 yr^{-1} of CH_4 emissions from lakes >0.1 km^2 could be anthropogenic (Figure 4). Similarly, CH_4 emissions from small lakes and ponds are influenced by human factors, with emissions increasing with eutrophication (Deemer and Holgerson, 2021), erosion and runoff in agricultural landscapes (Heathcote et al., 2013), and warming, the latter likely to have a disproportionately greater effect in small, shallow systems (Woolway et al., 2016). Thus, we adopt the same ⅓ number as for lakes for the proportion of anthropogenic emissions in small lakes and ponds (<0.1 km2), which amounts to 6 Tg CH_4 yr^{-1} (Figure 4).

There are also human-made small lakes and ponds, notably for agriculture, aquaculture, and recreation, that generally have conditions favourable for high CH_4 emissions (Downing, 2010; Holgerson and Raymond, 2016; Malerba et al., 2022; Ollivier et al., 2019; Zhao et al., 2021; Dong et al., 2023). Downing (2010) estimated that farm ponds comprise a global surface area of ~77,000 km^2; using a conservative emission rate of 265 mg CH_4 m^{-2} d^{-1} and an ice correction factor of 0.6 leads to an emission of 4.5 Tg yr^{-1} that is anthropogenically sourced from farm ponds. Here the value is rounded to 5 Tg yr^{-1} (Figure 4). Clearly, more work is required to assess the anthropogenic component of CH_4 emissions from lakes and ponds. It remains difficult to parse out an anthropogenic component to stream and river CH_4 fluxes. Although some studies have noticed a temperature dependence with stream sediments (Comer-Warner et al., 2018; Zhu et al., 2020), Rocher-Ros et al. (2023) noted a small temperature dependence of CH_4 emissions in streams and rivers compared to other freshwater ecosystems, potentially due to the many other external processes affecting fluxes in these dynamic flowing ecosystems. Urbanisation can lead to elevated river CH_4 emissions, particularly in regions with elevated organic matter and nutrient loading due to limited wastewater treatment (Begum et al., 2021; Nirmal Rajkumar et al., 2008; Wang et al., 2021a). Some studies have found agricultural streams and ditches can have higher effluxes due to inputs of fine sediments (Comer-Warner et al., 2018; Crawford and Stanley, 2016), organic carbon, and nutrients (Borges et al., 2018) that lead to in-situ methane production. Furthermore, the creation of drainage ditches in organic soils tap CH_4 rich waters from water-logged horizons and heighten emissions from ex-situ sources (Peacock et al., 2021), although limitations in both the geographic scope of existing ditch emission estimates our ability to estimate global surface area of ditches precludes their inclusion in this budget. Finally, extremely high rates of CH_4 emission have been linked to ongoing permafrost thaw in Asia's Qinghai–Tibet Plateau (Zhang et al., 2020). However, the loss and disconnection of wetlands to rivers may have resulted in a decrease in the input of dissolved CH_4 from this source. A recent expert elicitation (Rosentreter, et al. 2024) reported that 35% of all inland freshwater sources were anthropogenic and given that some of the river flux is from upstream reservoirs, we assign a 30% anthropogenic contribution to the stream and river flux (9 Tg CH_4 yr^{-1}, Figure 4), which approximates the expert elicitation via the impact of eutrophication and urban influences.

Combination (lakes, ponds, reservoirs, streams and rivers, farm ponds). Combining the aforementioned emissions from lakes >0.1 km^2 (33 [13-53] Tg CH$_4$ yr^{-1}), small lakes and ponds < 0.1 km^2 (20 [6-33] Tg CH$_4$ yr^{-1}), reservoirs (25 [13-65] Tg CH$_4$ yr^{-1}), streams and rivers (29 [12-46] Tg CH$_4$ yr^{-1}) and farm ponds (5 Tg CH$_4$ yr^{-1}), leads to a total of ~112 Tg CH$_4$ yr^{-1} from freshwater systems, with a range of [49-202] Tg CH$_4$ yr^{-1}. This estimate is about 50 Tg lower than in Saunois et al. (2020) and is broadly consistent with the recent regionalized estimate by Lauerwald et al. (2023b) compiled for the Regional Carbon Cycle Assessment and Processes (RECCAP2, https://www.globalcarbonproject.org/reccap/; 103 Tg CH$_4$ yr^{-1}, IQR= 82.1–134.8). The updated budget from these ecosystems and their anthropogenic components are represented in Fig. 4. The gridded products for emissions from lakes and ponds by Johnson et al. (2022), from reservoirs by Johnson et al. (2021) and from streams and rivers by Rocher-Ros et al. (2023) have been combined into a single map presented in Fig. 5.

Double-counting inland freshwater ecosystems in the bottom-up estimates. To address the differences found between bottom-up and top-down CH$_4$ budgets, and to acknowledge advances in addressing the central issue of double counting CH$_4$ emissions for inland freshwater ecosystems, we introduce here a new correction term. Historically, the bottom-up estimate of global CH$_4$ emissions has been higher than the top-down estimate, first recognized in Kirschke et al. (2013) and confirmed in Saunois et al. (2016, 2020). The larger bottom-up emissions estimate has been partly attributed to double-counting vegetated wetland emissions with inland freshwater emissions (including lakes, ponds, rivers, streams, and reservoirs) and also the emissions of CH$_4$ produced in vegetated wetlands and then transported via aquatic processes and emitted from inland freshwaters (Pangala et al., 2017; Kirk and Cohen, 2023). The Saunois et al. (2020) CH$_4$ budget addressed the issue of double counting through the use of a revised vegetated wetland area dataset, WAD2M v1.0 (Zhang et al., 2021), that removed inland waters from the SWAMPS (Jenson and McDonald, 2019) surface-inundation dataset, allowing for independent vegetated wetlands and inland freshwater CH$_4$ emissions to be compiled. Yet, the Saunois et al. (2020) CH$_4$ budget still had a ~150 Tg CH$_4$ yr^{-1} difference between bottom-up and top-down estimates. In this budget, we refined the vegetated wetland area dataset with WAD2M v2.0 (see section 3.2.1, where HydroLakes is used to remove lakes and ponds >0.1 km^2). Additionally, we applied numbers from peer-reviewed publications and expert elicitation to account for lateral CH$_4$ flux emissions. This most recent bottom-up budget estimates 159 [119-203] Tg CH$_4$ yr^{-1} from vegetated wetlands for 2010-2019 and 112 Tg CH$_4$ yr^{-1} from inland freshwaters that includes 83 Tg CH$_4$ yr^{-1} from lakes, ponds, and reservoirs and 29 Tg CH$_4$ yr^{-1} from rivers and streams, leading to a combined wetland and inland freshwater flux of 271 Tg CH$_4$ yr^{-1}. Here, we propose a correction of 20 Tg CH$_4$ yr^{-1} to account for double counting of small lakes and ponds (< 0.1 km^2) that are likely included in our vegetated wetlands estimate, and removing 1-3 Tg CH$_4$ yr^{-1} from river emissions due to lateral transport of CH$_4$ originating in adjacent vegetated wetlands. The river flux correction arises from assuming that for catchments with >10% wetlands, rivers provide 5-10% of vegetated CH$_4$ emissions. The total double-counting correction term of 23 Tg CH$_4$ reduces the bottom-up budget for combined wetlands and inland waters from 271 Tg CH$_4$ yr^{-1} to 248 Tg

1127 CH_4 yr^{-1} (see Fig. 4 and Table 3). Comparing the 2000-2009 decadal emissions from wetlands and inland freshwater
1128   ecosystems across the last three previous assessments of the budget shows a significant downward revision with 305
1129   (183+122) Tg CH_4 yr^{-1}, 356 (147+209) Tg CH_4 yr^{-1} and 248 (159+112-23) Tg CH_4 yr^{-1} (respectively from Saunois et al.
1130   (2016; 2020) and this work).

1131   Finally, it is worth noting that inland freshwater ecosystems can overlap with geological seepage systems in some areas,
1132   i.e., they may occur in correspondence with geological structures that emit fossil (microbial, thermogenic, or abiotic)
1133 CH_4 generated in the Earth's crust. Examples have been documented in the Fisherman Lake in Canada (Smith et al., 2005),
1134   in the Baikal lake (Schmid et al, 2007), and in rice paddies in Japan (Etiope et al., 2011). Thus, some gas emissions in
1135   freshwater environments, particularly as bubble plumes, can be incorrectly attributed to modern biological (ecosystem)
1136   activities if appropriate isotopic and molecular analyses are not performed.

3.2.3 Onshore and offshore geological sources

1138   Significant amounts of CH_4, produced within the Earth's crust, naturally migrate to the atmosphere through tectonic faults
1139   and fractured rocks. Major emissions are related to hydrocarbon formation in sedimentary basins (microbial and thermogenic
1140   methane), through continuous or episodic exhalations from onshore and shallow marine hydrocarbon seeps and through
1141   diffuse soil microseepage (Etiope, 2015). Specifically, five source categories have been considered. Four are onshore
1142   sources: gas-oil seeps, mud volcanoes, diffuse microseepage, and geothermal manifestations including volcanoes. One
1143   source is offshore: submarine seepage, which may include the same types of gas manifestations occurring on land. Etiope
1144   et al. (2019) have produced the first gridded maps of geological CH_4 emissions and their isotopic signature for these five
1145   categories, with a global total of 37.4 Tg CH_4 yr^{-1} (reproduced in Fig. 5). However, these maps are based on incomplete
1146   data on geological sites due to missing information and difficulties in defining all current geological emitting sites.
1147   Combining the best estimates for the five categories of geological sources (from grid maps or from previous statistical and
1148   process-based models), the breakdown by category reveals that onshore microseepage dominate (24 Tg CH_4 yr^{-1}), the other
1149   categories having similar smaller contributions: as mean values, 4.7 Tg CH_4 yr^{-1} for geothermal manifestations, about 7 Tg
1150 CH_4 yr^{-1} for submarine seepage and 9.6 Tg CH_4 yr^{-1} for onshore seeps and mud volcanoes. These values lead to a global
1151   bottom-up geological emission mean of 45 [27-63] Tg CH_4 yr^{-1} (Etiope and Schwietzke, 2019).
1152   While all bottom-up and some top-down estimates, following different and independent techniques from different authors,
1153   consistently suggest a global geo-CH_4 emission in the order of 40-50 Tg yr-1, the radiocarbon (^{14}C-CH_4) data in ice cores
1154   reported by Hmiel et al. (2020) appear to give a much lower estimate, with a minimum of about 1.6 Tg CH_4 yr^{-1} and a
1155   maximum value of 5.4 Tg CH_4 yr^{-1} (95 percent confidence) for the pre-industrial period. Dyonisius et al. (2020) also suggest
1156   a low range of geological emissions over the last deglaciation period and for the late Holocene (0-10 Tg CH_4 yr^{-1}). The
1157   discrepancy between Hmiel et al. (2020) and all other estimates has been discussed in Thornton et al. (2021), which
1158   demonstrated that the global near-zero geologic CH_4 emission estimate in Hmiel et al. (2020) is incompatible with the sum

of multiple independent bottom-up estimates, based on a wide variety of methodologies, from individual natural geological seepage areas: for example, from the Black Sea (up to 1 Tg CH_4 yr^{-1}), the Eastern Siberian Arctic Shelf (ESAS, up to 4.6 Tg CH_4 yr^{-1}, referring mostly to thermogenic gas), onshore Alaska (up to 1.4 Tg CH_4 yr^{-1}) and a single seepage site in Indonesia (releasing 0.1 Tg CH_4 yr^{-1} as estimated by satellite measurement) (see Thornton et al. (2021) and references therein). Jackson et al. (2020) expressed doubt about the low Hmiel et al. (2020) estimates, noting that they are difficult to reconcile with the results of many other researchers and with bottom-up approaches in general. This discrepancy highlights another main unresolved uncertainty in the methane budget and calls for further investigations to reconcile the different estimates and reduce the uncertainty on geological emissions. Waiting for further investigation to better understand discrepancies between radiocarbon approaches and other studies, we decided to keep the estimates from Etiope and Schwietzke (2019) for the mean values, and associate it to the lowest estimates reported in Etiope et al. (2019), as in Saunois et al. (2020). Thus, we report a total global geological emission of 45 [18-63] Tg CH_4 yr^{-1}, with a breakdown between offshore emissions of 7 [5-10] Tg CH_4 yr^{-1} and onshore emissions of 38 [13-53] Tg CH_4 yr^{-1} (Table 3), similar to Saunois et al. (2020). This bottom-up estimate is slightly lower than in the Saunois et al. (2016) budget mostly due to a reduction of estimated emissions of onshore and offshore seeps (see Sect. 3.2.6 for more offshore contribution explanations).

3.2.4 Termites

Termites are decomposers playing a central role in ecosystem nutrient fluxes at tropical and subtropical latitudes, in particular (Abe et al., 2000). Termites represent a natural CH4 source due to methanogenesis occurring in their hindgut during the symbiotic metabolic breakdown of lignocellulose (Sanderson, 1996; Brune, 2014). The upscaling of CH4 emissions from termites from site to global level is characterised by high uncertainty (Sanderson, 1996; Kirschke et al., 2013; Saunois et al., 2016) due to the combination of factors that need to be considered and the scarcity of information for each of these factors for global upscaling. Needed data include termite biomass density (Sanderson, 1996), species distribution within and among ecosystems (Sugimoto et al., 1998), variation of termite CH4 emission rates per species and dietary group (Sanderson, 1996), the role played by the termite mound structure in affecting the fraction of produced CH4 that is effectively released into the atmosphere (Sugimoto et al., 1998; Nauer et al., 2018). In Kirschke et al. (2013) and Saunois et al. (2016) a global upscaling of termite CH4 emissions was proposed, where CH4 emissions, E_{CH4} (kg CH_4 $ha^{-1}yr^{-1}$), were estimated as the product of three terms: termite biomass (Bio_{TERM} g fresh weight m^{-2}), a scalar correction factor (LU) expressing the effect of land use/cover change on termite biomass density, a termite CH4 emission factor (EF_{TERM}, µg CH_4 g^{-1} Bio_{TERM} h^{-1}) . The approach between the two re-analyses of CH4 emissions varied only for the data sources of gross primary productivity (GPP) and land use which were used to attribute biomass values of termite per ecosystem surface unit, in order to cover different time spans, 1980s, 1990s and 2000s in Kirschke et al. (2013) and 2000-2007 and 2010-2016 in Saunois et al. (2016). For the present update, additional changes have been introduced compared with the previous versions. Here we summarise the key data used for the new upscaling. CH4 fluxes were modelled between 45°S and 45°N and within

35°S and 35°N. The termite biomass density, Bio_{TERM}, for tropical ecosystems was estimated as function (Kirschke et al., 2013; $Bio_{TERM}=1.21 \cdot e^{0.0008 \cdot GPP}$) of the gross primary production (GPP, g C m^{-2} yr^{-1}) using the 0.25° native resolution VODCA2GPP dataset covering the period 2001-2020 (Wild et al., 2022). Wetlands, barren areas, water bodies and artificial surfaces were excluded from this estimation and set as no data (no emissions). The scalar correction factor LU of 0.4 (60%) for agricultural areas (i.e., croplands) (Kirschke et al., 2013) was applied to the GPP value of the nearest natural areas to account for anthropic disturbance. The annual (2001-2020) land cover information was obtained from the MODIS Terra+Aqua Combined Land Cover product (MCD12C1v006; https://lpdaac.usgs.gov/products/mcd12c1v006/), using the International Geosphere-Biosphere Programme (IGP) classification with a 0.05° spatial resolution. For desert and arid lands, within 35°S and 35°N, a fixed Bio_{TERM} value of 1.56 g m^{-2} was instead used (Sanderson, 1996; Heděnec et al., 2022). Similarly, fix values from the few available studies reported in literature were used to estimate Bio_{TERM} between 35°- 45° N and 35°- 45° S as follows: 1.83 g m^{-2} for temperate forests and grasslands (Wood and Sands, 1978; Petersen and Luxton, 1982; Sanderson, 1996; Bignell and Eggleton, 2000; King et al., 2013; conversion factor from dry to fresh biomass is 0.27 from Petersen and Luxton, 1982), 5.3 g m^{-2} for scrublands and Mediterranean areas of Australia (Sanderson, 1996), 1.09 g m^{-2} for the other Mediterranean shrubland ecosystems (Heděnec et al., 2022). Other climates and land covers were set as no data. Climate zoning was defined using the Climate Zones Köppen-Geiger dataset (Beck et al., 2018), this product is representative for the 1980-2016 time period and has a 0.0083° native resolution. The EF_{TERM} was revised compared with previous estimates (Kirschke et al., 2013; Saunois et al., 2016), in order to consider the different distribution of termite families and subfamilies in the different continents and ecosystems, characterised by different feeding habits and nest typologies, as reported by Sugimoto et al. (1998), which might influence the EF. The species of each family and subfamily of the two major groups of lower and higher termites, listed by Sugimoto et al. (1998) were associated with EF values based on emissions from in-vitro experiments as reported by Sanderson (1996) and Eggleton et al. (1999), to which a correction factor (cf_{MOUND}) of 0.5 (Nauer et al., 2018; Chiri et al., 2020; 2021) was applied in order to take into account the mound effect on the CH_4 produced by termites, once inside the nest. The average EF_{TERM} for tropical and temperate areas was hence estimated as the weighted EF_{TERM} derived from the product of the percentage weight of each family or subfamily of termites in the "community composition" in each geographical area and ecosystem (Sugimoto et al. (1998, Table 6), the respective calculated EF of each family or subfamily, a scalar or correction factor which considers the nest type (as in Table 5 from Sugimoto et al. 1998). For desert and arid lands and temperate areas, which were not reported in Sugimoto et al. (1998), EF rates were calculated directly from data reported in literature for the most representative species which were the genus *Amitermes* for the former (EF from data by Sanderson 1996, Eggleton et al. 1999, Jamali et al. 2011) and the genus *Reticulitermes* (family Rhinotermitidea) for the latter (EF from data by Odelson and Breznak, 1983; Sanderson, 1996; Eggleton et al., 1999; Myer et al., 2021). The following EF_{TERMS} were hence obtained to scale up emissions: 3.26 ± 1.79 µg CH_4 g^{-1} termite h^{-1} (28.56 mg CH_4 g^{-1} termite $year^{-1}$) for tropical ecosystems, 1.82 ± 1.54 µg CH_4 g^{-1} termite h^{-1} for temperate forests, grasslands, and Mediterranean areas, 1.24 ± 1.22 µg CH_4 g^{-1} termite h^{-1} for deserts and arid lands (warm climate).

Annual CH_4 fluxes were computed for all the years from 2001 to 2020 producing 20 global maps at 0.05° resolution of yearly total emissions. A further map of the estimated error representative of the entire time period was elaborated at the same resolution as the emissions dataset.

Termite CH_4 emissions over the period 2001-2020 varied between 9.7-10.8 Tg CH_4 yr^{-1}, with an average of 10.2 ± 6.2 Tg CH_4 yr^{-1}. Considering a 20-year average, tropical and subtropical moist broadleaf forests contributed to 46% of the total average flux, while tropical and subtropical grasslands, savannas, and shrublands to another 36%. In terms of regional contribution, 37.2% of fluxes were attributed to South America, 31.5% to Africa, 18.1% to Asia, 5.5% to Australia, 7.4% to North America and less than 1% to Europe. The present estimate value is within the range of previous up-scaling studies, spanning from 2 to 22 Tg CH_4 yr^{-1} (Ciais et al., 2013). In this study, we report a decadal value of 10 Tg CH_4 yr^{-1} with a range of [4-16] (Table 3).

3.2.5 Wild animals

Wild ruminants emit CH_4 through microbial fermentation that occurs in their rumen, similarly to domesticated livestock species (USEPA, 2010b). Using a total animal population of 100-500 million, Crutzen et al. (1986) estimated the global emissions of CH_4 from wild ruminants to be in the range of 2-6 Tg CH_4 yr^{-1}. More recently, Pérez-Barbería (2017) lowered this estimate to 1.1-2.7 Tg CH_4 yr^{-1} using a total animal population estimate of 214 million (range of 210-219), arguing that the maximum number of animals (500 million) used in Crutzen et al. (1986) was poorly justified. Moreover Pérez-Barbería (2017) also stated that the value of 15 Tg CH_4 yr^{-1} found in the last IPCC reports is much higher than their estimate because this value comes from an extrapolation of Crutzen's work for the last glacial maximum when the population of wild animals was much larger, as originally proposed by Chappellaz et al. (1993). Recently, based on the modelling of grassland extent, Kleinen et al. (2023) also suggest that the population of wild animal during the last glacial maximum proposed by Crutzen et al. (1986) and further used by Chappellaz et al. (1993) were overestimated. However, the estimate of 1-3 Tg CH_4 yr^{-1} seems underestimated when considering that Hempson et al. (2017) found actual CH_4 emissions from African wildlife alone to be around 9 Tg CH_4 yr^{-1} but without discussing the uncertainty of this value. As a result, high uncertainty remains and recalls the need for further investigation of this natural source of CH_4.

Based on these findings and waiting for further global estimates, the range adopted in this updated CH_4 budget is 2 [1-3] Tg CH_4 yr^{-1} (Table 3).

3.2.6 Coastal and oceanic sources

Coastal and oceanic sources comprise CH_4 release from estuaries, coastal vegetated habitats, as well as marine waters including seas and oceans. Possible sources of coastal and oceanic CH_4 include (1) in-situ biogenic production through various pathways in oxygenated sea-surface waters (Oremland, 1979; Karl et al., 2008; Lenhart et al., 2016; Repeta et al., 2016), a flux that can be enhanced in the coastal ocean because of submarine groundwater discharge (USEPA, 2010b); (2)

production from shallow and marine (bare and vegetated) sediments including free gas or destabilised hydrates and thawing subsea permafrost containing modern (^{14}C-bearing) microbial gas; (3) geological marine seepage (see also Sect. 3.2.3), including hydrates, containing fossil (^{14}C-free) microbial or thermogenic CH_4. CH_4 produced in marine sediments and seabed CH_4 seepage can be transported across the water column to the sea-surface by upwelling waters (once at the surface methane can cross the sea-air interface via diffusion) and gas bubble plumes (for instance from geological marine seeps; e.g., Judd, 2004; Etiope et al., 2019). Gas bubble plumes generally reach the atmosphere in relatively shallow waters (<400 m) of continental shelves depending on the intensity of the events (e.g., Westbrook et al., 2009); however massive deep-water seepage events could contribute a significant amount of CH4 to the atmosphere, even from depths > 1000 m (e.g., Schmale et al., 2005.; Greinert et al., 2006; Solomon et al., 2009). In coastal vegetated habitats, CH_4 can also be transported to the atmosphere through the aerenchyma of emergent aquatic plants (Purvaja et al., 2004).

We distinguish between coastal and oceanic "geological" and "modern biogenic" CH_4 sources. Coastal and oceanic "geological" emissions refer to CH_4 seepage from the Earth's crust (mostly in hydrocarbon-rich sedimentary basins), which is typically evaluated by combining geochemical analyses (isotopic and molecular, including radiocarbon, ^{14}C, analyses) and geological observations (degassing along faults, seeps, mud volcanoes). Geological emissions do not contain modern biogenic gas that is fossil (^{14}C-free). Coastal and oceanic "biogenic" CH_4 refers to CH_4 formed *in situ* in coastal and marine sediments and in the water column by recent or modern microbial activity (therefore with measurable amounts of radiocarbon (^{14}C)). To avoid double-counting, we assume that all diffusive CH_4 emissions outside of geological seepage regions (identified in global grid maps; Etiope et al., 2019) are fuelled by biogenic CH_4. Finally, we briefly discuss the case of CH_4 hydrates, which can be considered either a "geological" source when they host fossil CH_4 or a "biogenic" source when they host modern CH_4.

Coastal and oceanic modern biogenic methane emissions. Area-integrated diffusive modern biogenic CH_4 emissions from coastal ecosystems are 1-2 magnitudes lower than from inland freshwaters but significantly higher than biogenic emissions from the open ocean (Rosentreter et al., 2021; Rosentreter et al., 2023; Weber et al., 2019). Particularly the shallow vegetated coastline fringed by mangroves, salt marshes, and seagrasses is a CH_4 hotspot in the coastal ocean, characterised by significantly higher flux densities than other coastal settings such as estuaries or the continental shelves (Rosentreter et al., 2021; Rosentreter et al., 2023). Coastal ecosystems are thus being increasingly recognized as weak global sources to the atmosphere (Weber et al., 2019; Saunois et al., 2020; Rosentreter et al., 2021). Hydrogenotrophic and acetoclastic methanogenesis are largely outcompeted by sulphate reduction in coastal/marine sediments, which is often shown by a decreasing trend of CH_4 concentrations with increasing salinity from upper tidal (low salinity) to marine (high salinity) regions. Much of the CH_4 produced below the sulfate-reduction zone is indeed re-oxidized by sedimentary anaerobic methane oxidation or re-oxidized in the water column, leading to small emissions despite much larger production (Knittel and Boetius 2009; Regnier et al., 2011). Methylated compounds such as methylamines and methyl sulphides are non-competitive substrates that are exclusively used by methanogens, therefore methylated methanogenesis can occur in coastal

regions with high sulphate concentrations, for example, in organic-rich (Maltby et al., 2018), vegetated (Schorn et al., 2022), and hypersaline coastal sediments (Xiao et al., 2018). Coastal CH_4 can be driven by the exchange of pore water or groundwater (high in CH_4) with coastal surface waters in tidal systems, referred to as tidal pumping (Ovalle et al., 1990; Call et al., 2015). Anthropogenic impacts such as wastewater pollution and land-use change can increase CH_4 fluxes in estuaries (Wells et al., 2020). A large increase of CH_4 emissions follows the conversion of natural coastal habitats to aquaculture farms (Yuan et al., 2019; Yang et al., 2022).

Currently available global modern biogenic CH_4 flux data show high spatiotemporal variability within and between coastal systems, but also because of the overall global paucity of data. Therefore, global estimates have high uncertainties and show large ranges in both empirical (Rosentreter et al., 2021) and machine-learning based approaches (Weber et al., 2019). According to a recent data-driven meta-data analysis, global estuaries, including tidal systems and deltas, lagoons, and fjords, are estimated to emit median (Q1-Q3) 0.25 (0.07-0.46) Tg CH_4 yr^{-1} (Rosentreter et al., 2023). Coastal vegetation, including mangrove forests, salt marshes, and seagrasses are estimated to emit 0.77 (0.47-1.41) Tg CH_4 yr^{-1}, which is 3 times more than global estuaries (Rosentreter et al., 2023). The combined median (Q1-Q3) emission of 1.01 (0.54-1.87) Tg CH_4 yr^{-1} for coastal vegetation and estuaries by Rosentreter et al. (2023) is lower than the recent observation-based global synthesis including tidal flats and aquaculture ponds (median 1.49 (0.22-6.48) Tg CH_4 yr^{-1}) by Rosentreter et al. (2021). Total shallow coastal modern biogenic CH_4 emissions based on existing data including emissions from estuaries, coastal vegetation (Rosentreter et al., 2023), tidal flats, and man-made coastal aquaculture ponds (Rosentreter et al., 2021) amount to median (Q1-Q3) 1.8 (0.59-5.57) Tg CH_4 yr^{-1}. This range is about 3-4 times lower than the earlier global assessment by Borges and Abril (2011) and also lower than the value of 4-5 Tg CH_4 yr^{-1} reported in the previous CH_4 budget for inner and outer estuaries including marshes and mangroves (Saunois et al., 2020), which was based on a significantly smaller dataset (n=80) and larger estuarine surface areas (Laruelle et al., 2013) than used here (Laruelle et al., 2025).

The near-shore (0-50 m), inner shelf diffusive modern biogenic CH_4 flux of median (Q1-Q3) 1.33 (0.93-2.10) Tg CH_4 yr^{-1} by Weber et al. (2019) based on machine-learning is similar to the combined shallow coastal (estuaries and coastal vegetation) median by Rosentreter et al. (2021, 2023). Adding the diffusive modern biogenic CH_4 flux for the outer shelf (50-200 m) (median (Q1-Q3) of 0.54 (0.40-0.73) Tg CH_4 yr^{-1}) and for the slope (200-2000m) (median (Q1-Q3) of 0.28 (0.22-0.37) Tg CH_4 yr^{-1}) (Weber et al., 2019), and excluding geological seepage regions (Etiope et al., 2019; see below), gives a total median (Q1-Q3) of 3.95 (2.14-8.77) Tg CH_4 yr^{-1} for combined coastal shallow, near-shore, outer shelf and slope diffusive modern biogenic CH_4 emissions. The previous budget by Saunois (2020) also included poorly constrained emissions (upper bound value: 1-2 Tg CH_4 yr^{-1}) from large river plumes protruding onto the shelves. However, here we assume that emissions from large river plumes are accounted for in the near-shore and outer shelf estimates by Weber et al. (2019). Area-integrated diffusive CH_4 emissions from the open ocean and deep seas (>2000 m) are much lower than from other coastal systems but amount to median (Q1-Q3) 0.91 (0.75-1.12) Tg CH_4 yr^{-1} because of the large surface area of the open ocean (>300 x 10^6 km^2) (Weber et al., 2019). Overall, these marine biogenic emissions are sustained by a mixture of

sedimentary production and in-situ production in the sea-surface layers (including the methylphosphonate pathway) (e.g., Karl et al., 2008; Repeta et al., 2016; Resplandy et al., 2024). The total coastal and ocean diffusive modern biogenic emissions retained here amount to 5 (3-10) Tg CH_4 yr^{-1} (Table 3).

Coastal and oceanic geological methane emissions Submarine geological CH_4 emission is the offshore component of the general geological emissions of natural gas from the Earth's crust (Judd, 2004; Etiope, 2009; Etiope et al., 2019). The onshore components include terrestrial seeps, mud volcanoes, microseepage, and geothermal manifestations, addressed in Sect. 3.2.3. Natural gas seeping at the seabed as bubble plumes can reach the surface in relatively shallow waters (<400 m), but CH_4-rich bubble plumes reaching the atmosphere from depths >500 m have been observed in some cases (e.g., Solomon et al., 2009), and upwelling of bottom marine waters can, in theory, transport geological CH_4 (dissolved) to the surface from any depth. This represents, however, a small and poorly known fraction of geological CH_4 emission. Geological CH_4 can be either microbial or thermogenic, produced throughout diverse geological periods in hydrocarbon source rocks in sedimentary basins (therefore it is always fossil, ^{14}C-free). The seepage at the seafloor is typically related to tectonic faults, sometimes forming mud diapirs and mud volcanoes (Mazzini and Etiope, 2017). Published estimates of geological CH_4 submarine emissions range from 3 to 20 Tg yr^{-1}, with a best guess of 7 Tg yr^{-1} (Etiope and Schwietzke, 2019; Etiope et al., 2019 and references therein).

Here, the diffusive geological CH_4 emissions are estimated at 0.16 (0.11-0.24) Tg CH_4 yr^{-1} for near-shore (0-50 m), 0.03 (0.02-0.05) Tg CH_4 yr^{-1} for outer shelf (50-200 m), and 0.02 (0.01-0.03) Tg CH_4 yr^{-1} for slope (200-2000 m) by calculating the fraction of the Weber et al. (2019) diffusive fluxes that occur within the identified geological seepage regions from Etiope et al. (2019). No geological seepage regions were identified in the open ocean and deep seas (> 2000 m).

In this study, we consider the ebullitive flux as geologically sourced CH_4. While modern biogenic CH_4 gas production appears ubiquitous in shallow sediments (Fleischer et al., 2001; Best et al., 2006), no global dataset is currently available to estimate the biogenic ebullitive CH_4 flux to the atmosphere. Omission of this flux thus constitutes a significant knowledge gap in the coastal and oceanic CH_4 budget. Global geological CH_4 ebullition from continental shelf and slope, referring only to depths <200 m, were estimated at 5.06 (1.99-8.16) Tg CH_4 yr^{-1} (Weber et al., 2019). This estimate is based on prior estimates of the geological flux from the seafloor (Hovland et al., 1993) and bubble transfer efficiency to the ocean surface (McGinnis et al., 2006). Etiope et al. (2019) estimated a partial fraction of geological emissions in the form of gas bubbles of 3.9 (1.8-6) Tg CH_4 yr^{-1}, only referring to the sum of published estimates from 15 geological seepage regions, which are also deeper than 200 m. Global extrapolation including other 16 identified seepage zones (where flux data are not available) was suggested to be at least 7 (3-10) Tg CH_4 yr^{-1} (Etiope et al., 2019), and this value coincides with the mean emission value (best guess) derived by combining literature data, see Etiope and Schwietzke (2019) for further details. It is worth noting that the Weber et al. (2019) estimate of 5.06 (1.99-8.16) Tg CH_4 yr^{-1}, which considers only the continental shelf at depths <200 m, is compatible with the overall submarine emission of 7 (3-10) Tg CH_4 yr^{-1} (including seeps > 200 m deep) indicated

in Etiope and Schwietzke (2019) and Etiope et al. (2019). Although 300-400 m is considered a general depth limit for efficient transport (with limited oxidation and dissolution) of CH_4 bubbles to the atmosphere (e.g., Judd, 2004; Schmale et al., 2005; Etiope et al., 2019), in some cases oil coatings on bubbles inhibit gas dissolution so that CH_4-rich bubbles can reach the atmosphere from depths >500 m (e.g., Solomon et al., 2009). As mentioned above, a fraction of geological CH_4 released in deep seas (such as in the areas with gas-charged sediments inventoried in Fleischer et al., 2001) can also be transported to the surface by upwelling bottom waters. Further research is needed to better evaluate the atmospheric impact of such deep seeps.

Geological submarine emissions, thus, would amount to 0.21 (0.14-0.32) Tg CH_4 yr^{-1} in the form of a diffusive flux while the ebullitive flux would be 5.06 (3.01-7.88) Tg CH_4 yr^{-1}, considering only < 200 m deep seepage, and 7 (3-10) Tg CH_4 yr^{-1} considering all data available (Etiope and Schwietzke, 2019). Here, we select the Etiope and Schwietzke (2019) assessment in order to account for all potential seepage areas, including those located at water depths > 200m. While we use the estimate by Etiope and Schwietzke (2019) estimate, we acknowledge that high uncertainty remains and other studies suggest a lower ranges of emissions based on radiocarbon (^{14}C-CH_4) data in ice cores (e.g., Hmiel et al., 2020). The suggested estimate may overestimate this source and be part of the top-down bottom-up discrepancy as discussed in Section 5.1.2.

As a result, here we report a (rounded) median of 12 Tg CH_4 yr^{-1} with a range of 6-20 Tg CH_4 yr^{-1} for all coastal and oceanic sources (Table 3).

Methane emissions from gas hydrates. Among the different origins of coastal and oceanic CH_4, hydrates have attracted a lot of attention. CH_4 hydrates (or clathrates) are ice-like crystals formed under specific temperature and pressure conditions (Milkov, 2005). Hydrates may host either modern microbial CH_4, containing ^{14}C and formed *in situ* in shallow sediments (this type of hydrates is also called "autochthonous") or fossil, microbial or thermogenic CH_4, migrated from deeper sediments, generally from reservoirs in hydrocarbon-rich sedimentary basins (this type of hydrates is also called "allochthonous"; Milkov, 2005; Foschi et al., 2023). The total stock of marine CH_4 hydrates is large but uncertain, with global estimates ranging from hundreds to thousands of Pg CH_4 (Klauda and Sandler, 2005; Wallmann et al., 2012). Note that the highly climate-sensitive subsea permafrost reservoir beneath Arctic Ocean shelves also contributes to the hydrate inventory (Ruppel and Kassler, 2017).

Concerning more specifically atmospheric emissions from marine hydrates, Etiope (2015) points out that current estimates of CH_4 air–sea flux from hydrates (2–10 Tg CH_4 yr^{-1} in Ciais et al., 2013, or Kirschke et al., 2013) originate from the hypothetical values of Cicerone and Oremland (1988). No experimental data or estimation procedures have been explicitly described along the chain of references since then (Denman et al., 2007; IPCC, 2001; Kirschke et al., 2013; Lelieveld et al., 1998). It was estimated that ~473 Tg CH_4 has been released into the water column over 100 years (Kretschmer et al., 2015). Those few teragrams per year become negligible once consumption within the water column has been accounted for. While

events such as submarine slumps may trigger local releases of considerable amounts of CH_4 from hydrates that may reach the atmosphere (Etiope, 2015; Paull et al., 2002), on a global scale, present-day atmospheric CH_4 emissions from hydrates do not appear to be a significant source to the atmosphere, and at least formally, we should consider 0 (< 0.1) Tg CH_4 yr^{-1} emissions.

3.2.7 Terrestrial permafrost

Permafrost is defined as frozen soil, sediment, or rock having temperatures at or below 0°C for at least two consecutive years (Harris et al., 1988). The total extent of permafrost in the Northern Hemisphere is about 14 million km^2 or 15% of the exposed land surface (Obu et al., 2019). As the climate warms, a rise in soil temperatures has been observed across the permafrost region, and permafrost thaw occurs when temperatures pass 0°C, often associated with melting of ice in the ground (Biskaborn et al., 2019). Permafrost thaw is most pronounced in southern and spatially isolated permafrost zones, but also occurs in northern continuous permafrost (Obu et al., 2019). Thaw occurs either as a gradual, often widespread, deepening of the active layer (surface soils that thaw every summer) or as more rapid localised thaw associated with loss of massive ground ice (thermokarst) (Turetsky et al., 2020). A total of 1000 ± 200 Pg of carbon can be found in the upper 3 meters of permafrost region soils, or 1400-2000 Pg C for all permafrost (Hugelius et al., 2014; Strauss et al., 2021).

The thawing permafrost can generate direct and indirect CH_4 emissions. Direct CH_4 emissions are from the release of CH_4 contained within the thawing permafrost. This flux to the atmosphere is small and estimated to be a maximum of 1 Tg CH_4 yr^{-1} at present (USEPA, 2010b). Increased release of CH_4 from deep geogenic sources that occurs as seepage along permafrost boundaries and lake beds may also be considered a direct, and this is estimated to be 2±0.4 Tg CH_4 yr^{-1} (Walter Anthony et al., 2012). Indirect CH_4 emissions are probably more important. They are caused by 1) methanogenesis induced when the organic matter contained in thawing permafrost becomes available for microbial decomposition; 2) thaw induced soil wetting and changes in land surface hydrology possibly enhancing CH_4 production (McCalley et al., 2014; Schuur et al., 2022); and 3) the landscape topography changes driven by abrupt thaw processes and loss of ground ice, including the formation of thermokarst lakes, hill-slope thermokarst, and wetland thermokarst (Turetsky et al., 2020). Such CH_4 production is probably already significant today and is likely to become more important in the future associated with climate change and strong positive feedback from thawing permafrost (Schuur et al., 2022). However, indirect CH_4 emissions from permafrost thawing are difficult to estimate at present, with very few data to refer to, and in any case largely overlap with wetland and freshwater emissions occurring above or around thawing areas. In a recent synthesis of full permafrost region CH_4 budgets for the period 2000-2017, Hugelius et al. (2023) compared CH_4 budgets from bottom-up and top-down (atmospheric inversion models) approaches. They estimate an integrated bottom-up budget of 50 (23, 53; mean upper and lower 95% CI) Tg CH_4 yr^{-1} while the top-down estimate is 19 (15, 24) Tg CH_4 yr^{-1}. The bottom-up estimate is based on a combination of data-driven upscaling reported by Ramage et al. (2023) and process-based model estimates for wetland CH_4 flux calculated from model ensembles used in Saunois et al. (2020). The top-down estimate is calculated from

ensembles of atmospheric inversion models used in Saunois et al. (2020). Although it is difficult with direct process-attribution, fluxes of ca. 20-30 Tg CH_4 yr^{-1} in the bottom-up budget are caused by land cover types affected by previous permafrost thaw (thermokarst lakes, wetlands, hillslope). Because pre-thaw land cover types often have near neutral CH_4 balances (Ramage et al. 2023), these fluxes can largely be seen as driven by permafrost thaw, however the thaw may have occurred decades, or even centuries, before today.

Here, we choose to report only the direct emission range of 0-1 Tg CH_4 yr^{-1} (Table 3), keeping in mind that current wetland, thermokarst lakes and other freshwater methane emissions already likely include a significant indirect contribution originating from thawing permafrost.

3.2.8 Vegetation

Three distinct pathways for the production and emission of CH_4 by living vegetation are considered here (see Covey and Megonigal (2019) and Bastviken et al. (2023) for extensive reviews). Firstly, plants produce CH_4 through an abiotic photochemical process induced by stress (Keppler et al., 2006). This pathway was initially questioned (e.g., Dueck et al., 2007; Nisbet et al., 2009), and although numerous studies have since confirmed aerobic emissions from plants and better resolved its physical drivers (Fraser et al., 2015), global estimates still vary by two orders of magnitude (Liu et al., 2015). This plant source has not been confirmed in-field however, and although the potential implication for the global CH_4 budget remains unclear, emissions from this source are certainly much smaller than originally estimated in Keppler et al. (2006) (Bloom et al., 2010; Fraser et al., 2015). Second, and of clearer significance, plant stems act as "straws", drawing up and releasing microbially produced CH_4 from anoxic soils (Cicerone and Shetter, 1981; Rice et al., 2010; Nisbet et al., 2009). For instance, in the forested wetlands of Amazonia, tree stems are the dominant ecosystem flux pathway for soil-produced CH_4, therefore, including stem emissions in ecosystem budgets can reconcile regional bottom-up and top-down estimates (Pangala et al., 2017; Gauci et al., 2022). Third, the stems of both living trees (Covey et al., 2012) and dead wood (Covey et al., 2016) provide an environment suitable for microbial methanogenesis. Static chambers demonstrate locally significant through-bark flux from both soil- (Pangala et al., 2013, 2015), and tree stem-based methanogens (Pitz and Megonigal, 2017; Wang et al., 2016). A synthesis indicates stem CH_4 emissions significantly increase the source strength of forested wetlands, and modestly decrease the sink strength of upland forests (Covey and Megonigal, 2019). Recently, field-work suggested that trees may also act as a CH_4 sink (Machacova et al., 2021; Gorgolewski et al., 2023; Gauci et al., 2024). The scientific activity covering CH_4 emissions in forested ecosystems reveals a far more complex story than previously thought, with an interplay of productive/consumptive, aerobic/anaerobic, and biotic/abiotic processes occurring between upland/wetland soils, trees, and atmosphere. Understanding the complex processes that regulate CH_4 source–sink dynamics in forests and estimating their contribution to the global CH_4 budget requires cross-disciplinary research, more observations, and new models that can overcome the classical binary classifications of wetland versus upland forest and of emitting versus uptaking soils (Barba et al., 2019; Covey and Megonigal, 2019). Although we recognize these emissions are potentially large

1450 (particularly tree transport from inundated soil), global estimates for each of these pathways remain highly uncertain and/or

1451 are currently included here within other flux category sources (e/g. inland waters, wetlands, upland soils).

3.3 Methane sinks and lifetime

1453 CH_4 is the most abundant reactive trace gas in the troposphere and its reactivity is important to both tropospheric and

1454 stratospheric chemistry. The main atmospheric sink of CH_4 (~90% of the total sink mechanism) is oxidation by the hydroxyl

1455 radical (OH), mostly in the troposphere (Ehhalt, 1974). Other losses are by photochemistry in the stratosphere (reactions

1456 with chlorine atoms (Cl) and excited atomic oxygen ($O(^1D)$)), oxidation in soils (Curry, 2007; Dutaur and Verchot, 2007),

1457 and by photochemistry in the marine boundary layer (reaction with Cl; Allan et al. (2007), Thornton et al. (2010)).

1458 Uncertainties in the total sink of CH_4 as estimated by atmospheric chemistry models are in the order of 20-40% (Saunois et

1459 al., 2016). It is much less (10-20%) when using atmospheric proxy methods (e.g., methyl chloroform, see below) as in

1460 atmospheric inversions (Saunois et al., 2016). In the present release of the global CH_4 budget, we estimate bottom-up

1461 CH_4 chemical sinks and lifetime mainly based on global model results from the Chemistry Climate Model Initiative (CCMI)

1462 2022 activity (Plummer et al., 2021) and CMIP6 simulations (Collins et al., 2017).

3.3.1 Tropospheric OH oxidation

1464 OH radicals are produced following the photolysis of ozone (O_3) in the presence of water vapour. OH is destroyed by

1465 reactions with carbon monoxide (CO), CH_4, and non-methane volatile organic compounds.

1466 Following the Atmospheric Chemistry and Climate Model Intercomparison Project (ACCMIP), which studied the long-term

1467 changes in atmospheric composition between 1850 and 2100 (Lamarque et al., 2013), a new series of experiments was

1468 conducted by several chemistry-climate models and chemistry-transport models participating in the Chemistry-Climate

1469 Model Initiative (CCMI) (Plummer et al., 2021). Mass-weighted OH tropospheric concentrations do not directly represent

1470 CH_4 loss, as the spatial and vertical distributions of OH affect this loss through, in particular, the temperature dependency

1471 and the distribution of CH_4 (e.g., Zhao et al., 2019). However, estimating OH concentrations and, spatial and vertical

1472 distributions is a key step in estimating methane loss through OH. Over the period 2000-2010, the global mass-weighted

1473 OH tropospheric concentration is estimated at 13.3 [11.7-18.2] x 10^5 molecules cm^{-3} by 8 CCMI-2022 models and at 11. 8

1474 [9.4-13.5] x 10^5 molecules cm^{-3} by 9 models contributing CMIP6 historical run (Collins et al., 2021) (see supplementary

1475 Table S4). The ranges calculated here are similar to the ones proposed previously in Saunois et al. (2020), where the multi-

1476 model mean (11 models) global mass-weighted OH tropospheric concentration was 11.7±1.0 x 10^5 molecules cm^{-3} (range

1477 9.9-14.4 x 10^5 molecules cm^{-3}, Zhao et al. (2019)) consistent with the previous estimates from ACCMIP (11.7±1.0 x

1478 10^5 molecules cm^{-3}, with a range of 10.3-13.4 x 10^5 molecules cm^{-3}, Voulgarakis et al. (2013) for year 2000) and the

1479 estimates of Prather et al. (2012) of 11.2±1.3 x 10^5 molecules cm^{-3}. Nicely et al. (2017) attribute the differences in OH

1480 simulated by different chemistry transport models to, in decreasing order of importance, different chemical mechanisms,

various treatments of the photolysis rate of O_3, and modelled O_3 and CO. Besides the uncertainty on global OH concentrations, there is an uncertainty in the spatial and temporal distribution of OH. Models often simulate higher OH in the northern hemisphere (NH) than in the southern hemisphere (SH), leading to a NH/SH OH ratio greater than 1 (e.g., Zhao et al., 2019). However, there is evidence for parity in inter-hemispheric OH concentrations (Patra et al., 2014), which needs to be confirmed by other observational and model-derived estimates. The analysis of the latest CCMI (Plummer et al., 2021) and CMIP6 (Collins et al., 2021) model outputs show that structural uncertainties in the atmospheric chemistry models remain large, probably due to inherent biases in OH precursors. Such biases have been highlighted in the OH 3D fields simulated by two atmospheric chemistry models (Zhao et al., 2023), and were corrected using OH precursors observations. Such corrections resulted in tropospheric OH mean concentrations lowered by 2. 10^5 molecules cm^{-3}, leading to around 10 x 10^5 molecules cm^{-3}, and a NH/SH OH ratio closer to 1, in better agreement with methyl chloroform (MCF)-based approaches. This study highlights the need for further improvement of the atmospheric chemistry model.

OH concentrations and their changes can be sensitive to climate variability (e.g., Nicely et al., 2018; Anderson et al., 2021), biomass burning (e.g., Anderson et al., 2024), and anthropogenic emissions of precursors (Peng et al., 2022; Stevenson et al., 2020). OH distributions calculated by chemistry climate models show large regional differences and various vertical profiles (Zhao et al., 2019). OH changes present also regional differences over the long term (Stevenson et al., 2020). Despite large regional changes, the global mean OH concentration was suggested to have changed only slightly from 1850 to 1980, but followed by strong (9 %) increases up to the present day (Stevenson et al., 2020). This increase simulated by models over 2000-2015 are however not in agreement with observation-based approaches (Thompson et al., 2024; Patra et al., 2020; Nicely et al., 2018; Rigby et al., 2017; Turner et al., 2017) where OH decreases or remain constant over the period. CCMI and CMIP6 models show OH interannual variability ranging from 0. 9% to 1.8% over 2000-2010 (Table S4), in agreement with the values of IAV derived from some observationally constrained studies (e.g., Thompson et al., 2024; Montzka et al., 2011) but lower than value deduced from methyl chloroform measurements (Patra et al., 2021; Naus et al., 2021). However, chemistry climate simulations consider meteorology variability but not fully emission interannual variability (e.g., from biomass burning) and thus are expected to simulate lower OH inter annual variability than in reality. Using an empirical model constrained by global observations of O_3, water vapour, CH_4, and temperature as well as the simulated effects of changing NO_X emissions and tropical expansion, Nicely et al. (2017) found an interannual variability in OH of about 1.3-1.6% between 1980 and 2015, in agreement with methyl chloroform based estimates (Montzka et al., 2011).

Over 2000-2009, the tropospheric loss (tropopause height at 200 hPa) of CH_4 by OH oxidation derived from the ten and CCMI modelling activities (see supplementary Table S5) is estimated at of 546 [446-663] Tg CH_4 yr^{-1} (Table 3), which is similar to the one reported previously in Saunois et al. (2020) from CCMI model (553 [476-677] Tg CH_4 yr^{-1}) and still slightly higher than the one from the ACCMIP models (528 [454-617] Tg CH_4 yr^{-1} reported in Kirschke et al. (2013) and Saunois et al. (2016).

For the recent 2010-2019 decade, we report a climatological value based on only five models that contributed to CMIP6 runs (historical run followed by SSP3-7.0 projections starting in 2015, Collins et al. (2021)) to acknowledge the impact of the rise in atmospheric methane on the methane chemical sink. Hence, for 2010-2019, we report the climatological value of 563 [462-663] Tg CH_4 yr^{-1} (Table 3).

3.3.2 Stratospheric loss

In the stratosphere, CH_4 is lost through reactions with excited atomic oxygen $O(^1D)$, atomic chlorine (Cl), atomic fluorine (F), and OH (Brasseur and Solomon, 2005; le Texier et al., 1988). Uncertainties in the chemical loss of stratospheric CH_4 are large, due to uncertain interannual variability in stratospheric transport (Zhang et al., 2023) as well as its chemical interactions and feedbacks with stratospheric O_3 (Morgenstern et al., 2018). Particularly, the fraction of stratospheric loss due to the different oxidants is still uncertain, with possibly 20-35% due to halons, about 25% due to $O(^1D)$ mostly in the high stratosphere and the rest due to stratospheric OH (McCarthy et al., 2003).

In this study, six chemistry climate models that contributed to CMIP6 modelling activities (Table S5) provided estimates of CH_4 chemical loss, including reactions with OH, $O(^1D)$, and Cl; CH_4 photolysis is also included but occurs only above the stratosphere. Considering a 200 hPa tropopause height, these six CMIP6 simulations suggest an estimate of 34 [10-51] Tg CH_4 yr^{-1} for the CH_4 stratospheric sink for the 2000-2009 decade (Table S5), similar to the value derived from the previous CCMI activity reported in Saunois et al. (2020) (31 [12-41] Tg CH_4 yr^{-1}). The lowest estimate provided by a model (10 Tg CH_4 yr^{-1}) is quite unrealistic and would yield a methane stratospheric lifetime of several hundreds of years. As a result, this oulier is excluded and we prefer to report a mean of 39 Tg CH_4 yr^{-1} associated with a range of [27-51] for 2000-2009.

For 2010-2019, we report here a climatological range of 28-43 Tg CH_4 yr^{-1} associated with a mean value of 37 Tg CH_4 yr^{-1} (Table 3) based on five models that contributed to CMIP6 runs (historic followed by SSP3-7.0 projections starting in 2015; Table S5).

3.3.3 Tropospheric reaction with Cl

Halogen atoms can also contribute to the oxidation of CH_4 in the troposphere. Allan et al. (2005) measured mixing ratios of methane and $\delta^{13}C$-CH_4 at two stations in the southern hemisphere from 1991 to 2003, and found that the apparent kinetic isotope effect (KIE) of the atmospheric CH_4 sink was significantly larger than that explained by OH alone. A seasonally varying sink due to Cl in the marine boundary layer of between 13 and 37 Tg CH_4 yr^{-1} was proposed as the explanatory mechanism (Allan et al., 2007; Platt et al., 2004). This sink was estimated to occur mainly over coastal and marine regions, where sodium chloride (NaCl) from evaporated droplets of seawater react with NO_2 to eventually form Cl_2, which then UV-dissociates to Cl. However significant production of nitryl chloride ($ClNO_2$) at continental sites has been recently reported (Riedel et al., 2014) and suggests the broader presence of Cl, which in turn would expand the significance of the Cl sink in the troposphere. Recently, Hossaini et al. (2016), Sherwen et al. (2016), and Wang et al. (2019b, 2021b) have made

significant improvements in tropospheric chemistry modelling and they conclude to an oxidation contribution of 2.6%, 2%, 1% and 0.8%, respectively. These values correspond to a tropospheric CH$_4$ loss of around 12-13 Tg CH$_4$ yr^{-1}, 9 Tg CH$_4$ yr^{-1}, 5 Tg yr^{-1}, and 3 Tg CH$_4$ yr^{-1} respectively, much lower than the first estimates by Allan et al. (2007). The recent work of Wang et al. (2021b) is the most comprehensive modelling study and based upon Sherwen et al. (2016) and Wang et al. (2019b). Both the KIE approach and chemistry transport model simulations carry uncertainties (extrapolations based on only a few sites and use of indirect measurements, for the former and missing sources, coarse resolution, underestimation of some anthropogenic sources for the latter). However, Gromov et al. (2018) found that Cl can contribute only 0.23% the tropospheric sink of CH$_4$ (about 1 Tg CH$_4$ yr^{-1}) in order to balance the global ^{13}C(CO) budget (see their Table S1). While tropospheric Cl has a marginal impact on the total CH$_4$ sink (few percents), it influences more significantly the atmospheric isotopic δ^{13}C-CH$_4$ signal and improved estimates of the tropospheric Cl amount should be used for isotopic CH$_4$ modelling studies (Strode et al., 2020; Thanwerdas et al., 2022b).

Each recent Cl estimate suggests a reduced contribution to the methane loss than previously reported by Allan et al. (2007). As a result, we suggest here to use the mean, minimum and maximum of the last five estimates published since 2016, leading to a climatological value of 6 [1-13] Tg CH$_4$ yr^{-1} (Table 3), thus reducing both the magnitude and the uncertainty range compared to Saunois et al. (2020).

3.3.4 Soil uptake

Unsaturated oxic soils are sinks of atmospheric CH$_4$ due to the presence of methanotrophic bacteria, which consume CH$_4$ as a source of energy. Dutaur and Verchot (2007) conducted a comprehensive meta-analysis of field measurements of CH$_4$ uptake spanning a variety of ecosystems. Extrapolating to the global scale, they reported a range of 36 ± 23 Tg CH$_4$ yr^{-1}, but also showed that stratifying the results by climatic zone, ecosystem, and soil type led to a narrower range (and lower mean estimate) of 22 ± 12 Tg CH$_4$ yr^{-1}. Modelling studies, employing meteorological data as external forcing, have also produced a considerable range of estimates. Using a soil depth-averaged formulation based on Fick's law with parameterizations for diffusion and biological oxidation of CH$_4$, Ridgwell et al. (1999) estimated the global sink strength at 38 Tg CH$_4$ yr^{-1}, with a range 20-51 Tg CH$_4$ yr^{-1} reflecting the model structural uncertainty in the base oxidation parameter. Curry (2007) improved on the latter by employing an exact solution of the one-dimensional diffusion-reaction equation in the near-surface soil layer (i.e., exponential decrease in CH$_4$ concentration below the surface), a land surface hydrology model, and calibration of the oxidation rate to field measurements. This resulted in a global estimate of 28 Tg CH$_4$ yr^{-1} (9-47 Tg CH$_4$ yr^{-1}), the result reported by Zhuang et al. (2013), Kirschke et al. (2013) and Saunois et al. (2016). Ito and Inatomi (2012) used an ensemble methodology to explore the variation in estimates produced by these parameterizations and others, which spanned the range 25-35 Tg CH$_4$ yr^{-1}. For the period 2000-2020, as part of the wetland emissions modelling activity, JSBACH (Kleinen et al., 2020) and VISIT (Ito and Inatomi, 2012) models compute a global CH$_4$ soil uptake to 18 and 35 Tg CH$_4$ yr^{-1}, respectively.

Murguia-Flores et al. (2018) further refined the Curry (2007) model's structural and parametric representations of key drivers of soil methanotrophy, demonstrating good agreement with the observed latitudinal distribution of soil uptake (Dutaur and Verchot, 2007). Their model (MeMo) simulates a CH_4 soil sink of 37.5 Tg CH_4 yr^{-1} for the period 2010-2019 (Fig. S4), compared to 39.5 and 31.3 Tg CH_4 yr^{-1} using the Ridgwell et al. (1999) and Curry (2007) parameterizations, respectively, under the same meteorological forcing, run specifically for this study. For the 2000s period, the simulations estimate the soil uptake at 30.4, 36.7 and 38.3 Tg CH_4 yr^{-1} based on the parameterization of Curry, MeMo, and Ridgwell, respectively. As part of a more comprehensive model accounting for a range of CH_4 sources and sinks, Tian et al. (2010, 2015, 2016) computed vertically-averaged CH_4 soil uptake including the additional mechanisms of aqueous diffusion and plant-mediated (*aerenchyma*) transport, arriving at the estimate 30±19 Tg CH_4 yr^{-1} (Tian et al., 2016) for the 2000s. The still more comprehensive biogeochemical model of Riley et al. (2011) included vertically resolved representations of the same processes considered by Tian et al. (2016), in addition to grid cell fractional inundation and, importantly, the joint limitation of uptake by both CH_4 and O_2 availability in the soil column. Riley et al. (2011) estimated a global CH_4 soil sink of 31 Tg CH_4 yr^{-1} with a structural uncertainty of 15-38 Tg CH_4 yr^{-1} (a higher upper limit resulted from an elevated gas diffusivity to mimic convective transport; as this is not usually considered, we adopt the lower upper bound associated with no limitation of uptake at low soil moisture). A model of this degree of complexity is required to explicitly simulate situations where the soil water content increases enough to inhibit the diffusion of oxygen, and the soil becomes a methane source (Lohila et al., 2016). This transition can be rapid, thus creating areas (for example, seasonal wetlands) that can be either a source or a sink of methane depending on the season.

The previous Curry (2007) estimate can be revised upward slightly based on subsequent work and the increase in CH_4 concentration since that time. Indeed, Murgia-Flores et al. (2021) estimated that the global soil-uptake doubled between 1900 and 2015 and could further increase due to enhanced diffusion of CH_4 into soil as a result of increases in atmospheric CH_4 mole fraction. Further investigation of the soil uptake is required to better constrain this process at the global scale while it is highly dependent on local scale microbial activity and environmental conditions (e.g., D'Imperio et al., 2023; Fest et al., 2017).

Considering the latest estimates (based on VISIT, JSBACH, and Memo models, Table S6 in the supplementary) we report here a mean estimate of 31 [17-39] Tg CH_4 yr^{-1} for 2000-2009 and 32 [18-40] for 2010-2019 Tg CH_4 yr^{-1} (Table 3).

3.3.5 CH_4 lifetime

The atmospheric lifetime of a given gas in steady state may be defined as the global atmospheric burden (Tg) divided by the total sink (Tg yr^{-1}) (IPCC, 2001). This value is different from what is called perturbation lifetime. Perturbation lifetime is used to determine how a one-time pulse emission may decay as a function of time as needed for the calculation of Global Warming Potentials (GWPs), and as a result is related to a theoretical concept. For CH_4, the corresponding perturbation lifetime that should be used in the GWP calculation is 11.8 ± 1.8 years (Forster et al., 2021). In this section, we discuss the

1609 global atmospheric lifetime (also called 'burden lifetime' or 'turnover lifetime') that characterises the time required to turn

1610 over the global atmospheric burden and defined as the burden divided by the removal flux.

1611 Global models provide an estimate of the loss of the gas due to individual sinks, which can then be used to derive lifetime

1612 due to a specific sink. For example, the tropospheric lifetime of CH_4 is determined as the global atmospheric CH_4 burden

1613 divided by the loss from OH oxidation in the troposphere, sometimes called "chemical lifetime". The total lifetime of

1614 CH_4 corresponds to the global burden divided by the total loss including tropospheric loss from OH oxidation, stratospheric

1615 chemistry and soil uptake. The CCMI (Plummer et al., 2021) and CMIP6 (Collins et al., 2021) runs estimate the tropospheric

1616 methane lifetime at about 9.2 years (average over years 2000-2009), with a range of 7.5-11 years (see Table S5). This range

1617 agrees with previous values found in ACCMIP and CCMI (9.3 [7.1-10.6] years, Voulgarakis et al. (2013), 9 [7.2-10.1] years,

1618 Saunois et al. (2020)). Adding 31 Tg to account for the soil uptake to the total chemical loss of the CMIP6 and CCMI

1619 models, we derive a total CH_4 lifetime of 8.2 years (average over 2000-2009 with a range of 6.8-9.7 years). The lifetime

1620 calculated over 2010-2019 based on CMIP6 simulations is similar (Table S5). These updated model estimates of total

1621 CH_4 lifetime agree with the previous estimates from ACCMIP (8.2 [6.4-9.2] years for year 2000, Voulgarakis et al. (2013))

1622 and Saunois et al. (2020) based CCMI models. Reducing the large spread in CH_4 lifetime (between models, and between

1623 models and observation-based estimates) would 1) bring an improved constraint on global total methane emissions, and 2)

1624 ensure an accurate forecast of future climate.

1625 **4 Atmospheric observations and top-down inversions**

1626 **4.1 Atmospheric observations**

1627 Systematic atmospheric CH_4 observations began in 1978 (Blake et al., 1982) with infrequent measurements from discrete

1628 air samples collected in the Pacific at a range of latitudes from 67°N to 53°S. Because most of these air samples were from

1629 well-mixed oceanic air masses and the measurement technique was precise and accurate, they were sufficient to establish

1630 an increasing trend and the first indication of the latitudinal gradient of methane. Spatial and temporal coverage was greatly

1631 improved soon after (Blake and Rowland, 1986) with the addition of the Earth System Research Laboratory from US

1632 National Oceanic and Atmospheric Administration (NOAA/GML) flask network (Steele et al. (1987); Lan et al. (2024), Fig.

1633 1), and the Advanced Global Atmospheric Gases Experiment (AGAGE) (Cunnold et al., 2002; Prinn et al., 2018), the

1634 Commonwealth Scientific and Industrial Research Organisation (CSIRO, Francey et al. (1999)), the University of California

1635 Irvine (UCI, Simpson et al.. 2012) and in situ and flask measurements from regional networks, such as ICOS (Integrated

1636 Carbon Observation System) in Europe (https://www.icos-ri.eu/). The combined datasets provide the longest time series of

1637 globally averaged CH_4 abundances. Since the early-2000s, CH_4 column-averaged mole fractions have been retrieved through

1638 passive remote sensing from space (Buchwitz et al., 2005a, 2005b; Butz et al., 2011; Crevoisier et al., 2009; Frankenberg et

1639 al., 2005; Hu et al., 2018). Ground-based Fourier transform infrared (FTIR) measurements at fixed locations also provide

time-resolved CH_4 column observations during daylight hours, and a validation dataset against which to evaluate the satellite measurements such as the Total Carbon Column Observing Network (TCCON) network (e.g., Pollard et al., 2017; Wunch et al., 2011), or Network for Detection of Atmospheric Composition Change (NDACC) (e.g., Bader et al., 2017).

In this budget, in-situ observations from the different networks were used in the top-down atmospheric inversions to estimate CH_4 sources and sinks over the period 2000-2020. Satellite observations from the TANSO/FTS instrument on board the satellite GOSAT were used to estimate CH_4 sources and sinks over the period 2010-2020. Other atmospheric data (FTIR, airborne measurements, AirCore, isotopic measurements, etc.) have been used for validation by some groups, but not specifically in this study. However, further information is provided in Tables S7, S8, S9, S10, and S11 and a more comprehensive validation of the inversions is planned to use some of these data.

4.1.1 In situ CH_4 observations and atmospheric growth rate at the surface

We use globally averaged CH_4 mole fractions at the Earth's surface from the four observational networks (NOAA/GML, AGAGE, CSIRO and UCI). The data are archived at the World Data Centre for Greenhouse Gases (WDCGG) of the WMO Global Atmospheric Watch (WMO-GAW) program (https://gaw.kishou.go.jp/), including measurements from other sites that are not operated as part of the four networks. The CH_4 in-situ monitoring network has grown significantly over the last decade due to the emergence of laser diode spectrometers which are robust and accurate enough to allow deployments with low maintenance enabling the development of denser networks in developed countries (Stanley et al., 2018; Yver Kwok et al., 2015), and new stations in remote environments (Bian et al., 2015; Nisbet et al., 2019).

The networks differ in their sampling strategies, including the frequency of observations, spatial distribution, and methods of calculating globally averaged CH_4 mole fractions. Details are given in the supplementary material of Kirschke et al. (2013). The global average values of CH_4 abundances at Earth's surface presented in Fig. 1 are computed using long-term measurements from background conditions with minimal influence from immediate emissions. All measurements are calibrated against gas standards either on the current WMO reference scale or on independent scales with well-estimate differences from the WMO scale. The current WMO reference scale, maintained by NOAA/ESRL, WMO-X2004A (Dlugokencky et al., 2005) was updated in July 2015. NOAA and CSIRO global means are on this scale. AGAGE uses an independent standard scale (based on work by Tohoku University (Aoki et al., 1992) and maintained at Scripps Institution of Oceanography (SIO)), but direct comparisons of standards and indirect comparisons of atmospheric measurements show that differences are well below 5 ppb (Tans and Zwellberg, 2014; Vardag et al., 2014) and the TU-1987 scale used for AGAGE measurements is only 0.5 ppb difference from WMO-X2004A at 1900 ppb level. UCI uses another independent scale that was established in 1978 and is traceable to NIST (Flores et al., 2015; Simpson et al., 2012), but has not been included in standard exchanges with other networks so differences with the other networks cannot be quantitatively defined. Additional experimental details are presented in the supplementary material from Kirschke et al. (2013) and references therein.

In Fig. 1 (a) globally averaged CH_4 and (b) its growth rate (derivative of the deseasonalized trend curve) through to 2022 are plotted for the four measurement programs using a procedure of signal decomposition described in Thoning et al. (1989). We define the annual G_{ATM} as the increase in the atmospheric concentrations from Jan. 1 in one year to Jan. 1 in the next year. Agreement among the four networks is good for the global growth rate, especially since ~1990. The large differences observed mainly before 1990 probably reflect the different spatial coverage of each network. The long-term behaviour of globally averaged atmospheric CH_4 shows a positive growth rate (defined as the derivative of the deseasonalized mixing ratio) that is slowing down from the early-1980s through 1998, a near-stabilisation of CH_4 concentrations from 1999 to 2006, and a renewed period with positive persistent overall accelerating growth rates since 2007, slightly larger after 2014. From 1999 to 2006, the annual increase of atmospheric CH_4 was remarkably small at 0.6±0.1 ppb yr^{-1}. After 2006, the atmospheric growth rate has increased to a level similar to that of the mid-1990s (~5 ppb yr^{-1}), and for 2014 and 2015 even to that of the 1980s (>10 ppb yr^{-1}). In the two recent years 2020 and 2021, the highest growth rates of 15 ppb yr^{-1} and 18 ppb yr^{-1} (see Sect. 6) were unprecedented since the 1980s. On decadal timescales, the annual increase is on average 2.2±0.3 ppb yr^{-1} for 2000-2009, 7.6±0.3 ppb yr^{-1} for 2010-2019 and 15.2±0.4 ppb yr^{-1} for the year 2020 (Table 3). Both climate variability and anthropogenic emission changes are responsible for variations in atmospheric CH_4 growth rates. Indeed, climate variation such as El Nino Southern Oscillation induce changes in emissions such as biomass burning or wetland emission but also impact OH oxidation (e.g., Rowlinson et al., 2019; Zhao et al., 2020b; Peng et al., 2022).

4.1.2 Satellite data of column average CH_4

In this budget, we use satellite data from the JAXA satellite Greenhouse Gases Observing SATellite (GOSAT) launched in January 2009 (Butz et al., 2011; Morino et al., 2011) containing the TANSO-FTS instrument, which observes in the shortwave infrared (SWIR). Different retrievals of CH_4 based on TANSO-FTS/GOSAT products are made available to the community: from NIES (Yoshida et al., 2013), from SRON (Schepers et al., 2012) and from University of Leicester (Parker et al., 2020; Parker and Boesch, 2020). The three retrievals are used by the top-down systems (Table 4 and S6). Although GOSAT retrievals still show significant unexplained biases and limited sampling in cloud covered regions and in the high latitude winter, it represents an important improvement compared to the first satellite measuring CH_4 from space, SCIAMACHY (Scanning Imaging Absorption spectrometer for Atmospheric CartograpHY) both for random and systematic observation errors (see Table S2 of Buchwitz et al. (2016)).

Here, as in Saunois et al. (2020), only inversions using GOSAT retrievals are used.

4.2 Top-down inversions used in the budget

An atmospheric inversion is the optimal combination of atmospheric observations, of a model of atmospheric transport and chemistry, of a prior estimate of CH_4 sources and sinks, and of their uncertainties, to provide improved estimates of the

sources and sinks, and their uncertainty. The theoretical principle of CH_4 inversions is detailed in the Supplementary Material and an overview of the different methods applied to CH_4 is presented in Houweling et al. (2017).

We consider an ensemble of inversions gathering various chemistry transport models, differing in vertical and horizontal resolutions, meteorological forcing, advection and convection schemes, and boundary layer mixing. Including these different systems is a conservative approach that allows us to cover different potential uncertainties of the inversion, among them: model transport, set-up issues, and prior dependency. General characteristics of the inversion systems are provided in Table 4. Further details can be found in the referenced papers and in the Supplementary Material. Each group was asked to provide gridded flux estimates for the period 2000-2020, using either surface or satellite data, but no additional constraints were imposed so that each group could use their preferred inversion setup. Two sets of prior emission distributions were built from the most recent inventories or model-based estimates (see Supplementary Material), but its use was not mandatory (see Table S8 to S11 for the inversion characteristics). This approach corresponds to a flux assessment, but not to a model inter-comparison as the protocol was not too stringent. Estimating posterior uncertainty is time and computer resource consuming, especially for the 4D-var approaches and Monte Carlo methods. Posterior uncertainties have not been requested for this study, but they were found to be lower than the ensemble spread in Saunois et al. (2020). Indeed, chemistry transport models differ in inter-hemispheric transport, stratospheric CH_4 profiles, and OH distribution, limitations which are not fully considered in the individual posterior uncertainty. As a result, we report the minimum-maximum range among the different top-down approaches.

Seven atmospheric inversion systems using global Eulerian transport models were used in this study; they contributed to the previous budgets that included eight atmospheric inversion systems in Saunois et al. (2016) and nine in Saunois et al. (2020). Each inversion system provided one or several simulations, including sensitivity tests varying the assimilated observations (surface or satellite), the OH interannual variability, or the prior fluxes ensemble. This represents a total of 24 inversion runs with different time coverage: generally, 2000-2020 for surface-based observations, and 2010-2020 for GOSAT-based inversions (Table 4 and Table S7). In poorly observed regions, top-down surface inversions may rely on the prior estimates and bring little or no additional information to constrain (often) spatially overlapping emissions (e.g., in India, China). Also, we recall that many top-down systems solve for the total fluxes at the surface only or for some categories that may differ from the GCP categories. When multiple sensitivity tests were performed the mean of this ensemble was used not to overweight one particular inverse system. It should also be noticed that some satellite-based inversions are in fact combined satellite and surface inversions as they use surface-based inversions to correct the latitudinal bias of the satellite retrievals against the optimised atmosphere measurements to correct for errors in the transport model especially in the stratosphere (e.g., Segers et al., 2022; Maasakkers et al., 2019). Nevertheless, these inversions are still referred to as satellite-based inversions. Most of the top-down models use the OH distribution from the TRANSCOM experiment (Patra et al., 2011) either as fixed over the period or with the interannual variability derived by Patra et al. (2021).

Each group provided gridded monthly maps of emissions for both their prior and posterior total and for sources per category (see the categories Sect. 2.3). Results are reported in Sect. 5. Atmospheric sinks from the top-down approaches have been provided for this budget, and are compared with the values reported in Saunois et al. (2020). Not all inverse systems report their chemical sink; as a result, the global mass imbalance for the top-down budget is derived as the difference between total sources and total sinks for each model when both fluxes were reported.

5 Methane budget: top-down and bottom-up comparison

5.1 Global methane budget

5.1.1 Global total methane emissions

Top-down estimates. At the global scale, the total annual emissions inferred by the ensemble of 24 inversions is 575 [553-586] Tg CH_4 yr^{-1} for the 2010-2019 decade (Table 3), with the highest ensemble mean emission of 608 [581-627] Tg CH_4 yr^{-1} for 2020. Global emissions for 2000-2009 (543 Tg CH_4 yr^{-1}) are consistent with Saunois et al. (2016, 2020) and the range for global emissions, 526-558 Tg CH_4 yr^{-1} falls within the range in Saunois et al. (2016) (535-569) and Saunois et al. (2020) (524-560), although the ensemble of inverse systems contributing to this budget is different from Saunois et al. (2016, 2020). Changes in ensemble members contributing to the different budgets are a feature of each new GMB release and, therefore, introduce a source of variation (Table S7). The range reported gives the minimum and maximum values among studies and does not reflect the individual full uncertainties. In addition, most of the top-down models use the same OH distribution from the TRANSCOM experiment (Patra et al., 2011), which introduces less variability to the global budget than is likely justified, and so contributes to the rather low range (10%) compared to bottom-up estimates (see below). We recall here that Zhao et al. (2020a) found an uncertainty of about 17% in global methane emissions (518 to 611 Tg CH_4 yr^{-1} for the early 2000s) due to changes in OH burden and distribution (OH ranging from 10.3 to 12.6 10^5 molec cm^{-3})

Bottom-up estimates. The bottom-up estimates considered here differ substantially from the top-down results, with annual global emissions being about 15% larger at 669 [512-849] Tg CH_4 yr^{-1} for 2010-2019 (Table 3). Yet, thanks to the double counting corrections in this budget, bottom-up and top-down budgets are in better agreement compared to previous GMB releases. For the period 2000-2009, the discrepancy between bottom-up and top-down was about 30% of the top-down estimates in Saunois et al. (2016, 2020) (167 and 156 Tg CH_4 yr^{-1}, respectively), a value that has been reduced significantly in this budget (now 95 Tg CH_4 yr^{-1} (<17%) for the same 2000-2009 period). This reduction is due to improvements from an important decrease in the estimate of emissions from natural and indirect anthropogenic emissions from bottom-up approaches, and more specifically inland freshwater emissions. From the previous budget, the estimate for inland freshwater emissions (lakes, ponds, reservoirs, rivers, and streams) has decreased from 159 Tg CH_4 yr^{-1} to 112 Tg CH_4 yr^{-1} (47 Tg decrease). Then, 23 Tg have been removed in the total freshwater ecosystem emissions due to double counting between vegetated wetlands and mostly small ponds and lakes (Sect. 3.2.2). As a result, the combined wetland and inland freshwater

emissions are estimated to be 242 Tg CH_4 yr^{-1} for 2000-2009 (Table 3), compared with 306 Tg CH_4 yr^{-1} in Saunois et al. (2020).

This budget is the first that reconciles bottom-up and top-down total emissions within the uncertainty ranges. However, the uncertainty in the global budget remains high because of the large range reported for emissions from freshwater systems. Still, the upper bound of global emissions from bottom-up approaches is not consistent with top-down estimates that rely on OH burden constrained by methyl chloroform atmospheric observations and is still likely overestimated.

5.1.2 Global methane emissions per source category

The global CH_4 emissions from natural and anthropogenic sources (see Sect. 2.3) for 2010-2019 are presented in Fig. 6, Fig. 7, and Table 3. Top-down estimates attribute about 65% of total emissions to anthropogenic activities (range of 55-70%), and 35% to natural emissions. Bottom-up estimates attribute 57% of emissions to direct anthropogenic and the rest to natural plus indirect anthropogenic emissions. A current predominant role of direct anthropogenic sources of CH_4 emissions is consistent with and strongly supported by available ice core and atmospheric CH_4 records. These data indicate that atmospheric CH_4 varied around 700 ppb during the last millennium before increasing by a factor of 2.6 to ~1800 ppb since pre-industrial times. Accounting for the decrease in mean-lifetime over the industrial period, Prather et al. (2012) estimated from these data a total source of 554±56 Tg CH_4 in 2010 of which about 64% (352±45 Tg CH_4) was of direct anthropogenic origin, consistent with the range in our top-down estimates.

Natural and indirect anthropogenic emissions. Although smaller than in previous Global Methane Budget releases, the main remaining discrepancy between top-down and bottom-up budgets is found for the natural and indirect anthropogenic emission total (105 Tg), with 311 [183-462] Tg CH_4 yr^{-1} for bottom-up and only 206 [188-225] Tg CH_4 yr^{-1} for top-down over the 2010-2019 decade (Table 3). In the bottom-up estimates, this discrepancy comes first from the estimates in both inland freshwater sources (64 Tg) and second from other natural sources (20 Tg from geological sources, termites, oceans, and permafrost). The top-down approaches may be biased due to missing fluxes (mainly inland freshwaters) in their prior estimates.

For 2010-2019, the top-down and bottom-up derived estimates for wetlands emissions of 165 [145-214] Tg CH_4 yr^{-1} and 159 [119-203] Tg CH_4 yr^{-1} (Table 3), respectively, are comparable within their range. Based on diagnostic wetland area values (see notes in Table 3), bottom-up mean wetland emissions for the 2000-2009 period are smaller in this study than those of Saunois et al. (2016) but larger than in Saunois et al. (2020). The changes in wetland emissions from bottom-up models may be related to updates on the wetland extent data set (WAD2M), the use of two different meteorological forcings for this study and a different set of models (see Sect. 3.2.1). Conversely, the current 2000-2009 mean top-down wetland estimates are lower than those of Saunois et al. (2016) and Saunois et al. (2020) (Table 3). In the bottom-up estimates, the amplitude of the range of emissions of 116-189 is roughly similar to Saunois et al. (2016) (151-222) and Saunois et al.

(2020) (102-179) for 2000-2009. Here, the larger range in bottom-up estimates of wetland emissions is due to the use of GSWP3-W5E5 and greater sensibilities of some models to the climate parameters, as discussed in Sect. 3.2.1. Bottom-up and top-down estimates for wetland emissions agree better in this study (~5 Tg yr^{-1} for 2000-2009) than in Saunois et al. (2016, 2020) (~17 Tg yr^{-1} and ~30 Tg yr^{-1}, respectively). Natural emissions from inland freshwater systems were not included in the prior fluxes used in the top-down approaches, due to unavailable or uncertain gridded products at the start of the modelling activity. However, emissions from these inland freshwater systems may be implicitly included in the posterior estimates of the top-down models, as these two sources are close and probably overlap at the rather coarse resolution of the top-down models. This is the reason why the 'wetland emissions' in the top-down budget in fact better correspond to the sum of combined wetland and inland freshwaters emissions in the bottom-up budget. The double-counting of 23 Tg CH_4 reduces the bottom-up budget for combined wetland and inland freshwaters from 271 Tg CH_4 yr^{-1} to 248 Tg CH_4 yr^{-1} (Sect. 3.2.2). Comparing the 2000-2009 decadal emissions from wetlands and inland freshwater ecosystems estimated by the bottom-up approaches across the last three Global Methane Budgets shows an upward and then a downward revision with 305 (183+122) Tg CH_4 yr^{-1}, 356 (147+209) Tg CH_4 yr^{-1} and 248 (159+112-23) Tg CH_4 yr^{-1} (respectively from Saunois et al. (2016, 2020) and this work; the sum in bracket corresponds to the sum of vegetated wetland emissions and inland water emissions estimated through the different budgets). The combined wetland and inland freshwater emissions discrepancy between bottom-up and top-down approaches amount to 105 Tg CH_4 yr^{-1} for the 2010-2019 decade. From a top-down point of view, the sum of all the natural sources is more robust than the partitioning between wetlands, inland waters, and other natural sources. Including all known spatio-temporal distributions of natural emissions in top-down prior fluxes would be a step forward to consistently compare natural versus anthropogenic total emissions between top-down and bottom-up approaches.

In the top-down budget, wetlands represent 28% on average of the total methane emissions but only 24% in the bottom-up budget (because of higher total emissions inferred) (see Table 3). Given the large uncertainties, neither bottom-up nor top-down approaches included in this study point to significant changes in wetland emissions between the two decades 2000-2009 and 2010-2019 at the global scale.

For the 2010-2019 decade, top-down inversions infer "Other natural emissions" (Table 3) at 43 [40-46] Tg CH_4 yr^{-1}, whereas the sum of the individual bottom-up emissions is 63 [24-93] Tg CH_4 yr^{-1}, contributing to a 20 Tg discrepancy between bottom-up and top-down approaches. Atmospheric inversions infer the same amount over the decade 2000-2009 as over 2010-2019, which is almost half of the value reported in Saunois et al. (2016) (68 [21-130] Tg CH_4 yr^{-1}). This reduction in magnitude and uncertainty is due to 1) a more consistent way of considering other natural emissions in the various inverse systems (same prior estimate as in this budget) and 2) a difference in the ensemble of top-down inversions reported here compared to previous releases. It is worth noting that, most of the top-down models include about the same ocean and onshore geological emissions and termite emissions in their prior scenarios. However,, none include freshwater or permafrost emissions in their prior fluxes, and thus in their posterior estimates.

Geological emissions are associated with relatively large uncertainties, and marine seepage emissions are still widely debated (Thornton et al., 2020). However, summing up all bottom-up fossil-CH_4 related sources (including anthropogenic emissions) leads to a total of 165 [135-190] Tg CH_4 yr^{-1} in 2010-2019, which is about 29% of the top-down global CH_4 emissions, and 25% of the bottom-up total global estimate. These results agree with the value inferred from ^{14}C atmospheric isotopic analyses of 30% contribution of fossil-CH_4 to global emissions (Etiope et al., 2008; Lassey et al., 2007b). This total fossil fuel emissions from bottom-up approaches agrees well with the ^{13}C-based estimate of Schwietzke et al. (2016) of 192 ± 32 Tg CH_4 yr^{-1}. In the bottom-up budget, the larger total emissions (due to uncertainties in bottom-up estimates of natural emissions) leads to a lower fossil fuel contribution compared to Lassey et al. (2007b).

Anthropogenic direct emissions. Total anthropogenic direct emissions for the period 2010-2019 were assessed to be statistically consistent between top-down (369 Tg CH_4 yr^{-1}, range 350-391) and bottom-up approaches (358 Tg CH_4 yr^{-1}, range 329-387), albeit top-down approaches infer direct anthropogenic emissions larger by 11 Tg CH_4 yr^{-1} on average compared to bottom-up approaches (Table 3). The partitioning of anthropogenic direct emissions between agriculture and waste, fossil fuels extraction and use, and biomass and biofuel burning, also shows good consistency between top-down and bottom-up approaches, though top-down approaches still suggest less fossil fuel and more agriculture and waste emissions than bottom-up estimates (Table 3 and Fig. 6 and 7). For 2010-2019, agriculture and waste contributed an estimated 228 [213-242]Tg CH_4 yr^{-1} in the top-down budget and 211 [195-231]Tg CH_4 yr^{-1} in the bottom-up budget. Fossil fuel emissions contributed 115 [100-124] Tg CH_4 yr^{-1}in the top-down budget and 120 [117-125] Tg CH_4 yr^{-1} in the bottom-up budget. Biomass and biofuel burning contributed 27 [26-27] Tg CH_4 yr^{-1} in the top-down budget and 28 [21-39]Tg CH_4 yr^{-1} in the bottom-up budget. Biofuel CH_4 emissions rely on very few estimates currently (Wuebbles and Hayhoe, 2002). Although biofuel is a small source globally (~12 Tg CH_4 yr^{-1}), more estimates are needed to allow a proper uncertainty assessment. Overall for top-down inversions the global fraction of total emissions for the different source categories is 40% for agriculture and waste, 20% for fossil fuels, and 5% for biomass and biofuel burning. With the exception of biofuel emissions, the uncertainty associated with global anthropogenic emissions appears to be smaller than that of natural sources but with an asymmetric uncertainty distribution (mean significantly different than median). The relative agreement between top-down and bottom-up approaches may indicate a limited capability of the inversion to separate emissions and a dependency to their prior fluxes; this agreement should therefore be treated with caution. Indeed, in poorly observed regions, top-down inversions rely on the prior estimates and bring little or no additional information to constrain (often) spatially overlapping emissions (e.g., in India, China). Also, as many top-down systems solve for the total fluxes at the surface or for some categories that may differ from the GCP categories, their posterior partitioning relies on the prior ratio between categories that are prescribed using bottom-up inventories.

5.1.3 Global budget of total methane sinks

Top-down estimates. The annual CH_4 chemical removal from the atmosphere is estimated to be 521 Tg CH_4 yr^{-1} averaged over the period 2010-2019, with an uncertainty of about ±2% (range 485-532 Tg CH_4 yr^{-1}) (Table 3). All the inverse models account for CH_4 oxidation by OH and O(^{1}D), and some include stratospheric Cl oxidation (Table S8 to S11). Most of the top-down models use the OH distribution from the TRANSCOM experiment (Patra et al., 2011) either as fixed over the period or including interannual variability from Patra et al. (2021). This study shows no trend in OH and IAV below ±4%, in agreement with Thompson et al. (2024) (no significant OH trend and IAV < 2%). As a result, the range of the top-down sink estimates is rather low compared to bottom-up estimates (see below). Differences between transport models affect the chemical removal of CH_4, leading to different chemical loss rates, even with the same OH distribution. However, uncertainties in the OH distribution and magnitude (around ±10% at the global scale, Zhao et al., 2019) are not considered in our study, while they could contribute to a significant change in the chemical sink, and then in the derived posterior emissions through the inverse process ((Zhao et al., 2020), around ±17% at the global scale, much larger than the model spread derived here. The chemical sink represents more than 90% of the total sink, the rest being attributable to soil uptake (35 [35-36] Tg CH_4 yr^{-1}). The rather narrow range is due to the use of the same climatological soil sink provided within the modelling protocol which is based on Murgia-Flores et al. (2018). This sink estimate used as prior in the inversions is a bit higher than the mean estimate of the soil sink calculated by bottom-up models (30 Tg CH_4 yr^{-1}, Sec. 3.3.4).

Bottom-up estimates. The total chemical loss for the 2010s reported here is 602 Tg CH_4 yr^{-1} with an uncertainty of 21% (~125 Tg CH_4 yr^{-1}). Differences in chemistry schemes in the models (especially in the stratosphere) and in the volatile organic compound treatment probably explain most of the discrepancies among models (Zhao et al., 2019).

5.2 Latitudinal and regional methane budgets

The latitudinal and regional breakdown of the bottom-up budget is based on crude assumptions that we acknowledge here. Natural and indirect anthropogenic emissions are based on wetland gridded products from land surface models and the combination of the maps from lakes and ponds from Johnson et al. (2022), reservoirs from Johnson et al. (2022) and streams and rivers from Rocher-Ros et al. (2023), the sum of those three scaled to 89 Tg CH_4 yr^{-1} (shown in Fig. 5) to artificially include the double counting (estimated only at the global scale) and match the global estimate. However, we acknowledge that this procedure distributes the double counting relatively to the final emission distribution and not according to the freshwater ecosystems where the double counting probably occurs. Wild animal and permafrost maps do not exist and are missing from the calculation, leading to at least 3 Tg CH_4 yr^{-1} of discrepancy. However, as aforementioned (Sections 3.2.5 and 3.2.7) this 3 Tg CH_4 yr^{-1} estimate is probably underestimated in the bottom-up budget. Geological and ocean sources are based on Etiope et al. (2019) and Weber et al. (2019) gridded products scaled to 50 Tg CH_4 yr^{-1} to be consistent to the reported global values. Finally, we use the termite emission map produced for this budget and used in the global budget.

1891   The latitudinal budget does not include the estimates from FAO and USEPA for the direct anthropogenic emissions as they

1892   are only provided at country scale.

5.2.1 Latitudinal budget of total methane emissions

1894   The latitudinal breakdown of emissions inferred from atmospheric inversions reveals a dominance of emissions in the

1895   latitudinal band 90°S-30°N of 364 [337-390] Tg CH_4 yr^{-1}, representing 64% of the global total (Table 5 and 6). As emissions

1896   in the Tropics (30°S-30°N) dominate this latitudinal contribution, we may refer to 90°S-30°N as the Tropics in the following

1897   32% of the emissions are from the mid-latitudes (187 [160-204] Tg CH_4 yr^{-1}) and 4% from high latitudes (above 60°N). The

1898   amounts of emissions depend on the land surface area of the region, however the 90°S-30°N latitudinal band represents 53%

1899   of global land surfaces and the boreal region 60°N-90°N around 13%. Hence, the relative contribution of the emissions from

1900   the 90°S-30°N region is much larger (11 points of percent more) than the percentage of its land surface areas, on the contrary

1901   the boreal regions (60°N-90°N) emissions contribute significantly less than the surface area percentage of this region (9

1902   points of percent less). The ranges around the mean latitudinal emissions are larger than for the global CH_4 sources. While

1903   the top-down uncertainty is less than ±5% at the global scale, it increases to ±7% for the tropics, to ±12% the northern mid-

1904   latitudes and to more than ±20% in the northern high-latitudes (for 2010-2019, Table 5). Both top-down and bottom-up

1905   approaches consistently show that CH_4 decadal emissions have increased by +21-27 Tg CH_4 yr^{-1} in the tropics, and by +5-

1906   16 Tg CH_4 yr^{-1} in the northern mid-latitudes between 2000-2009 and 2010-2019 using the mean ensemble estimate.

1907   Over 2010-2019, at the global scale, satellite-based inversions infer almost identical emissions to ground-based inversions

1908   (difference of +1 [-3-9] Tg CH_4 yr^{-1}, with GOSAT based inversion a bit higher than surface measurements-based inversions),

1909   when comparing consistently surface versus satellite-based inversions for each system, similar to Saunois et al. (2020). This

1910   difference is much lower than the range derived between the different systems (range of 20 Tg CH_4 yr^{-1} using surface- or

1911   satellite-based inversions). This result reflects that differences in atmospheric transport among the systems probably have

1912   more impact on the estimated global emissions than the types of observations assimilated.

1913   As expected, considering the different coverage of observation datasets, regional distributions of inferred emissions differ

1914   depending on the nature of the observations used (satellite or surface). The largest differences (satellite-based minus surface-

1915   based inversions) are observed over the tropical region, between -10 and +43 Tg CH_4 yr^{-1} (90°S to 30°N), and the northern

1916   mid-latitudes (between -36 and -2 Tg CH_4 yr^{-1}). Satellite data provide stronger constraints on fluxes in tropical regions than

1917   surface data, due to a much larger spatial coverage. It is therefore not surprising that differences between these two types of

1918   observations are found in the tropical band, and consequently in the northern mid-latitudes to balance total emissions, thus

1919   affecting the north-south gradient of emissions. However, the regional patterns of these differences are not consistent

1920   through the different inverse systems. Indeed, some systems found higher emissions in the tropics when using GOSAT

1921   instead of surface observations, while others found the opposite. This difference between inversion systems may depend on

1922 whether or not a bias correction is applied to the satellite data based on surface observations, and also on the modelled
1923 horizontal and vertical transports, in the troposphere and in the stratosphere.

5.2.2 Latitudinal methane emissions per source category

1925 The analysis of the latitudinal CH_4 budget per source category (Fig. 8 and Table 6) can be performed both for bottom-up
1926 and top-down approaches but with limitations. Bottom-up estimates of natural and indirect anthropogenic emissions are
1927 based on assumptions as specified at the beginning of this section 5.2. For top-down estimates, as already noted, the
1928 partitioning of emissions per source category has to be considered with caution. Indeed, using only atmospheric
1929 CH_4 observations to constrain CH_4 emissions makes this partitioning largely dependent on prior emissions. However,
1930 differences in spatial patterns and seasonality of emissions can be utilised to constrain emissions from different categories
1931 by atmospheric methane observations (for those inversions solving for different sources categories, see Sect. 2.3).
1932 Agriculture and waste are the largest sources of CH_4 emissions in the tropics and southern hemisphere (140 [121-150] Tg
1933 CH_4 yr^{-1} in the bottom-up budget and 150 [135-168] Tg CH_4 yr^{-1} in the top-down budget, about 40% of total CH_4 emissions
1934 in this region) (Table 6). However, combined wetland and inland freshwater emissions are nearly as large with 151 [85-234]
1935 Tg CH_4 yr^{-1} in the bottom-up budget and 128 [112-155] Tg CH_4 yr^{-1} in the top-down budget (Table 6). Anthropogenic
1936 emissions dominate in the northern mid-latitudes, with the highest contribution from agriculture and waste emissions (40%
1937 of total emissions in the top-down budget), closely followed by fossil fuel emissions (32% of total emissions, top-down
1938 budget). Boreal regions are largely dominated by inland freshwater emissions (41% and 54% of total emissions, top-down
1939 and bottom-up budget, respectively) (Table 6).
1940 The largest discrepancies between the top-down and the bottom-up budgets are found in the mid-latitudes and boreal regions
1941 from the natural and indirect sources with bottom-up estimates twice as large as the top-down ones, especially in the inland
1942 freshwater category.
1943 The uncertainty for wetlands and inland freshwater emissions is larger in the bottom-up models than in the top-down models
1944 (mostly wetlands), while uncertainty in anthropogenic emissions is larger in the top-down models than in the bottom-up
1945 inventories. The large uncertainty in tropical inland freshwater emissions (mostly wetlands) of ±44% results from large
1946 regional differences between the bottom-up land-surface models. Although they are using the same forcings, their responses
1947 in terms of flux density show different sensitivities to temperature, water vapour pressure, precipitation, and radiation.

5.2.3 Regional budget for total emissions

1949 The regional breakdown of emissions is provided for 18 continental regions (see map in Fig. S3 and Table S1 with the
1950 country aggregation in the supplementary materials).
1951 At the regional scale and, for the 2010-2019 decade (Table 7), total methane emissions are dominated by South East Asia
1952 with 63 [52-71] Tg CH_4 yr^{-1}, China with 57 [37-72] Tg CH_4 yr^{-1}, and South Asia with 52 [43-60] Tg CH_4 yr^{-1} (top-down

budget). These top three emitters contribute 30% of total global CH_4 emissions. The following high emitting regions are Brazil 47 [41-58] Tg CH_4 yr^{-1}, Equatorial Africa 47 [39-59] Tg CH_4 yr^{-1}, USA 38 [32-46] Tg CH_4 yr^{-1}, Southwest South America 38 [30-48] Tg CH_4 yr^{-1}, Russia 36 [27-45] Tg CH_4 yr^{-1}, Europe 31 [24-36] Tg CH_4 yr^{-1}, Middle East 31 [24-39] Tg CH_4 yr^{-1}, Northern Africa 25 [23-29] Tg CH_4 yr^{-1}, and Canada 20 [17-24] Tg CH_4 yr^{-1}. Other regions contribute less than 20 Tg CH_4 yr^{-1}.

5.2.4 Regional budget per source category

Natural and indirect anthropogenic emissions versus direct anthropogenic emissions. In agreement with Stavert et al. (2021), natural and indirect anthropogenic emissions are dominated by Brazil, Canada, Russia, Equatorial Africa and Southeast Asia, contributing 126 Tg CH_4 yr^{-1} in the bottom-up and 105 Tg CH_4 yr^{-1} in the top-down budget (Table 7), i.e., 47% and 50% of the global natural and indirect anthropogenic emissions in these budgets, respectively. At regional scale also, the range of uncertainty in natural and indirect anthropogenic emissions are much larger in the bottom-up budget than in the top-down budget (Fig. S5). Except for 4 regions (Canada, Brazil, Northern South America, Southwest South America), direct anthropogenic emissions contribute more than half of the total regional emissions. Due to the large uncertainty and discrepancies in natural and indirect emissions estimates, the regional direct anthropogenic fractions may differ between the bottom-up and top-down budgets. However, in absolute values, the highest direct anthropogenic emitters are the same in the two budgets with China and South Asia being the top two by far, contributing 56 [51-66] Tg CH_4 yr^{-1} and 45 [44-47] Tg CH_4 yr^{-1}, respectively (bottom-up values, Fig. 9 and Table 7). These two regions contribute 28% (26%) of the global direct anthropogenic emissions in the bottom-up (top-down) budget. The ranks of direct anthropogenic emitters are similar to those presented in the last budget (Stavert et al., 2021). Southeast Asia, United States of America, Middle East, Europe, Equatorial Africa, and Russia emit between 32 Tg CH_4 yr^{-1} and 23 Tg CH_4 yr^{-1} as direct anthropogenic emissions (bottom-up values, Fig 8). Brazil, Northern Africa, and Southwest South America emit between 10 CH_4 yr^{-1} and 20 CH_4 yr^{-1}, while the rest of the regions emit less than 10 CH_4 yr^{-1} direct anthropogenic emissions (Table 7 and Fig. S5).

Sectoral emissions. The sectoral partitioning at the regional scale has been derived from both bottom-up and top-down approaches. However, the top-down budget has more limitations, as the sectoral partitioning is usually based on the prior fluxes fractions at the pixel scale, and assimilating only total methane observations does not allow to disentangle the different source sectors overlapping in a pixel grid. However, differences in spatial patterns and seasonality of emissions can still be constrained by atmospheric CH_4 observations for those inversions solving for different sources categories (see Sect. 2.3). Bottom-up approaches allow deeper sectorial splitting, especially in terms of direct anthropogenic emissions (Fig. 9). Table 7, Fig. 9 and Fig. 10 present the estimations of CH_4 emissions on average over 2010-2019. Fig. 10 presents the budgets for three main categories (Combined wetland and inland freshwaters, Fossil fuels and Agriculture & Waste), a more detailed figure and table including the five categories is available in the supplementary material (Fig. S6 and Table S13 to S18).

1985   Values for each individual data-set for the decades 2000-2009, 2010-2019, and the last year 2020 are made available in a

1986   spreadsheet (see Data Availability).

1987   For most regions, "Combined wetland and inland freshwater emissions" are the most uncertain in the bottom-up budget,

1988   and generally their range is larger than in the top-down budget. In the top-down budget for 2010-2019 (Table 7), this category

1989   contributes the most to the regional emissions in Brazil 24 [20-33] Tg CH_4 yr^{-1}, Southeast Asia 24 [14-29] Tg CH_4 yr^{-1}

1990   (though similar to their Agriculture and Waste emissions 24 [21-31] Tg CH_4 yr^{-1}), Equatorial Africa 22 [19-28] Tg CH_4 yr-

1991 ^{1}, Southwest South America 22 [14-33] Tg CH_4 yr^{-1}, Canada 12 [9-18] Tg CH_4 yr^{-1}, Northern South America 8 [6-10] Tg

1992 CH_4 yr^{-1}, Southern Africa 7 [4-9] Tg CH_4 yr^{-1}. Agriculture and Waste emissions dominates in South Asia 39 [33-43] Tg CH_4

1993   yr^{-1}, China 30 [13-37] Tg CH_4 yr^{-1}, Europe 19 [16-23] Tg CH_4 yr^{-1}, United States of America 13 [9-16] Tg CH_4 yr^{-1}, Northern

1994   Africa 13 [12-14] Tg CH_4 yr^{-1}, Central America 9 [8-10] Tg CH_4 yr^{-1}, and Korea and Japan 3 [3-4] Tg CH_4 yr^{-1}. Fossil fuel

1995   emissions dominate in the Middle East 18 [11-24] Tg CH_4 yr^{-1} and Russia 14 [8-23] Tg CH_4 yr^{-1} (close to their combined

1996   wetland and inland freshwater emissions of 11 [8-13] Tg CH_4 yr^{-1}).

1997   The four largest contributors to the Fossil Fuel sector remain China, the Middle East, Russia, and the United States of

1998   America. Altogether they contribute 67 (64) Tg CH_4 yr^{-1} in the bottom-up (top-down) budget, around 55% of the global

1999   fossil fuel emissions. The bottom-up and top-down approaches generally agree in terms of ensemble mean, except for China

2000   for which the top-down estimates suggest lower emissions than the inventories. While Chinese fossil fuel emissions occur

2001   mainly through coal mining activity (88%), the Middle East, Russia and the USA extract mainly oil and gas (100%, 80%,

2002   72%).

2003   The three largest contributors to the Agriculture and Waste sector remain South Asia, China, and Southeast Asia. Together

2004   they contribute 88 (92) Tg CH_4 yr^{-1} in the bottom-up (top-down) budget, around 40% of the global agriculture and Waste

2005   sector (Table 7). While the ensemble means tend to agree between bottom-up and top-down budgets, the uncertainty derived

2006   from the top-down approaches is larger, especially for these three regions. CH_4 emissions due to rice cultivation originate

2007   mostly from these same three regions (South East Asia, China and South Asia). Livestock management emissions occurs

2008   mainly in South Asia 20 [18-22] Tg CH_4 yr^{-1}, Brazil 12 [11-13] Tg CH_4 yr^{-1}, China 11 [8-16] Tg CH_4 yr^{-1}, and Europe 11

2009   [10-12] Tg CH_4 yr^{-1} (bottom-up estimates, Table 7). The United States of America, Equatorial Africa, Northern Africa and

2010   Southwest South America emit between 7 Tg CH_4 yr^{-1} and 10 Tg CH_4 yr^{-1} in this sub-sector. Other regions emit less than 4

2011   Tg CH_4 yr^{-1} in the livestock management sector. The Waste sector emissions are dominated by three regions: China 11 [6-

2012   14] Tg CH_4 yr^{-1}, South Asia 9 [4-11] Tg CH_4 yr^{-1}, and Europe 8 [6-12] Tg CH_4 yr^{-1} (bottom-up estimates, Table 7). These

2013   three regions contribute around 40% of the global emissions of the Waste sector. It is worth noting that the uncertainty in

2014   the inventory estimates at the regional scale is around 40% (from the min-max range of the estimate, not including the

2015   uncertainty from each inventory).

6 Insights on the methane cycle from 2020-2022 during which there has been unprecedented high growth rates of methane emissions

The mean emissions estimate for the last year of the budget (2020) was 608 [581-627] Tg CH$_4$ yr^{-1} (Top-down),) with 65% of the emissions from direct anthropogenic sources. This is 65 Tg CH$_4$ yr^{-1} higher (11%) than the mean emissions of the 2000-2009 decade and 6% higher than 2010-2019. In Jackson et al. (2024), we estimated that total methane emissions increased by around 20% between the early 2000s (2000-2002) and the late 2010s (2018-2020). 2020 was a second highest year in terms of atmospheric CH$_4$ growth rate (+15.2 ppb/yr) since systematic measurements began in the late 1980s, coming in just behind the highest in 2021 at 17.97 ppb/yr. A few studies analysed the large growth rate increase between 2019 (+9.7 ppb/yr) and 2020 (+15.2 ppb/yr) of +5.4 ppb/yr (corresponding to +14.4 ± 2.0 Tg CH$_4$ yr^{-1}) (Peng et al., 2022; Stevenson et al., 2022). Peng et al. (2022) estimated that the 2019-2020 growth rate change was almost equally due to an increase in wetland emissions (6.9 ± 2.1 Tg CH$_4$ yr^{-1}) and a decrease of the OH chemical loss (7.5 ± 0.8 Tg CH$_4$ yr^{-1}) due to reduced OH precursor emissions during the COVID lockdown (Laughner et al., 2021). The COVID19 lockdown resulted in decreased NO$_x$ emissions and reduced fossil fuel related CH$_4$ emissions (Thorpe et al., 2023), leading to less OH production. At the global scale, Feng et al. (2023) calculated an emission increase of 27 Tg CH$_4$ yr^{-1} between 2019 and 2020 considering constant OH, and a smaller increase of 21 Tg CH$_4$ yr^{-1} when including a 1.4% decrease of OH. Increased emissions were mainly found in the northern tropics. Qu et al. (2022) also inferred a 31 Tg CH$_4$ yr^{-1} increase of emissions, mostly in the tropics, half of it in Africa. Furthermore, Niwa et al. (2024) suggested emission increases by 10–18 Tg CH4 yr-1 in 15°S—10°N and by 20 Tg CH4 yr-1 in 10–35°N from 2016–2019 to 2020–2022. Such a result is compatible with wetland driven abnormal emissions during a consecutive 3-year La Nina event spanning from 2020 to 2022 (Zhang et al., 2023; Nisbet et al., 2023). The difference in terms of methodology and approaches between these three studies make it difficult to compare them quantitatively but provide a robust understanding on the possible causes. Importantly, all the studies indicate, in various proportions, increasing CH$_4$ emissions in the tropics and in the boreal region, potentially driven by microbial emission from wetlands due to wetter and warmer climate , and a significant contribution of reduced OH concentrations due to COVID lockdown.

Based on our ensemble of data, we find that top-down approaches infer a much larger change in CH$_4$ emissions (median [Q1-Q3] at +23 [10-31] Tg CH$_4$ yr^{-1}) than bottom-up approaches (-1 [-5-3] Tg CH$_4$ yr^{-1}) between 2019 and 2020 (Fig. S7). Bottom-up approaches suggest a very small increase in wetland emissions (around (+1 [0-3] Tg CH$_4$ yr^{-1}), while top-down approaches suggest on average a larger increase for wetlands of +8 [5-11] Tg CH$_4$ yr^{-1}, mainly in the tropics and mid-latitudes. It is worth noting that large uncertainties exist for a given year and that the inter annual variability is much lower than the ensemble spread. While bottom-up approaches suggest almost constant fossil fuel emissions and slight increase in agriculture and waste (+3 Tg CH$_4$ yr^{-1}), top-down approaches tend to derive higher emissions changes (+6 Tg CH$_4$ yr^{-1} from the fossil fuel sector and +11 Tg CH$_4$ yr^{-1} from agriculture and waste as the median over the ensemble). Biomass

burning emissions decreased using both approaches by about 5 Tg CH_4 yr^{-1} in agreement with Peng et al. (2022). Some inversions were run with IAV of OH from Patra et al. (2021) and others with constant OH. However, the inferred OH IAV in 2019 and 2020 are rather low (0.3% and 0.15% on yearly average) in Patra et al. (2021), leading to a small impact in terms of emissions changes between 2019-2020, with +22 [9-31] (median [Q1-Q3]) based on the inversions with constant OH and 19 [7-28] based on the inversions with varying OH (Fig S8).

This first analysis based on our ensemble shows how challenging it is to attribute CH_4 emissions changes to a specific sector or region between two years, because related uncertainties remain much larger than the targeted signal to explain. This calls again for further improvement of both approaches.

NOAA estimates of 2021 and 2022 methane atmospheric growth rates 17.8.0±0.5 ppb/yr and 14.0±0.8 ppb/yr, respectively (Lan et al., 2024). They show a continuation of very high growth rates, challenging again our understanding of the methane budget. The very high values of CH_4 growth rate over 2020-2022 have also been accompanied by a sharp decline in the stable isotopic signal, $\delta^{13}C_{CH_4}$, which suggest that this recent increase of methane growth rate is at least partly explained by increased emissions from microbial sources such as those found in wetlands, inland waters, agriculture and waste systems (Nisbet et al., 2023; Michel et al., 2024). However, it is worth noting that almost all published top-down studies aforementioned include constraints only on CH_4, and do not discuss the consistency with the atmospheric isotopic signal.

As of the time of submission of this manuscript, bottom-up estimates for anthropogenic emissions for 2021 and 2022 are only available from the EDGARv8 data set (https://edgar.jrc.ec.europa.eu/dataset_ghg80; EDGAR, 2023). This research inventory suggests that anthropogenic emissions continued to increase from 2020 (374 Tg CH_4 yr^{-1}) to 2021 (379 Tg CH_4 yr^{-1}) and 2022 (386 Tg CH_4 yr^{-1}) with around 62% of the increase due to the fossil fuel sources, 23 % from the Waste sector, and 14% from the agriculture sector (Table S19). The bottom-up estimate of wetland emissions for 2021-2023, derived from a single wetland model, indicates positive anomalies of 26 Tg CH_4 yr^{-1} in 2020, 23 Tg CH_4 yr^{-1} in 2021, and 21 Tg CH_4 yr^{-1} 2022 relative to the 2000-2006 baseline (https://earth.gov/ghgcenter/data-catalog/lpjwsl-wetlandch4-grid-v1; Zhang et al., 2023).

7 Future developments, missing elements, and remaining uncertainties

In this budget, robust features and uncertainties on sources and sinks estimated by bottom-up or top-down approaches have been highlighted as well as discrepancies between the two budgets. Limitations of the different approaches have also been highlighted. Four shortcomings of the CH_4 budget were already identified in Kirschke et al. (2013) and Saunois et al. (2016, 2020) and are revisited below pointing to key research areas. Although much progress has been made, they are still relevant, and actions are needed. However, these actions fall into different timescales and actors. Here, we revisit the four shortcomings of the contemporary methane budget and discuss how each weakness has been addressed since Saunois et al. (2020). Each section ends by discussing remaining research needs with a list of suggestions, from higher to lower priority.

1. Shortcoming 1: *Towards a decrease of the high uncertainty in the amount of methane emitted by wetland and inland water systems, and a weakened double counting issue.*

This first shortcoming has probably received the largest interest in the last few years with significant improvements. First a community effort has been made based on more studies, documenting, or modelling more inland freshwater systems and synthesising emissions from the complex and heterogeneous ensemble of emitting areas: wetlands, ponds, lakes, reservoirs, streams, rivers, estuaries, and marine systems. The range of wetland and inland water emissions has been narrowed down with improved wetland extent and refined estimates for inland freshwater systems. Double counting between inland freshwater systems has been estimated for the first time and accounted for in this budget. All these improvements decreased the discrepancy between top-down and bottom-up estimate of combined wetland and inland freshwater emissions from 156 Tg CH_4 yr^{-1} in Saunois et al. (2020) down to 85 Tg CH_4 yr^{-1} in this update for the 2000-2009 decade. Gridded maps for lakes, ponds, reservoirs, and streams and rivers freshwater emissions have been produced over the past years (Johnson et al., 2021, 2022; Rocher-Ros et al., 2023) making the spatial distribution of CH_4 sources almost complete for the first time and allowing better description of prior emissions in future top-down inversions.

Next steps include on the short term from highest to lowest priority include:

(i) integration of spatial distribution of inland waters in atmospheric inversion models to reach a full description of prior methane sources and sinks.

(ii) refinement of double counting estimation and its possible reduction with more precise spatial and temporal distributions of the different systems contributing to inland freshwater emissions by using very high-resolution satellite data (down to metre resolutions) to properly separate them. The development of a dynamical global high-resolution (typically few metres) classification of saturated soils and inundated surfaces based on satellite data (visible and microwave), surface inventories, and expert knowledge.

(iii) continuation of ongoing efforts to calibrate and evaluate land surface models for wetland emissions against in-situ observations such as FLUXNET-CH4 (Knox et al., 2019; Delwiche et al., 2021) or BAWLD-CH4 (Kuhn et al., 2021) for boreal regions and avoid dependence on top-down estimates. It is still critical to increase the limited number of tropical observations and to assimilate them in the inverse systems to help address the issue (e.g., Kallingal et al., 2024).

(iv) continuation of ongoing efforts to develop a diversity of modelling approaches (among them process-based model or machine learning approaches) to estimate wetland and inland freshwater CH4 emissions, including lateral fluxes, and reducing upscaling issues, as done by e.g. Zhuang et al. (2023) for lakes.

(v) continuous integration of collected flux measurements such as in the FLUXNET-CH4 activity (Knox et al., 2019; Delwiche et al., 2021) or in BAWLD-CH4 data set (Kuhn et al., 2021) to provide global flux maps based on machine learning approaches or other approaches (Peltola et al., 2019, McNicol et al., 2023).

Over the long run, developing measurement systems will help to improve estimates of the diversity of wetland and inland freshwater sources, and further reduce uncertainties:

- More systematic measurements of CH_4 fluxes and their isotopic signatures from sites reflecting the diversity of environment of wetlands and inland waters, complemented with environmental meta-data (e.g., soil temperature and moisture, vegetation types, water temperature, acidity, nutrient concentrations, NPP, soil carbon density for wetlands, lake morphologies) will allow us to better understand and estimate the processes of production and transport to the atmosphere (diffusive, ebullitive, plants mediated..) and to better constrain methane fluxes and their isotopic signatures in the different modelling approaches (Glagolev et al., 2011; Turetsky et al., 2014).

2. Shortcoming 2: *Towards a better assessment of uncertainties for global methane sinks in top-down and bottom-up budgets.*

The inverse systems used here have similar caveats than those described in Saunois et al. (2016, 2020) (same OH field, same kind of proxy method to optimise it) leading to quite constrained atmospheric sink and therefore total global CH_4 sources. Although we have used the latest release of CCMI-2022 (Plummer et al., 2021) and CMIP6 simulations (Collins et al., 2017), the uncertainty of derived CH4 chemical loss from the chemistry climate models remains at the same (large) level compared to the previous intercomparison project ACCMIP (Lamarque et al., 2013). The causes of uncertainties on the CH_4 loss and the differences between the different OH fields derived from Chemistry Transport Models (CTM) and Climate Chemistry Models (CCM) have been widely discussed (e.g., Nicely et al., 2017; Zhao et al., 2019, 2020a). These results emphasise the need to first assess, and then improve, atmospheric transport and chemistry models, especially vertically, and to integrate robust representation of OH fields in atmospheric models. Recently, numerous efforts based on satellite data have been made to constrain OH distribution, variability and trends (e.g, Anderson, 2023,2024; Pimlott et al. 2022; Zhao et al., 2023; Zhu et al., 2022). Finally, soil uptake estimates rely on very few studies, and interannual variations remain underconstrained.

Next steps, in the short term, could include developments by the modelling community in:

- Estimating the soil uptake with different land surface models (creating an ensemble) and discussing its variations over the past decade.
- Assessing the impact of using updated and varying soil uptake estimates, especially considering a warmer climate in the top-down approach. Indeed, for top-down models resolving for the net flux of CH_4 at the surface integrating a larger estimate of soil uptake would allow larger emissions, and then reduce the uncertainty with the bottom-up estimates of total CH_4 sources.
- Further studying the reactivity of the air parcels in the chemistry climate models and defining new diagnostics to assess modelled CH4 lifetimes such as in Prather et al. (2023).

- Developing benchmarking of CTM and CCM regarding simulated OH distribution and variability (as in Zhao et al. (2019) for example) to increase efforts to assess biases and improve atmospheric chemical schemes in CTM and CCM.

- Developing methods to better constrain OH. Numerous have been proposed: satellite CH_4 observations (Zhang et al., 2018; Anderson et al., 2023; 2024) could afford this but strategy is needed (see Duncan et al., 2024 and references therein); using halogenated compounds beyond methyl chloroform (MCF), such as done in box models (Thompson et al., 2024) to derive a 3D dynamical OH. Such methods should be able to reach very low uncertainty for OH burden and trends (<2%) in order to really better constrain the CH_4 budget. Duncan et al. (2024) discuss the existing satellite-based methods and propose a strategy to constrain OH from space-based approaches.

- Integrating the aforementioned different potential OH chemical fields, including also inter annual variability, to assess the impact on the methane budget following Zhao et al. (2020).

Over the long run, other parameters should be (better) integrated into top-down approaches, among them:

- The magnitude of the CH_4 loss through oxidation by tropospheric Cl, a process debated in the recent literature. More modelling (e.g., Thanwerdas et al., 2022b) and instrumental studies should be devoted to reducing the uncertainty of this potential additional sink before integrating it in top-down models. This would be especially critical if inversions using ^{13}C-CH4 observations are included in GMB in the future.

3. Shortcoming 3: Towards a better partitioning of methane sources and sinks by region and process using top-down models

In this work, we report inversions assimilating satellite data from GOSAT, which bring more constraints than provided by surface stations alone, especially over tropical continents. However, we still found that satellite- and surface-based inversions, and the different inversion systems do not consistently infer the same regional flux distribution.

The estimates contributing to the Global Methane budget are further used in more specific studies focusing on the comparison of the estimates from bottom-up and top-down approaches at national (Deng et al., 2022) and regional scales, including efforts from the GCP-REgional Carbon Cycle Assessment and Processes (RECCAP2) (Petrescu et al., 2021; 2023; Tibrewal et al., 2024; Lauerwald et al., 2023b; and other RECCAP-2 publications to come, see https://www.globalcarbonproject.org/reccap/publications.htm).

Next steps, in the short term, could integrate developments to be made by the top-down community:

- Including GOSAT 2 retrievals (Noël et al., 2022; Imasu et al., 2023) for the GOSAT-based inversions and considering TROPOMI-based inversions (as done in Tsuruta et al. (2023), Shen et al. (2023), Chen et al. (2022), Qu et al. (2021)   or Y   u et al. (2023)) in the next releases once at least 8 years of data are available to provide a decadal estimate and biases are reduced for global scale use (Lorente et al., 2023; Balasu et al., 2023). Indeed,

2175 recent satellite developments have provided higher temporal and spatial resolutions of CH_4 observations in regions

2176 with poor in-situ measurements (Figure S9, such as TROPOMI observations in North Africa).

2177 - Integrating the newly available updated gridded products for the different natural sources of CH_4 in their prior

2178 fluxes (e.g. inland freshwaters) to reach a full spatial description of sources and sinks, and to be able to better

2179 compare the top-down budget with the bottom-up budget.

2180 - Integration of the newly developed 4D variational inversion systems using isotopic species in the top-down budget

2181 (Basu et al., 2022; Thanwerdas et al., 2024; Drinkwater et al. 2023; Mannisenaho et al., 2023).

2182 - Improving the availability of in-situ data at high temporal resolution for the scientific community, especially ones

2183 covering poorly documented regions such as China (Liu et al., 2021b; Guo et al., 2020), India (Nomura et al., 2021;

2184 Lin et al., 2015; Tiwari and Kumar, 2012) and Siberia (Sasakawa et al., 2010, 2017; Fujita et al., 2020; Winderlich

2185 et al., 2010), which are not delivered so far to international databases, or only at poor temporal resolution.

2186 - Integrating the information from imagery satellites (e.g., TROPOMI, Carbon Mapper, Methane Sat, GHG Sat.) of

2187 high to super-emitters to improve prior fluxes of anthropogenic emissions in terms of quantity and locations for

2188 each covered sector.

2189 Over the long run, integrating more measurements and regional studies will help to improve the top-down systems, and

2190 further reduce the uncertainties:

2191 - Extending the CH_4 surface networks to poorly observed regions (e.g., Tropics, China, India, high latitudes) and to

2192 the vertical dimension: aircraft regular measurements (e.g., Filges et al., 2015; Brenninkmeijer et al., 2007; Paris

2193 et al., 2010; Sweeney et al., 2015); Aircore campaigns (e.g., Andersen et al., 2018; Membrive et al., 2017) ; TCCON

2194 observations (e.g., Wunch et al., 2011, 2019) remains critical to complement satellite data that do not observe well

2195 in cloudy regions and at high latitudes, and also to evaluate and eventually correct satellite biases (Buchwitz et al.,

2196 2016).

2197 - Extending and developing continuous isotopic measurements of CH_4 to help partitioning methane sources and to

2198 be integrated in 4D variational isotopic inversions (e.g., Yacovitch et al., 2021).

2199 - Integrating global data from future satellite instruments with intrinsic low-bias, such as active LIDAR techniques

2200 with MERLIN (Ehret et al., 2017), that are promising to overcome issues of systematic errors (Bousquet et al.,

2201 2018) and should provide measurements over the Arctic, contrary to the existing and planned passive missions.

2202 - Other co-emitted species such as radiocarbon for fossil/non-fossil emissions (Lassey et al., 2007a, 2007b; Petrenko

2203 et al., 2017), CO (e.g., Zheng et al., 2019) for biomass burning emissions, and ethane for fugitive emissions (e.g.,

2204 Ramsden et al., 2022) could bring additional information for partitioning emissions.

2205

2206 4. Shortcoming 4: *Towards reducing uncertainties in the modelling of atmospheric transport in the models used in the*

2207 *top-down budget*

The TRANSCOM experiment synthesised in Patra et al. (2011) showed a large sensitivity of the representation of atmospheric transport on CH_4 abundances in the atmosphere. In particular, the modelled CH_4 budget appeared to depend strongly on the troposphere-stratosphere exchange rate and thus on the model vertical grid structure and circulation in the lower stratosphere. Also, regional changes in the CH_4 budget depend on the characteristics of the atmospheric transport models used in the inversion (Bruhwiler et al., 2017; Locatelli et al., 2015). This axis of research is demanding important development from the atmospheric modelling community. Waiting for future improvements (finer horizontal and vertical resolutions, more accurate physical parameterization, increase in computing resources…), assessing atmospheric transport error and the impact on the top-down budget remain crucial and mostly rely on the use of an ensemble of models. Methodology changes that could be integrated into the next methane budget releases include:

- Evaluating more deeply the inversions provided against independent measurements such as aircraft regular campaigns available through for example the CH4 GLOBALVIEWplus v6.0 ObsPack (Schuldt et al., 2023), the IAGOS data portal (https://iagos.aeris-data.fr/download/), the NIES portal (https://db.cger.nies.go.jp/ged/en/datasetlist/index.html) for CONTRAIL (e.g., Machida et al., 2008) and Siberian measurements (e.g., Sasakawa et al., 2017), the WDCGG data portal (https://gaw.kishou.go.jp/) for additional flights over three other Japanese airports and Orléans, France ; Aircore campaigns data set can be downloaded through the NOAA Global Monitoring Laboratory website (https://gml.noaa.gov/ccgg/arc/?id=144, Baier et al., 2021) and the French AIrCore Program for atmospheric sampling (https://aircore.aeris-data.fr, Membrive et al., 2017); TCCON observations (https://tccondata.org; e.g., Wunch et al., 2011, 2019), and use this evaluation to weight the different models used in the CH_4 budget.

Next steps, in the short term, could include some development to be addressed by the top-down community to reduce atmospheric transport errors:

- Developing further methodologies to extract stratospheric partial column abundances from observations such as TCCON data (Saad et al., 2014; Wang et al., 2014), Aircore (e.g. Andersen et al., 2018; Membrive et al., 2017) or, ACE-FTS (De Mazière et al., 2018) or MIPAS (Glatthor et al., 2023) satellite data.
- Combining SWIR and TIR measurements from space to better constrain the tropospheric column, from TROPOMI and IASI for example in the MethanePlus ESA project (https://methaneplus.eu/#docs, Buchwitz etal., 2023) or GOSAT (Kuze et al., 2020).
- Porting transport models codes to run on Graphics processing Units (GPU) to achieve sub-degrees resolution global inversions (Chevallier et al., 2023).

In the long run, developments within the dynamical core of the atmospheric transport models through the implementation of hexagonal-icosaedric grid with finer resolution (Dubos et al., 2015; Niwa et al., 2017, 2022; Lloret et al., 2023), and improvements in the simulated boundary layer dynamics or troposphere-stratosphere exchanges are promising to reduce atmospheric transport errors.

8 Conclusions

We have built an updated global methane budget by using and synthesising a large ensemble of published methods and new results using a consistent, transparent, and traceable approach, including atmospheric observations and inversions (top-down models), process-based models for land surface emissions and atmospheric chemistry, and inventories of anthropogenic emissions (bottom-up models and inventories). For the 2010-2019 decade, global CH_4 emissions are 575 Tg CH_4 yr^{-1} (range of 553-586 Tg CH_4 yr^{-1}), as estimated by top-down inversions. About 65% of global emissions are anthropogenic (range of 63-68%). Bottom-up models and inventories suggest larger global emissions (669 Tg CH_4 yr^{-1} [512-849]) mostly because of larger and more uncertain natural emissions from inland freshwater systems, natural wetlands, and geological seepage , and likely some unresolved double counting of these sources. It is also likely that some of the individual bottom-up emission estimates are too high, leading to larger global emissions from the bottom-up approach than the atmospheric constraints suggest. However, the important progress in this update is that for the first time, the bottom-up and top-down budgets agree within their uncertainty ranges. This is substantial progress toward defining more accurate global methane emissions.

The latitudinal breakdown inferred from the top-down approach reveals a dominant role of tropical emissions (~64%) compared to mid (~32%) and high (~4%) northern latitudes (above 60°N) emissions.

Our results, including an extended set of atmospheric inversions, are compared with the previous budget syntheses of Kirschke et al. (2013) and Saunois et al. (2016; 2020). They show overall good consistency when comparing the same decade (2000-2009) at the global and latitudinal scales. The magnitude and uncertainty of most natural or indirect anthropogenic sources have been revised and updated. In particular, this new budget benefits from large efforts and collaborations from the research community to provide improved estimates of the magnitude and uncertainty of the different freshwater sources and helps reduce the potential double counting at the global scale. Of note, newly available gridded datasets for lakes, ponds, reservoirs, streams, and rivers allow building latitudinal and regional estimates for all these sources for the first time in these estimates. In the next review, we hope to be able to reduce uncertainties in emissions from inland freshwater systems by better quantifying the emission factors of each contributing sub-systems (streams, rivers, lakes, ponds) and estimating double counting at regional scale or avoiding double counting by better defining the surface areas of each ecosystem. Another important priority for improvements is the uncertainty on the chemical loss of CH_4 which still needs to be better assessed in both the top-down and the bottom-up budgets. Building on the improvement of the points detailed in Sect. 7, our aim is to update this budget synthesis as a living review paper regularly (~every three or four years). Each update will produce a more recent decadal CH_4 budget, highlight changes in emissions and trends, and incorporate newly available data and model improvements.

It is still under debate why exactly there is a sustained increase of atmospheric CH_4 (more than +5 ppb yr^{-1}) since 2007 (Nisbet et al., 2019; Nisbet et al., 2023; Turner et al., 2019). Some likely explanations, already introduced by Saunois et al.

2274 (2017) and further investigated by Jackson et al. (2020; 2024) and other studies, include, by decreasing order of certainty:

2275 1) a positive contribution from microbial and fossil sources (e.g., Nisbet et al., 2019; Nisbet et al., 2023; Schwietzke et al.,

2276 2016; Jackson et al., 2020), a negative contribution from biomass burning emissions before 2014 (Giglio et al., 2013;

2277 Worden et al., 2017); 2) a negligible role of Arctic emission changes (e.g., Nisbet et al., 2019; Saunois et al., 2017); and 3)

2278 a tropical dominance of the increasing emissions (e.g., Saunois et al., 2017; Jackson et al., 2020; Wilson et al., 2021;

2279 Drinkwater et al., 2023). Although the accelerated atmospheric methane growth rate in 2020 (15.2 ppb/yr) has found some

2280 explanation with the impact of the world Pandemia in 2020, the sustained observed growth rates in 2021 (17.8 ppb/yr) and

2281 2022 (14 ppb/yr) still challenge our understanding of the global methane cycle. While in Jackson et al. (2020; 2024), the

2282 increase in CH_4 emissions over the last two decades is almost attributed entirely to direct anthropogenic emissions, the

2283 uncertainty range from the GMB ensemble is large, and the contribution from natural emissions (wetlands) is still largely

2284 uncertain. Besides the decadal change in CH_4 emissions, large interannual variability can occur from these natural emissions.

2285 The recent high record of CH_4 growth rate highlights the potential of large variations from natural emissions from one year

2286 to another, in particular wetland emissions (e.g., Peng et al., 2022; Feng et al., 2023). These remain the challenges to be

2287 overcome in better quantifying global methane emissions.

2288 Further investigation is needed in follow-up studies to (1) compare these results to the official UNFCCC declarations and

2289 to important assessment (as those of IEA) as done previously for example in Deng et al. (2022; 2024) or more specifically

2290 for fossil fuel emissions in Tibrewal et al. (2024) and (2) further discuss the trend and interannual variability of CH_4 sources

2291 and sinks at sectoral and regional scales as in Jackson et al. (2020, 2024), Stavert et al. (2021) or RECCAP-2 related

2292 publications (e.g., Petrescu et al., 2021; 2023; Lauerwald et al., 2023b), and discuss the compatibility of the budget against

2293 the atmospheric isotopic signal such as in Saunois et al. (2017). The next budgets will be critical to assess whether the Global

2294 Methane Pledge is successful and assess methane mitigation efforts.

2295 The GCP will continue to support and coordinate the development of improved flux estimates for all budget components

2296 and new underlying science to support improved modelling, acquisition of observations, and data integration. At regular

2297 intervals (3-4 years), we will continue to bring all flux components together to produce an improved and updated global

2298 CH_4 budget, and provide a global benchmark for other CH_4 products and assessments.

9 Data availability

2300 The data presented here are made available in the belief that their dissemination will lead to greater understanding and new

2301 scientific insights on the methane budget and changes to it, and help to reduce its uncertainties. For research projects, if the

2302 data used are essential to the work to be published, or if the conclusion or results largely depend on the data, co-authorship

2303 should be considered. Full contact details and information on how to cite the data are given in the accompanying database.

The accompanying database includes a netcdf file defining the regions used, an archive with the maps of prior fluxes used in the top-down activity, an archive with data corresponding to Fig. 3 and 5, and one Excel file organised in the following spreadsheets.

The file Global_Methane_Budget_2000-2020_v1.0.xlsx includes (1) a summary, (2) the methane observed mixing ratio and growth rate from the four global networks (NOAA, AGAGE, CSIRO and UCI), (3) the evolution of global anthropogenic methane emissions (including biomass burning emissions) used to produce Fig. 2, (4) the global and latitudinal budgets over 2000–2009 based on bottom-up approaches, (5) the global and latitudinal budgets over 2000–2009 based on top-down approaches, (6) the global and latitudinal budgets over 2010–2019 based on bottom-up approaches, (7) the global and latitudinal budgets over 2010– 2019 based on top-down approaches, (8) the global and latitudinal budgets for year 2020 based on bottom-up approaches, (9) the global and latitudinal budgets for year 2020 based on top-down approaches, and (10) the list of contributors to contact for further information on specific data.

This database is available from ICOS Carbon Portal (https://doi.org/10.18160/GKQ9-2RHT, Martinez et al., 2024).

Author contributions.

MS, AM, and JT gathered the bottom-up and top-down data sets and performed the post processing and analysis.

MS, BP, PB, PeC, and RJ coordinated the global budget. MS, BP, PB, PeC, RJ, PP and PCi contributed to the update of the full text and all coauthors appended comments. AM, ED, and XL produced the figures. DJB, NG, PH, AI, AJ, TK, TL, XL, KMcD, JMe, JMu, SP, CP, WR, HT, YY, WZ, ZZ, Qing Z, Qiuan Z and Qianlai Z performed surface land model simulations to compute wetland emissions. GA, DB, SC, BRD, GE, MAH, GH, MSJ, RL, SN, GRR, JAR, EHS, PRa, PRe, and TSW provided data sets useful for natural emission estimates and/or contributed to text on bottom-up natural emissions. LHI, SJS, TNF, GRvW, and MC provided anthropogenic data sets and contributed to the text for this section. AM, JT, PP, DBe, RJ, YN, AS, AT, and BZ performed atmospheric inversions to compute top-down methane emission estimates for sources and sinks. EJD, XL, DRB, PBK, JM, RJP, MR, MS, DWo, and YYo are PI of atmospheric observations used in top-down inversions and/or contributed the text describing atmospheric methane observations. FD, MS, and JT contributed to the bottom-up chemical sink section by providing data sets, processing data and/or contributing to the text. FMF provided data for the soil sink.

Competing interests. At least one of the (co-)authors is a member of the editorial board of Earth System Science Data.

Acknowledgements

This paper is the result of a collaborative international effort under the umbrella of the Global Carbon Project, a project of Future Earth and a research partner of the World Climate Research Programme (WCRP). We acknowledge all the people and institutions who provided the data used in the global methane budget as well as the institutions funding parts of this

effort (see Table A3). We are very grateful for the help provided by Alex Vermeulen in publishing the Global Methane Budget dataset on the Integrated Carbon Observation System (ICOS) website. We acknowledge the modelling groups for making their simulations available for this analysis, the joint WCRP Stratosphere-troposphere Processes And their Role in Climate/International Global Atmospheric Chemistry (SPARC/IGAC) Chemistry-Climate Model Initiative (CCMI) for organising and coordinating the model data analysis activity, and the British Atmospheric Data Centre (BADC) for collecting and archiving the CCMI model output. We acknowledge the long-term support provided by the Commonwealth Scientific and Industrial Research Organisation (CSIRO) and the National Environmental Science Program - Climate Systems Hub to coordinate and support activities of the Global Carbon Project. We are grateful to the Emissions Databse for Global Atmospheric Research (EDGAR) team (M. Crippa, D. Guizzardi, F. Pagani, M. Banja, E. Schaaf, M. Muntean, W. Becker, F. Monforti-Ferrario) for the work needed to publish the EDGAR greenhouse gas emission datasets used in this work (https://edgar.jrc.ec.europa.eu/). We are particularly indebted to the dedicated station/instrumental operators/scientists that have gathered the data and ensured their high quality.

We acknowledge more specifically Katherine Jensen for her contribution to the Surface Water Microwave Product Series SWAMPS, Fortunat Joos for his contribution to simulations with the Land surface Processes and eXchanges model (LPX Bern), Ray Langenfeld for his contribution to CSIRO network, Paul Miller for his contribution to simulations with the Lund-Potsdam-Jena General Ecosystem Simulator (LPJ-GUESS), Peng Shushi for his contribution to simulations with the Organising Carbon and Hydrology In Dynamic Ecosystems (ORCHIDEE) model, Shamil Maksyutov for his contribution for simulations with the inverse model at the National Institute for Environmental Studies (NIES), Isobel Simpson for her contribution to the University of California Irvine (UCI) network, Paul Steele for his former contribution to CSIRO network, Ray Weiss for his contribution to the Advanced Global Atmospheric Gases Experiment (AGAGE) network, Christine Widenmeyer for her contribution with the Fire INventory from the National Center for Atmospheric Research (FINN) database, Xiaoming Xu for his contribution to simulations with with the The Integrated Science Assessment Model (ISAM), Yuanzhi Yao for his contribution to simulations with the Dynamicl Land Ecosystem Model (DLEM), Diego Guizzardi for his contribution to EDGAR, Maria Tenkanen for her contribution with the Crabon Tracker – Europe (CTE) outputs, Giulia Conchedda for her contribution to the Food and Agriculture Organization (FAO) database. FAOSTAT data collection, analysis, and dissemination is funded through FAO regular budget funds. The contribution of relevant experts in member countries is gratefully acknowledged. We acknowledge Juha Hatakka from the Finnish Meteorological Institute (FMI) for making methane measurements at the Pallas station and sharing the data with the community. We thank Ariana Sutton-Grier and Lisamarie Windham-Myers for reviewing an earlier version of this manuscript. Any use of trade, firm, or product names is for descriptive purposes only and does not imply endorsement by the US Government. We warmly thank the three anonymous reviewers for their time and their feedbacks that helped improving greatly the manuscript.

References

Abe, Y., Bignell, D. E. and Higashi, T., Eds.: Termites: Evolution, Sociality, Symbioses, Ecology, Springer Netherlands, Dordrecht., 2000.

Aho, K.S., J.H. Fair, J.D. Hosen, E.D. Kyzivat, L.A. Logozzo, G. Rocher-Ros, L.C. Weber, B. Yoon, and P.A. Raymond: Distinct concentration-discharge dynamics in temperate streams and rivers: CO2 exhibits chemostasis while CH_4 exhibits source limitation due to temperature control, Limnology and Oceanography, 66(10): p. 3656-3668., 2021

Allan, W., Lowe, D. C., Gomez, A. J., Struthers, H. and Brailsford, G. W.: Interannual variation of ^{13}C in tropospheric methane: Implications for a possible atomic chlorine sink in the marine boundary layer, J. Geophys. Res.-Atmospheres, 110(D11), doi:10.1029/2004JD005650, 2005.

Allan, W., Struthers, H. and Lowe, D. C.: Methane carbon isotope effects caused by atomic chlorine in the marine boundary layer: Global model results compared with Southern Hemisphere measurements, J. Geophys. Res.-Atmospheres, 112(D4), D04306, doi:10.1029/2006jd007369, 2007.

Allen, G. H., & Pavelsky, T. M.: Global extent of rivers and streams. Science, 361(6402), 585–588. https://doi.org/10.1126/science.aat0636, 2018

Andersen, T., Scheeren, B., Peters, W. and Chen, H.: A UAV-based active AirCore system for measurements of greenhouse gases, Atmospheric Meas. Tech., 11(5), 2683–2699, doi:10.5194/amt-11-2683-2018, 2018.

Anderson, D. C., Duncan, B. N., Fiore, A. M., Baublitz, C. B., Follette-Cook, M. B., Nicely, J. M., and Wolfe, G. M.: Spatial and temporal variability in the hydroxyl (OH) radical: understanding the role of large-scale climate features and their influence on OH through its dynamical and photochemical drivers, Atmos. Chem. Phys., 21, 6481–6508, https://doi.org/10.5194/acp-21-6481-2021, 2021.

Anderson, D. C., Duncan, B. N., Nicely, J. M., Liu, J., Strode, S. A., and Follette-Cook, M. B.: Technical note: Constraining the hydroxyl (OH) radical in the tropics with satellite observations of its drivers – first steps toward assessing the feasibility of a global observation strategy, Atmos. Chem. Phys., 23, 6319–6338, https://doi.org/10.5194/acp-23-6319-2023, 2023.

Anderson, D. C., Duncan, B. N., Liu, J., Nicely, J. M., Strode, S. A., Follette-Cook, M. B., Souri, A. H., Ziemke , J. R., Gonzales-Abad, G. and Ayazpour, Z.: Trends and interannual variability of the hydroxyl radical in the remote tropics during boreal autumn inferred from satellite proxy data. Geophysical Research Letters, 51, e2024GL108531, https://doi.org/10.1029/2024GL108531, 2024

André, J.-C., Boucher, O., Bousquet, P., Chanin, M.-L., Chappellaz, J. and Tardieu, B.: Le méthane : d'où vient-il et quel est son impact sur le climat ?, EDP Sciences, Académie des Sciences et Technologies, Paris., 2014.

Aoki, S., Nakazawa, T., Murayama, S. and Kawaguchi, S.: Measurements of atmospheric methane at the Japanese Antarctic Station. Syowa., Tellus, 44B(4), 273–281, doi:10.1034/j.1600-0889.1992.t01-3-00005.x., 1992.

Arora, V. K., Melton, J. R. and Plummer, D.: An assessment of natural methane fluxes simulated by the CLASS-CTEM

model, Biogeosciences, 15(15), 4683–4709, doi:10.5194/bg-15-4683-2018, 2018.

Bader, W., Bovy, B., Conway, S., Strong, K., Smale, D., Turner, A. J., Blumenstock, T., Boone, C., Collaud Coen, M., Coulon, A., Garcia, O., Griffith, D. W. T., Hase, F., Hausmann, P., Jones, N., Krummel, P., Murata, I., Morino, I., Nakajima, H., O'Doherty, S., Paton-Walsh, C., Robinson, J., Sandrin, R., Schneider, M., Servais, C., Sussmann, R. and Mahieu, E.: The recent increase of atmospheric methane from 10 years of ground-based NDACC FTIR observations since 2005, Atmospheric Chem. Phys., 17(3), 2255–2277, doi:10.5194/acp-17-2255-2017, 2017.

Baicich, P.: The Birds and Rice Connection, Bird Watch. Dig. [online] Available from: http://www.greatbirdingprojects.com/images/BWD_J-A_13_BIRDS_N_RICE.pdf, 2013.

Baier, B., Sweeney, C., Newberger, T., Higgs, J., Wolter, S., & NOAA Global Monitoring Laboratory : NOAA AirCore atmospheric sampling system profiles (Version 20230831) [Data set]. NOAA GML. https://doi.org/10.15138/6AV0-MY81, 2021

Balasus, N., Jacob, D. J., Lorente, A., Maasakkers, J. D., Parker, R. J., Boesch, H., Chen, Z., Kelp, M. M., Nesser, H., and Varon, D. J.: A blended TROPOMI+GOSAT satellite data product for atmospheric methane using machine learning to correct retrieval biases, Atmos. Meas. Tech., 16, 3787–3807, https://doi.org/10.5194/amt-16-3787-2023, 2023.

Bansal, S., Van Der Berg, M.P., Fern, R.R., Jones, J.W., Lo, R., McKenna, O.P., Tangen, B.A., Zhang, Z., and Gleason, R.A.: Large increases in methane emissions expected from North America's largest wetland complex, Sci. Adv., 9, eade1112, doi:10.1126/sciadv.ade1112, 2023.

Barba, J., Bradford, M. A., Brewer, P. E., Bruhn, D., Covey, K., van Haren, J., Megonigal, J. P., Mikkelsen, T. N., Pangala, S. R., Pihlatie, M., Poulter, B., Rivas-Ubach, A., Schadt, C. W., Terazawa, K., Warner, D. L., Zhang, Z. and Vargas, R.: Methane emissions from tree stems: a new frontier in the global carbon cycle, New Phytol., 222(1), 18–28, doi:10.1111/nph.15582, 2019.

Barker, P. A., Allen, G., Gallagher, M., Pitt, J. R., Fisher, R. E., Bannan, T., Nisbet, E. G., Bauguitte, S. J.-B., Pasternak, D., Cliff, S., Schimpf, M. B., Mehra, A., Bower, K. N., Lee, J. D., Coe, H., and Percival, C. J.: Airborne measurements of fire emission factors for African biomass burning sampled during the MOYA campaign, Atmos. Chem. Phys., 20, 15443–15459, https://doi.org/10.5194/acp-20-15443-2020, 2020.

Bastviken, D., Tranvik, L. J., Downing, J. A., Crill, P. M. and Enrich-Prast, A.: Freshwater Methane Emissions Offset the Continental Carbon Sink, Science, 331(6013), 50–50, doi:10.1126/science.1196808, 2011.

Bastviken, D., C.C. Treat, S.R. Pangala, V. Gauci, A. Enrich-Prast, M. Karlson, M. Gålfalk, M.B. Romano, and H.O. Sawakuchi, The importance of plants for methane emission at the ecosystem scale. Aquatic Botany, 184: p. 103596, 2023.

Basu, S., Lan, X., Dlugokencky, E., Michel, S., Schwietzke, S., Miller, J. B., Bruhwiler, L., Oh, Y., Tans, P. P., Apadula, F., Gatti, L. V., Jordan, A., Necki, J., Sasakawa, M., Morimoto, S., Di Iorio, T., Lee, H., Arduini, J., and Manca, G.: Estimating emissions of methane consistent with atmospheric measurements of methane and δ^{13}C of methane, Atmos.

Chem. Phys., 22, 15351–15377, https://doi.org/10.5194/acp-22-15351-2022, 2022.

Beaulieu, J.J., DelSontro, T. & Downing, J.A.: Eutrophication will increase methane emissions from lakes and impoundments during the 21st century. *Nat Commun* 10, 1375 , https://doi.org/10.1038/s41467-019-09100-5, 2019

Beck, H., Zimmermann, N., McVicar, T. *et al*. Present and future Köppen-Geiger climate classification maps at 1-km resolution. *Sci Data* **5**, 180214, doi.org/10.1038/sdata.2018.214, 2018

Beerling, D.J., Woodward, F.I., Vegetation and the Terrestrial Carbon Cycle: Modelling the First 400 Million Years. Cambridge University Press, Cambridge, 2001

Begum, M.S., M.J. Bogard, D.E. Butman, E. Chea, S. Kumar, X. Lu, O.K. Nayna, L. Ran, J.E. Richey, S.M. Tareq, D.T. Xuan, R. Yu, and J.-H. Park, Localized Pollution Impacts on Greenhouse Gas Dynamics in Three Anthropogenically Modified Asian River Systems. Journal of Geophysical Research: Biogeosciences, 126(5): p. e2020JG006124, 2021

Bergamaschi, P., Houweling, S., Segers, A., Krol, M., Frankenberg, C., Scheepmaker, R. A., Dlugokencky, E., Wofsy, S. C., Kort, E. A., Sweeney, C., Schuck, T., Brenninkmeijer, C., Chen, H., Beck, V. and Gerbig, C.: Atmospheric CH_4 in the first decade of the 21st century: Inverse modeling analysis using SCIAMACHY satellite retrievals and NOAA surface measurements, J. Geophys. Res. Atmospheres, 118(13), 7350–7369, doi:10.1002/jgrd.50480, 2013.

Bergamaschi, P., DANILA, A. M., Weiss, R., Thompson, R. L., Brunner, D., Levin, I., meijer, Y., Chevallier, F., Janssens-Maenhout, G., Bovensmann, H., Crisp, D., Basu, S., Dlugockencky, E. J., Engelen, R., Gerbig, C., Günther, D., Hammer, S., Henne, S., Houweling, S., Karstens, U., Kort, E. A., Maione, M., Manning, A. J., Miller, J., Montzka, S., Pandey, S., Peters, W., Peylin, P., Pinty, B., Ramonet, M., Reimann, S., Röckmann, T., Schmidt, M., Strogies, M., Sussams, J., Tarasova, O., Van Aardenne, J., Vermeulen, A. and Vogel, F.: Atmospheric monitoring and inverse modelling for verification of greenhouse gas inventories, EUR - Scientific and Technical Research Reports, Publications Office of the European Union. [online] Available from: https://ec.europa.eu/jrc/en/publication/eur-scientific-and-technical-research-reports/atmospheric-monitoring-and-inverse-modelling-verification-greenhouse-gas-inventories (Accessed 17 March 2020a), 2018.

Best, A. I., Richardson, M. D., Boudreau, B. P., Judd, A. G., Leifer, I., Lyons, A. P., et al.: Shallow Seabed Methane Gas Could Pose Coastal hazard. Eos Trans. AGU 87 (22), 213–217. doi:10.1029/2006EO220001, 2006

Bian, L., Gao, Z., Sun, Y., Ding, M., Tang, J. and Schnell, R. C.: CH4 Monitoring and Background Concentration at Zhongshan Station, Antarctica, Atmospheric Clim. Sci., 6(1), 135–144, doi:10.4236/acs.2016.61012, 2015.

Bignell, D.E., Eggleton, P. Termites in ecosystems. In: Abe, T., Higashi, M. and Bignell, D.E. (Eds), Termites: Evolution, Sociality, Symbioses, Ecology. Kluwer, Dordrecht, Netherlands, 363–387, 2000.

Biskaborn, B.K., Smith, S.L., Noetzli, J. *et al*. Permafrost is warming at a global scale. *Nat Commun* **10**, 264, https://doi-org.insu.bib.cnrs.fr/10.1038/s41467-018-08240-4, 2019

Blake, D. R. and Rowland, F. S.: World-wide increase in tropospheric methane, 1978–1983, J. Atmospheric Chem., 4, 43–62, 1986.

Blake, D. R., Mayer, E. W., Tyler, S. C., Makide, Y., Montague, D. C. and Rowland, F. S.: Global Increase in Atmospheric Methane Concentrations between 1978 and 1980, Geophys. Res. Lett., 9(4), 477–480, 1982.

Bloom, A. A., Lee-Taylor, J., Madronich, S., Messenger, D. J., Palmer, P. I., Reay, D. S. and McLeod, A. R.: Global methane emission estimates from ultraviolet irradiation of terrestrial plant foliage, New Phytol., doi:10.1111/j.1469-8137.2010.03259.x, 2010.

Bohn, T. J., Melton, J. R., Ito, A., Kleinen, T., Spahni, R., Stocker, B. D., Zhang, B., Zhu, X., Schroeder, R., Glagolev, M. V., Maksyutov, S., Brovkin, V., Chen, G., Denisov, S. N., Eliseev, A. V., Gallego-Sala, A., McDonald, K. C., Rawlins, M. A., Riley, W. J., Subin, Z. M., Tian, H., Zhuang, Q. and Kaplan, J. O.: WETCHIMP-WSL: Ïntercomparison of wetland methane emissions models over West Siberia, Biogeosciences, 12(11), 3321–3349, doi:10.5194/bg-12-3321-2015, 2015.

Bodmer, P., Vroom, R. J. E., Stepina, T., del Giorgio, P. A., Kosten, S.: Methane dynamics in vegetated habitats in inland waters: quantification, regulation, and global significance, Frontiers in Water, 5, DOI=10.3389/frwa.2023.1332968, 2024

Borges, A. V. and Abril, G.: Carbon Dioxide and Methane Dynamics in Estuaries, in Treatise on Estuarine and Coastal Science, vol. 5, pp. 119–161, Academic Press, Waltham. [online] Available from: doi:10.1016/B978-0-12-374711-2.00504-0, 2011.

Borges, A., G. Abril, and S. Bouillon: Carbon dynamics and CO2 and CH4 outgassing in the Mekong delta, Biogeosciences, 15: p. 1093-1114., 2018

Borges, A.V., F. Darchambeau, T. Lambert, C. Morana, G.H. Allen, E. Tambwe, A. Toengaho Sembaito, T. Mambo, J. Nlandu Wabakhangazi, J.P. Descy, C.R. Teodoru, and S. Bouillon: Variations in dissolved greenhouse gases (CO2, CH4, N2O) in the Congo River network overwhelmingly driven by fluvial-wetland connectivity, Biogeosciences, 16(19): p. 3801-3834, 2019

Borges, A. V., Deirmendjian, L., Bouillon, S., Okello, W., Lambert, T., Roland, F.A. E., Razanamahandry, V. F. , Voarintsoa, NR. G., Darchambeau, F., Kimirei, I. A. , Descy, J-P., Allen, G. H. and Morana, C.: Greenhouse gas emissions from African lakes are no longer a blind spot.Sci. Adv.8, eabi8716, DOI:10.1126/sciadv.abi8716, 2022

Bousquet, P., Ciais, P., Miller, J. B., Dlugokencky, E. J., Hauglustaine, D. A., Prigent, C., Van der Werf, G. R., Peylin, P., Brunke, E. G., Carouge, C., Langenfelds, R. L., Lathiere, J., Papa, F., Ramonet, M., Schmidt, M., Steele, L. P., Tyler, S. C. and White, J.: Contribution of anthropogenic and natural sources to atmospheric methane variability, Nature, 443(7110), 439–443, 2006.

Bousquet, P., Pierangelo, C., Bacour, C., Marshall, J., Peylin, P., Ayar, P. V., Ehret, G., Bréon, F.-M., Chevallier, F., Crevoisier, C., Gibert, F., Rairoux, P., Kiemle, C., Armante, R., Bès, C., Cassé, V., Chinaud, J., Chomette, O., Delahaye, T., Edouart, D., Estève, F., Fix, A., Friker, A., Klonecki, A., Wirth, M., Alpers, M. and Millet, B.: Error Budget of the MEthane Remote LIdar missioN and Its Impact on the Uncertainties of the Global Methane Budget, J.

Geophys. Res. Atmospheres, 123(20), 11,766-11,785, doi:10.1029/2018JD028907, 2018.

Brandt, A. R., Heath, G. A., Kort, E. A., O'Sullivan, F., Pétron, G., Jordaan, S. M., Tans, P., Wilcox, J., Gopstein, A. M., Arent, D., Wofsy, S., Brown, N. J., Bradley, R., Stucky, G. D., Eardley, D. and Harriss, R.: Methane Leaks from North American Natural Gas Systems, Science, 343(6172), 733–735, doi:10.1126/science.1247045, 2014.

Brasseur, G. P. and Solomon, S.: Aeronomy of the Middle Atmosphere: Chemistry and Physics of the Stratosphere and Mesosphere, 3rd ed., Springer Netherlands., 2005.

Brenninkmeijer C. A. M., Crutzen, P., Boumard, F., Dauer, T., Dix, B., Ebinghaus, R., Filippi, D., Fischer, H., Franke, H., Fries, U., Heintzenberg, J., Helleis, F., Hermann, M., Kock, H. H., Koeppel, C., Lelieveld, J., Leuenberger, M., Martinsson, B. G., Miemczyk, S., Moret, H. P., Nguyen, H. N., Nyfeler, P., Oram, D., O'Sullivan, D., Penkett, S., Platt, U., Pupek, M., Ramonet, M., Randa, B., Reichelt, M., Rhee, T. S., Rohwer, J., Rosenfeld, K., Scharffe, D., Schlager, H., Schumann, U., Slemr, F., Sprung, D., Stock, P., Thaler, R., Valentino, F., van Velthoven, P., Waibel, A., Wandel, A., Waschitschek, K., Wiedensohler, A., Xueref- Remy, I., Zahn, A., Zech, U., and Ziereis, H.: Civil Aircraft for the regular investigation of the atmosphere based on an instrumented container: The new CARIBIC system, Atmos. Chem. Phys., 7, 4953-4976, doi:10.5194/acp-7-4953-2007, 2007.

Bruhwiler, L. M., Basu, S., Bergamaschi, P., Bousquet, P., Dlugokencky, E., Houweling, S., Ishizawa, M., Kim, H.-S., Locatelli, R., Maksyutov, S., Montzka, S., Pandey, S., Patra, P. K., Petron, G., Saunois, M., Sweeney, C., Schwietzke, S., Tans, P. and Weatherhead, E. C.: U.S. CH4 emissions from oil and gas production: Have recent large increases been detected?, J. Geophys. Res. Atmospheres, 122(7), 4070–4083, doi:10.1002/2016JD026157, 2017.

Brune, A.: Symbiotic digestion of lignocellulose in termite guts, *Nat Rev Microbiol* 12, 168–180, doi.org/10.1038/nrmicro3182., 2014

Buchwitz, M., de Beek, R., Burrows, J. P., Bovensmann, H., Warneke, T., Notholt, J., Meirink, J. F., Goede, A. P. H., Bergamaschi, P., Korner, S., Heimann, M. and Schulz, A.: Atmospheric methane and carbon dioxide from SCIAMACHY satellite data: initial comparison with chemistry and transport models, Atmospheric Chem. Phys., 5, 941–962, 2005a.

Buchwitz, M., de Beek, R., Noel, S., Burrows, J. P., Bovensmann, H., Bremer, H., Bergamaschi, P., Korner, S. and Heimann, M.: Carbon monoxide, methane and carbon dioxide columns retrieved from SCIAMACHY by WFM-DOAS: year 2003 initial data set, Atmospheric Chem. Phys., 5, 3313–3329, 2005b.

Buchwitz, M., Dils, B., Boesch, H., Crevoisier, C., Detmers, R., Frankenberg, C., Hasekamp, O., Hewson, W., Laeng, A., Noel, S., Nothold, J., Parker, R., Reuter, M. and Schneising, O.: Product Validation and Intercomparison Report (PVIR) for the Essential Climate Variable (ECV) Greenhouse Gases (GHG), ESA Climate Change Initiative (CCI), report version 4, Feb 2016, http://www.esa-ghg-cci.org/?q=webfm_send/300., 2016.

Buchwitz, M., Schneising, O., Vanselow, S., Houweling, S., van Peet, J., Siddans, R., Kerridge, B., Ventress, L., Knappett, D., Crevoisier, C., Meilhac, N., Borsdof, T., Lorente, A. and Aben, I. : Final Report of the Methane Plus ESA project,

2535   TN-D15/16-CH4PLUS, https://methaneplus.eu/#docs, Accessed on February 13 2024, 202

2536   Butz, A., Guerlet, S., Hasekamp, O., Schepers, D., Galli, A., Aben, I., Frankenberg, C., Hartmann, J. M., Tran, H., Kuze,
2537   A., Keppel-Aleks, G., Toon, G., Wunch, D., Wennberg, P., Deutscher, N., Griffith, D., Macatangay, R.,
2538   Messerschmidt, J., Notholt, J. and Warneke, T.: Toward accurate CO_2 and CH_4 observations from GOSAT, Geophys.
2539   Res. Lett., 38(14), L14812, doi:10.1029/2011gl047888, 2011.

2540   Cai, Z. C., Xing, G., Yan, X., Xu, H., Tsuruta, H., Yagi, K. and Minami, K.: Methane and nitrous oxide emissions from
2541   rice paddy fields as affected by nitrous fertilizers and water management, Plant Soil, 196, 7–14, 1997.

2542   Cael, B.B., J. Biggs, and D.A. Seekell, The size-distribution of earth's lakes and ponds: Limits to power-law behavior.
2543   Frontiers in Environmental Science, 10.-, 2022

2544   Call, M., D. T. Maher, I. R. Santos, and others.: Spatial and temporal variability of carbon dioxide and methane fluxes
2545   over semi-diurnal and spring–neap–spring timescales in a mangrove creek. Geochim. Cosmochim. Acta **150**: 211–225.
2546   doi:10.1016/j.gca.2014.11.023, 2015

2547   Canadell, J.G., P.M.S. Monteiro, M.H. Costa, L. Cotrim da Cunha, P.M. Cox, A.V. Eliseev, S. Henson, M. Ishii, S. Jaccard,
2548   C. Koven, A. Lohila, P.K. Patra, S. Piao, J. Rogelj, S. Syampungani, S. Zaehle, and K. Zickfeld: Global Carbon and
2549   other Biogeochemical Cycles and Feedbacks. In *Climate Change 2021: The Physical Science Basis. Contribution of*
2550   *Working Group I to the Sixth Assessment Report of the Intergovernmental Panel on Climate Change* [Masson-
2551   Delmotte, V., P. Zhai, A. Pirani, S.L. Connors, C. Péan, S. Berger, N. Caud, Y. Chen, L. Goldfarb, M.I. Gomis, M.
2552   Huang, K. Leitzell, E. Lonnoy, J.B.R. Matthews, T.K. Maycock, T. Waterfield, O. Yelekçi, R. Yu, and B. Zhou (eds.)].
2553   Cambridge University Press, Cambridge, United Kingdom and New York, NY, USA, pp. 673–816, doi:
2554   10.1017/9781009157896.007, 2021

2555   Carlson, K. M., Gerber, J. S., Mueller, N. D., Herrero, M., MacDonald, G. K., Brauman, K. A., Havlik, P., O'Connell, C.
2556   S., Johnson, J. A., Saatchi, S. and West, P. C.: Greenhouse gas emissions intensity of global croplands, Nat. Clim.
2557   Change, 7(1), 63–68, doi:10.1038/nclimate3158, 2017.

2558   Castelán-Ortega, O. A., Carlos Ku-Vera, J. and Estrada-Flores, J. G.: Modeling methane emissions and methane
2559   inventories for cattle production systems in Mexico, Atmósfera, 27(2), 185–191, doi:10.1016/S0187-6236(14)71109-
2560   9, 2014.

2561   Cathles, L., Brown, L., Taam, M. and Hunter, A.: A commentary on "The greenhouse-gas footprint of natural gas in shale
2562   formations" by R.W. Howarth, R. Santoro, and Anthony Ingraffea, Clim. Change, 113(2), 525–535,
2563   doi:10.1007/s10584-011-0333-0, 2012.

2564   Chandra, N., P. K. Patra, J. S. H. Bisht, A. Ito, T. Umezawa, S. Morimoto, S. Aoki, G. Janssens-Maenhout, R. Fujita,
2565   M. Takigawa, S. Watanabe, N. Saitoh, J.G. Canadell, Emissions from the oil and gas sectors, coal mining and ruminant
2566   farming drive methane growth over the past three decades, J. Meteorol. Soc. Jpn., 99(2), doi:10.2151/jmsj.2021-015,
2567   2021.

Chandra, N., Patra, P.K., Fujita, R., Höglund-Isaksson, L., Umezawa, T., Goto, D., Morimoto, S., Vaughn, B. H., and Röckmann, T.: Methane emissions decreased in fossil fuel exploitation and sustainably increased in microbial source sectors during 1990–2020, Comm. Earth Environ., 5, https://doi.org/10.1038/s43247-024-01286-x, 2024

Chang, J., Peng, S., Ciais, P., Saunois, M., Dangal, S. R. S., Herrero, M., Havlík, P., Tian, H. and Bousquet, P.: Revisiting enteric methane emissions from domestic ruminants and their δ 13 C CH4 source signature, Nat. Commun., 10(1), 1–14, doi:10.1038/s41467-019-11066-3, 2019.

Chang, J., Peng, S., Yin, Y., Ciais, P., Havlik, P., & Herrero, M.: The key role of production efficiency changes in livestock methane emission mitigation. AGU Advances, 2, e2021AV000391, https://doi.org/10.1029/2021AV000391, 2021

Chappellaz, J., Bluniert, T., Raynaud, D., Barnola, J. M., Schwander, J. and Stauffert, B.: Synchronous changes in atmospheric CH4 and Greenland climate between 40 and 8 kyr BP, Nature, 366(6454), 443–445, doi:10.1038/366443a0, 1993.

Chen, H., Zhu, Q., Peng, C., Wu, N., Wang, Y., Fang, X., Jiang, H., Xiang, W., Chang, J., Deng, X. and Yu, G.: Methane emissions from rice paddies natural wetlands, lakes in China: Synthesis new estimate, Glob. Change Biol., 19(1), 19–32, doi:10.1111/gcb.12034, 2013.

Chen, Y. H. and Prinn, R. G.: Estimation of atmospheric methane emissions between 1996 and 2001 using a three-dimensional global chemical transport model, J. Geophys. Res.-Atmospheres, 111(D10307), doi:10.1029/2005JD006058, 2006.

Chen, Z., Jacob, D. J., Nesser, H., Sulprizio, M. P., Lorente, A., Varon, D. J., Lu, X., Shen, L., Qu, Z., Penn, E., and Yu, X.: Methane emissions from China: a high-resolution inversion of TROPOMI satellite observations, Atmos. Chem. Phys., 22, 10809–10826, https://doi.org/10.5194/acp-22-10809-2022, 2022.

Chen, Y., Hall, J., van Wees, D., Andela, N., Hantson, S., Giglio, L., van der Werf, G. R., Morton, D. C., and Randerson, J. T.: Multi-decadal trends and variability in burned area from the fifth version of the Global Fire Emissions Database (GFED5), Earth Syst. Sci. Data, 15, 5227–5259, https://doi.org/10.5194/essd-15-5227-2023, 2023.

Chevallier, F., Lloret, Z., Cozic, A., Takache, S., and Remaud, M.: Toward high-resolution global atmospheric inverse modeling using graphics accelerators. *Geophysical Research Letters*, 50(5), 1–9. https://doi.org/10.1029/2022GL102135, 2023

Chiri, E., Greening, C., Lappan, R., Waite D. W., Jirapanjawat, T., Dong, X, Arndt, S. K., and Nauer, P. A.: Termite mounds contain soil-derived methanotroph communities kinetically adapted to elevated methane concentrations. ISME J 14, 2715–273, https://doi.org/10.1038/s41396-020-0722-3, 2020

Chiri, E., Nauer, P. A., Lappan, R., Jirapanjawat, T., Waite, D. W., Handley, K. M., Hugenholtz, P., Cook, P. L. M., Arndt, S. K., and Greening, C.: Termite gas emissions select for hydrogenotrophic microbial communities in termite mounds. Proceedings of the National Academy of Sciences of the United States of America, 118(30), e2102625118.

2601 https://doi.org/10.1073/pnas.2102625118, 2021

2602 Ciais, P., Sabine, C., Bala, G., Bopp, L., Brovkin, V., Canadell, J., Chhabra, A., DeFries, R., Galloway, J., Heimann. M,

2603 Jones, C., Le Quéré, C., Myneni, R. B., Piao, S. and Thornton, P.: Carbon and Other Biogeochemical Cycles, in In

2604 Climate Change 2013: The Physical Science Basis. Contribution of Working Group I to the Fifth Assessment Report

2605 of IPCC, edited by T. F. Stocker, D. Qin, G.-K. Plattner, M. Tignor, S. K. Allen, J. Boschung, A. Nauels, Y. Xia, V.

2606 Bex, and P. M. Midgley, Cambridge University Press, Cambridge., 2013.

2607 Cicerone, R. J. and Oremland, R. S.: Biogeochemical aspects of atmospheric methane, Glob. Biogeochem. Cycles, 2, 299–

2608 327, 1988.

2609 Cicerone, R. J. and Shetter, J. D.: Sources of atmospheric methane: Measurements in rice paddies and a discussion, J.

2610 Geophys. Res., 86, 7203–7209, 1981.

2611 Collins, W. J., Lamarque, J. F., Schulz, M., Boucher, O., Eyring, V, Hegglin, M. I., Maycock, A., Myhre, G., Prather, M.,

2612 Shindell, D. and Smith, S.J.: AerChemMIP: quantifying the effects of chemistry and aerosols in CMIP6. Geoscientific

2613 Model Development 10, 585–607. doi:10.5194/ gmd-10-585-2017, 2017.

2614 Comer-Warner, S.A., P. Romeijn, D.C. Gooddy, S. Ullah, N. Kettridge, B. Marchant, D.M. Hannah, and S.

2615 Krause:Thermal sensitivity of CO_2 and CH_4 emissions varies with streambed sediment properties. Nature

2616 Communications, 9(1): p. 2803, 2018

2617 Conley, S., Franco, G., Faloona, I., Blake, D. R., Peischl, J. and Ryerson, T. B.: Methane emissions from the 2015 Aliso

2618 Canyon blowout in Los Angeles, CA, Science, 351(6279), 1317–1320, doi:10.1126/science.aaf2348, 2016.

2619 Conrad, R., Klose, M. and Claus, P.: Phosphate Inhibits Acetotrophic Methanogenesis on Rice Roots, Appl. Environ.

2620 Microbiol., 66(2), 828–831, 2000.

2621 Covey, K. R. and Megonigal, J. P.: Methane production and emissions in trees and forests, New Phytol., 222(1), 35–51,

2622 doi:10.1111/nph.15624, 2019.

2623 Covey, K. R., Wood, S. A., Warren, R. J., Lee, X. and Bradford, M. A.: Elevated methane concentrations in trees of an

2624 upland forest, Geophys. Res. Lett., 39(15), doi:10.1029/2012gl052361, 2012.

2625 Covey, K. R., de Mesquita, C. P. B., Oberle, B., Maynard, D. S., Bettigole, C., Crowther, T. W., Duguid, M. C., Steven,

2626 B., Zanne, A. E., Lapin, M., Ashton, M. S., Oliver, C. D., Lee, X. and Bradford, M. A.: Greenhouse trace gases in

2627 deadwood, Biogeochemistry, 130(3), 215–226, doi:10.1007/s10533-016-0253-1, 2016.

2628 Crawford, J.T. and E.H. Stanley: Controls on methane concentrations and fluxes in streams draining human-dominated

2629 landscapes. Ecological Applications, 26(5): p. 1581-1591, 2016

2630 Crevoisier, C., Nobileau, D., Fiore, A. M., Armante, R., Chedin, A. and Scott, N. A.: Tropospheric methane in the tropics

2631 - first year from IASI hyperspectral infrared observations, Atmospheric Chem. Phys., 9(17), 6337–6350, 2009.

2632 Crippa, M., Guizzardi, D., Solazzo, E., Muntean, M., Schaaf, E., Monforti-Ferrario, F., Banja, M., Olivier, J.G.J., Grassi,

2633 G., Rossi, S., Vignati, E.,GHG emissions of all world countries - 2021 Report, EUR 30831 EN, Publications Office of

2634   the European Union, Luxembourg, 2021, ISBN 978-92-76-41547-3, doi:10.2760/173513, JRC126363, 2021

2635 Crippa, M., Guizzardi, D., Pagani, F., Banja, M., Muntean, M., Schaaf E., Becker, W., Monforti-Ferrario, F., Quadrelli,

2636   R., Risquez Martin, A., Taghavi-Moharamli, P., Köykkä, J., Grassi, G., Rossi, S., Brandao De Melo, J., Oom, D.,

2637   Branco, A., San-Miguel, J., Vignati, E., GHG emissions of all world countries, Publications Office of the European

2638   Union, Luxembourg, 2023, doi:10.2760/953322, JRC134504, 2023

2639 Crutzen, P. J., Aselmann, I. and Seiler, W.: Methane production by domestic animals, wild ruminants, other herbivorous

2640   fauna, and humans, Tellus B, 38B(3–4), 271–284, doi:10.1111/j.1600-0889.1986.tb00193.x, 1986.

2641 Cucchi, M., Weedon, G. P., Amici, A., Bellouin, N., Lange, S., Müller Schmied, H., Hersbach, H. and Buontempo, C.:

2642   WFDE5: bias-adjusted ERA5 reanalysis data for impact studies. Earth System Science Data, 12, 2097–2120, 2020

2643 Cunnold, D. M., Steele, L. P., Fraser, P. J., Simmonds, P. G., Prinn, R. G., Weiss, R. F., Porter, L. W., O'Doherty, S.,

2644   Langenfelds, R. L., Krummel, P. B., Wang, H. J., Emmons, L., Tie, X. X. and Dlugokencky, E. J.: In situ measurements

2645   of atmospheric methane at GAGE/AGAGE sites during 1985-2000 and resulting source inferences, J. Geophys. Res.

2646   - Atmospheres, 107(D14), doi:10.1029/2001jd001226, 2002.

2647 Curry, C. L.: Modeling the soil consumption of atmospheric methane at the global scale, Glob. Biogeochem. Cycles, 21(4),

2648   GB4012, doi:10.1029/2006gb002818, 2007.

2649 Dalsøren, S. B., Isaksen, I. S. A., Li, L. and Richter, A.: Effect of emission changes in Southeast Asia on global hydroxyl

2650   and methane lifetime, Tellus B, 61(4), 588–601, doi:10.1111/j.1600-0889.2009.00429.x, 2009.

2651 Darmenov, A. and da Silva, A.: The quick fire emissions dataset (QFED) - Documentation of versions 2.1, 2.2 and

2652   2.4, Technical Report Series on Global Modeling and Data Assimilation, NASA Global Modeling and Assimilation

2653   Office,. [online] Available from: https://gmao.gsfc.nasa.gov/pubs/docs/Darmenov796.pdf (Accessed 11 March 2020),

2654   2015.

2655 De Mazière, M., Vigouroux, C., Bernath, P. F., Baron, P., Blumenstock, T., Boone, C., Brogniez, C., Catoire, V., Coffey,

2656   M., Duchatelet, P., Griffith, D., Hannigan, J., Kasai, Y., Kramer, I., Jones, N., Mahieu, E., Manney, G. L., Piccolo, C.,

2657   Randall, C., Robert, C., Senten, C., Strong, K., Taylor, J., Tétard, C., Walker, K. A., and Wood, S.: Validation of ACE-

2658   FTS v2.2 methane profiles from the upper troposphere to the lower mesosphere, Atmos. Chem. Phys., 8, 2421–2435,

2659   https://doi.org/10.5194/acp-8-2421-2008, 2008.

2660 Deemer, B. R., Harrison, J. A., Li, S., Beaulieu, J. J., DelSontro, T., Barros, N., Bezerra-Neto, J. F., Powers, S. M., dos

2661   Santos, M. A. and Vonk, J. A.: Greenhouse Gas Emissions from Reservoir Water Surfaces: A New Global Synthesis,

2662   BioScience, 66(11), 949–964, doi:10.1093/biosci/biw117, 2016.

2663 Deemer, B.R. and M.A. Holgerson, Drivers of Methane Flux Differ Between Lakes and Reservoirs, Complicating Global

2664   Upscaling Efforts. Journal of Geophysical Research: Biogeosciences 126(4): p. e2019JG005600., 2021.

2665 Defratyka, S. M., Paris, J.-D., Yver-Kwok, C., Fernandez, J. M., Korben, P., and Bousquet, P.: Mapping Urban Methane

2666   Sources in Paris, France, Environmental Science & Technology, 55, 8583-8591, 10.1021/acs.est.1c00859, 2021.

2667 DelSontro, T., Beaulieu, J. J. and Downing, J. A.: Greenhouse gas emissions from lakes and impoundments: Upscaling in
2668   the face of global change, Limnol. Oceanogr. Lett., 3(3), 64–75, doi:10.1002/lol2.10073, 2018.

2669 Delwiche, K. B., Knox, S. H., Malhotra, A., Fluet-Chouinard, E., McNicol, G., Feron, S., Ouyang, Z., Papale, D., Trotta,
2670   C., Canfora, E., Cheah, Y.-W., Christianson, D., Alberto, Ma. C. R., Alekseychik, P., Aurela, M., Baldocchi, D.,
2671   Bansal, S., Billesbach, D. P., Bohrer, G., Bracho, R., Buchmann, N., Campbell, D. I., Celis, G., Chen, J., Chen, W.,
2672   Chu, H., Dalmagro, H. J., Dengel, S., Desai, A. R., Detto, M., Dolman, H., Eichelmann, E., Euskirchen, E., Famulari,
2673   D., Fuchs, K., Goeckede, M., Gogo, S., Gondwe, M. J., Goodrich, J. P., Gottschalk, P., Graham, S. L., Heimann, M.,
2674   Helbig, M., Helfter, C., Hemes, K. S., Hirano, T., Hollinger, D., Hörtnagl, L., Iwata, H., Jacotot, A., Jurasinski, G.,
2675   Kang, M., Kasak, K., King, J., Klatt, J., Koebsch, F., Krauss, K. W., Lai, D. Y. F., Lohila, A., Mammarella, I., Belelli
2676   Marchesini, L., Manca, G., Matthes, J. H., Maximov, T., Merbold, L., Mitra, B., Morin, T. H., Nemitz, E., Nilsson, M.
2677   B., Niu, S., Oechel, W. C., Oikawa, P. Y., Ono, K., Peichl, M., Peltola, O., Reba, M. L., Richardson, A. D., Riley, W.,
2678   Runkle, B. R. K., Ryu, Y., Sachs, T., Sakabe, A., Sanchez, C. R., Schuur, E. A., Schäfer, K. V. R., Sonnentag, O.,
2679   Sparks, J. P., Stuart-Haëntjens, E., Sturtevant, C., Sullivan, R. C., Szutu, D. J., Thom, J. E., Torn, M. S., Tuittila, E.-
2680   S., Turner, J., Ueyama, M., Valach, A. C., Vargas, R., Varlagin, A., Vazquez-Lule, A., Verfaillie, J. G., Vesala, T.,
2681   Vourlitis, G. L., Ward, E. J., Wille, C., Wohlfahrt, G., Wong, G. X., Zhang, Z., Zona, D., Windham-Myers, L., Poulter,
2682   B., and Jackson, R. B.: FLUXNET-CH4: a global, multi-ecosystem dataset and analysis of methane seasonality from
2683   freshwater wetlands , Earth Syst. Sci. Data, 13, 3607–3689, https://doi.org/10.5194/essd-13-3607-2021, 2021.

2684 Deng, Z., Ciais, P., Tzompa-Sosa, Z. A., Saunois, M., Qiu, C., Tan, C., Sun, T., Ke, P., Cui, Y., Tanaka, K., Lin, X.,
2685   Thompson, R. L., Tian, H., Yao, Y., Huang, Y., Lauerwald, R., Jain, A. K., Xu, X., Bastos, A., Sitch, S., Palmer, P. I.,
2686   Lauvaux, T., d'Aspremont, A., Giron, C., Benoit, A., Poulter, B., Chang, J., Petrescu, A. M. R., Davis, S. J., Liu, Z.,
2687   Grassi, G., Albergel, C., Tubiello, F. N., Perugini, L., Peters, W., and Chevallier, F.: Comparing national greenhouse
2688   gas budgets reported in UNFCCC inventories against atmospheric inversions, Earth Syst. Sci. Data, 14, 1639–1675,
2689   https://doi.org/10.5194/essd-14-1639-2022, 2022.

2690 Deng, Z., Ciais, P., Hu, L., Martinez, A., Saunois, M., Thompson, R. L., Tibrewal, K., Peters, W., Byrne, B., Grassi, G.,
2691   Palmer, P. I., Luijkx, I. T., Liu, Z., Liu, J., Fang, X., Wang, T., Tian, H., Tanaka, K., Bastos, A., Sitch, S., Poulter, B.,
2692   Albergel, C., Tsuruta, A., Maksyutov, S., Janardanan, R., Niwa, Y., Zheng, B., Thanwerdas, J., Belikov, D., Segers,
2693   A., and Chevallier, F.: Global Greenhouse Gas Reconciliation 2022, Earth Syst. Sci. Data Discuss. [preprint],
2694   https://doi.org/10.5194/essd-2024-103, in review, 2024.

2695 Denman, K. L., G. Brasseur, A. Chidthaisong, P. Ciais, P. M. Cox, R. E. Dickinson, D. Hauglustaine, C. Heinze, E.
2696   Holland, D. Jacob, U. Lohmann, S Ramachandran, P. L. da Silva Dias, S. C. Wofsy and X. Zhang: Couplings Between
2697   Changes in the Climate System and Biogeochemistry, Cambridge University Press, Cambridge, United Kingdom and
2698   New York, NY, USA., 2007.

2699 D'Imperio, L., B.-B. Li, J. M. Tiedje, Oh, Y., Christiansen, J.R., Kepfer-Rojas, S., Westergaard-Nielsen, A., Brandt, K.

K., Holm P.E., Wang, P., Ambus, P., and Elberling, B.: Spatial Controls of Methane Uptake in Upland Soils Across Climatic and Geological Regions in Greenland, Communications Earth & Environment, 4-46, https://doi.org/10.1038/s43247-023-01143-3, 2023.

Dirmeyer, P. A., Gao, X., Zhao, M., Guo, Z., Oki, T., and Hanasaki, N. GSWP-2: Multimodel analysis and impli- cations for our perception of the land surface. Bulletin of the American Meteorological Society, 87(10):1381–1398, 2006.

Dlugokencky, E. J., Dutton, E. G., Novelli, P. C., Tans, P. P., Masarie, K. A., Lantz, K. O. and Madronich, S.: Changes in CH_4 and CO growth rates after the eruption of Mt Pinatubo and their link with changes in tropical tropospheric UV flux, Geophys. Res. Lett., 23(20), 2761–2764, 1996.

Dlugokencky, E. J., Myers, R. C., Lang, P. M., Masarie, K. A., Crotwell, A. M., Thoning, K. W., Hall, B. D., Elkins, J. W. and Steele, L. P.: Conversion of NOAA atmospheric dry air CH4 mole fractions to a gravimetrically prepared standard scale, J Geophys Res, 110(D18306), doi:10.1029/2005JD006035., 2005.

Dlugokencky, E. J., Bruhwiler, L., White, J. W. C., Emmons, L. K., Novelli, P. C., Montzka, S. A., Masarie, K. A., Lang, P. M., Crotwell, A. M., Miller, J. B. and Gatti, L. V.: Observational constraints on recent increases in the atmospheric CH4 burden, Geophys. Res. Lett., 36, 5 PP., doi:200910.1029/2009GL039780, 2009.

Dlugokencky, E. J., Nisbet, E. G., Fisher, R. and Lowry, D.: Global atmospheric methane: budget, changes and dangers, Philos. Trans. R. Soc. - Math. Phys. Eng. Sci., 369(1943), 2058–2072, 2011.

Dong, B., Xi, Y., Cui, Y., and Peng, S.: Quantifying Methane Emissions from Aquaculture Ponds in China, Environ. Sci. Technol., 57, 1576–1583, https://doi.org/10.1021/acs.est.2c05218, 2023.

Downing, J.: Emerging global role of small lakes and ponds: Little things mean a lot. Limnetica, 29: p. 9-24, 2010

Drinkwater, A., Palmer, P. I., Feng, L., Arnold, T., Lan, X., Michel, S. E., Parker, R., and Boesch, H.: Atmospheric data support a multi-decadal shift in the global methane budget towards natural tropical emissions, Atmos. Chem. Phys., 23, 8429–8452, https://doi.org/10.5194/acp-23-8429-2023, 2023.

Dubos, T., Dubey, S., Tort, M., Mittal, R., Meurdesoif, Y. and Hourdin, F.: DYNAMICO-1.0, an icosahedral hydrostatic dynamical core designed for consistency and versatility, Geosci. Model Dev., 8(10), 3131–3150, doi:10.5194/gmd-8-3131-2015, 2015.

Dueck, T. A., de Visser, R., Poorter, H., Persijn, S., A. Gorissen, A., W. de Visser, W., Schapendonk, A., Verhagen, J., Snel, J., Harren, F. J. M., Ngai, A. K. Y., Verstappen, F., Bouwmeester, H., Voesenek, L. A. C. J. and van der Werf, A.: No evidence for substantial aerobic methane emission by terrestrial plants: a ^{13}C-labelling approach, New Phytol., doi:10.1111/j.1469-8137.2007.02103.x, 2007.

Duncan, B., Anderson, D., Fiore, A., Joiner, J., Krotkov, N., Li, C., Millet, D., Nicely, J., Oman, L., St. Clair, J., Shutter, J., Souri, A., Strode, S., Weir, B., Wolfe, G., Worden, H., and Zhu, Q.: Opinion: Beyond Global Means: Novel Space-Based Approaches to Indirectly Constrain the Concentrations, Trends, and Variations of Tropospheric Hydroxyl Radical (OH), EGUsphere [preprint], https://doi.org/10.5194/egusphere-2024-2331, 2024.

2733 Dutaur, L. and Verchot, L. V.: A global inventory of the soil CH_4 sink, Glob. Biogeochem Cycles, 21, GB4012,
2734   doi:10.1029/2006GB002734, 2007.

2735 Dyonisius, M. N., Petrenko, V. V., Smith, A. M., Hua, Q., Yang, B., Schmitt, J., Beck, J., Seth, B., Bock, M., Hmiel, B.,
2736   Vimont, I., Menking, J. A., Shackleton, S. A., Baggenstos, D., Bauska, T. K., Rhodes, R. H., Sperlich, P., Beaudette,
2737   R., Harth, C., Kalk, M., Brook, E.J., Fisher , H., Severinghaus, J.P., and Weiss, R. F.: Old carbon reservoirs were not
2738   important in the deglacial methane budget, Science, 367(6480), 907–910. https://doi.org/10.1126/science.aax0504,
2739   2020

2740 EDGAR (Emissions Database for Global Atmospheric Research) Community GHG Database (a collaboration between
2741   the European Commission, Joint Research Centre (JRC), the International Energy Agency (IEA), and comprising IEA-
2742   EDGAR CO2, EDGAR CH4, EDGAR N2O, EDGAR F-GASES version 7.0, European Commission, JRC (Datasets),
2743   available at https://edgar.jrc.ec.europa.eu/dataset_ghg70#sources, 2022

2744 EDGAR (Emissions Database for Global Atmospheric Research) Community GHG Database, a collaboration between the
2745   European Commission, Joint Research Centre (JRC), the International Energy Agency (IEA), and comprising IEA-
2746   EDGAR CO2, EDGAR CH4, EDGAR N2O, EDGAR F-GASES version 8.0, European Commission, JRC (Datasets),
2747   available at https://edgar.jrc.ec.europa.eu/dataset_ghg80, 2023

2748 Eggleton, P., Homathevi, R., Jones, D., MacDonald, J., Jeeva, D., Bignell, D., Davies, R., and Maryati, M.: Termite
2749   assemblages, forest disturbance and greenhouse gas fluxes in Sabah, East Malaysia, Philos. T. Roy. Soc. B, 354, 1791–
2750   1802, doi: 10.1098/rstb.1999.0521, 1999

2751 Ehhalt, D., Prather, M., Dentener, F., Derwent, R., Dlugokencky, E., Holland, E., Isaksen, I., Katima, J., Kirchhoff, V.,
2752   Matson, P., Midgley, P. and Wang, M.: Atmospheric chemistry and greenhouse gases. In: Climate Change 2001: The
2753   Scientific Basis. Contribution of Working Group I to the Third Assessment Report of the Intergovernmental Panel on
2754   Climate Change. [Houghton, J.T., et al. (eds.)]. Cambridge University Press, Cambridge, United Kingdom and New
2755   York, NY, USA, pp. 239-287, 2001.

2756 Ehhalt, D. H.: The atmospheric cycle of methane, Tellus, 26(1–2), 58–70, doi:10.1111/j.2153-3490.1974.tb01952.x, 1974.

2757 Ehret, G., Bousquet, P., Pierangelo, C., Alpers, M., Millet, B., Abshire, J. B., Bovensmann, H., Burrows, J. P., Chevallier,
2758   F., Ciais, P., Crevoisier, C., Fix, A., Flamant, P., Frankenberg, C., Gibert, F., Heim, B., Heimann, M., Houweling, S.,
2759   Hubberten, H. W., Jockel, P., Law, K., Low, A., Marshall, J., Agusti-Panareda, A., Payan, S., Prigent, C., Rairoux, P.,
2760   Sachs, T., Scholze, M. and Wirth, M.: MERLIN: A French-German Space Lidar Mission Dedicated to Atmospheric
2761   Methane, Remote Sens., 9(10), 2017.

2762 Etiope, G.: Natural Gas Seepage. The Earth's Hydrocarbon Degassing, Springer International Publishing., 2015.

2763 Etiope G.: Natural emissions of methane from geological seepage in Europe. Atmosph. Environment, 43, 1430-1443,
2764   doi:10.1016/j.atmosenv.2008.03.014., 2009

2765 Etiope, G. and Schwietzke, S.: Global geological methane emissions: an update of top-down and bottom-up estimates,

Elem Sci Anth, 7(1), 47, doi:10.1525/elementa.383, 2019.

Etiope, G., Lassey, K. R., Klusman, R. W. and Boschi, E.: Reappraisal of the fossil methane budget and related emission from geologic sources, Geophys. Res. Lett., 35(9), L09307, doi:10.1029/2008gl033623, 2008.

Etiope, G., Nakada, R., Tanaka, K. and Yoshida, N.: Gas seepage from Tokamachi mud volcanoes, onshore Niigata Basin (Japan): origin, post-genetic alterations and CH_4-CO_2 fluxes. *App. Geochem.,* 26, 348-359, 2011.

Etiope, G., Ciotoli, G., Schwietzke, S. and Schoell, M.: Gridded maps of geological methane emissions and their isotopic signature, Earth Syst Sci Data, 11(1), 1–22, doi:10.5194/essd-11-1-2019, 2019.

EU-Landfill-Directive: https://eur-lex.europa.eu/legal-content/EN/TXT/?uri=CELEX:31999L0031, 1999.

FAO: FAOSTAT Emissions Land Use database. Food and Agriculture Organization of the United Nations. Statistical Division., [online] Available from: http://www.fao.org/faostat/en/#data/GL (Accessed December 2022), 2022.

Federici, S., Tubiello, F. N., Salvatore, M., Jacobs, H. and Schmidhuber, J.: New estimates of CO2 forest emissions and removals: 1990–2015, For. Ecol. Manag., 352, 89–98, doi:10.1016/j.foreco.2015.04.022, 2015.

Feng, L., Braun, C., Arnold, S. R. and Gidden, M.: iiasa/emissions_downscaling: Supplemental Data, doi:10.5281/zenodo.2538194, 2019.

Feng, L., Palmer, P. I., Parker, R. J., Lunt, M. F., and Bösch, H.: Methane emissions are predominantly responsible for record-breaking atmospheric methane growth rates in 2020 and 2021, Atmos. Chem. Phys., 23, 4863–4880, https://doi.org/10.5194/acp-23-4863-2023, 2023.

Fest, B. J., Hinko-Najera, N., Wardlaw, T., Griffith, D. W. T., Livesley, S. J., and Arndt, S. K.: Soil methane oxidation in both dry and wet temperate eucalypt forests shows a near-identical relationship with soil air-filled porosity, Biogeosciences, 14, 467–479, https://doi.org/10.5194/bg-14-467-2017, 2017.

Filges, A., Gerbig, C., Chen, H., Franke, H., Klaus, C., and Jordan, A.: The IAGOS-core greenhouse gas package: a measurement system for continuous airborne observations of CO2, CH4, H2O and CO, Tellus B, 68, 27989, https://doi.org/10.3402/tellusb.v67.27989, 2015.

Fleischer, P., Orsi, T. H., Richardson, M. D., and Anderson, A. L. (2001). Distribution of free gas in marine sediments: a global overview. Geo-Marine Lett., 21, 103–122, 2001.

Flores, E., Rhoderick, G. C., Viallon, J., Moussay, P., Choteau, T., Gameson, L., Guenther, F. R. and Wielgosz, R. I.: Methane standards made in whole and synthetic air compared by cavity ring down spectroscopy and gas chromatography with flame ionization detection for atmospheric monitoring applications, Anal. Chem., 87(6), 3272–3279, doi:10.1021/ac5043076, 2015.

Fluet-Chouinard, E, Stocker, BD, Zhang, Z, Malhotra, A, Melton, JR, Poulter, B, Kaplan, JO, Goldewijk, KK, Siebert, S, Minayeva, T, Hugelius, G, Joosten, H, Barthelmes, A, Prigent, C, Aires, F, Hoyt, AM, Davidson, N, Finlayson, CM, Lehner, B, Jackson, RB, McIntyre, PB: Extensive global wetland loss over the past three centuries, Nature, 614(7947) 281-286, doi:10.1038/s41586-022-05572-6, 2023

2799   Forster, P., T. Storelvmo, K. Armour, W. Collins, J.-L. Dufresne, D. Frame, D.J. Lunt, T. Mauritsen, M.D. Palmer, M.
2800   Watanabe, M. Wild, and H. Zhang: The Earth's Energy Budget, Climate Feedbacks, and Climate Sensitivity. In
2801   Climate Change 2021: The Physical Science Basis. Contribution of Working Group I to the Sixth Assessment Report
2802   of the Intergovernmental Panel on Climate Change [Masson-Delmotte, V., P. Zhai, A. Pirani, S.L. Connors, C. Péan,
2803   S. Berger, N. Caud, Y. Chen, L. Goldfarb, M.I. Gomis, M. Huang, K. Leitzell, E. Lonnoy, J.B.R. Matthews, T.K.
2804   Maycock, T. Waterfield, O. Yelekçi, R. Yu, and B. Zhou (eds.)]. Cambridge University Press, Cambridge, United
2805   Kingdom and New York, NY, USA, pp. 923–1054, doi: 10.1017/9781009157896.009, 2021

2806   Foschi M., Etiope G., Cartwright J.A.: Seismic evidence of extensive microbial gas migration and trapping in submarine
2807   marine   hydrates   (Rakhine   Basin,   Bay   of   Bengal).   Mar.   Petrol.   Geol.,   149,   106100,
2808   https://doi.org/10.1016/j.marpetgeo.2023.106100., 2023

2809   France, J. L., Lunt, M. F., Andrade, M., Moreno, I., Ganesan, A. L., Lachlan-Cope, T., Fisher, R. E., Lowry, D., Parker,
2810   R. J., Nisbet, E. G., and Jones, A. E.: Very large fluxes of methane measured above Bolivian seasonal wetlands, P.
2811   Natl. Acad. Sci. USA, 119, e2206345119, https://doi.org/10.1073/pnas.2206345119, 2022.

2812   Francey, R. J., Steele, L. P., Langenfelds, R. L. and Pak, B. C.: High precision long-term monitoring of radiatively active
2813   and related trace gases at surface sites and from aircraft in the southern hemisphere atmosphere, J. Atmospheric Sci.,
2814   56(2), 279–285, 1999.

2815   Frankenberg, C., Meirink, J. F., van Weele, M., Platt, U. and Wagner, T.: Assessing methane emissions from global space-
2816   borne observations, Science, 308(5724), 1010–1014, 2005.

2817   Fraser, P. J., Rasmussen, R. A., Creffield, J. W., French, J. R. and Khalil, M. A. K.: Termites and global methane – Another
2818   assessment, J. Atmospheric Chem., 4, 295–310, 1986.

2819   Fraser, W. T., Blei, E., Fry, S. C., Newman, M. F., Reay, D. S., Smith, K. A. and McLeod, A. R.: Emission of methane,
2820   carbon monoxide, carbon dioxide and short-chain hydrocarbons from vegetation foliage under ultraviolet irradiation,
2821   Plant Cell Environ., 38(5), 980–989, doi:10.1111/pce.12489, 2015.

2822   Fujita, R., Morimoto, S., Maksyutov, S., Kim, H.-S., Arshinov, M., Brailsford, G., Aoki, S. and Nakazawa, T.: Global and
2823   Regional CH4 Emissions for 1995–2013 Derived From Atmospheric CH4, δ13C-CH4, and δD-CH4 Observations and
2824   a   715   Chemical   Transport   Model.   J.   Geophys.   Res.   Atmos.,   125:   e2020JD032903.
2825   https://doi.org/10.1029/2020JD032903, 2020

2826   Gauci, V., Figueiredo, V., Gedney, N., Pangala, S. R., Stauffer, T., Weedon, G., P. and Enrich-Prast A. Non-flooded
2827   riparian Amazon trees are a regionally significant methane source   , *Phil. Trans. R. Soc. A,*   3802020044620200446
2828   http://doi.org/10.1098/rsta.2020.0446,   2022.

2829   Gauci, V., Pangala, S.R., Shenkin, A., Barba, J., Bastviken, D., Figueiredo, V., Gomez, C., Enrich-Prast A., Sayer, E., s-
2830   Stauufer, T., Welch, B., Elias, D., McNamara, N., Allen, M, and Malhi Y.: Global atmospheric methane uptake by
2831   upland tree woody surfaces, Nature, 631, 796–800 , https://doi.org/10.1038/s41586-024-07592-w, 2024

Gedney, N., Huntinford, C., Comyn Platt, E. and Wiltshire, A. Significant feedbacks of wetland methane release on climate change and the causes of their uncertainty. Env. Res. Letts. 14, 084027 doi:10.1088/1748-9326/ab2726, 2019.

Gidden, M. J., Riahi, K., Smith, S. J., Fujimori, S., Luderer, G., Kriegler, E., Vuuren, D. P. van, Berg, M. van den, Feng, L., Klein, D., Calvin, K., Doelman, J. C., Frank, S., Fricko, O., Harmsen, M., Hasegawa, T., Havlik, P., Hilaire, J., Hoesly, R., Horing, J., Popp, A., Stehfest, E. and Takahashi, K.: Global emissions pathways under different socioeconomic scenarios for use in CMIP6: a dataset of harmonized emissions trajectories through the end of the century, Geosci. Model Dev., 12(4), 1443–1475, doi:10.5194/gmd-12-1443-2019, 2019.

Giglio, L., Randerson, J. T. and van der Werf, G. R.: Analysis of daily, monthly, and annual burned area using the fourth-generation global fire emissions database (GFED4), J. Geophys. Res. - Biogeosciences, 118(1), 317–328, doi:10.1002/jgrg.20042, 2013.

Glagolev, M., Kleptsova, I., Filippov, I., Maksyutov, S. and Machida, T.: Regional methane emission from West Siberia mire landscapes, Environ. Res. Lett., 6(4), 045214, doi:doi:10.1088/1748-9326/6/4/045214, 2011.

Glatthor, N., von Clarmann, T., Funke, B., Garcia-Comas, M., Grabowski, U., Höpfner, M., Kellmann, S., Kiefer, M., Laeng, A., Linden, A., Lopez-Puertas, M., and Stiller, G. P.: IMK/IAA MIPAS retrievals version 8: CH4 and N2O, EGUsphere [preprint], https://doi.org/10.5194/egusphere-2023-919, 2023.

Global Methane Pledge, Global Methane Pledge website: Pledges, 1 September. https://www.globalmethanepledge.org/#pledges. Accessed 28 September 2023, 2023.

Gorgolewski, A. S., Caspersen, J. P., Vantellingen, J., and Thomas, S. C.: Tree foliage is a methane sink in upland temperate forests, Ecosystems, 26, 174–186, 2023.

Greinert, J., Artemov, Y., Egorov, V., De Batist, M., McGinnis, D.: 1300-m-high rising bubbles from mud volcanoes at 2080 m in the Black Sea: Hydroacoustic characteristics and temporal variability, Earth and Planetary Science Letters, 244, 1-2, https://doi.org/10.1016/j.epsl.2006.02.011, 2006

Griffiths, K., A. Jeziorski, D. Antoniades, M. Beaulieu, J.P. Smol, and I. Gregory-Eaves, Pervasive changes in algal indicators since pre-industrial times: A paleolimnological study of changes in primary production and diatom assemblages from ~200 Canadian lakes. Science of The Total Environment, 838: p. 155938., 2022.

Grinham, A., M. Dunbabin, D. Gale, and J. Udy, Quantification of ebullitive and diffusive methane release to atmosphere from a water storage. Atmospheric Environment, 45(39): p. 7166-7173., 2011.

Gromov, S., Brenninkmeijer, C. A. M. and Jöckel, P.: A very limited role of tropospheric chlorine as a sink of the greenhouse gas methane, Atmospheric Chem. Phys., 18(13), 9831–9843, doi:10.5194/acp-18-9831-2018, 2018.

Guo, M., Fang, S., Liu, S., Liang, M., Wu, H., Yang, L., Li, Z., Liu, P., Zhang, F: Comparison of atmospheric CO2, CH4, and CO at two stations in the Tibetan Plateau of China, *Earth Space Sci, 7*, e2019EA001051, 2020

Gurney, K. R., Law, R. M., Denning, A. S., Rayner, P. J., Pak, B. C., Baker, D., Bousquet, P., Bruhwiler, L., Chen, Y. H., Ciais, P., Fung, I. Y., Heimann, M., John, J., Maki, T., Maksyutov, S., Peylin, P., Prather, M. and Taguchi, S.: Transcom

3 inversion intercomparison: Model mean results for the estimation of seasonal carbon sources and sinks, Glob. Biogeochem. Cycles, 18(1), GB2010, doi:10.1029/2003gb002111, 2004.

Harris, S. A., French, H. M., Heginbottom, J. A., Johnston, G. H., Ladanyi, B., Sego, D. C. and van Everdingen, R. O.: Glossary of permafrost and related ground-ice terms, National Research Council of Canada. Associate Committee on Geotechnical Research. Permafrost Subcommittee., 1988.

Harris, I., Jones, P.D., Osborn, T.J. and Lister, D.H.: Updated high-resolution grids of monthly climatic observations – the CRU TS3.10 Dataset, Int. J. Climatol., 34: 623-642. https://doi.org/10.1002/joc.3711, 2014

Harrison, J.A., Y.T. Prairie, S. Mercier-Blais, and C. Soued: Year-2020 Global Distribution and Pathways of Reservoir Methane and Carbon Dioxide Emissions According to the Greenhouse Gas From Reservoirs (G-res) Model. Global Biogeochemical Cycles 35(6): p. e2020GB006888, 2021.

Heathcote, A. J., C. T. Filstrup, and J. A. Downing (2013): Watershed sediment losses to lakes accelerating despite agricultural soil conservation efforts, *PLoS One*, 8(1), e53554, doi:10.1371/journal.pone.0053554, 2013

Heděnec, P., Jiménez, J.J., Moradi, J. *et al.*: Global distribution of soil fauna functional groups and their estimated litter consumption across biomes. Sci Rep 12, 17362, https://doi.org/10.1038/s41598-022-21563-z, 2022

Hempson, G.P., Archibald, S, and Bond, W.J.: The consequences of replacing wildlife with livestock in Africa, Sci Rep, 7, 17196, https://doi.org/10.1038/s41598-017-17348-4, 2017

Hill, J., McSweeney, C., Wright, A.-D. G., Bishop-Hurley, G., and Kalantar-zadeh, K.: Measuring Methane Production from Ruminants, Trends in Biotechnology, Volume 34, Issue 1, doi:10.1016/j.tibtech.2015.10.004, 2016

Hmiel, B., Petrenko, V. V., Dyonisius, M. N., Buizert, C., Smith, A. M., Place, P. F., Harth, C., Beaudette, R., Hua, Q., Yang, B., Vimont, I., Michel, S. E., Severinghaus, J. P., Etheridge, D., Bromley, T., Schmitt, J., Faïn, X., Weiss, R. F. and Dlugokencky, E.: Preindustrial 14 CH 4 indicates greater anthropogenic fossil CH 4 emissions, Nature, 578(7795), 409–412, doi:10.1038/s41586-020-1991-8, 2020.

Ho, J.C., A.M. Michalak, and N. Pahlevan: Widespread global increase in intense lake phytoplankton blooms since the 1980s. Nature, 574(7780): p. 667-670, 2019

Hoesly, R. M., Smith, S. J., Feng, L., Klimont, Z., Janssens-Maenhout, G., Pitkanen, T., Seibert, J. J., Vu, L., Andres, R. J., Bolt, R. M., Bond, T. C., Dawidowski, L., Kholod, N., Kurokawa, J. I., Li, M., Liu, L., Lu, Z., Moura, M. C. P., O'Rourke, P. R. and Zhang, Q.: Historical (1750–2014) anthropogenic emissions of reactive gases and aerosols from the Community Emissions Data System (CEDS), Geosci Model Dev, 11(1), 369–408, doi:10.5194/gmd-11-369-2018, 2018.

Höglund-Isaksson, L.: Bottom-up simulations of methane and ethane emissions from global oil and gas systems 1980 to 2012, Environ. Res. Lett., 12(2), 024007, doi:10.1088/1748-9326/aa583e, 2017.

Höglund-Isaksson, L., Thomson, A., Kupiainen, K., Rao, S. and Janssens-Maenhout, G.: Anthropogenic methane sources, emissions and future projections, Chapter 5 in AMAP Assessment 2015: Methane as an Arctic Climate Forcer, p. 39-

59, available at http://www.amap.no/documents/doc/AMAP-Assessment-2015-Methane-as-an-Arctic-climate-forcer/1285., 2015.

Höglund-Isaksson, L., Gómez-Sanabria, A., Klimont, Z., Rafaj, P., Schöpp, W.,: Technical potentials and costs for reducing global anthropogenic methane emissions in the 2050 timeframe -results from the GAINS model, Environ. Res. Comm. 2(2), https://iopscience.iop.org/article/10.1088/2515-7620/ab7457 , 2020

Holgerson, M. A. and Raymond, P. A.: Large contribution to inland water CO 2 and CH 4 emissions from very small ponds, Nat. Geosci., 9(3), 222–226, doi:10.1038/ngeo2654, 2016.

Holmes, C. D., Prather, M. J., Søvde, O. A. and Myhre, G.: Future methane, hydroxyl, and their uncertainties: key climate and emission parameters for future predictions, Atmospheric Chem. Phys., 13(1), 285–302, doi:10.5194/acp-13-285-2013, 2013.

Hopcroft,P.O. , P.J. Valdes & D.J. Beerling, (2011). Simulating idealised Dansgaard-Oeschger events and their potential influence on the global methane cycle, Quaternary Science Reviews, 30, 3258-3268,

doi: 10.1016/j.quascirev.2011.08.01., 2011

Hossaini, R., Chipperfield, M. P., Saiz-Lopez, A., Fernandez, R., Monks, S., Feng, W., Brauer, P. and Glasow, R. von: A global model of tropospheric chlorine chemistry: Organic versus inorganic sources and impact on methane oxidation, J. Geophys. Res. Atmospheres, 121(23), 14,271-14,297, doi:10.1002/2016JD025756, 2016.

Houweling, S., Bergamaschi, P., Chevallier, F., Heimann, M., Kaminski, T., Krol, M., Michalak, A. M. and Patra, P.: Global inverse modeling of CH4 sources and sinks: an overview of methods, Atmospheric Chem. Phys., 17(1), 235–256, doi:10.5194/acp-17-235-2017, 2017.

M. Hovland, A.G. Judd, R.A. Burke: The global flux of methane from shallow submarine sediments, Chemosphere, Volume 26, Issues 1–4, Pages 559-578, doi:10.1016/0045-6535(93)90442-8., 1993

Howarth, R. W.: Ideas and perspectives: is shale gas a major driver of recent increase in global atmospheric methane?, Biogeosciences, 16(15), 3033–3046, doi:10.5194/bg-16-3033-2019, 2019.

Hu, H., Landgraf, J., Detmers, R., Borsdorff, T., Brugh, J. A. de, Aben, I., Butz, A. and Hasekamp, O.: Toward Global Mapping of Methane With TROPOMI: First Results and Intersatellite Comparison to GOSAT, Geophys. Res. Lett., 45(8), 3682–3689, doi:10.1002/2018GL077259, 2018.

Hugelius, G., Tarnocai, C., Broll, G., Canadell, J. G., Kuhry, P., & Swanson, D. K.. The Northern Circumpolar Soil Carbon Database: spatially distributed datasets of soil coverage and soil carbon storage in the northern permafrost regions. *Earth System Science Data*, 5(1), 3–13. https://doi.org/10.5194/essd-5-3-2013, 2013

Hugelius, G., Strauss, J., Zubrzycki, S., Harden, J. W., Schuur, E. A. G., Ping, C. L., Schirrmeister, L., Grosse, G., Michaelson, G. J., Koven, C. D., O'Donnell, J. A., Elberling, B., Mishra, U., Camill, P., Yu, Z., Palmtag, J. and Kuhry, P.: Estimated stocks of circumpolar permafrost carbon with quantified uncertainty ranges and identified data gaps, Biogeosciences, 11(23), 6573–6593, doi:10.5194/bg-11-6573-2014, 2014.

Hugelius, Gustaf, Loisel, J., Chadburn, S., Jackson, R. B., Jones, M., MacDonald, G., et al. : Large stocks of peatland carbon and nitrogen are vulnerable to permafrost thaw. Proceedings of the National Academy of Sciences, 117(34), 20438–20446. https://doi.org/10.1073/pnas.1916387117, 2020

Hugelius, G., Ramage, J.L., Burke, E.J., Chatterjee, A., Smallman, T.L., Aalto, T., Bastos, A., Biasi, C., Canadell, J.G., Chandra, N. and Chevallier, F., et al. Two decades of permafrost region CO2, CH4, and N2O budgets suggest a small net greenhouse gas source to the atmosphere. Preprint in ESS Open Archive. September 11, 2023. DOI: 10.22541/essoar.169444320.01914726/v1, 2023

IEA, *Coal Information: Overview*, IEA, Paris https://www.iea.org/reports/coal-information-overview, License: CC BY 4.0, Accessed 17 January 2024, 2021

IEA (2023), Energy Statistics Data Browser, IEA, Paris https://www.iea.org/data-and-statistics/data-tools/energy-statistics-data-browser, Accessed 17 January 2024, 2023a

IEA, US natural gas production by source, 2013-2023, IEA, Paris https://www.iea.org/data-and-statistics/charts/us-natural-gas-production-by-source-2013-2023, IEA. Licence: CC BY 4.0,Accessed 17 January 2024, 2023b

Imasu, R.; Matsunaga, T.; Nakajima, M.; Yoshida, Y.; Shiomi, K.; Morino, I.; Saitoh, N.; Niwa, Y.; Someya, Y.; Oishi, Y.; et al. Greenhouse Gases Observing SATellite 2 (GOSAT-2): Mission Overview. Prog. Earth Planet. Sci., *10*, 33., 2023,

Inoue, M., Morino, I., Uchino, O., Nakatsuru, T., Yoshida, Y., Yokota, T., Wunch, D., Wennberg, P. O., Roehl, C. M., Griffith, D. W. T., Velazco, V. A., Deutscher, N. M., Warneke, T., Notholt, J., Robinson, J., Sherlock, V., Hase, F., Blumenstock, T., Rettinger, M., Sussmann, R., Kyrö, E., Kivi, R., Shiomi, K., Kawakami, S., Mazière, M. D., Arnold, S. G., Feist, D. G., Barrow, E. A., Barney, J., Dubey, M., Schneider, M., Iraci, L. T., Podolske, J. R., Hillyard, P. W., Machida, T., Sawa, Y., Tsuboi, K., Matsueda, H., Sweeney, C., Tans, P. P., Andrews, A. E., Biraud, S. C., Fukuyama, Y., Pittman, J. V., Kort, E. A. and Tanaka, T.: Bias corrections of GOSAT SWIR XCO_2 and XCH_4 with TCCON data and their evaluation using aircraft measurement data, Atmospheric Meas. Tech., 9(8), 3491–3512, doi:10.5194/amt-9-3491-2016, 2016.

IPCC: Good Practice Guidance and Uncertainty Management in National Greenhouse Gas Inventories. Intergovernmental Panel on Climate Change, National Greenhouse Gas Inventories Programme. Montreal, IPCC-XVI/Doc.10(1.IV.2000), May 2000., 2000.

IPCC: Climate change 2001: The scientific basis. Contribution of working group I to the third assessment report of the Intergovernmental Panel on Climate Change, Cambridge University Press, Cambridge, United Kingdom and New York, NY, USA., 2001.

IPCC: IPCC Guidelines for National Greenhouse Gas Inventories. The National Greenhouse Gas Inventories Programme, Eggleston H.S., Buendia L., Miwa K., Ngara T. and Tanabe K. (eds). The Intergovernmental Panel on Climate Change, IPCC TSU NGGIP, IGES. Institute for Global Environmental Strategy, Hayama, Kanagawa, Japan. Available online

at: http://www.ipcc-nggip.iges.or.jp/support/Primer_2006GLs.pdf., 2006.

IPCC: 2019 Refinement to the 2006 IPCC Guidelines for National Greenhouse Gas Inventories — IPCC. [online] Available from: https://www.ipcc.ch/report/2019-refinement-to-the-2006-ipcc-guidelines-for-national-greenhouse-gas-inventories/ (Accessed 17 March 2020), 2019.

Ito, A. and Inatomi, M.: Use of a process-based model for assessing the methane budgets of global terrestrial ecosystems and evaluation of uncertainty, Biogeosciences, 9(2), 759–773, doi:10.5194/bg-9-759-2012, 2012.

Jacob, D. J., Varon, D. J., Cusworth, D. H., Dennison, P. E., Frankenberg, C., Gautam, R., Guanter, L., Kelley, J., McKeever, J., Ott, L. E., Poulter, B., Qu, Z., Thorpe, A. K., Worden, J. R., and Duren, R. M.: Quantifying methane emissions from the global scale down to point sources using satellite observations of atmospheric methane, Atmos. Chem. Phys., 22, 9617–9646, https://doi.org/10.5194/acp-22-9617-2022, 2022.

Jackson, R. B., Down, A., Phillips, N. G., Ackley, R. C., Cook, C. W., Plata, D. L. and Zhao, K.: Natural gas pipeline leaks across Washington, D.C, Environ. Sci. Technol., 48(3), 2051–2058, doi:10.1021/es404474x, 2014a.

Jackson, R. B., Saunois, M., Bousquet, P., Canadell, J. G., Poulter, B., Stavert, A. R., Poulter, B., Bergamaschi, P., Niwa, Y., Segers, A., Tsuruta, A.: Increasing anthropogenic methane emissions arise equally from agricultural and fossil fuel sources, Environmental Research Letters, 15, 7, https://doi.org/10.1088/1748-9326/ab9ed2, 2020

Jackson, R. B., Saunois, M., Martinez, A., Canadell, J. G., Yu, X., Li, M., Poulter, B., Raymind, P., Regnier, P., Davis, S.J., and Patra, P.: Human activities now fuel two-thirds of global methane emissions, Environmental Research Letters, 19, 101002, DOI:10.1088/1748-9326/ad6463, 2024

Jamali, H., Livesley, S.J., Dawes, T.Z. *et al.* Termite mound emissions of CH_4 and CO_2 are primarily determined by seasonal changes in termite biomass and behaviour. *Oecologia* 167, 525–534, doi.org/10.1007/s00442-011-1991-3, 2011

Janssens-Maenhout, G., Crippa, M., Guizzardi, D., Muntean, M., Schaaf, E., Dentener, F., Bergamaschi, P., Pagliari, V., Olivier, J., Peters, J., van Aardenne, J., Monni, S., Doering, U., Petrescu, R., Solazzo, E. and Oreggioni, G.: EDGAR v4.3.2 Global Atlas of the three major Greenhouse Gas Emissions for the period 1970-2012, Earth Syst Sci Data Discuss, 2019, 1–52, doi:10.5194/essd-2018-164, 2019.

JAXA: GOSAT-2: Greenhouse gases Observing SATellite-2@ibuki2_JAXA"IBUKI-2", [online] Available from: https://global.jaxa.jp/projects/sat/gosat2/index.html (Accessed 25 March 2020), 2019.

Jensen, K. and Mcdonald, K.: Surface Water Microwave Product Series Version 3: A Near-Real Time and 25-Year Historical Global Inundated Area Fraction Time Series From Active and Passive Microwave Remote Sensing, IEEE Geosci. Remote Sens. Lett., 16(9), 1402–1406, doi:10.1109/LGRS.2019.2898779, 2019.

Jiang, Y., Groenigen, K. J. van, Huang, S., Hungate, B. A., Kessel, C. van, Hu, S., Zhang, J., Wu, L., Yan, X., Wang, L., Chen, J., Hang, X., Zhang, Y., Horwath, W. R., Ye, R., Linquist, B. A., Song, Z., Zheng, C., Deng, A. and Zhang, W.: Higher yields and lower methane emissions with new rice cultivars, Glob. Change Biol., 23(11), 4728–4738,

2997   doi:10.1111/gcb.13737, 2017.

2998   Johnson, D. E., Phetteplace, H. W. and Seidl, A. F.: Methane, nitrous oxide and carbon dioxide emissions from ruminant
2999   livestock production systems, edited by J. Takahashi and B. A. Young, pp. 77–85, Elsevier, Amsterdam, The
3000   Netherlands., 2002.

3001   Johnson, M.S., E. Matthews, J. Du, V. Genovese, and D. Bastviken, Methane Emission From Global Lakes: New
3002   Spatiotemporal Data and Observation-Driven Modeling of Methane Dynamics Indicates Lower Emissions, Journal of
3003   Geophysical Research: Biogeosciences, 127(7): p. e2022JG006793, 2022

3004   Johnson, M. S., E. Matthews, D. Bastviken, B. Deemer, J. Du, and V. Genovese, Spatiotemporal methane emission from
3005   global reservoirs, Journal of Geophysical Research: Biogeosciences, 126, e2021JG006305,
3006   https://doi.org/10.1029/2021JG006305, 2021

3007   Judd, A.G. (2004). Natural seabed seeps as sources of atmospheric methane, Environ. Geol., 46, 988–996, 2004.

3008   Jung, M., Reichstein, M., Margolis, H. A., Cescatti, A., Richardson, A. D., Arain, M. A., Arneth, A., Bernhofer, C., Bonal,
3009   D., Chen, J., Gianelle, D., Gobron, N., Kiely, G., Kutsch, W., Lasslop, G., Law, B. E., Lindroth, A., Merbold, L.,
3010   Montagnani, L., Moors, E. J., Papale, D., Sottocornola, M., Vaccari, F., and Williams, C.: Global patterns of land-
3011   atmosphere fluxes of carbon dioxide, latent heat, and sensible heat derived from eddy covariance, satellite, and
3012   meteorological observations, J. Geophys. Res., 116, G00J07,https://doi.org/10.1029/2010jg001566, 2011.

3013   Kai, F. M., Tyler, S. C., Randerson, J. T. and Blake, D. R.: Reduced methane growth rate explained by decreased Northern
3014   Hemisphere microbial sources, Nature, 476(7359), 194–197, 2011.

3015   Kaiser, J. W., Heil, A., Andreae, M. O., Benedetti, A., Chubarova, N., Jones, L., Morcrette, J. J., Razinger, M., Schultz,
3016   M. G., Suttie, M. and van der Werf, G. R.: Biomass burning emissions estimated with a global fire assimilation system
3017   based on observed fire radiative power, Biogeosciences, 9(1), 527–554, doi:10.5194/bg-9-527-2012, 2012.

3018   Kallingal, J. T., Lindström, J., Miller, P. A., Rinne, J., Raivonen, M., and Scholze, M.: Optimising CH_4 simulations from
3019   the LPJ-GUESS model v4.1 using an adaptive Markov chain Monte Carlo algorithm, Geosci. Model Dev., 17, 2299–
3020   2324, https://doi.org/10.5194/gmd-17-2299-2024, 2024.

3021   Karl, D., Beversdorf, L., Björkman, K. *et al.* Aerobic production of methane in the sea. *Nature Geosci* **1**, 473–478 ,
3022   https://doi.org/10.1038/ngeo234), 2008

3023   Karlson, M., and Bastviken, D.: Multi-Source Mapping of Peatland Types Using Sentinel-1, Sentinel-2, and Terrain
3024   Derivatives—A Comparison Between Five High-Latitude Landscapes. Journal of Geophysical Research:
3025   Biogeosciences 128, e2022JG007195. https://doi.org/10.1029/2022JG007195, 2023

3026   Keppler, F., Hamilton, J. T. G., Brass, M. and Rockmann, T.: Methane emissions from terrestrial plants under aerobic
3027   conditions, Nature, 439, 187–191, doi:10.1038/nature04420, 2006.

3028   Kholod, N., Evans, M., Pilcher, R. C., Roshchanka, V., Ruiz, F., Coté, M. and Collings, R.: Global methane emissions
3029   from coal mining to continue growing even with declining coal production, J. Clean. Prod., 256, 120489,

3030   doi:10.1016/j.jclepro.2020.120489, 2020.

3031 Kim H., Global Soil Wetness Project Phase 3 Atmospheric Boundary Conditions (Experiment 1) [Data set]. Data
3032   Integration and Analysis System (DIAS)., https://doi.org/10.20783/DIAS.501, 2017

3033 King, J.R., Warren, R.J., Bradford, M.A. Correction: Social Insects Dominate Eastern US Temperate Hardwood Forest
3034   Macroinvertebrate Communities in Warmer Regions. PLOS ONE 8(10): 10.1371/annotation/87285c86-f1df-4f8b-
3035   bc08-d64643d351f4, 2013.

3036 Kirk, L, and MJ Cohen: River Corridor Sources Dominate CO_2 Emissions From a Lowland River Network. Journal of
3037   Geophysical Research, Biogeosciences, 128(1), e2022JG006954, 2023.

3038 Kirschke, S., Bousquet, P., Ciais, P., Saunois, M., Canadell, J. G., Dlugokencky, E. J., Bergamaschi, P., Bergmann, D.,
3039   Blake, D. R., Bruhwiler, L., Cameron-Smith, P., Castaldi, S., Chevallier, F., Feng, L., Fraser, A., Heimann, M.,
3040   Hodson, E. L., Houweling, S., Josse, B., Fraser, P. J., Krummel, P. B., Lamarque, J. F., Langenfelds, R. L., Le Quere,
3041   C., Naik, V., O'Doherty, S., Palmer, P. I., Pison, I., Plummer, D., Poulter, B., Prinn, R. G., Rigby, M., Ringeval, B.,
3042   Santini, M., Schmidt, M., Shindell, D. T., Simpson, I. J., Spahni, R., Steele, L. P., Strode, S. A., Sudo, K., Szopa, S.,
3043   van der Werf, G. R., Voulgarakis, A., van Weele, M., Weiss, R. F., Williams, J. E. and Zeng, G.: Three decades of
3044   global methane sources and sinks, Nat. Geosci., 6(10), 813–823, doi:10.1038/ngeo1955, 2013.

3045 Klauda, J. B. and Sandler, S. I.: Global distribution of methane hydrate in ocean sediment, Energy Fuels, 19(2), 459–470,
3046   2005.

3047 Kleinen, T., Brovkin, V. and Schuldt, R. J.: A dynamic model of wetland extent and peat accumulation: results for the
3048   Holocene, Biogeosciences, 9(1), 235–248, doi:10.5194/bg-9-235-2012, 2012.

3049 Kleinen, T., Mikolajewicz, U., and Brovkin, V.: Terrestrial methane emissions from the Last Glacial Maximum to the
3050   preindustrial period, Clim. Past, 16, 575–595, doi:10.5194/cp-16-575-2020, 2020.

3051 Kleinen, T., Gromov, S., Steil, B., and Brovkin, V.: Atmospheric methane underestimated in future climate projections,
3052   Environ. Res. Lett., 16, 094006, doi:10.1088/1748-9326/ac1814, 2021.

3053 Kleinen, T., Gromov, S., Steil, B., and Brovkin, V.: Atmospheric methane since the last glacial maximum was driven by
3054   wetland sources, Clim. Past, 19, 1081–1099, doi:10.5194/cp-19-1081-2023, 2023

3055 Knittel K and Boetius A : Anaerobic oxidation of methane: progress with an unknown process methane. Annu Rev
3056   Microbiol 63:311–334, 2009

3057 Knox, S. H., Jackson, R. B., Poulter, B., McNicol, G., Fluet-Chouinard, E., Zhang, Z., Hugelius, G., Bousquet, P.,
3058   Canadell, J. G., Saunois, M., Papale, D., Chu, H., Keenan, T. F., Baldocchi, D., Torn, M. S., Mammarella, I., Trotta,
3059   C., Aurela, M., Bohrer, G., Campbell, D. I., Cescatti, A., Chamberlain, S., Chen, J., Chen, W., Dengel, S., Desai, A.
3060   R., Euskirchen, E., Friborg, T., Gasbarra, D., Goded, I., Goeckede, M., Heimann, M., Helbig, M., Hirano, T., Hollinger,
3061   D. Y., Iwata, H., Kang, M., Klatt, J., Krauss, K. W., Kutzbach, L., Lohila, A., Mitra, B., Morin, T. H., Nilsson, M. B.,
3062   Niu, S., Noormets, A., Oechel, W. C., Peichl, M., Peltola, O., Reba, M. L., Richardson, A. D., Runkle, B. R. K., Ryu,

Y., Sachs, T., Schäfer, K. V. R., Schmid, H. P., Shurpali, N., Sonnentag, O., Tang, A. C. I., Ueyama, M., Vargas, R., Vesala, T., Ward, E. J., Windham-Myers, L., Wohlfahrt, G. and Zona, D.: FLUXNET-CH4 Synthesis Activity: Objectives, Observations, and Future Directions, Bull. Am. Meteorol. Soc., 100(12), 2607–2632, doi:10.1175/BAMS-D-18-0268.1, 2019.

Knox, S. H., Bansal, S., McNicol, G., Schafer, K., Sturtevant, C., Ueyama, M., et al.:. Identifying dominant environmental predictors of freshwater wetland methane fluxes across diurnal to seasonal time scales. *Global Change Biology*, 27(15), 3582–3604. https://doi.org/10.1111/gcb.15661, 2021

Kretschmer, K., Biastoch, A., Rüpke, L. and Burwicz, E.: Modeling the fate of methane hydrates under global warming, Glob. Biogeochem Cycles, 29(5), 610–625, doi:1002/2014GB005011, 2015.

Kuhn, M.A., Varner, R.K., Bastviken, D., Crill, P., MacIntyre, S., Turetsky, M., Walter Anthony, K., McGuire, A.D., and Olefeldt, D. (2021). BAWLD-CH4: a comprehensive dataset of methane fluxes from boreal and arctic ecosystems. Earth Syst. Sci. Data 13, 5151-5189. 10.5194/essd-13-5151-2021.

Kuze A, Kikuchi N, Kataoka F, Suto H, Shiomi K, Kondo Y. Detection of Methane Emission from a Local Source Using GOSAT Target Observations. *Remote Sensing*, 12(2):267. https://doi.org/10.3390/rs12020267, 2020

Kyzivat, E.D., L.C. Smith, F. Garcia-Tigreros, C. Huang, C. Wang, T. Langhorst, J.V. Fayne, M.E. Harlan, Y. Ishitsuka, D. Feng, W. Dolan, L.H. Pitcher, K.P. Wickland, M.M. Dornblaser, R.G. Striegl, T.M. Pavelsky, D.E. Butman, and C.J. Gleason, The Importance of Lake Emergent Aquatic Vegetation for Estimating Arctic-Boreal Methane Emissions. Journal of Geophysical Research: Biogeosciences 127(6): p. e2021JG006635, 2022.

Lamarque, J. F., Shindell, D. T., Josse, B., Young, P. J., Cionni, I., Eyring, V., Bergmann, D., Cameron-Smith, P., Collins, W. J., Doherty, R., Dalsoren, S., Faluvegi, G., Folberth, G., Ghan, S. J., Horowitz, L. W., Lee, Y. H., MacKenzie, I. A., Nagashima, T., Naik, V., Plummer, D., Righi, M., Rumbold, S. T., Schulz, M., Skeie, R. B., Stevenson, D. S., Strode, S., Sudo, K., Szopa, S., Voulgarakis, A. and Zeng, G.: The Atmospheric Chemistry and Climate Model Intercomparison Project (ACCMIP): overview and description of models, simulations and climate diagnostics, Geosci. Model Dev., 6(1), 179–206, doi:10.5194/gmd-6-179-2013, 2013.

Lamb, B. K., Edburg, S. L., Ferrara, T. W., Howard, T., Harrison, M. R., Kolb, C. E., Townsend-Small, A., Dyck, W., Possolo, A. and Whetstone, J. R.: Direct Measurements Show Decreasing Methane Emissions from Natural Gas Local Distribution Systems in the United States, Environ. Sci. Technol., 49(8), 5161–5169, doi:10.1021/es505116p, 2015.

Lan, X., K.W. Thoning, and E.J. Dlugokencky: Trends in globally-averaged CH4, N2O, and SF6 determined from NOAA Global Monitoring Laboratory measurements. Version 2024-02, https://doi.org/10.15138/P8XG-AA10, 2024

Lange S., WFDE5 over land merged with ERA5 over the ocean (W5E5). V. 1.0. 2019. doi:10.5880/pik.2019.023, 2019

Laruelle, G. G., Dürr, H. H., Lauerwald, R., Hartmann, J., Slomp, C. P., Goossens, N. and Regnier, P. A. G.: Global multi-scale segmentation of continental and coastal waters from the watersheds to the continental margins, Hydrol. Earth Syst. Sci., 17(5), 2029–2051, doi:10.5194/hess-17-2029-2013, 2013.

Laruelle, G.G., Rosentreter, J.A. and Regnier, P.: Extrapolation-Based Regionalized Re-evaluation of the Global Estuarine Surface Area. Estuaries and Coasts, 48, 34, https://doi.org/10.1007/s12237-024-01463-3, 2025

Lassey, K. R., Etheridge, D. M., Lowe, D. C., Smith, A. M. and Ferretti, D. F.: Centennial evolution of the atmospheric methane budget: what do the carbon isotopes tell us?, Atmospheric Chem. Phys., 7(8), 2119–2139, 2007a.

Lassey, K. R., Lowe, D. C. and Smith, A. M.: The atmospheric cycling of radiomethane and the "fossil fraction" of the methane source, Atmospheric Chem. Phys., 7(8), 2141–2149, 2007b.

Lauerwald, R., Allen, G.H., Deemer, B.R., Liu, S., Maavara, T., Raymond, P., Alcott, L., Bastviken, D., Hastie, A., Holgerson, M.A., Johnson, M.S., Lehner, B., Lin, P., Marzadri, A., Ran, L., Tian, H., Yang, X., Yao, Y. and Regnier, P. Inland water greenhouse gas budgets for RECCAP2: 1. State-of- the-art of global scale assessments. *Global Biogeochemical Cycles*, *37*, e2022GB007657. https://doi. org/10.1029/2022GB007657, 2023a.

Lauerwald, R., Allen, G.H., Deemer, B.R., Liu, S., Maavara, T., Raymond, P., Alcott, L., Bastviken, D., Hastie, A., Holgerson, M.A., Johnson, M.S., Lehner, B., Lin, P., Marzadri, A., Ran, L., Tian, H., Yang, X., Yao, Y. and Regnier, P. Inland water greenhouse gas budgets for RECCAP2: 2 Regionalization and homogenization of estimates following the RECCAP2 framework, *Global Biogeochemical Cycles*, *37*, e2022GB007658. https://doi. org/10.1029/2022GB007658, 2023b.

Laughner, J. L., Neu, J. L., Schimel, D., Wennberg, P. O., Barsanti, K., Bowman, K. W., Chatterjee, A., Croes, B. E., Fitzmaurice, H. L., Henze, D. K., Kim, J., Kort, E. A., Liu, Z., Miyazaki, K., Turner, A. J., Anenberg, S., Avise, J., Cao, H., Crisp, D., de Gouw, J., Eldering, A., Fyfe, J. C., Goldberg, D. L., Gurney, K. R., Hasheminassab, S., Hopkins, F., Ivey, C. E., Jones, D. B. A., Liu, J., Lovenduski, N. S., Martin, R. V., McKinley, G. A., Ott, L., Poulter, B., Ru, M., Sander, S. P., Swart, N., Yung, Y. L., and Zeng, Z.-C.: Societal shifts due to COVID-19 reveal large-scale complexities and feedbacks between atmospheric chemistry and climate change, P. Natl. Acad. Sci. USA, 118, e2109481118, https://doi.org/10.1073/pnas.2109481118, 2021.

Lauvaux, T., Giron, C., Mazzolini, M., d'Aspremont, A., Duren, R., Cusworth, D., Shindell, D., and Ciais, P.: Global assessment of oil and gas methane ultra-emitters, Science, 375, 557–561, https://doi.org/10.1126/science.abj4351, 2022.

Lelieveld, J., Crutzen, P. J. and Dentener, F. J.: Changing concentration, lifetime and climate forcing of atmospheric methane, Tellus Ser. B-Chem. Phys. Meteorol., 50(2), 128–150, doi:10.1034/j.1600-0889. 1998. t01-1-00002.x, 1998.

Lelieveld, J., Lechtenbohmer, S., Assonov, S. S., Brenninkmeijer, C. A. M., Dienst, C., Fischedick, M. and Hanke, T.: Greenhouse gases: Low methane leakage from gas pipelines, Nature, 434(7035), 841–842, doi:10.1038/434841a, 2005.

Lenhart, K., Klintzsch, T., Langer, G., Nehrke, G., Bunge, M., Schnell, S. and Keppler, F.: Evidence for methane production by the marine algae *Emiliania huxleyi*, Biogeosciences, 13(10), 3163–3174, doi:10.5194/bg-13-3163-2016, 2016.

Lewan, M. D.: Comment on Ideas and perspectives: is shale gas a major driver of recent increase in global atmospheric

methane? by Robert W. Howarth (2019), Biogeosciences Discuss., 1–10, doi:10.5194/bg-2019-419, 2020.

Li, C., Frolking, S., Xiao, X., Moore, B., Boles, S., Qiu, J., Huang, Y., Salas, W. and Sass, R.: Modeling impacts of farming management alternatives on CO_2, CH_4, and N_2O emissions: A case study for water management of rice agriculture of China, Glob. Biogeochem. Cycles, 19(3), doi:10.1029/2004gb002341, 2005.

Li T, Huang Y, Zhang W, Song C: CH4MODwetland: A biogeophysical model for simulating methane emissions from natural wetlands. Ecological Modelling 221: 666–680, 2010.

Li, Y., J. Shang, C. Zhang, W. Zhang, L. Niu, L. Wang, and H. Zhang, The role of freshwater eutrophication in greenhouse gas emissions: A review. Science of The Total Environment, 768: p. 144582., 2021

Li, H. Z., Seymour, S. P. , MacKay, K., Wang, J. S., Warren, J., Guanter, L., Zavala-Araiza, D., Smith, M.L., and Xie, D.: Direct measurements of methane emissions from key facilities in Alberta's oil and gas supply chain, Science of The Total Environment, Volume 912, 169645, ISSN 0048-9697, doi:10.1016/j.scitotenv.2023.169645, 2024.

Lin, X., Indira, N. K., Ramonet, M., Delmotte, M., Ciais, P., Bhatt, B. C., Reddy, M. V., Angchuk, D., Balakrishnan, S., Jorphail, S., Dorjai, T., Mahey, T. T., Patnaik, S., Begum, M., Brenninkmeijer, C., Durairaj, S., Kirubagaran, R., Schmidt, M., Swathi, P. S., Vinithkumar, N. V., Yver Kwok, C. and Gaur, V. K.: Long-lived atmospheric trace gases measurements in flask samples from three stations in India, Atmospheric Chem. Phys., 15(17), 9819–9849, doi:10.5194/acp-15-9819-2015, 2015.

Lin, P., Pan, M., Beck, H. E., Yang, Y., Yamazaki, D., Frasson, R., et al.: Global reconstruction of naturalized river flows at 2.94 million reaches. *Water Resources Research*, 55, 6499–6516. https://doi.org/10.1029/2019WR025287, 2019

Liu, Z., Guan, D., Wei, W., Davis, S. J., Ciais, P., Bai, J., Peng, S., Zhang, Q., Hubacek, K., Marland, G., Andres, R. J., Crawford-Brown, D., Lin, J., Zhao, H., Hong, C., Boden, T. A., Feng, K., Peters, G. P., Xi, F., Liu, J., Li, Y., Zhao, Y., Zeng, N. and He, K.: Reduced carbon emission estimates from fossil fuel combustion and cement production in China, Nature, 524(7565), 335–338, doi:10.1038/nature14677, 2015.

Liu, G., Peng, S., Lin, X., Ciais, P., Li, X., Xi, Y., Lu, Z., Chang, J., Saunois, M., Wu, Y., Patra, P., Chandra, N., Zeng, H., and Piao, S.: Recent Slowdown of Anthropogenic Methane Emissions in China Driven by Stabilized Coal Production, Environ. Sci. Technol. Lett., 8, 739–746, https://doi.org/10.1021/acs.estlett.1c00463, 2021a.

Liu, S., Fang, S., Liu, P., Liang, M., Guo, M., and Feng, Z.: Measurement report: Changing characteristics of atmospheric CH4 in the Tibetan Plateau: records from 1994 to 2019 at the Mount Waliguan station, Atmos. Chem. Phys., 21, 393–413, https://doi.org/10.5194/acp-21-393-2021, 2021b

Liu, S., C. Kuhn, G. Amatulli, K. Aho, D.E. Butman, G.H. Allen, P. Lin, M. Pan, D. Yamazaki, C. Brinkerhoff, C. Gleason, X. Xia, and P.A. Raymond: The importance of hydrology in routing terrestrial carbon to the atmosphere via global streams and rivers. Proceedings of the National Academy of Sciences, 119(11): p. e2106322119, 2022.

Lloret, Z., Chevallier, F., Cozic, A., Remaud, M., and Meurdesoif, Y.: Simulating the variations of carbon dioxide in the global atmosphere on the hexagonal grid of DYNAMICO coupled with the LMDZ6 model, Geosci. Model Dev. Discuss. [preprint], https://doi.org/10.5194/gmd-2023-140, in review, 2023.

Locatelli, R., Bousquet, P., Saunois, M., Chevallier, F. and Cressot, C.: Sensitivity of the recent methane budget to LMDz sub-grid-scale physical parameterizations, Atmospheric Chem. Phys., 15(17), 9765–9780, doi:10.5194/acp-15-9765-2015, 2015.

Lohila, A., Aalto, T., Aurela, M., Hatakka, J., Tuovinen, J.-P., Kilkki, J., Penttilä, T., Vuorenmaa, J., Hänninen, P., Sutinen, R., Viisanen, Y. and Laurila, T.: Large contribution of boreal upland forest soils to a catchment-scale CH_4 balance in a wet year, Geophys. Res. Lett., 43(6), 2946–2953, doi:10.1002/2016gl067718, 2016.

Lorente, A., Borsdorff, T., Martinez-Velarte, M. C., and Landgraf, J.: Accounting for surface reflectance spectral features in TROPOMI methane retrievals, Atmos. Meas. Tech., 16, 1597–1608, https://doi.org/10.5194/amt-16-1597-2023, 2023.

Lu, X., Jacob, D. J., Zhang, Y., Maasakkers, J. D., Sulprizio, M. P., Shen, L., Qu, Z., Scarpelli, T. R., Nesser, H., Yantosca, R. M., Sheng, J., Andrews, A., Parker, R. J., Boesch, H., Bloom, A. A., and Ma, S.: Global methane budget and trend, 2010–2017: complementarity of inverse analyses using in situ (GLOBALVIEWplus CH4 ObsPack) and satellite (GOSAT) observations, Atmos. Chem. Phys., 21, 4637–4657, https://doi.org/10.5194/acp-21-4637-2021, 2021

Lu, X., Jacob, D. J., Zhang, Y., Maasakkers, J. D., Zhang, Y., Qu, Z., Chen, Z., Sulprizio, M. P., Varon, D., Hmiel, H., Park, R. J., Boesch, H., and Fan, S.: Observation-derived 2010–2019 trends in methane emissions and intensities from US oil and gas fields tied to activity metrics, P. Natl. Acad. Sci. USA, 120, e2217900120, https://doi.org/10.1073/pnas.2217900120, 2023.

Maasakkers, J. D., Jacob, D. J., Sulprizio, M. P., Scarpelli, T. R., Nesser, H., Sheng, J.-X., Zhang, Y., Hersher, M., Bloom, A. A., Bowman, K. W., Worden, J. R., Janssens-Maenhout, G., and Parker, R. J.: Global distribution of methane emissions, emission trends, and OH concentrations and trends inferred from an inversion of GOSAT satellite data for 2010–2015, Atmos. Chem. Phys., 19, 7859–7881, https://doi.org/10.5194/acp-19-7859-2019, 2019.

Maasakkers, J. D., Jacob, D. J., Sulprizio, M. P., Scarpelli, T. R., Nesser, H., Sheng, J., Zhang, Y., Lu, X., Bloom, A. A., Bowman, K. W., Worden, J. R., and Parker, R. J.: 2010–2015 North American methane emissions, sectoral contributions, and trends: a high-resolution inversion of GOSAT observations of atmospheric methane, Atmos. Chem. Phys., 21, 4339–4356, https://doi.org/10.5194/acp-21-4339-2021, 2021.

Maavara, T., Lauerwald, R., Regnier, P. and Van Capellen P.: Global perturbation of organic carbon cycling by river damming, Nat Commun 8, 153, https://doi.org/10.1038/ncomms15347, 2017.

Machacova, K., Borak, L., Agyei, T., Schindler, T., Soosaar, K., Mander, Ü., and Ah-Peng, C: Trees as net sinks for methane (CH_4) and nitrous oxide (N_2O) in the lowland tropical rain forest on volcanic Réunion Island, The New phytologist, 229(4), 1983–1994, https://doi.org/10.1111/nph.17002, 2021

3194   Machida, T., H. Matsueda, Y. Sawa, Y. Nakagawa, K. Hirotani, N. Kondo, K. Goto, N. Nakazawa, K. Ishikawa and T.

3195   Ogawa: Worldwide measurements of atmospheric CO2 and other trace gas species using commercial airlines, J. Atmos.

3196   Oceanic Technol., 25(10), 1744-1754, doi:10.1175/2008JTECHA1082.1, 2008

3197   Maksyutov, S., Oda, T., Saito, M., Janardanan, R., Belikov, D., Kaiser, J. W., Zhuravlev, R., Ganshin, A., Valsala, V. K.,

3198   Andrews, A., Chmura, L., Dlugokencky, E., Haszpra, L., Langenfelds, R. L., Machida, T., Nakazawa, T., Ramonet,

3199   M., Sweeney, C. and Worthy, D.: Technical note: A high-resolution inverse modelling technique for estimating surface

3200 CO_2 fluxes based on the NIES-TM – FLEXPART coupled transport model and its adjoint, Atmospheric Chem.

3201   Phys. Discuss., 1–33, doi:10.5194/acp-2020-251, 2020.

3202   Malerba, M.E., T. de Kluyver, N. Wright, L. Schuster, and P.I. Macreadie: Methane emissions from agricultural ponds are

3203   underestimated in national greenhouse gas inventories. Communications Earth & Environment, 3(1): p. 306, 2022

3204   Maltby, J., L. Steinle, C. R. Löscher, H. W. Bange, M. A. Fischer, M. Schmidt, and T. Treude: Microbial methanogenesis

3205   in the sulfate-reducing zone of sediments in the Eckernförde Bay, SW Baltic Sea. Biogeosciences **15**: 137–157.

3206   doi:10.5194/bg-15-137-2018, 2018

3207   Manning, F. C. , Kho, L. K., Hill, T. C., Cornulier, T., and Teh, Y A: Carbon Emissions From Oil Palm Plantations on

3208   Peat Soil, Front. For. Glob. Change, Sec. Tropical Forests, Volume 2 , https://doi.org/10.3389/ffgc.2019.0003, 2019

3209   Mannisenaho V, Tsuruta A, Backman L, Houweling S, Segers A, Krol M, Saunois M, Poulter B, Zhang Z, Lan X, et al.

3210   Global Atmospheric $\delta^{13}CH_4$ and CH_4 Trends for 2000–2020 from the Atmospheric Transport Model TM5 Using CH_4

3211   from Carbon Tracker Europe–CH4 Inversions. *Atmosphere*, 14(7):1121. https://doi.org/10.3390/atmos14071121, 2023

3212   van Marle, M. J. E., Kloster, S., Magi, B. I., Marlon, J. R., Daniau, A.-L., Field, R. D., Arneth, A., Forrest, M., Hantson,

3213   S., Kehrwald, N. M., Knorr, W., Lasslop, G., Li, F., Mangeon, S., Yue, C., Kaiser, J. W. and Werf, G. R. van der:

3214   Historic global biomass burning emissions for CMIP6 (BB4CMIP) based on merging satellite observations with

3215   proxies and fire models (1750–2015), Geosci. Model Dev., 10(9), 3329–3357, doi:10.5194/gmd-10-3329-2017, 2017.

3216   Martinez, A., Saunois, M., Poulter B., Zhen, Z., Raymond, P., Regnier, P. Canadell, J. G., Jackson, R. B., Patra, P. K.,

3217   Bousquet, P., Ciais, P., Dlugokencky, E.J., Lan, X., Allen, G., Bastviken,D., Beerling, D. J., Belikov, D., Blake, D.,

3218   Castaldi, S., Crippa, M., Deemer, B.R., Dennison, F., Etiope, G., Gedney, N., Höglund-Isaksson, L., Holgerson, M.A.,

3219   Hopcroft, P. O. , Hugelius, G., Ito, A., Jain, A. K., Janardanan, R., Johnson, M. S., Kleinen, T, Krummel, P. B.,

3220   Lauerwald, R., Li, T., Liu, X., McDonald, K. C., Melton, J. R., Mühle, J., Müller, J., Murguia-Flores, F., Niwa, Y.,

3221   Noce, S., Pan, S., Parker, R. J., Peng, C., Ramonet, M., Riley, W. J., Rocher-Ros, G., Rosentreter, J. A., Sasakawa,

3222   M., Segers A. , Smith, S. J., Stanley, E. H.,Thanwerdas, J., Tian, H., Tsuruta, A., Tubiello, F. N., Weber, T. S., van

3223   der Werf, G. R., Worthy, D. E. J., Xi, Y., Yoshida Y. , Zhang, W. , Zheng, B. , Zhu, Qing , Zhu, Qiuan, and Zhuang,

3224   Q.: *Supplemental data of the Global Carbon Project Methane Budget 2024* v1. [Data set],

3225   https://doi.org/10.18160/GKQ9-2RHT, 2024

3226   Matthews, E. and Fung, I.: Methane emission from natural wetlands: Global distribution, area, and environmental

characteristics of sources, Glob. Biogeochem. Cycles, 1(1), 61–86, doi:d10.1029/GB001i001p00061, 1987.

Mazzini A., Etiope G. (2017). Mud volcanism: an updated review. Earth Sci. Rev., 168, 81-112. http://dx.doi.org/10.1016/j.earscirev.2017.03.001., 2017

McCalley, C. K., Woodcroft, B. J., Hodgkins, S. B., Wehr, R. A., Kim, E.-H., Mondav, R., Crill, P. M., Chanton, J. P., Rich, V. I., Tyson, G. W. and Saleska, S. R.: Methane dynamics regulated by microbial community response to permafrost thaw, Nature, 514(7523), 478–481, doi:10.1038/nature13798, 2014.

McCarthy, M. C., Boering, K. A., Rice, A. L., Tyler, S. C., Connell, P. and Atlas, E.: Carbon and hydrogen isotopic compositions of stratospheric methane: 2. Two-dimensional model results and implications for kinetic isotope effects, J. Geophys. Res. Atmospheres, 108(D15), doi:10.1029/2002JD003183, 2003.

McGinnis, D. F., J. Greinert, Y. Artemov, S. E. Beaubien, and A. Wüest: Fate of rising methane bubbles in stratified waters: How much methane reaches the atmosphere?, J. Geophys. Res., 111, C09007, doi:10.1029/2005JC003183, 2006

McGuire, A. D., Christensen, T. R., Heroult, A., Miller, P. A., Hayes, D., Euskirchen, E., Kimball, J. S., Yi, Y., Koven, C., Lafleur, P., Oechel, W., Peylin, P. and Williams, M.: An assessment of the carbon balance of Arctic tundra, Comp. Obs. Process Models Atmospheric Inversions, 9(Article), 3185–3204, doi:10.5194/bg-9-3185-2012, 2012.

McKain, K., Down, A., Raciti, S. M., Budney, J., Hutyra, L. R., Floerchinger, C., Herndon, S. C., Nehrkorn, T., Zahniser, M. S., Jackson, R. B., Phillips, N. and Wofsy, S. C.: Methane emissions from natural gas infrastructure and use in the urban region of Boston, Massachusetts, Proc. Natl. Acad. Sci., 112(7), 1941–1946, doi:10.1073/pnas.1416261112, 2015.

McNicol, G., Fluet-Chouinard, E., Ouyang, Z., Knox, S., Zhang, Z., Aalto, T., et al.: Upscaling wetland methane emissions from the FLUXNET-CH4 eddy covariance network (UpCH4 v1.0): Model development, network assessment, and budget comparison. AGU Advances, 4, e2023AV000956. https://doi.org/10.1029/2023AV000956, 2023

Meinshausen, M., Smith, S., Calvin, K., Daniel, J., Kainuma, M., Lamarque, J. F., Matsumoto, K., Montzka, S., Raper, S., Riahi, K., Thomson, A., Velders, G. and van Vuuren, D. P.: The RCP greenhouse gas concentrations and their extensions from 1765 to 2300, Clim. Change, 109(1), 213–241, doi:10.1007/s10584-011-0156-z, 2011.

Meinshausen, M., Vogel, E., Nauels, A., Lorbacher, K., Meinshausen, N., Etheridge, D. M., Fraser, P. J., Montzka, S. A., Rayner, P. J., Trudinger, C. M., Krummel, P. B., Beyerle, U., Canadell, J. G., Daniel, J. S., Enting, I. G., Law, R. M., Lunder, C. R., O'Doherty, S., Prinn, R. G., Reimann, S., Rubino, M., Velders, G. J. M., Vollmer, M. K., Wang, R. H. J., and Weiss, R.: Historical greenhouse gas concentrations for climate modelling (CMIP6), Geosci. Model Dev., 10, 2057–2116, https://doi.org/10.5194/gmd-10-2057-2017, 2017.

Meinshausen, M., Nicholls, Z. R. J., Lewis, J., Gidden, M. J., Vogel, E., Freund, M., Beyerle, U., Gessner, C., Nauels, A., Bauer, N., Canadell, J. G., Daniel, J. S., John, A., Krummel, P. B., Luderer, G., Meinshausen, N., Montzka, S. A.,

Rayner, P. J., Reimann, S., Smith, S. J., van den Berg, M., Velders, G. J. M., Vollmer, M. K., and Wang, R. H. J.: The shared socio-economic pathway (SSP) greenhouse gas concentrations and their extensions to 2500, Geosci. Model Dev., 13, 3571–3605, https://doi.org/10.5194/gmd-13-3571-2020, 2020.

Melton, J. R. and Arora, V. K.: Competition between plant functional types in the Canadian Terrestrial Ecosystem Model (CTEM) v. 2.0, Geosci. Model Dev., 9(1), 323–361, doi:10.5194/gmd-9-323-2016, 2016.

Melton, J. R., Wania, R., Hodson, E. L., Poulter, B., Ringeval, B., Spahni, R., Bohn, T., Avis, C. A., Beerling, D. J., Chen, G., Eliseev, A. V., Denisov, S. N., Hopcroft, P. O., Lettenmaier, D. P., Riley, W. J., Singarayer, J. S., Subin, Z. M., Tian, H., Zürcher, S., Brovkin, V., van Bodegom, P. M., Kleinen, T., Yu, Z. C. and Kaplan, J. O.: Present state of global wetland extent and wetland methane modelling: conclusions from a model intercomparison project (WETCHIMP), Biogeosciences, 10(2), 753–788, doi:10.5194/bg-10-753-2013, 2013.

Membrive, O., Crevoisier, C., Sweeney, C., Danis, F., Hertzog, A., Engel, A., Bönisch, H. and Picon, L.: AirCore-HR: a high-resolution column sampling to enhance the vertical description of CH_4 and CO_2, Atmospheric Meas. Tech., 10(6), 2163–2181, doi:10.5194/amt-10-2163-2017, 2017.

Messager, M. L., Lehner, B., Grill, G., Nedeva, I. and Schmitt, O.: Estimating the volume and age of water stored in global lakes using a geo-statistical approach, Nat. Commun., 7(1), 1–11, doi:10.1038/ncomms13603, 2016.

Michel, SE, Lan, X, Miller, J, Tans, P, Clark, JR, Schaefer, H, Sperlich, P, Brailsford, G, Morimoto, S, Moossen, H, Li, J.: Rapid shift in methane carbon isotopes suggests microbial emissions drove record high atmospheric methane growth in 2020-2022, Proc Natl Acad Sci U S A, 121(44):e2411212121, doi: 10.1073/pnas.2411212121, 2024.

Mijling, B., van der A, R. J. and Zhang, Q.: Regional nitrogen oxides emission trends in East Asia observed from space, Atmospheric Chem. Phys., 13(23), 12003–12012, doi:doi:10.5194/acp-13-12003-2013, 2013.

Milkov, A. V.: Molecular and stable isotope compositions of natural gas hydrates: A revised global dataset and basic interpretations in the context of geological settings, Org. Geochem., 36(5), 681–702, 2005.

Minkkinen, K. and Laine, J.: Vegetation heterogeneity and ditches create spatial variability in methane fluxes from peatlands drained for forestry, Plant Soil, 285(1), 289–304, doi:10.1007/s11104-006-9016-4, 2006.

Monforti Ferrario, Fabio; Crippa, Monica; Guizzardi, Diego; Muntean, Marilena; Schaaf, Edwin; Lo Vullo, Eleonora; Solazzo, Efisio; Olivier, Jos; Vignati, Elisabetta: EDGAR v6.0 Greenhouse Gas Emissions. European Commission, Joint Research Centre (JRC) [Dataset] PID: http://data.europa.eu/89h/97a67d67-c62e-4826-b873-9d972c4f670b, 2021

Montzka, S. A., Krol, M., Dlugokencky, E., Hall, B., Jockel, P. and Lelieveld, J.: Small Interannual Variability of Global Atmospheric Hydroxyl, Science, 331(6013), 67–69, 2011.

Morgenstern, O., Hegglin, M. I., Rozanov, E., O'Connor, F. M., Abraham, N. L., Akiyoshi, H., Archibald, A. T., Bekki, S., Butchart, N., Chipperfield, M. P., Deushi, M., Dhomse, S. S., Garcia, R. R., Hardiman, S. C., Horowitz, L. W., Jöckel, P., Josse, B., Kinnison, D., Lin, M., Mancini, E., Manyin, M. E., Marchand, M., Marécal, V., Michou, M., Oman, L. D., Pitari, G., Plummer, D. A., Revell, L. E., Saint-Martin, D., Schofield, R., Stenke, A., Stone, K., Sudo,

K., Tanaka, T. Y., Tilmes, S., Yamashita, Y., Yoshida, K., and Zeng, G.: Review of the global models used within phase 1 of the Chemistry–Climate Model Initiative (CCMI), Geosci. Model Dev., 10, 639–671, https://doi.org/10.5194/gmd-10-639-2017, 2017.

Morgenstern, O., Stone, K. A., Schofield, R., Akiyoshi, H., Yamashita, Y., Kinnison, D. E., Garcia, R. R., Sudo, K., Plummer, D. A., Scinocca, J., Oman, L. D., Manyin, M. E., Zeng, G., Rozanov, E., Stenke, A., Revell, L. E., Pitari, G., Mancini, E., Di Genova, G., Visioni, D., Dhomse, S. S., and Chipperfield, M. P.: Ozone sensitivity to varying greenhouse gases and ozone-depleting substances in CCMI-1 simulations, Atmos. Chem. Phys., 18, 1091–1114, https://doi.org/10.5194/acp-18-1091-2018, 2018.

Morino, I., Uchino, O., Inoue, M., Yoshida, Y., Yokota, T., Wennberg, P. O., Toon, G. C., Wunch, D., Roehl, C. M., Notholt, J., Warneke, T., Messerschmidt, J., Griffith, D. W. T., Deutscher, N. M., Sherlock, V., Connor, B., Robinson, J., Sussmann, R. and Rettinger, M.: Preliminary validation of column-averaged volume mixing ratios of carbon dioxide and methane retrieved from GOSAT short-wavelength infrared spectra, Atmospheric Meas. Tech., 4(6), 1061–1076, 2011.

Murguia-Flores, F., Arndt, S., Ganesan, A. L., Murray-Tortarolo, G. and Hornibrook, E. R. C.: Soil Methanotrophy Model (MeMo v1.0): a process-based model to quantify global uptake of atmospheric methane by soil, Geosci. Model Dev., 11(6), 2009–2032, doi:10.5194/gmd-11-2009-2018, 2018.

Murguia-Flores, F., Ganesan, A. L., Arndt, S., and Hornibrook, E. R. C.: Global uptake of atmospheric methane by soil from 1900 to 2100, Global Biogeochemical Cycles, 35, e2020GB006774, https://doi.org/10.1029/2020GB006774, 2021.

Myer, A., Myer, M.H., Trettin, C.C. and Forschler, B.T.: The fate of carbon utilized by the subterranean termite *Reticulitermes flavipes*. *Ecosphere* 12 (12):e03872,doi:10.1002/ecs2.3872, 2021

Myhre, G., Shindell, D., Bréon, F.-M., Collins, W., Fuglestvedt, J., Huang, J., Koch, D., Lamarque, J.-F., Lee, D., Mendoza, B., Nakajima, T., Robock, A., Stephens, G., Takemura, T. and Zhang, H.: Anthropogenic and Natural Radiative Forcing., in In Climate Change 2013: The Physical Science Basis. Contribution of Working Group I to the Fifth Assessment Report of the Intergovernmental Panel on Climate Change., edited by T. F. Stocker, D. D. Qin, G.-K. Plattner, M. Tignor, S. K. Allen, J. Boschung, A. Nauels, Y. Xia, V. Bex, and P. M. Midgley, Cambridge University Press, Cambridge, United Kingdom and New York, NY, USA., 2013.

Naik, V., Voulgarakis, A., Fiore, A. M., Horowitz, L. W., Lamarque, J. F., Lin, M., Prather, M. J., Young, P. J., Bergmann, D., Cameron-Smith, P. J., Cionni, I., Collins, W. J., Dalsoren, S. B., Doherty, R., Eyring, V., Faluvegi, G., Folberth, G. A., Josse, B., Lee, Y. H., MacKenzie, I. A., Nagashima, T., van Noije, T. P. C., Plummer, D. A., Righi, M., Rumbold, S. T., Skeie, R., Shindell, D. T., Stevenson, D. S., Strode, S., Sudo, K., Szopa, S. and Zeng, G.: Preindustrial to present day changes in tropospheric hydroxyl radical and methane lifetime from the Atmospheric Chemistry and Climate Model Intercomparison Project (ACCMIP), Atmospheric Chem. Phys., 13(10), 5277–5298, doi:10.5194/acp-13-5277-

2013, 2013.

Nakazawa, T., Machida, T., Tanaka, M., Fujii, Y., Aoki, S. and Watanabe, O.: Differences of the atmospheric CH4 concentration between the Arctic and Antarctic regions in pre-industrial/pre-agricultural era, Geophys. Res. Lett., 20(10), 943–946, doi:10.1029/93GL00776, 1993.

Natchimuthu, S., I. Sundgren, M. Gålfalk, L. Klemedtsson, P. Crill, Å. Danielsson, and D. Bastviken, Spatio-temporal variability of lake CH4 fluxes and its influence on annual whole lake emission estimates. Limnology and Oceanography, 61(S1): p. S13-S26, 2016.

Nauer, P. A., Hutley, L. B., and Arndt, S. K.: Termite mounds mitigate half of termite methane emissions, P. Natl. Acad. Sci. USA, 115, 13306–13311, 2018.

Naus, S., Montzka, S. A., Patra, P. K., and Krol, M. C.: A three-dimensional-model inversion of methyl chloroform to constrain the atmospheric oxidative capacity, Atmos. Chem. Phys., 21, 4809–4824, https://doi.org/10.5194/acp-21-4809-2021, 2021.

Nicely, J. M., Salawitch, R. J., Canty, T., Anderson, D. C., Arnold, S. R., Chipperfield, M. P., Emmons, L. K., Flemming, J., Huijnen, V., Kinnison, D. E., Lamarque, J.-F., Mao, J., Monks, S. A., Steenrod, S. D., Tilmes, S. and Turquety, S.: Quantifying the causes of differences in tropospheric OH within global models, J. Geophys. Res. Atmospheres, 122(3), 1983–2007, doi:10.1002/2016JD026239, 2017.

Nicely, J. M., Canty, T. P., Manyin, M., Oman, L. D., Salawitch, R. J., Steenrod, S. D., Strahan, S. E., and Strode, S. A.: Changes in Global Tropospheric OH Expected as a Result of Climate Change Over the Last Several Decades, J. Geophys. Res.-Atmos., 123, 10774–10795, https://doi.org/10.1029/2018JD028388, 2018.

Nirmal Rajkumar, A., J. Barnes, R. Ramesh, R. Purvaja, and R.C. Upstill-Goddard, Methane and nitrous oxide fluxes in the polluted Adyar River and estuary, SE India. Marine Pollution Bulletin, 56(12): p. 2043-2051, 2008

Nisbet, R. E. R., Fisher, R., Nimmo, R. H., Bendall, D. S., Crill, P. M., Gallego-Sala, A. V., Hornibrook, E. R. C., Lopez-Juez, E., Lowry, D., Nisbet, P. B. R., Shuckburgh, E. F., Sriskantharajah, S., Howe, C. J. and Nisbet, E. G.: Emission of methane from plants, Proc. R. Soc. B-Biol. Sci., 276(1660), 1347–1354, 2009.

Nisbet, E. G., Manning, M. R., Dlugokencky, E. J., Fisher, R. E., Lowry, D., Michel, S. E., Myhre, C. L., Platt, S. M., Allen, G., Bousquet, P., Brownlow, R., Cain, M., France, J. L., Hermansen, O., Hossaini, R., Jones, A. E., Levin, I., Manning, A. C., Myhre, G., Pyle, J. A., Vaughn, B., Warwick, N. J. and White, J. W. C.: Very strong atmospheric methane growth in the four years 2014-2017: Implications for the Paris Agreement, Glob. Biogeochem. Cycles, 0(ja), doi:10.1029/2018GB006009, 2019.

Nisbet, E. G., Fisher, R. E., Lowry, D., France, J. L., Allen, G., Bakkaloglu, S., Broderick, T.J., Cain, M., Coleman, M., Fernandez, J., Forster, G., Griffiths, P.T., Iverach, C.P., Keely, B.F.J., Manning, M.R., Nisbet-Jones, B.R., Pyle, J.A., Townsend-Samll, A., al-Shallan, A., Warwick, N. and Zazzeri, G.: Methane mitigation: methods to reduce emissions, on the path to the Paris agreement. Reviews of Geophysics, 58, e2019RG000675.

https://doi.org/10.1029/2019RG000675, 2020

Nisbet, E. G., Manning, M. R., Dlugokencky, E. J., Michel, S. E., Lan, X., Röckmann, T., van der Denier Gon, H. A., Schmitt, J., Palmer, P. I., Dyonisius, M. N., Oh, Y., Fisher, R. E., Lowry, D., France, J. L., White, J. W. C., Brailsford, G., and Bromley, T.: Atmospheric methane: Comparison between methane's record in 2006–2022 and during glacial terminations, Global Biogeochem. Cy., 37, e2023GB007875, https://doi.org/10.1029/2023GB007875, 2023.

Nisbet, E.G.: Climate feedback on methane from wetlands, Nat. Clim. Chang., 13, 421–422. https://doi.org/10.1038/s41558-023-01634-3, 2023

Niwa, Y., Fujii, Y., Sawa, Y., Iida, Y., Ito, A., Satoh, M., Imasu, R., Tsuboi, K., Matsueda, H. and Saigusa, N.: A 4D-Var inversion system based on the icosahedral grid model (NICAM-TM 4D-Var v1.0) – Part 2: Optimization scheme and identical twin experiment of atmospheric CO_2 inversion, Geosci. Model Dev., 10(6), 2201–2219, doi:10.5194/gmd-10-2201-2017, 2017.

Niwa, Y., Ishijima, K., Ito, A. and Iida, Y.: Toward a long-term atmospheric CO_2 inversion for elucidating natural carbon fluxes: technical notes of NISMON-CO_2 v2021.1. Prog. Earth Planet Sci. 9, 42, doi:10.1186/s40645-022-00502-6, 2022

Niwa, Y., Tohjima, Y., Terao, Y., Saeki, T., Ito, A., Umezawa, T., Yamada, K., Sasakawa, M., Machida, T., Nakaoka, S.-I., Nara, H., Tanimoto, H., Mukai, H., Yoshida, Y., Morimoto, S., Takatsuji, S., Tsuboi, K., Sawa, Y., Matsueda, H., Ishijima, K., Fujita, R., Goto, D., Lan, X., Schuldt, K., Heliasz, M., Biermann, T., Chmura, L., Necki, J., and Xueref-Remy, I.: Multi-observational estimation of regional and sectoral emission contributions to the persistent high growth rate of atmospheric CH4 for 2020–2022, EGUsphere [preprint], https://doi.org/10.5194/egusphere-2024-2457, 2024.

Noël, S., Reuter, M., Buchwitz, M., Borchardt, J., Hilker, M., Schneising, O., Bovensmann, H., Burrows, J. P., Di Noia, A., Parker, R. J., Suto, H., Yoshida, Y., Buschmann, M., Deutscher, N. M., Feist, D. G., Griffith, D. W. T., Hase, F., Kivi, R., Liu, C., Morino, I., Notholt, J., Oh, Y.-S., Ohyama, H., Petri, C., Pollard, D. F., Rettinger, M., Roehl, C., Rousogenous, C., Sha, M. K., Shiomi, K., Strong, K., Sussmann, R., Té, Y., Velazco, V. A., Vrekoussis, M., and Warneke, T.: Retrieval of greenhouse gases from GOSAT and GOSAT-2 using the FOCAL algorithm, Atmos. Meas. Tech., 15, 3401–3437, https://doi.org/10.5194/amt-15-3401-2022, 2022.

Nomura, S., Naja, M., Ahmed, M. K., Mukai, H., Terao, Y., Machida, T., Sasakawa, M., and Patra, P. K.: Measurement report: Regional characteristics of seasonal and long-term variations in greenhouse gases at Nainital, India, and Comilla, Bangladesh, Atmos. Chem. Phys., 21, 16427–16452, https://doi.org/10.5194/acp-21-16427-2021, 2021

Obu, J., Westermann, S., Bartsch, A., Berdnikov, N., Christiansen, H. H., Dashtseren, A., Delaloye, R., Elberling, B., Etzelmüller, B., Kholodov, A., Khomutov, A., Kääb, A., Leibman, M. O., Lewkowicz, A. G., Panda, S. K., Romanovsky, V., Way, R. G., Westergaard-Nielsen, A., Wu, T., Yamkhin, J. and Zou, D.: Northern Hemisphere permafrost map based on TTOP modelling for 2000–2016 at 1 km2 scale, Earth-Sci. Rev., 193, 299–316, doi:10.1016/j.earscirev.2019.04.023, 2019.

3392 Ocko, I. B, Sun, T., Shindell, D., Oppenheimer, M., Hristov, A. N, Pacala, S. W, Mauzerall, D. L, Xu, Y. and Hamburg,
3393   S. P: Acting rapidly to deploy readily available methane mitigation measures by sector can immediately slow global
3394   warming, Environ. Res. Lett., 16, 054042, doi :10.1088/1748-9326/abf9c8, 2021

3395 Odelson, D.A. and Breznak, J. A. Volatile fatty acid production by the hindgut microbiota of xilophagus termites. Applied
3396   and Environmental Microbiology, 45, 1602-1613, 1983. doi: 10.1128/aem.45.5.1602-1613.1983.

3397   Ollivier, Q. R., Maher, D. T., Pitfield, C. and Macreadie, P. I.: Punching above their weight: Large release of greenhouse
3398   gases from small agricultural dams, Glob. Change Biol., 25(2), 721–732, doi:10.1111/gcb.14477, 2019.

3399 Omara, M, Zavala-Araiza,D, Lyon, DR, Hmiel, B, Roberts, KA, Hamburg, SP :Methane emissions from US low
3400   production oil and natural gas well sites, Nat Commun, 13(1):2085, doi: 10.1038/s41467-022-29709-3, 2022

3401 O'Neill, B. C., Tebaldi, C., Vuuren, D. P. van, Eyring, V., Friedlingstein, P., Hurtt, G., Knutti, R., Kriegler, E., Lamarque,
3402   J.-F., Lowe, J., Meehl, G. A., Moss, R., Riahi, K. and Sanderson, B. M.: The Scenario Model Intercomparison Project
3403   (ScenarioMIP) for CMIP6, Geosci. Model Dev., 9(9), 3461–3482, doi: 10.5194/gmd-9-3461-2016, 2016.

3404 Oreggioni, G. D., F. Monforti Ferrario, M. Crippa, M. Muntean, E. Schaaf, D. Guizzardi, E. Solazzo, M. Duerr, M. Perry
3405   and E. Vignati: Climate change in a changing world: Socio-economic and technological transitions, regulatory
3406   frameworks and trends on global greenhouse gas emissions from EDGAR v.5.0, Global Environmental Change,
3407   doi:10.1016/j.gloenvcha.2021.10235, 2021

3408 Oremland, R. S. Methanogenic activity in plankton samples and fish intestines: a mechanism for *in situ* methanogenesis
3409   in oceanic surface waters. *Limnol. Oceanogr.* **24,** 1136–1141, 1979.

3410 O'Rourke, P. R, Smith, S. J., Mott, A., Ahsan, H., McDuffie, E. E., Crippa, M., Klimont, S., McDonald, B., Z., Wang,
3411   Nicholson, M. B, Feng, L., and Hoesly, R. M., CEDS v-2021-02-05 Emission Data 1975-2019 (Version Feb-05-2021).
3412   Zenodo. http://doi.org/10.5281/zenodo.4509372, 2021

3413 Ovalle, A. R. C., C. E. Rezende, L. D. Lacerda, and C. A. R. Silva: Factors affecting the hydrochemistry of a mangrove
3414   tidal creek, Sepetiba Bay, Brazil. Estuar. Coast. Shelf Sci. 31: 639–650. doi:10.1016/0272-7714(90)90017-L, 1990

3415 Pacala, S. W.: Verifying greenhouse gas emissions: Methods to support international climate agreements, National
3416   Academies Press., 2010

3417 Pandey, S., Gautam, R., Houweling, S., Gon, H. D. van der, Sadavarte, P., Borsdorff, T., Hasekamp, O., Landgraf, J., Tol,
3418   P., Kempen, T. van, Hoogeveen, R., Hees, R. van, Hamburg, S. P., Maasakkers, J. D. and Aben, I.: Satellite
3419   observations reveal extreme methane leakage from a natural gas well blowout, Proc. Natl. Acad. Sci., 116(52), 26376–
3420   26381, doi:10.1073/pnas.1908712116, 2019.

3421 Pangala, S. R., Moore, S., Hornibrook, E. R. C. and Gauci, V.: Trees are major conduits for methane egress from tropical
3422   forested wetlands, New Phytol., 197(2), 524–531, doi:10.1111/nph.12031, 2013.

3423 Pangala, S. R., Hornibrook, E. R. C., Gowing, D. J. and Gauci, V.: The contribution of trees to ecosystem methane
3424   emissions in a temperate forested wetland, Glob. Change Biol., 21(7), 2642–2654, doi:10.1111/gcb.12891, 2015.

3425 Pangala, S. R., Enrich-Prast, A., Basso, L. S., Peixoto, R. B., Bastviken, D., Hornibrook, E. R. C., Gatti, L. V., Marotta,
3426   H., Calazans, L. S. B., Sakuragui, C. M., Bastos, W. R., Malm, O., Gloor, E., Miller, J. B. and Gauci, V.: Large
3427   emissions from floodplain trees close the Amazon methane budget, Nature, 552(7684), 230–234,
3428   doi:10.1038/nature24639, 2017.

3429 Paris, J.-D., Ciais, P., Nedelec, P., Stohl, A., Belan, B. D., Arshinov, M. Y., Carouge, C., Golitsyn, G. S. and Granberg, I.
3430   G.: New insights on the chemical composition of the Siberian air shed from the YAK AEROSIB aircraft campaigns,
3431   Bull. Am. Meteorol. Soc., 91(5), 625–641, doi:10.1175/2009BAMS2663.1., 2010.

3432 Parker, R. J., Webb, A., Boesch, H., Somkuti, P., Barrio Guillo, R., Di Noia, A., Kalaitzi, N., Anand, J. S., Bergamaschi,
3433   P., Chevallier, F., Palmer, P. I., Feng, L., Deutscher, N. M., Feist, D. G., Griffith, D. W. T., Hase, F., Kivi, R., Morino,
3434   I., Notholt, J., Oh, Y.-S., Ohyama, H., Petri, C., Pollard, D. F., Roehl, C., Sha, M. K., Shiomi, K., Strong, K., Sussmann,
3435   R., Té, Y., Velazco, V. A., Warneke, T., Wennberg, P. O., and Wunch, D.: A decade of GOSAT Proxy satellite CH4
3436   observations, Earth Syst. Sci. Data, 12, 3383–3412, https://doi.org/10.5194/essd-12-3383-2020, 2020.

3437 Parker, R. and Boesch, H. (2020): University of Leicester GOSAT Proxy XCH4 v9.0. Centre for Environmental Data
3438   Analysis, 07 May 2020. https://dx.doi.org/10.5285/18ef8247f52a4cb6a14013f8235cc1eb, 2020

3439 Parker, R. J., Wilson, C., Comyn-Platt, E., Hayman, G., Marthews, T. R., Bloom, A. A., Lunt, M. F., Gedney, N., Dadson,
3440   S. J., McNorton, J., Humpage, N., Boesch, H., Chipperfield, M. P., Palmer, P. I., and Yamazaki, D.: Evaluation of
3441   wetland CH4 in the Joint UK Land Environment Simulator (JULES) land surface model using satellite observations,
3442   Biogeosciences, 19, 5779–5805, https://doi.org/10.5194/bg-19-5779-2022, 2022.

3443 Pathak, H., Li, C. and Wassmann, R.: Greenhouse gas emissions from Indian rice fields: calibration and upscaling using
3444   the DNDC model, Biogeosciences, 1(1), 1–11, 2005.

3445 Patra, P. K., Houweling, S., Krol, M., Bousquet, P., Belikov, D., Bergmann, D., Bian, H., Cameron-Smith, P., Chipperfield,
3446   M. P., Corbin, K., Fortems-Cheiney, A., Fraser, A., Gloor, E., Hess, P., Ito, A., Kawa, S. R., Law, R. M., Loh, Z.,
3447   Maksyutov, S., Meng, L., Palmer, P. I., Prinn, R. G., Rigby, M., Saito, R. and Wilson, C.: TransCom model simulations
3448   of CH4 and related species: linking transport, surface flux and chemical loss with CH4 variability in the troposphere
3449   and lower stratosphere, Atmospheric Chem. Phys., 11(24), 12,813-12,837, doi:10.5194/acp-11-12813-2011, 2011.

3450 Patra, P. K., Krol, M. C., Montzka, S. A., Arnold, T., Atlas, E. L., Lintner, B. R., Stephens, B. B., Xiang, B., Elkins, J. W.,
3451   Fraser, P. J., Ghosh, A., Hintsa, E. J., Hurst, D. F., Ishijima, K., Krummel, P. B., Miller, B. R., Miyazaki, K., Moore,
3452   F. L., Mühle, J., O'Doherty, S., Prinn, R. G., Steele, L. P., Takigawa, M., Wang, H. J., Weiss, R. F., Wofsy, S. C. and
3453   Young, D.: Observational evidence for interhemispheric hydroxyl-radical parity, Nature, 513(7517), 219–223,
3454   doi:10.1038/nature13721, 2014.

3455 Patra, P. K., Takigawa, M., Watanabe, S., Chandra, N., Ishijima, K. and Yamashita, Y.: Improved Chemical Tracer
3456   Simulation by MIROC4.0-based Atmospheric Chemistry-Transport Model (MIROC4-ACTM), SOLA, 14(0), 91–96,
3457   doi:10.2151/sola.2018-016, 2018.

Patra, P. K., Krol, M. C., Prinn, R. G., Takigawa, M., Mühle, J., Montzka, S. A., Lal, S., Yamashita, Y., Naus, S., Chandra, N., Weiss, R. F., Krummel, P. B., Fraser, P. J., O'Doherty, S., and Elkins, J. W.: Methyl Chloroform Continues to Constrain the Hydroxyl (OH) Variability in the Troposphere, J. Geophys. Res.-Atmos., 126, e2020JD033862, https://doi.org/10.1029/2020JD033862, 2021.

Paull, C. K., Brewer, P. G., Ussler, W., Peltzer, E. T., Rehder, G. and Clague, D.: An experiment demonstrating that marine slumping is a mechanism to transfer methane from seafloor gas-hydrate deposits into the upper ocean and atmosphere, Geo-Mar. Lett., 22(4), 198–203, doi:10.1007/s00367-002-0113-y, 2002.

Peacock, M., J. Audet, D. Bastviken, M.N. Futter, V. Gauci, A. Grinham, J.A. Harrison, M.S. Kent, S. Kosten, C.E. Lovelock, A.J. Veraart, and C.D. Evans, Global importance of methane emissions from drainage ditches and canals. Environmental Research Letters, 16(4): p. 044010., 2021

Pekel, J.-F., Cottam, A., Gorelick, N. and Belward, A. S.: High-resolution mapping of global surface water and its long-term changes, Nature, 540(7633), 418–422, doi:10.1038/nature20584, 2016.

Peltola, O., Vesala, T., Gao, Y., Räty, O., Alekseychik, P., Aurela, M., Chojnicki, B., Desai, A. R., Dolman, A. J., Euskirchen, E. S., Friborg, T., Göckede, M., Helbig, M., Humphreys, E., Jackson, R. B., Jocher, G., Joos, F., Klatt, J., Knox, S. H., Kowalska, N., Kutzbach, L., Lienert, S., Lohila, A., Mammarella, I., Nadeau, D. F., Nilsson, M. B., Oechel, W. C., Peichl, M., Pypker, T., Quinton, W., Rinne, J., Sachs, T., Samson, M., Schmid, H. P., Sonnentag, O., Wille, C., Zona, D. and Aalto, T.: Monthly gridded data product of northern wetland methane emissions based on upscaling eddy covariance observations, Earth Syst. Sci. Data, 11(3), 1263–1289, doi:10.5194/essd-11-1263-2019, 2019.

Peng, S. S., Piao, S. L., Bousquet, P., Ciais, P., Li, B. G., Lin, X., Tao, S., Wang, Z. P., Zhang, Y. and Zhou, F.: Inventory of anthropogenic methane emissions in Mainland China from 1980 to 2010, Atmospheric Chem. Phys. Discuss., 2016, 1–29, doi:10.5194/acp-2016-139, 2016.

Peng, S., Lin, X., Thompson, R. L., Xi, Y., Liu, G., Hauglustaine, D., Lan, X., Poulter, B., Ramonet, M., Saunois, M., Yin, Y., Zhang, Z., Zheng, B., and Ciais, P.: Wetland emission and atmospheric sink changes explain methane growth in 2020, Nature, 612, 477–482, https://doi.org/10.1038/s41586-022-05447-w, 2022.

Pérez-Barbería, F. J.: Scaling methane emissions in ruminants and global estimates in wild populations, Sci. Total Environ., 579, 1572–1580, doi:10.1016/j.scitotenv.2016.11.175, 2017.

Petersen, H. and Luxton, M. A comparative analysis of soil fauna populations and their role in decomposition processes. Oikos 39: 287–388, doi.org/10.2307/3544689., 1982

Petrenko, V. V., Smith, A. M., Schaefer, H., Riedel, K., Brook, E., Baggenstos, D., Harth, C., Hua, Q., Buizert, C., Schilt, A., Fain, X., Mitchell, L., Bauska, T., Orsi, A., Weiss, R. F. and Severinghaus, J. P.: Minimal geological methane emissions during the Younger Dryas–Preboreal abrupt warming event, Nature, 548, 443, doi:10.1038/nature23316 https://www.nature.com/articles/nature23316#supplementary-information, 2017.

Petrescu, A. M. R., Qiu, C., Ciais, P., Thompson, R. L., Peylin, P., McGrath, M. M., Solazzo, E., Janssens-Maenhout, G., Tubiello, F. N., Bergamaschi, P., Brunner, D., Peters, G. P., Höglund- Isaksson, L., Regnier, P., Lauerwald, R., Bastviken, D., Tsuruta, A., Winiwarter, W., Patra, P. P., Kuhnert, M., Oreggioni, G. D., Crippa, M., Saunois, M., Perugini, L., Markkanen, T., Aalto, T., Groot Zwaaftink, C. C., Yao, Y., Wilson, C. C., Conchedda, G., Günther, D., Leip, A., Smith, P., Haussaire, J. M., Leppänen, A., Manning, A. J., McNorton, J., Brockmann, P., & Dolman, A. J. H. A. The consolidated European synthesis of CH4 and N2O emissions for the European Union and United Kingdom: 1990-2017. Earth System Science Data, 13(5), 2307-2362. doi:10.5194/ essd-13-2307- 2021, 2021.

Petrescu, A. M. R., Qiu, C., McGrath, M. J., Peylin, P., Peters, G. P., Ciais, P., Thompson, R. L., Tsuruta, A., Brunner, D., Kuhnert, M., Matthews, B., Palmer, P. I., Tarasova, O., Regnier, P., Lauerwald, R., Bastviken, D., Höglund-Isaksson, L., Winiwarter, W., Etiope, G., Aalto, T., Balsamo, G., Bastrikov, V., Berchet, A., Brockmann, P., Ciotoli, G., Conchedda, G., Crippa, M., Dentener, F., Groot Zwaaftink, C. D., Guizzardi, D., Günther, D., Haussaire, J.-M., Houweling, S., Janssens-Maenhout, G., Kouyate, M., Leip, A., Leppänen, A., Lugato, E., Maisonnier, M., Manning, A. J., Markkanen, T., McNorton, J., Muntean, M., Oreggioni, G. D., Patra, P. K., Perugini, L., Pison, I., Raivonen, M. T., Saunois, M., Segers, A. J., Smith, P., Solazzo, E., Tian, H., Tubiello, F. N., Vesala, T., van der Werf, G. R., Wilson, C., and Zaehle, S.: The consolidated European synthesis of CH4 and N2O emissions for the European Union and United Kingdom: 1990–2019, Earth Syst. Sci. Data, 15, 1197–1268, https://doi.org/10.5194/essd-15-1197-2023, 2023.

Phillips, N. G., Ackley, R., Crosson, E. R., Down, A., Hutyra, L. R., Brondfield, M., Karr, J. D., Zhao, K. and Jackson, R. B.: Mapping urban pipeline leaks: Methane leaks across Boston, Environ. Pollut., 173, 1–4, doi:10.1016/j.envpol.2012.11.003, 2013.

Pimlott, M.A., Pope, R.J., Kerridge, B.J., Latter, B.G., Knappett, D.S., Heard, D.E., Ventress, L.J., Siddans, R., Feng, W., and Chipperfield, M.P.: Investigating the global OH radical distribution using steady-state approximations and satellite data. Atmos. Chem. Phys., 22, 10467–10488, doi:10.5194/acp-22-10467-2022, 2022

Pison, I., Ringeval, B., Bousquet, P., Prigent, C. and Papa, F.: Stable atmospheric methane in the 2000s: key-role of emissions from natural wetlands, Atmospheric Chem. Phys. Discuss., 13(4), 9017–9049, doi:10.5194/acpd-13-9017-2013, 2013.

Pitz, S. and Megonigal, J. P.: Temperate forest methane sink diminished by tree emissions, New Phytol., 214(4), 1432–1439, doi:10.1111/nph.14559, 2017.

Platt, U., Allan, W. and Lowe, D.: Hemispheric average Cl atom concentration from $^{13}C/^{12}C$ ratios in atmospheric methane, Atmos Chem Phys, 4, 2393–2399, 2004.

Plummer, D., Nagashima, T., Tilmes, S., Archibald, A., Chiodo, G., Fadnavis, S., Garny, H., Josse, B., Kim, J., Lamarque, J.-F., Morgenstern, O., Murray, L., Orbe, C., Tai, A., Chipperfield, M., Funke, B., Juckes, M., Kinnison, D., Kunze, M., Luo, B., Matthes, K., Newman, P. A., Pascoe, C. and Peter, T.: CCMI- 2022: a new set of Chemistry–Climate Model Initiative (CCMI) community simulations to update the assessment of models and support upcoming ozone

3524   assessment activities. SPARC Newsletter 57, 22–30, 2021.

3525   Pollard, D. F., Sherlock, V., Robinson, J., Deutscher, N. M., Connor, B. and Shiona, H.: The Total Carbon Column
3526   Observing Network site description for Lauder, New Zealand, Earth Syst. Sci. Data, 9(2), 977–992, doi:10.5194/essd-
3527   9-977-2017, 2017.

3528   Portmann, F. T., Siebert, S. & Döll, P. : MIRCA2000 – Global monthly irrigated and rainfed crop areas around the year
3529   2000: A new high-resolution data set for agricultural and hydrological modeling, Global Biogeochemical Cycles, 24,
3530   GB 1011, doi:10.1029/2008GB003435, 2010

3531   Portmann, R. W., Daniel, J. S. and Ravishankara, A. R.: Stratospheric ozone depletion due to nitrous oxide: influences of
3532   other gases, Philos. Trans. R. Soc. Lond. B Biol. Sci., 367(1593), 1256–1264, doi:10.1098/rstb.2011.0377, 2012.

3533   Poulter, B., Bousquet, P., Canadell, J. G., Ciais, P., Peregon, A., Saunois, M., Arora, V. K., Beerling, D. J., Brovkin, V.,
3534   Jones, C. D., Joos, F., Gedney, N., Ito, A., Kleinen, T., Koven, C. D., McDonald, K., Melton, J. R., Peng, C. H., Peng,
3535   S. S., Prigent, C., Schroeder, R., Riley, W. J., Saito, M., Spahni, R., Tian, H. Q., Taylor, L., Viovy, N., Wilton, D.,
3536   Wiltshire, A., Xu, X. Y., Zhang, B. W., Zhang, Z. and Zhu, Q. A.: Global wetland contribution to 2000-2012
3537   atmospheric methane growth rate dynamics, Environ. Res. Lett., 12(9), doi:10.1088/1748-9326/aa8391, 2017.

3538   Prairie, Y.T., J. Alm, J. Beaulieu, N. Barros, T. Battin, J. Cole, P. del Giorgio, T. DelSontro, F. Guérin, A. Harby, J.
3539   Harrison, S. Mercier-Blais, D. Serça, S. Sobek, and D. Vachon, Greenhouse Gas Emissions from Freshwater
3540   Reservoirs: What Does the Atmosphere See? Ecosystems, 21(5): p. 1058-1071, 2018

3541   Prather, M. J., Holmes, C. D. and Hsu, J.: Reactive greenhouse gas scenarios: Systematic exploration of uncertainties and
3542   the role of atmospheric chemistry, Geophys. Res. Lett., 39(9), L09803, doi:10.1029/2012gl051440, 2012.

3543 Prather, M. J., Guo, H., and Zhu, X.: Deconstruction of tropospheric chemical reactivity using aircraft measurements: the
3544 Atmospheric Tomography Mission (ATom) data, Earth Syst. Sci. Data, 15, 3299–3349, https://doi.org/10.5194/essd-15-
3545 3299-2023, 2023.

3546   Prinn, R. G., Weiss, R. F., Arduini, J., Arnold, T., DeWitt, H. L., Fraser, P. J., Ganesan, A. L., Gasore, J., Harth, C. M.,
3547   Hermansen, O., Kim, J., Krummel, P. B., Li, S., Loh, Z. M., Lunder, C. R., Maione, M., Manning, A. J., Miller, B. R.,
3548   Mitrevski, B., Mühle, J., O'Doherty, S., Park, S., Reimann, S., Rigby, M., Saito, T., Salameh, P. K., Schmidt, R.,
3549   Simmonds, P. G., Steele, L. P., Vollmer, M. K., Wang, R. H., Yao, B., Yokouchi, Y., Young, D., and Zhou, L.: History
3550   of chemically and radiatively important atmospheric gases from the Advanced Global Atmospheric Gases Experiment
3551   (AGAGE), *Earth Syst. Sci. Data*, 10, 985–1018, https://doi.org/10.5194/essd-10-985-2018, 2018.

3552   Prosperi, P., Bloise, M., Tubiello, F.N. *et al.* New estimates of greenhouse gas emissions from biomass burning and peat
3553   fires using MODIS Collection 6 burned areas. *Climatic Change* **161**, 415–432, https://doi.org/10.1007/s10584-020-
3554   02654-0, 2020

3555   Purvaja, R., Ramesh, R., & Frenzel, P.: Plant-mediated methane emission from an Indian mangrove, *Global Change*
3556   *Biology*, 10, 1825–1834, 2004

Qin, B., Zhou, J., Elser, J.J., Gardner, W.S., Deng, J., and J.D. Brookes: Water depth underpins the relative roles and fates of nitrogen and phosphorus in lakes, Environmental Science & Technology 2020 *54* (6), 3191-3198, DOI: 10.1021/acs.est.9b05858, 2020.

Qu, Z., Jacob, D. J., Shen, L., Lu, X., Zhang, Y., Scarpelli, T. R., Nesser, H., Sulprizio, M. P., Maasakkers, J. D., Bloom, A. A., Worden, J. R., Parker, R. J., and Delgado, A. L.: Global distribution of methane emissions: a comparative inverse analysis of observations from the TROPOMI and GOSAT satellite instruments, Atmos. Chem. Phys., 21, 14159–14175, https://doi.org/10.5194/acp-21-14159-2021, 2021.

Qu, Z., Jacob, D. J., Zhang, Y., Shen, L., Varon, D. J., Lu, X., Scarpelli, T., Bloom, A., Worden, J., and Parker, R. J.: Attribution of the 2020 surge in atmospheric methane by inverse analysis of GOSAT observations, Environ. Res. Lett., 17, 094003, https://doi.org/10.1088/1748-9326/ac8754, 2022.

Randerson, J. T., Chen, Y., van der Werf, G. R., Rogers, B. M. and Morton, D. C.: Global burned area and biomass burning emissions from small fires, J. Geophys. Res. Biogeosciences, 117, G4, doi:10.1029/2012jg002128, 2012.

Ramage, J.L., Kuhn, M., Virkkala, A.M., Voigt, C., Marushchak, M.E., Bastos, A., Biasi, C., Canadell, J.G., Ciais, P., Ĺopez-Blanco, E. Natali, S.M., et al.: The net GHG balance and budget of the permafrost region (2000-2020) from ecosystem flux upscaling. Preprint in ESS Open Archive. September 11, 2023. DOI: 10.22541/essoar.169447408.86275712/v1, 2023

Ramsden, A. E., Ganesan, A. L., Western, L. M., Rigby, M., Manning, A. J., Foulds, A., France, J. L., Barker, P., Levy, P., Say, D., Wisher, A., Arnold, T., Rennick, C., Stanley, K. M., Young, D., and O'Doherty, S.: Quantifying fossil fuel methane emissions using observations of atmospheric ethane and an uncertain emission ratio, Atmos. Chem. Phys., 22, 3911–3929, https://doi.org/10.5194/acp-22-3911-2022, 2022.

Ray, N.E., Holgerson, M.A., Andersen, M.R., Bikše, J., Bortolotti, L.E., Futter, M., Kokorīte, I., Law, A., McDonald, C., Mesman, J.P., Peacock, M., Richardson, D.C., Arsenault, J., Bansal, S., Cawley, K., Kuhn, M., Shahabinia, A.R. and Smufer, F.: Spatial and temporal variability in summertime dissolved carbon dioxide and methane in temperate ponds and shallow lakes. Limnol Oceanogr, 68: 1530-1545. https://doi.org/10.1002/lno.12362, 2023

Regnier P., Arndt, S., Dale, A.W., LaRowe, D.E., Mogollon, J. and Van Cappellen, P. Advances in the biogeochemical modeling of anaerobic oxidation of methane (AOM). Earth Science Reviews. 106, 105-130, 2011;

Ren, W. E. I., Tian, H., Xu, X., Liu, M., Lu, C., Chen, G., Melillo, J., Reilly, J. and Liu, J.: Spatial and temporal patterns of CO_2 and CH_4 fluxes in China's croplands in response to multifactor environmental changes, Tellus B, 63(2), 222–240, doi:10.1111/j.1600-0889.2010.00522.x, 2011.

Repeta, D. J., Ferrón, S., Sosa, O. A., Johnson, C. G., Repeta, L. D., Acker, M., DeLong, E. F. and Karl, D. M.: Marine methane paradox explained by bacterial degradation of dissolved organic matter, Nat. Geosci., 9(12), 884–887, doi:10.1038/ngeo2837, 2016.

Resplandy, L., Hogikyan, A., Müller, J.D., Najjar, R.G., Bange, H., W., Bianchi, D., Weber, T., Cai, W.-J., Doney, S. C., Fennel, K., Gehlen, M., Hauck, J., Lacroix, F., Landschützer, P., Le Quéré, C., Roobaert, A., Schwinger, J., Berthet, S., Bopp, L., Chau, T.T.T., Dai, M., Gruber, N., Ilyina, T., Kock, A., Manizza, M., Lachkar, Z., Laruelle, G. G., Liao, E., Lima, I. D., Nissen, C., Rödenbeck, C., Séférian, R., Toyama, K., Tsujino, H., and Regnier, P.: A synthesis of global coastal ocean greenhouse gas fluxes, Global Biogeochemical Cycles, 38, e2023GB007803. https://doi.org/10.1029/2023GB007803, 2024

Riahi, K., van Vuuren, D. P., Kriegler, E., Edmonds, J., O'Neill, B. C., Fujimori, S., Bauer, N., Calvin, K., Dellink, R., Fricko, O., Lutz, W., Popp, A., Cuaresma, J. C., Kc, S., Leimbach, M., Jiang, L., Kram, T., Rao, S., Emmerling, J., Ebi, K., Hasegawa, T., Havlik, P., Humpenöder, F., Da Silva, L. A., Smith, S., Stehfest, E., Bosetti, V., Eom, J., Gernaat, D., Masui, T., Rogelj, J., Strefler, J., Drouet, L., Krey, V., Luderer, G., Harmsen, M., Takahashi, K., Baumstark, L., Doelman, J. C., Kainuma, M., Klimont, Z., Marangoni, G., Lotze-Campen, H., Obersteiner, M., Tabeau, A. and Tavoni, M.: The Shared Socioeconomic Pathways and their energy, land use, and greenhouse gas emissions implications: An overview, Glob. Environ. Change, 42, 153–168, doi:10.1016/j.gloenvcha.2016.05.009, 2017.

Rice, A. L., Butenhoff, C. L., Shearer, M. J., Teama, D., Rosenstiel, T. N. and Khalil, M. A. K.: Emissions of anaerobically produced methane by trees, Geophys. Res. Lett., 37, L03807, doi:10.1029/2009GL041565, 2010.

Ridgwell, A. J., Marshall, S. J. and Gregson, K.: Consumption of atmospheric methane by soils: A process-based model, Glob. Biogeochem. Cycles, 13(1), 59–70, doi:10.1029/1998gb900004, 1999.

Riedel, T. P., Wolfe, G. M., Danas, K. T., Gilman, J. B., Kuster, W. C., Bon, D. M., Vlasenko, A., Li, S. M., Williams, E. J., Lerner, B. M., Veres, P. R., Roberts, J. M., Holloway, J. S., Lefer, B., Brown, S. S. and Thornton, J. A.: An MCM modeling study of nitryl chloride ($ClNO_2$) impacts on oxidation, ozone production and nitrogen oxide partitioning in polluted continental outflow, Atmospheric Chem. Phys., 14(8), 3789–3800, doi:10.5194/acp-14-3789-2014, 2014.

Rigby, M., Montzka, S. A., Prinn, R. G., White, J. W. C., Young, D., O'Doherty, S., Lunt, M. F., Ganesan, A. L., Manning, A. J., Simmonds, P. G., Salameh, P. K., Harth, C. M., Mühle, J., Weiss, R. F., Fraser, P. J., Steele, L. P., Krummel, P. B., McCulloch, A. and Park, S.: Role of atmospheric oxidation in recent methane growth, Proc. Natl. Acad. Sci., 114(21), 5373, 2017.

Riley, W. J., Subin, Z. M., Lawrence, D. M., Swenson, S. C., Torn, M. S., Meng, L., Mahowald, N. M. and Hess, P.: Barriers to predicting changes in global terrestrial methane fluxes: analyses using CLM4Me, a methane biogeochemistry model integrated in CESM, Biogeosciences, 8(7), 1925–1953, doi:10.5194/bg-8-1925-2011, 2011.

Ringeval, B., Friedlingstein, P., Koven, C., Ciais, P., de Noblet-Ducoudre, N., Decharme, B. and Cadule, P.: Climate-CH_4 feedback from wetlands and its interaction with the climate-CO_2 feedback, Biogeosciences, 8(8), 2137–2157, doi:10.5194/bg-8-2137-2011, 2011.

Robison, A.L., W.M. Wollheim, B. Turek, C. Bova, C. Snay, and R.K. Varner, Spatial and temporal heterogeneity of methane ebullition in lowland headwater streams and the impact on sampling design, Limnology and Oceanography,

66(12): p. 4063-4076, 2021

Rocher-Ros, G., Stanley, E.H., Loken, L.C., Casson, N.J., Raymond, P.A., Liu, S., Amatulli, G. and Sponseller, R.A., Global methane emissions from rivers and streams. *Nature*, pp.1-6.,621, 530–535, https://doi.org/10.1038/s41586-023-06344-6, 2023

Rosentreter, J. A., Maher, D. T., Erler, D. V., Murray, R. H. and Eyre, B. D.: Methane emissions partially offset "blue carbon" burial in mangroves, Sci. Adv., 4(6), eaao4985, doi:10.1126/sciadv.aao4985, 2018.

Rosentreter, J. A., A. V Borges, B. R. Deemer, and others : Half of global methane emissions come from highly variable aquatic ecosystem sources. Nat. Geosci. **14**: 225–230. doi:10.1038/s41561-021-00715-2, 2021

Rosentreter, J.A., Laruelle, G.G., Bange, H.W., Bianchi, T.S., Busecke, J.J.M., Cai, W-J, Eyre, B.D., Forbrich, I., Kwon, E.Y., Mavara, T., Moosdorf, N., Van Dam, B. and Regnier, P. Coastal vegetation and estuaries are collectively a greenhouse gas sink. Nature Climate Change, 13, 579–587, doi: 10.1038/s41558-023-01682-9, 2023.

Rosentreter, J. A., Alcott, L., Maavara, T., Sun, X., Zhou, Y., Planavsky, N. J., and Raymond, P. A.: Revisiting the global methane cycle through expert opinion, Earth's Future, 12, e2023EF004234, https://doi.org/10.1029/2023EF004234 , 2024

Rowlinson, M. J., Rap, A., Arnold, S. R., Pope, R. J., Chipperfield, M. P., McNorton, J., Forster, P., Gordon, H., Pringle, K. J., Feng, W., Kerridge, B. J., Latter, B. L., and Siddans, R.: Impact of El Niño–Southern Oscillation on the interannual variability of methane and tropospheric ozone, Atmos. Chem. Phys., 19, 8669–8686, https://doi.org/10.5194/acp-19-8669-2019, 2019.

Ruppel, C. D., and J. D. Kessler (2017), The interaction of climate change and methane hydrates, Rev. Geophys., 55, 126-168, doi:10.1002/2016RG000534, 2017

Saad, K. M., Wunch, D., Toon, G. C., Bernath, P., Boone, C., Connor, B., Deutscher, N. M., Griffith, D. W. T., Kivi, R., Notholt, J., Roehl, C., Schneider, M., Sherlock, V. and Wennberg, P. O.: Derivation of tropospheric methane from TCCON CH_4 and HF total column observations, Atmospheric Meas. Technol., 7(9), 2907–2918, doi:10.5194/amt-7-2907-2014, 2014.

Sanderson, M. G.: Biomass of termites and their emissions of methane and carbon dioxide: A global database, Glob. Biogeochem. Cycles, 10(4), 543–557, doi:10.1029/96gb01893, 1996.

Sasakawa, M., Shimoyama, K., Machida, T., Tsuda, N., Suto, H., Arshinov, M., Davydov, D., Fofonov, A., Krasnov, O., Saeki, T., Koyama, Y. and Maksyutov, S.: Continuous measurements of methane from a tower network over Siberia, Tellus B, 62(5), 403–416, doi:10.1111/j.1600-0889.2010.00494.x, 2010.

Sasakawa, M., Machida, T., Ishijima, K., Arshinov, M., Patra, P. K., Ito, A., Aoki, S., and Petrov, V.: Temporal characteristics of CH4 vertical profiles observed in the West Siberian Lowland over Surgut from 1993 to 2015 and Novosibirsk from 1997 to 2015. Journal of Geophysical Research: Atmospheres, 122, 11,261– 11,273. https://doi.org/10.1002/2017JD026836, 2017.

3655 Saunois, M., Bousquet, P., Poulter, B., Peregon, A., Ciais, P., Canadell, J. G., Dlugokencky, E. J., Etiope, G., Bastviken,
3656   D., Houweling, S., Janssens-Maenhout, G., Tubiello, F. N., Castaldi, S., Jackson, R. B., Alexe, M., Arora, V. K.,
3657   Beerling, D. J., Bergamaschi, P., Blake, D. R., Brailsford, G., Brovkin, V., Bruhwiler, L., Crevoisier, C., Crill, P.,
3658   Covey, K., Curry, C., Frankenberg, C., Gedney, N., Höglund-Isaksson, L., Ishizawa, M., Ito, A., Joos, F., Kim, H. S.,
3659   Kleinen, T., Krummel, P., Lamarque, J. F., Langenfelds, R., Locatelli, R., Machida, T., Maksyutov, S., McDonald, K.
3660   C., Marshall, J., Melton, J. R., Morino, I., Naik, V., O'Doherty, S., Parmentier, F. J. W., Patra, P. K., Peng, C., Peng,
3661   S., Peters, G. P., Pison, I., Prigent, C., Prinn, R., Ramonet, M., Riley, W. J., Saito, M., Santini, M., Schroeder, R.,
3662   Simpson, I. J., Spahni, R., Steele, P., Takizawa, A., Thornton, B. F., Tian, H., Tohjima, Y., Viovy, N., Voulgarakis,
3663   A., van Weele, M., van der Werf, G. R., Weiss, R., Wiedinmyer, C., Wilton, D. J., Wiltshire, A., Worthy, D., Wunch,
3664   D., Xu, X., Yoshida, Y., Zhang, B., Zhang, Z. and Zhu, Q.: The global methane budget 2000–2012, Earth Syst Sci
3665   Data, 8(2), 697–751, doi:10.5194/essd-8-697-2016, 2016.
3666 Saunois, M., Bousquet, P., Poulter, B., Peregon, A., Ciais, P., Canadell, J. G., Dlugokencky, E. J., Etiope, G., Bastviken,
3667   D., Houweling, S., Janssens-Maenhout, G., Tubiello, F. N., Castaldi, S., Jackson, R. B., Alexe, M., Arora, V. K.,
3668   Beerling, D. J., Bergamaschi, P., Blake, D. R., Brailsford, G., Bruhwiler, L., Crevoisier, C., Crill, P., Covey, K.,
3669   Frankenberg, C., Gedney, N., Höglund-Isaksson, L., Ishizawa, M., Ito, A., Joos, F., Kim, H. S., Kleinen, T., Krummel,
3670   P., Lamarque, J. F., Langenfelds, R., Locatelli, R., Machida, T., Maksyutov, S., Melton, J. R., Morino, I., Naik, V.,
3671   O'Doherty, S., Parmentier, F. J. W., Patra, P. K., Peng, C., Peng, S., Peters, G. P., Pison, I., Prinn, R., Ramonet, M.,
3672   Riley, W. J., Saito, M., Santini, M., Schroeder, R., Simpson, I. J., Spahni, R., Takizawa, A., Thornton, B. F., Tian, H.,
3673   Tohjima, Y., Viovy, N., Voulgarakis, A., Weiss, R., Wilton, D. J., Wiltshire, A., Worthy, D., Wunch, D., Xu, X.,
3674   Yoshida, Y., Zhang, B., Zhang, Z. and Zhu, Q.: Variability and quasi-decadal changes in the methane budget over the
3675   period 2000-2012, Atmospheric Chem. Phys., 17(18), 11135–11161, doi:10.5194/acp-17-11135-2017, 2017.
3676 Saunois, M., Stavert, A. R., Poulter, B., Bousquet, P., Canadell, J. G., Jackson, R. B., Raymond, P. A., Dlugokencky, E.
3677   J., Houweling, S., Patra, P. K., Ciais, P., Arora, V. K., Bastviken, D., Bergamaschi, P., Blake, D. R., Brailsford, G.,
3678   Bruhwiler, L., Carlson, K. M., Carrol, M., Castaldi, S., Chandra, N., Crevoisier, C., Crill, P. M., Covey, K., Curry, C.
3679   L., Etiope, G., Frankenberg, C., Gedney, N., Hegglin, M. I., Höglund-Isaksson, L., Hugelius, G., Ishizawa, M., Ito, A.,
3680   Janssens-Maenhout, G., Jensen, K. M., Joos, F., Kleinen, T., Krummel, P. B., Langenfelds, R. L., Laruelle, G. G., Liu,
3681   L., Machida, T., Maksyutov, S., McDonald, K. C., McNorton, J., Miller, P. A., Melton, J. R., Morino, I., Müller, J.,
3682   Murguia-Flores, F., Naik, V., Niwa, Y., Noce, S., O'Doherty, S., Parker, R. J., Peng, C., Peng, S., Peters, G. P., Prigent,
3683   C., Prinn, R., Ramonet, M., Regnier, P., Riley, W. J., Rosentreter, J. A., Segers, A., Simpson, I. J., Shi, H., Smith, S.
3684   J., Steele, L. P., Thornton, B. F., Tian, H., Tohjima, Y., Tubiello, F. N., Tsuruta, A., Viovy, N., Voulgarakis, A., Weber,
3685   T. S., van Weele, M., van der Werf, G. R., Weiss, R. F., Worthy, D., Wunch, D., Yin, Y., Yoshida, Y., Zhang, W.,
3686   Zhang, Z., Zhao, Y., Zheng, B., Zhu, Q., Zhu, Q., and Zhuang, Q.: The Global Methane Budget 2000–2017, Earth
3687   Syst. Sci. Data, 12, 1561–1623, https://doi.org/10.5194/essd-12-1561-2020, 2020.

3688 Sayers, M.J., Grimm, A.G., Shuchman, R.A., Deines, A.M., Bunnel, D.B., Raymer, Z.B., Rogers, M.W., Woelmer, W.,
3689   Bennion, D.H., Brooks, C.N., Whitley, MA.A., Warner, D.M, and J. Mychek-Londer: A new method to generate a
3690   high-resolution global distribution map of lake chlorophyll, International Journal of Remote Sensing, 36:7, 1942-1964,
3691   DOI: 10.1080/01431161.2015.1029099, 2015

3692 Schepers, D., Guerlet, S., Butz, A., Landgraf, J., Frankenberg, C., Hasekamp, O., Blavier, J. F., Deutscher, N. M., Griffith,
3693   D. W. T., Hase, F., Kyro, E., Morino, I., Sherlock, V., Sussmann, R. and Aben, I.: Methane retrievals from Greenhouse
3694   Gases Observing Satellite (GOSAT) shortwave infrared measurements: Performance comparison of proxy and physics
3695   retrieval algorithms, J. Geophys. Res. Atmospheres, 117, D10, doi:10.1029/2012jd017549, 2012.

3696 Schmale O, Greinert J, Rehder G (2005) Methane emission from high-intensity marine gas seeps in the Black Sea into the
3697   atmosphere. Geophys Res Lett 32:L07609. doi:10.1029/2004GL021138, 2005

3698 Schmid, M., Batist, M.D., Granin, N.G., Kapitanov, V.A., McGinnis, D.F., Mizandrontsev, I.B., Obzhirov, A.I., and
3699   Wüest, A.. Sources and sinks of methane in Lake Baikal: A synthesis of measurements and modelling. Limnol.
3700   Oceanogr., 52(5), 1824–1837. doi: 10.4319/lo.2007.52.5.1824, 2007

3701   Schneising, O., Buchwitz, M., Reuter, M., Vanselow, S., Bovensmann, H., and Burrows, J. P.: Remote sensing of
3702   methane leakage from natural gas and petroleum systems revisited, Atmos. Chem. Phys., 20, 9169–9182,
3703   https://doi.org/10.5194/acp-20-9169-2020, 2020.

3704 Schorn, S., S. Ahmerkamp, E. Bullock, and others. : Diverse methylotrophic methanogenic archaea cause high methane
3705   emissions from seagrass meadows. Proc. Natl. Acad. Sci. **119**: 1–12. doi:10.1073/pnas.2106628119, 2022

3706 Schuldt, K. N., Mund, J., Aalto, T., Arlyn Andrews, Apadula, F., Jgor Arduini, Arnold, S., Baier, B., Bäni, L., Bartyzel,
3707   J., Bergamaschi, P., Biermann, T., Biraud, S. C., Pierre-Eric Blanc, Boenisch, H., Brailsford, G., Brand, W. A.,
3708   Brunner, D., Bui, T. P. V., … Miroslaw Zimnoch. : *Multi-laboratory compilation of atmospheric carbon dioxide data*
3709   *for the period 1983-2022; obspack_ch4_1_GLOBALVIEWplus_v6.0_2023-12-01* [Data set]. NOAA Global
3710   Monitoring Laboratory. https://doi.org/10.25925/20231001, 2023

3711 Schuur, E.A., Abbott, B.W., Commane, R., Ernakovich, J., Euskirchen, E., Hugelius, G., Grosse, G., Jones, M., Koven,
3712   C., Leshyk, V. and Lawrence, D. (2022) Permafrost and climate change: carbon cycle feedbacks from the warming
3713   Arctic. Annual Review of Environment and Resources, 47, pp.343-371. https://doi.org/10.1146/annurev-environ-
3714   012220-011847, 2022

3715 Schwietzke, S., Sherwood, O. A., Bruhwiler, L. M. P., Miller, J. B., Etiope, G., Dlugokencky, E. J., Michel, S. E., Arling,
3716   V. A., Vaughn, B. H., White, J. W. C. and Tans, P. P.: Upward revision of global fossil fuel methane emissions based
3717   on isotope database, Nature, 538(7623), 88–91, doi:10.1038/nature19797, 2016.

3718 Segers, A., Steinke, T., and Houweling, S.: Description of the CH4 Inversion Production Chain, CAMS (Copernicus
3719   Atmospheric   Monitoring   Service)   Report..   [online]   Available   from:
3720   https://atmosphere.copernicus.eu/sites/default/files/2022-10/CAMS255_2021SC1_D55.5.2.1-

3721   2021CH4_202206_production_chain_CH4_v1.pdf (Accessed 1 février 2024), 2022.

3722   Shaw, J. T., Allen, G., Barker, P., Pitt, J. R., Pasternak, D., Bauguitte, S. J.-B., Lee, J., Boewer, K. N., Daly, M. C., Lunt, M. F., Ganesan, A. L., Vaughan, A. R., Chibesakunda, F., Lambakasa, M., Fisher, R. E., France, J. L., Lowry, D., Palmer, P. I., Metzger, S., Parker, R. J., Gedney, N., Bateson, P., Cain, M., Lorente, A., Borsdorff, T., and Nisbet, E. G.: Large methane emission fluxes observed from tropical wetlands in Zambia, Global Biogeochem. Cy., 36, e2021GB007261, https://doi.org/10.1029/2021GB007261, 2022.

3727   Shen, L., Gautam, R., Omara, M., Zavala-Araiza, D., Maasakkers, J. D., Scarpelli, T. R., Lorente, A., Lyon, D., Sheng, J., Varon, D. J., Nesser, H., Qu, Z., Lu, X., Sulprizio, M. P., Hamburg, S. P., and Jacob, D. J.: Satellite quantification of oil and natural gas methane emissions in the US and Canada including contributions from individual basins, Atmos. Chem. Phys., 22, 11203–11215, https://doi.org/10.5194/acp-22-11203-2022, 2022.

3731   Shen, L., Jacob, D.J., Gautam, R. et al. National quantifications of methane emissions from fuel exploitation using high resolution inversions of satellite observations. Nat Commun 14, 4948 , https://doi.org/10.1038/s41467-023-40671-6, 2023

3734   Sherwen, T., Schmidt, J. A., Evans, M. J., Carpenter, L. J., Großmann, K., Eastham, S. D., Jacob, D. J., Dix, B., Koenig, T. K., Sinreich, R., Ortega, I., Volkamer, R., Saiz-Lopez, A., Prados-Roman, C., Mahajan, A. S., and Ordóñez, C.: Global impacts of tropospheric halogens (Cl, Br, I) on oxidants and composition in GEOS-Chem, Atmos. Chem. Phys., 16, 12239–12271, https://doi.org/10.5194/acp-16-12239-2016, 2016.

3738   Sherwin, E. D., Rutherford, J. S., Zhang, Z., Chen, Y., Wetherley, E. B., Yakovlev, P. V., Berman, E. S. F., Jones, B. B., Cusworth, D. H., Thorpe, A. K., Ayasse, A. K., Duren, R. M., and Brandt, A. R.: US oil and gas system emissions from nearly one million aerial site measurements, Nature, 627(8003), 328–334, doi:10.1038/s41586-024-07117-5, 2024

3742   Shindell, D, Sadavarte, P, Aben, I, Bredariol, TdO, Dreyfus, G, Höglund-Isaksson, L, Poulter, B, Saunois, M, Schmidt, GA, Szopa, S, Rentz, K, Parsons, L, Qu, Z, Faluvegi, G and Maasakkers, JD. : The methane imperative, Front Sci, 2:1349770, doi: 10.3389/fsci.2024.1349770, 2024

3745   Shindell, D., Kuylenstierna, J. C. I., Vignati, E., van Dingenen, R., Amann, M., Klimont, Z., Anenberg, S. C., Muller, N., Janssens-Maenhout, G., Raes, F., Schwartz, J., Faluvegi, G., Pozzoli, L., Kupiainen, K., Höglund-Isaksson, L., Emberson, L., Streets, D., Ramanathan, V., Hicks, K., Oanh, N. T. K., Milly, G., Williams, M., Demkine, V. and Fowler, D.: Simultaneously Mitigating Near-Term Climate Change and Improving Human Health and Food Security, Science, 335(6065), 183–189, doi:10.1126/science.1210026, 2012.

3750   Shorter, J. H., Mcmanus, J. B., Kolb, C. E., Allwine, E. J., Lamb, B. K., Mosher, B. W., Harriss, R. C., Partchatka, U., Fischer, H., Harris, G. W., Crutzen, P. J. and Karbach, H.-J.: Methane emission measurements in urban areas in Eastern Germany, J. Atmospheric Chem., 124(2), 121–140, 1996.

3753   Shu, S., Jain, A.K. and Kheshgi, H.S.: Investigating Wetland and Nonwetland Soil Methane Emissions and Sinks Across

3754   the Contiguous United States Using a Land Surface Model. Global Biogeochem. Cycles, 34: e2019GB006251.

3755   https://doi-org.insu.bib.cnrs.fr/10.1029/2019GB006251, 2020

3756 Simpson, I. J., Thurtell, G. W., Kidd, G. E., Lin, M., Demetriades-Shah, T. H., Flitcroft, I. D., Kanemasu, E. T., Nie, D.,

3757   Bronson, K. F. and Neue, H. U.: Tunable diode laser measurements of methane fluxes from an irrigated rice paddy

3758   field in the Philippines, J. Geophys. Res. Atmospheres, 100(D4), 7283–7290, doi:10.1029/94jd03326, 1995.

3759 Simpson, I. J., Sulbaek Andersen, M. P., Meinardi, S., Bruhwiler, L., Blake, N. J., Helmig, D., Rowland, F. S. and Blake,

3760   D. R.: Long-term decline of global atmospheric ethane concentrations and implications for methane, Nature,

3761   488(7412), 490–494, doi:10.1038/nature11342, 2012.

3762 Smith I.R., Grasby S.E., Lane L.S.: An investigation of gas seeps and aquatic chemistry in Fisherman Lake, southwest

3763   Northwest Territories. Geological Survey of Canada, Current Research 2005-A3, 8 p., 2005

3764 Solomon EA, Kastner M, MacDonald IR, Leifer I: Considerable methane fluxes to the atmosphere from hydrocarbon

3765   seeps in the Gulf of Mexico. Nat Geosci 2:561–565, 2009

3766 Spahni, R., Wania, R., Neef, L., van Weele, M., Pison, I., Bousquet, P., Frankenberg, C., Foster, P. N., Joos, F., Prentice,

3767   I. C. and van Velthoven, P.: Constraining global methane emissions and uptake by ecosystems, Biogeosciences, 8(6),

3768   1643–1665, doi:10.5194/bg-8-1643-2011, 2011.

3769 Stanley, E. H., Casson, N. J., Christel, S. T., Crawford, J. T., Loken, L. C. and Oliver, S. K.: The ecology of methane in

3770   streams and rivers: patterns, controls, and global significance, Ecol. Monogr., doi:10.1890/15-1027, 2016.

3771 Stanley, K. M., Grant, A., O'Doherty, S., Young, D., Manning, A. J., Stavert, A. R., Spain, T. G., Salameh, P. K., Harth,

3772   C. M., Simmonds, P. G., Sturges, W. T., Oram, D. E. and Derwent, R. G.: Greenhouse gas measurements from a UK

3773   network of tall towers: technical description and first results, Atmospheric Meas. Tech., 11(3), 1437–1458,

3774   doi:10.5194/amt-11-1437-2018, 2018.

3775 Stanley, E. H., Loken, L. C., Casson, N. J., Oliver, S. K., Sponseller, R. A., Wallin, M. B., Zhang, L., and Rocher-Ros,

3776   G.: GRiMeDB: the Global River Methane Database of concentrations and fluxes, Earth Syst. Sci. Data, 15, 2879–

3777   2926, https://doi.org/10.5194/essd-15-2879-2023, 2023.

3778 Stavert, A. R., Saunois, M., Canadell, J. G., Poulter, B., Jackson, R. B., Regnier, P., Lauerwald, R., Raymond, P. A.,

3779   Allen, G. H., Patra, P. K., Bergamaschi, P., Bousquet, P., Chandra, N., Ciais, P., Gustafson, A., Ishizawa, M., Ito,

3780   A., Kleinen, T., Maksyutov, S., Joe McNorton, Joe R. Melton, Jurek Müller, Yosuke Niwa, Shushi Peng, William

3781   J. Riley, Arjo Segers, Hanqin Tian, Aki Tsuruta, Yi Yin, Zhen Zhang, Bo Zheng, Zhuang, Q. Regional trends

3782   and drivers of the global methane budget. *Global Change Biology*, 28, 182–200. https://doi.org/10.1111/gcb.15901,

3783   2021

3784 Steele, L. P., Fraser, P. J., Rasmussen, R. A., Khalil, M. A. K., Conway, T. J., Crawford, A. J., Gammon, R. H., Masarie,

3785   K. A. and Thoning, K. W.: The global distribution of methane in the troposphere, J. Atmospheric Chem., 5, 125–171,

3786   1987.

3787 Stevenson, D. S., Zhao, A., Naik, V., O'Connor, F. M., Tilmes, S., Zeng, G., Murray, L. T., Collins, W. J., Griffiths, P. T.,
3788   Shim, S., Horowitz, L. W., Sentman, L. T., and Emmons, L.: Trends in global tropospheric hydroxyl radical and
3789   methane lifetime since 1850 from AerChemMIP, Atmos. Chem. Phys., 20, 12905–12920, https://doi.org/10.5194/acp-
3790   20-12905-2020, 2020.

3791 Stevenson, D. S., Derwent, R. G., Wild, O., and Collins, W. J.: COVID-19 lockdown emission reductions have the
3792   potential to explain over half of the coincident increase in global atmospheric methane, Atmos. Chem. Phys., 22,
3793   14243–14252, https://doi.org/10.5194/acp-22-14243-2022, 2022.

3794 Stocker, B. D., Spahni, R. and Joos, F.: DYPTOP: a cost-efficient TOPMODEL implementation to simulate sub-grid
3795   spatio-temporal dynamics of global wetlands and peatlands, Geosci. Model Dev., 7(6), 3089–3110, doi:10.5194/gmd-
3796   7-3089-2014, 2014.

3797 Strauss, J., Abbott, B.W., Hugelius, G., Schuur, E., Treat, C., Fuchs, M., Schädel, C., Ulrich, M., Turetsky, M., Keuschnig,
3798   M. and Biasi, C. (2021) Chapter 9. Permafrost. In FAO Recarbonizing global soils–A technical manual of
3799   recommended management practices: Volume 2–Hot spots and bright spots of soil organic carbon, p.130, 2021

3800 Strode, S. A., Wang, J. S., Manyin, M., Duncan, B., Hossaini, R., Keller, C. A., Michel, S. E., and White, J. W. C.: Strong
3801   sensitivity of the isotopic composition of methane to the plausible range of tropospheric chlorine, Atmos. Chem. Phys.,
3802   20, 8405–8419, https://doi.org/10.5194/acp-20-8405-2020, 2020.

3803 Sugimoto, A., Inoue, T., Kitibutr, N., Abe, T: Methane oxidation by termite mounds estimate by the carbon isotope
3804   composition of methane. Glob. Biogeochem. Cy. 12, 595-605. 1998.

3805 Sweeney, C., Karion, A., Wolter, S., Newberger, T., Guenther, D., Higgs, J. A., Andrews, A. E., Lang, P. M., Neff, D.,
3806   Dlugokencky, E., Miller, J. B., Montzka, S. A., Miller, B. R., Masarie, K. A., Biraud, S. C., Novelli, P. C., Crotwell,
3807   M., Crotwell, A. M., Thoning, K. and Tans, P. P.: Seasonal climatology of CO_2 across North America from aircraft
3808   measurements in the NOAA/ESRL Global Greenhouse Gas Reference Network, J. Geophys. Res. Atmospheres,
3809   120(10), 5155–5190, doi:10.1002/2014jd022591, 2015.

3810 Szopa, S., V. Naik, B. Adhikary, P. Artaxo, T. Berntsen, W.D. Collins, S. Fuzzi, L. Gallardo, A. Kiendler-Scharr, Z.
3811   Klimont, H. Liao, N. Unger, and P. Zanis: Short-Lived Climate Forcers. In Climate Change 2021: The Physical Science
3812   Basis. Contribution of Working Group I to the Sixth Assessment Report of the Intergovernmental Panel on Climate
3813   Change [Masson-Delmotte, V., P. Zhai, A. Pirani, S.L. Connors, C. Péan, S. Berger, N. Caud, Y. Chen, L. Goldfarb,
3814   M.I. Gomis, M. Huang, K. Leitzell, E. Lonnoy, J.B.R. Matthews, T.K. Maycock, T. Waterfield, O. Yelekçi, R. Yu,
3815   and B. Zhou (eds.)]. Cambridge University Press, Cambridge, United Kingdom and New York, NY, USA, pp. 817–
3816   922, doi:10.1017/9781009157896.008., 2021Tan, Z. and Zhuang, Q.: Methane emissions from pan-Arctic lakes during
3817   the 21st century: An analysis with process-based models of lake evolution and biogeochemistry, J. Geophys. Res.
3818   Biogeosciences, 120(12), 2641–2653, doi:10.1002/2015JG003184, 2015.

3819 Tans, P. and Zwellberg, C.: 17th WMO/IAEA Meeting on Carbon Dioxide, Other Greenhouse Gases and Related Tracers

Measurement Techniques (GGMT-2013), GAW Report, WMO, Geneva. [online] Available from: https://library.wmo.int/index.php?lvl=notice_display&id=16373#.XnpBPW7jIq8, 2014.

Taranu, Z.E., I. Gregory-Eaves, P.R. Leavitt, L. Bunting, T. Buchaca, J. Catalan, I. Domaizon, P. Guilizzoni, A. Lami, S. McGowan, H. Moorhouse, G. Morabito, F.R. Pick, M.A. Stevenson, P.L. Thompson, and R.D. Vinebrooke: Acceleration of cyanobacterial dominance in north temperate-subarctic lakes during the Anthropocene. Ecology Letters, 18(4): p. 375-384., 2015

Taylor, P. G., Bilinski, T. M., Fancher, H. R. F., Cleveland, C. C., Nemergut, D. R., Weintraub, S. R., Wieder, W. R. and Townsend, A. R.: Palm oil wastewater methane emissions and bioenergy potential, Nat. Clim. Change, 4(3), 151–152, doi:10.1038/nclimate2154, 2014.

le Texier, H., Solomon, S. and Garcia, R. R.: The role of molecular hydrogen and methane oxidation in the water vapour budget of the stratosphere, Q. J. R. Meteorol. Soc., 114(480), 281–295, doi:10.1002/qj.49711448002, 1988.

Thanwerdas, J., Saunois, M., Berchet, A., Pison, I., Vaughn, B. H., Michel, S. E., and Bousquet, P.: Variational inverse modeling within the Community Inversion Framework v1.1 to assimilate $\delta 13C(CH4)$ and $CH4$: a case study with model LMDz-SACS, Geosci. Model Dev., 15, 4831–4851, https://doi.org/10.5194/gmd-15-4831-2022, 2022a.

Thanwerdas, J., Saunois, M., Pison, I., Hauglustaine, D., Berchet, A., Baier, B., Sweeney, C., and Bousquet, P.: How do Cl concentrations matter for the simulation of $CH4$ and $\delta 13C(CH4)$ and estimation of the $CH4$ budget through atmospheric inversions?, Atmos. Chem. Phys., 22, 15489–15508, https://doi.org/10.5194/acp-22-15489-2022, 2022b.

Thanwerdas, J., Saunois, M., Berchet, A., Pison, I., and Bousquet, P.: Investigation of the renewed methane growth post-2007 with high-resolution 3-D variational inverse modeling and isotopic constraints, Atmos. Chem. Phys., 24, 2129–2167, https://doi.org/10.5194/acp-24-2129-2024, 2024.

Thompson, R. L., Montzka, S. A., Vollmer, M. K., Arduini, J., Crotwell, M., Krummel, P. B., Lunder, C., Mühle, J., O'Doherty, S., Prinn, R. G., Reimann, S., Vimont, I., Wang, H., Weiss, R. F., and Young, D.: Estimation of the atmospheric hydroxyl radical oxidative capacity using multiple hydrofluorocarbons (HFCs), Atmos. Chem. Phys., 24, 1415–1427, https://doi.org/10.5194/acp-24-1415-2024, 2024.

Thoning, K. W., Tans, P. P. and Komhyr, W. D.: Atmospheric carbon dioxide at Mauna Loa Observatory. 2. Analysis of the NOAA GMCC data, 1974,1985, J. Geophys. Res., 94(D6), 8549–8565, 1989.

Thorneloe, S. A., Barlaz, M. A., Peer, R., Huff, L. C., Davis, L. and Mangino, J.: Waste management, in Atmospheric Methane: Its Role in the Global Environment, edited by M. Khalil, pp. 234–262, Springer-Verlag, New York., 2000.

Thornton, B. F., Prytherch, J., Andersson, K., Brooks, I. M., Salisbury, D., Tjernström, M. and Crill, P. M.: Shipborne eddy covariance observations of methane fluxes constrain Arctic sea emissions, Sci. Adv., 6(5), eaay7934, doi:10.1126/sciadv.aay7934, 2020.

Thornton B.F., Etiope G., Schwietzke S., Milkov A.V., Klusman R.W., Judd A., Oehler D.Z.: Conflicting estimates of natural geologic methane emissions. Elem. Sci. Anth., 9, 1, doi:https:// doi.org/10.1525/elementa.2021.00031, 2021

Thornton, J. A., Kercher, J. P., Riedel, T. P., Wagner, N. L., Cozic, J., Holloway, J. S., Dubé, W. P., Wolfe, G. M., Quinn, P. K., Middlebrook, A. M., Alexander, B. and Brown, S. S.: A large atomic chlorine source inferred from mid-continental reactive nitrogen chemistry, Nature, 464(7286), 271–274, doi:10.1038/nature08905, 2010.

Thorpe, A. K. , Kort, E. A. , Cusworth, D. H. , Ayasse, A. K. , Bue, B. D. ,Yadav, V. ,Thompson, D. R. , Frankenberg, C. , Herner, J. , Falk, M. ,Green, R. O. ,Miller, C. E. , and Duren, R. M.: Methane emissions decline from reduced oil, natural gas, and refinery production during COVID-19, Environmental Research Communications, 5, 021006, 2023

Tian, H., Xu, X., Liu, M., Ren, W., Zhang, C., Chen, G. and Lu, C.: Spatial and temporal patterns of CH_4 and N_2O fluxes in terrestrial ecosystems of North America during 1979–2008: application of a global biogeochemistry model, Biogeosciences, 7(9), 2673–2694, doi:10.5194/bg-7-2673-2010, 2010.

Tian, H., Xu, X., Lu, C., Liu, M., Ren, W., Chen, G., Melillo, J. and Liu, J.: Net exchanges of CO_2, CH_4, and N_2O between China's terrestrial ecosystems and the atmosphere and their contributions to global climate warming, J. Geophys. Res. Biogeosciences, 116, G2, doi:10.1029/2010jg001393, 2011.

Tian, H., Chen, G., Lu, C., Xu, X., Ren, W., Zhang, B., Banger, K., Tao, B., Pan, S., Liu, M., Zhang, C., Bruhwiler, L. and Wofsy, S.: Global methane and nitrous oxide emissions from terrestrial ecosystems due to multiple environmental changes, Ecosyst. Health Sustain., 1(1), 1–20, doi:doi:10.1890/ehs14-0015.1, 2015.

Tian, H., Lu, C., Ciais, P., Michalak, A. M., Canadell, J. G., Saikawa, E., Huntzinger, D. N., Gurney, K. R., Sitch, S., Zhang, B., Yang, J., Bousquet, P., Bruhwiler, L., Chen, G., Dlugokencky, E., Friedlingstein, P., Melillo, J., Pan, S., Poulter, B., Prinn, R., Saunois, M., Schwalm, C. R. and Wofsy, S. C.: The terrestrial biosphere as a net source of greenhouse gases to the atmosphere, Nature, 531(7593), 225–228, doi:10.1038/nature16946, 2016.

Tian, H., Xu, R., Canadell, J. G., Thompson, R. L., Winiwarter, W., Suntharalingam, P., Davidson, E. A., Ciais, P., Jackson, R. B., Janssens-Maenhout, G., Prather, M. J., Regnier, P., Pan, N., Pan, S., Peters, G. P., Shi, H., Tubiello, F. N., Zaehle, S., Zhou, F., Arneth, A., Battaglia, G., Berthet, S., Bopp, L., Bouwman, A. F., Buitenhuis, E. T., Chang, J., Chipperfield, M. P., Dangal, S. R. S., Dlugokencky, E., Elkins, J. W., Eyre, B. D., Fu, B., Hall, B., Ito, A., Joos, F., Krummel, P. B., Landolfi, A., Laruelle, G. G., Lauerwald, R., Li, W., Lienert, S., Maavara, T., MacLeod, M., Millet, D. B., Olin, S., Patra, P. K., Prinn, R. G., Raymond, P. A., Ruiz, D. J., van der Werf, G. R., Vuichard, N., Wang, J., Weiss, R. F., Wells, K. C., Wilson, C., Yang, J., and Yao, Y.: A comprehensive quantification of global nitrous oxide sources and sinks, Nature, 586, 248–256, https://doi.org/10.1038/s41586-020-2780-0, 2020.

Tian, H., Yao, Y., Li, Y., Shi, H., Pan, S., Najjar, R. G., et al. (2023). Increased terrestrial carbon export and CO2 evasion from global inland waters since the preindustrial era. *Global Biogeochemical Cycles*, 37, e2023GB007776. https://doi.org/10.1029/2023GB007776, 2023

Tibrewal, K., Ciais, P., Saunois, M. Martinez, A., Lin, X., Thanwerdas, J., Deng, Z. , Chevallier, F. , Giron, C., Albergel, C., Tanaka, K., Patra, P., Tsuruta, A., Zheng, B., Belikov, D., Niwa, Y. , Janardanan, R. , Maksyutov, S., Segers, A., Tzompa-Sosa, Z. A., Bousquet, P., and Sciare, J.: Assessment of methane emissions from oil, gas and coal sectors

across inventories and atmospheric inversions, Commun Earth Environ 5, 26, https://doi.org/10.1038/s43247-023-01190-w, 2024

Tiwari, Y. K. and Kumar, K. R.: GHG observation programs in India, Asian GAWgreenhouse Gases 3 Korea Meteorol. Adm. Chungnam South Korea, 2012.

Tsuruta, A., Aalto, T., Backman, L., Hakkarainen, J., Laan-Luijkx, I. T. van der, Krol, M. C., Spahni, R., Houweling, S., Laine, M., Dlugokencky, E., Gomez-Pelaez, A. J., Schoot, M. van der, Langenfelds, R., Ellul, R., Arduini, J., Apadula, F., Gerbig, C., Feist, D. G., Kivi, R., Yoshida, Y. and Peters, W.: Global methane emission estimates for 2000–2012 from CarbonTracker Europe-CH₄ v1.0, Geosci. Model Dev., 10(3), 1261–1289, doi:10.5194/gmd-10-1261-2017, 2017.

Tsuruta, A.; Kivimäki, E.; Lindqvist, H.; Karppinen, T.; Backman, L.; Hakkarainen, J.; Schneising, O.; Buchwitz, M.; Lan, X.; Kivi, R.; et al. CH4 Fluxes Derived from Assimilation of TROPOMI XCH4 in CarbonTracker Europe-CH4: Evaluation of Seasonality and Spatial Distribution in the Northern High Latitudes. Remote Sens. 2023, 15, 1620. https://doi.org/10.3390/rs15061620, 2023

Tubiello, F. N.: Greenhouse Gas Emissions Due to Agriculture, in Elsevier Encyclopedia of Food Systems., 2019.

Tubiello, F. N., Salvatore, M., Rossi, S., Ferrara, A., Fitton, N. and Smith, P.: The FAOSTAT database of greenhouse gas emissions from agriculture, Environ. Res. Lett., 8(1), 015009, doi:10.1088/1748-9326/8/1/015009, 2013.

Tubiello, F. N., Karl, K., Flammini, A., Gütschow, J., Obli-Laryea, G., Conchedda, G., Pan, X., Qi, S. Y., Halldórudóttir Heiðarsdóttir, H., Wanner, N., Quadrelli, R., Rocha Souza, L., Benoit, P., Hayek, M., Sandalow, D., Mencos Contreras, E., Rosenzweig, C., Rosero Moncayo, J., Conforti, P., and Torero, M.: Pre- and post-production processes increasingly dominate greenhouse gas emissions from agri-food systems, Earth Syst. Sci. Data, 14, 1795–1809, https://doi.org/10.5194/essd-14-1795-2022, 2022.

Turetsky, M. R., Kotowska, A., Bubier, J., Dise, N. B., Crill, P., Hornibrook, E. R. C., Minkkinen, K., Moore, T. R., Myers-Smith, I. H., Nykänen, H., Olefeldt, D., Rinne, J., Saarnio, S., Shurpali, N., Tuittila, E.-S., Waddington, J. M., White, J. R., Wickland, K. P. and Wilmking, M.: A synthesis of methane emissions from 71 northern, temperate, and subtropical wetlands, Glob. Change Biol., 20(7), 2183–2197, doi:10.1111/gcb.12580, 2014.

Turetsky, M. R., Abbott, B. W., Jones, M. C., Anthony, K. W., Olefeldt, D., Schuur, E. A. G., et al.: Carbon release through abrupt permafrost thaw. *Nature Geoscience*, 13(2), 138–143. https://doi.org/10.1038/s41561-019-0526-0, 2020

Turner, A. J., Fung, I., Naik, V., Horowitz, L. W. and Cohen, R. C.: Modulation of hydroxyl variability by ENSO in the absence of external forcing, Proc. Natl. Acad. Sci., 115(36), 8931–8936, doi:10.1073/pnas.1807532115, 2018.

Turner, A. J., Frankenberg, C. and Kort, E. A.: Interpreting contemporary trends in atmospheric methane, Proc. Natl. Acad. Sci., 116(8), 2805, doi:10.1073/pnas.1814297116, 2019.

UNEP, United Nations Environment Programme and Climate and Clean Air Coalition. Global Methane Assessment:

3919   Benefits and Costs of Mitigating Methane Emissions. Nairobi: United Nations Environment Programme., 2021

3920   UNEP, United Nations Environment Programme/Climate and Clean Air Coalition. Global Methane Assessment: 2030
3921   Baseline Report. Nairobi, 2022

3922   USEPA: Greenhouse Gas Emissions Estimation Methodologies for Biogenic Emissions from Selected Source Categories:
3923   Solid Waste Disposal Wastewater Treatment Ethanol Fermentation, Measurement Policy Group, US EPA. [online]
3924   Available from: https://www3.epa.gov/ttnchie1/efpac/ghg/GHG_Biogenic_Report_draft_Dec1410.pdf (Accessed 11
3925   March 2020a), 2010a.

3926   USEPA: Office of Atmospheric Programs (6207J), Methane and Nitrous Oxide Emissions From Natural Sources, U.S.
3927   Environmental Protection Agency, EPA 430-R-10-001. Available online at http://nepis.epa.gov/, Washington, DC
3928   20460., 2010b.

3929   USEPA: Draft: Global Anthropogenic Non-CO_2 Greenhouse Gas Emissions: 1990-2030. EPA 430-R-03-002, United
3930   States Environmental Protection Agency, Washington D.C., 2011.

3931   USEPA: Global Anthropogenic Non-CO_2 Greenhouse Gas Emissions 1990-2030, EPA 430-R-12-006, US Environmental
3932   Protection Agency, Washington DC., 2012.

3933   USEPA: Draft Inventory of U.S. Greenhouse gas Emissions and Sinks: 1990-2014. EPA 430-R-16-002. February 2016.
3934   U.S. Environmental protection Agency, Washington, DC, USA., 2016.

3935   USEPA: Global Non-CO2 Greenhouse Gas Emission Projections & Mitigation Potential: 2015-2050, EPA-430-R-19-010,
3936   U.S. Environmental protection Agency, Washington, DC, USA., 2019

3937   Valentine, D. W., Holland, E. A. and Schimel, D. S.: Ecosystem and physiological controls over methane production in
3938   northern wetlands, J. Geophys. Res., 99(D1), 1563–1571, 1994.

3939   Vardag, S. N., Hammer, S., O'Doherty, S., Spain, T. G., Wastine, B., Jordan, A. and Levin, I.: Comparisons of continuous
3940   atmospheric CH_4, CO_2 and N_2O measurements – results from a travelling instrument campaign at Mace Head,
3941   Atmospheric Chem. Phys., 14(16), 8403–8418, doi:10.5194/acp-14-8403-2014, 2014.

3942   Varon, D. J., Jacob, D. J., Hmiel, B., Gautam, R., Lyon, D. R., Omara, M., Sulprizio, M., Shen, L., Pendergrass, D., Nesser,
3943   H., Qu, Z., Barkley, Z. R., Miles, N. L., Richardson, S. J., Davis, K. J., Pandey, S., Lu, X., Lorente, A., Borsdorff, T.,
3944   Maasakkers, J. D., and Aben, I.: Continuous weekly monitoring of methane emissions from the Permian Basin by
3945   inversion of TROPOMI satellite observations, Atmos. Chem. Phys., 23, 7503–7520, https://doi.org/10.5194/acp-23-
3946   7503-2023, 2023.

3947   VODCA2GPP – a new, global, long-term (1988–2020) gross primary production dataset from microwave remote sensing,
3948   Earth Syst. Sci. Data, 14, 1063–1085, https://doi.org/10.5194/essd-14-1063-2022, 2022.

3949   Voulgarakis, A., Naik, V., Lamarque, J. F., Shindell, D. T., Young, P. J., Prather, M. J., Wild, O., Field, R. D., Bergmann,
3950   D., Cameron-Smith, P., Cionni, I., Collins, W. J., Dals√∏ren, S. B., Doherty, R. M., Eyring, V., Faluvegi, G., Folberth,
3951   G. A., Horowitz, L. W., Josse, B., MacKenzie, I. A., Nagashima, T., Plummer, D. A., Righi, M., Rumbold, S. T.,

Stevenson, D. S., Strode, S. A., Sudo, K., Szopa, S. and Zeng, G.: Analysis of present day and future OH and methane lifetime in the ACCMIP simulations, Atmospheric Chem. Phys., 13(5), 2563–2587, doi:10.5194/acp-13-2563-2013, 2013.

Voulgarakis, A., Marlier, M. E., Faluvegi, G., Shindell, D. T., Tsigaridis, K. and Mangeon, S.: Interannual variability of tropospheric trace gases and aerosols: The role of biomass burning emissions, J. Geophys. Res. Atmospheres, 120(14), 7157–7173, doi:10.1002/2014jd022926, 2015.

Wallmann, K., Pinero, E., Burwicz, E., Haeckel, M., Hensen, C., Dale, A. and Ruepke, L.: The Global Inventory of Methane Hydrate in Marine Sediments: A Theoretical Approach, Energies, 5(7), 2449, 2012.

Walter Anthony, K.M., Anthony, P., Grosse, G. and Chanton, J.: Geologic methane seeps along boundaries of Arctic permafrost thaw and melting glaciers. Nature Geoscience, 5(6), pp.419-426., DOI: 10.1038/ngeo1480, 2012

Wang, F., Maksyutov, S., Tsuruta, A., Janardanan, R., Ito, A., Sasakawa, M., Machida, T., Morino, I., Yoshida, Y., Kaiser, J. W., Janssens-Maenhout, G., Dlugokencky, E. J., Mammarella, I., Lavric, J. V. and Matsunaga, T.: Methane Emission Estimates by the Global High-Resolution Inverse Model Using National Inventories, Remote Sens., 11(21), 2489, doi:10.3390/rs11212489, 2019a.

Wang, G., X. Xia, S. Liu, L. Zhang, S. Zhang, J. Wang, N. Xi, and Q. Zhang, Intense methane ebullition from urban inland waters and its significant contribution to greenhouse gas emissions. Water Research, 189: p. 116654, 2021a

Wang, X., Jacob, D. J., Eastham, S. D., Sulprizio, M. P., Zhu, L., Chen, Q., Alexander, B., Sherwen, T., Evans, M. J., Lee, B. H., Haskins, J. D., Lopez-Hilfiker, F. D., Thornton, J. A., Huey, G. L. and Liao, H.: The role of chlorine in global tropospheric chemistry, Atmospheric Chem. Phys., 19(6), 3981–4003, doi:10.5194/acp-19-3981-2019, 2019b.

Wang, X., Jacob, D. J., Downs, W., Zhai, S., Zhu, L., Shah, V., Holmes, C. D., Sherwen, T., Alexander, B., Evans, M. J., Eastham, S. D., Neuman, J. A., Veres, P. R., Koenig, T. K., Volkamer, R., Huey, L. G., Bannan, T. J., Percival, C. J., Lee, B. H., and Thornton, J. A.: Global tropospheric halogen (Cl, Br, I) chemistry and its impact on oxidants, Atmos. Chem. Phys., 21, 13973–13996, https://doi.org/10.5194/acp-21-13973-2021, 2021b.

Wang, Z., Deutscher, N. M., Warneke, T., Notholt, J., Dils, B., Griffith, D. W. T., Schmidt, M., Ramonet, M. and Gerbig, C.: Retrieval of tropospheric column-averaged CH_4 mole fraction by solar absorption FTIR-spectrometry using N_2O as a proxy, Atmospheric Meas. Tech., 7(10), 3295–3305, doi:10.5194/amt-7-3295-2014, 2014.

Wang, Z.-P., Gu, Q., Deng, F.-D., Huang, J.-H., Megonigal, J. P., Yu, Q., Lü, X.-T., Li, L.-H., Chang, S., Zhang, Y.-H., Feng, J.-C. and Han, X.-G.: Methane emissions from the trunks of living trees on upland soils, New Phytol., 211(2), 429–439, doi:10.1111/nph.13909, 2016.

Wania, R., I. Ross and I. C. Prentice: Implementation and evaluation of a new methane model within a dynamic global vegetation model: LPJ-WHyMe v1.3, Geosci. Model Dev. Discuss., 3, 1–59, 2010.

Wania, R., Melton, J. R., Hodson, E. L., Poulter, B., Ringeval, B., Spahni, R., Bohn, T., Avis, C. A., Chen, G., Eliseev, A. V., Hopcroft, P. O., Riley, W. J., Subin, Z. M., Tian, H., van Bodegom, P. M., Kleinen, T., Yu, Z. C., Singarayer, J.

S., Zurcher, S., Lettenmaier, D. P., Beerling, D. J., Denisov, S. N., Prigent, C., Papa, F. and Kaplan, J. O.: Present state of global wetland extent and wetland methane modelling: Methodology of a model inter-comparison project (WETCHIMP), Geosci. Model Dev., 6(3), 617–641, 2013.

Wassmann, R., Lantin, R. S., Neue, H. U., Buendia, L. V., Corton, T. M. and Lu, Y.: Characterization of methane emissions in Asia III: Mitigation options and future research needs, Nutr. Cycl. Agroecosystems, 58, 23–36, 2000.

Weber, T., Wiseman, N. A. and Kock, A.: Global ocean methane emissions dominated by shallow coastal waters, Nat. Commun., 10(1), 1–10, doi:10.1038/s41467-019-12541-7, 2019.

Wells, N. S., J. J. Chen, D. T. Maher, P. Huang, D. V. Erler, M. Hipsey, and B. D. Eyre: Changing sediment and surface water processes increase CH4 emissions from human-impacted estuaries. Geochim. Cosmochim. Acta **280**: 130–147. doi:10.1016/j.gca.2020.04.020, 2020

van der Werf, G. R., Randerson, J. T., Giglio, L., Collatz, G. J., Mu, M., Kasibhatla, P. S., Morton, D. C., DeFries, R. S., Jin, Y. and van Leeuwen, T. T.: Global fire emissions and the contribution of deforestation, savanna, forest, agricultural, and peat fires (1997-2009), Atmospheric Chem. Phys., 10(23), 11,707-11,735, 2010.

van der Werf, G. R., Randerson, J. T., Giglio, L., Leeuwen, T. T. van, Chen, Y., Rogers, B. M., Mu, M., Marle, M. J. E. van, Morton, D. C., Collatz, G. J., Yokelson, R. J. and Kasibhatla, P. S.: Global fire emissions estimates during 1997–2016, Earth Syst. Sci. Data, 9(2), 697–720, doi:10.5194/essd-9-697-2017, 2017.

Westbrook, G. K., Thatcher, K. E., Rohling, E. J., Piotrowski, A. M., Pälike, H., Osborne, A. H., Nisbet, E. G., Minshull, T. A., Lanoisellé, M., James, R. H., Hühnerbach, V., Green, D., Fisher, R. E., Crocker, A. J., Chabert, A.,Bolton, C., Beszczynska-Möller, A., Berndt, C., and Aquilina, A.: Escape of methane gas from the seabed along the West Spitsbergen continental margin, Geophys. Res. Lett., 36, L15608, https://doi.org/10.1029/2009GL039191, 2009.

Whalen, S. C.: Biogeochemistry of Methane Exchange between Natural Wetlands and the Atmosphere, Environ. Eng. Sci., 22(1), 73–94, doi:10.1089/ees.2005.22.73, 2005.

Wiedinmyer, C., Kimura, Y., McDonald-Buller, E. C., Emmons, L. K., Buchholz, R. R., Tang, W., Seto, K., Joseph, M. B., Barsanti, K. C., Carlton, A. G., and Yokelson, R.: The Fire Inventory from NCAR version 2.5: an updated global fire emissions model for climate and chemistry applications, EGUsphere [preprint], https://doi.org/10.5194/egusphere-2023-124, 2023.

Wik, M., Thornton, B. F., Bastviken, D., Uhlbäck, J. and Crill, P. M.: Biased sampling of methane release from northern lakes: A problem for extrapolation, Geophys. Res. Lett., 43(3), 1256–1262, doi:10.1002/2015gl066501, 2016a.

Wik, M., Varner, R. K., Anthony, K. W., MacIntyre, S. and Bastviken, D.: Climate-sensitive northern lakes and ponds are critical components of methane release, Nat. Geosci., 9(2), 99–105, doi:10.1038/ngeo2578, 2016b.

Wild, B., Teubner, I., Moesinger, L., Zotta, R.-M., Forkel, M., van der Schalie, R., Sitch, S., and Dorigo, W.: VODCA2GPP – a new, global, long-term (1988–2020) gross primary production dataset from microwave remote sensing, Earth Syst. Sci. Data, 14, 1063–1085, https://doi.org/10.5194/essd-14-1063-2022, 2022.

Williams, J. P., Omara, M., Himmelberger, A., Zavala-Araiza, D., MacKay, K., Benmergui, J., Sargent, M., Wofsy, S. C., Hamburg, S. P., and Gautam, R.: Small emission sources disproportionately account for a large majority of total methane emissions from the US oil and gas sector, EGUsphere [preprint], https://doi.org/10.5194/egusphere-2024-1402, 2024.

Winderlich, J., Chen, H., Gerbig, C., Seifert, T., Kolle, O., Lavrič, J. V., Kaiser, C., Höfer, A. and Heimann, M.: Continuous low-maintenance CO_2/CH_4/H_2O measurements at the Zotino Tall Tower Observatory (ZOTTO) in Central Siberia, Atmospheric Meas. Tech., 3(4), 1113–1128, doi:10.5194/amt-3-1113-2010, 2010.

Wilson, C., Chipperfield, M. P., Gloor, M., Parker, R. J., Boesch, H., McNorton, J., Gatti, L. V., Miller, J. B., Basso, L. S., and Monks, S. A.: Large and increasing methane emissions from eastern Amazonia derived from satellite data, 2010–2018, Atmos. Chem. Phys., 21, 10643–10669, https://doi.org/10.5194/acp-21-10643-2021, 2021.

Wood, T.G. and Sands, W.A. The role of termites in ecosystems. In: Brian, M.V. (Ed.), Production Ecology of Ants and Termites. Cambridge University Press, Cambridge, UK, 245–292, 1978.

Woodward G, Perkins D.M., and Brown L. E.: Climate change and freshwater ecosystems: impacts across multiple levels of organization, Philos Trans R Soc Lond B Biol Sci. ,365(1549), 2093-106, doi: 10.1098/rstb.2010.0055, 2010

Woodward, G., Gessner, M. O., Giller, P. S., Gulis, V., Hladyz, S., Lecerf, A., Malmqvist, B., McKie, B. G., Tiegs, S. D., Cariss, H., Dobson, M., Elosegi, A., Ferreira, V., Graça, M. A. S., Fleituch, T., Lacoursière, J. O., Nistorescu, M., Pozo, J., Risnoveanu, G., Schindler, M., Vadineanu, A., Vought, L. B.-M. and Chauvet, E.: Continental-Scale Effects of Nutrient Pollution on Stream Ecosystem Functioning, Science, 336(6087), 1438–1440, doi:10.1126/science.1219534, 2012.

Woolway RI, Jones ID, Maberly SC, French JR, Livingstone DM, Monteith DT, et al.: Diel Surface Temperature Range Scales with Lake Size, PLoS ONE 11(3): e0152466, doi:10.1371/journal.pone.0152466, 2016

Worden, J. R., Bloom, A. A., Pandey, S., Jiang, Z., Worden, H. M., Walker, T. W., Houweling, S. and Röckmann, T.: Reduced biomass burning emissions reconcile conflicting estimates of the post-2006 atmospheric methane budget, Nat. Commun., 8(1), 2227, doi:10.1038/s41467-017-02246-0, 2017.

Wu, Z., Li, J., Sun, Y. *et al.* : Imbalance of global nutrient cycles exacerbated by the greater retention of phosphorus over nitrogen in lakes. *Nat. Geosci.* 15, 464–468, https://doi.org/10.1038/s41561-022-00958-7, 2022

Wuebbles, D. J. and Hayhoe, K.: Atmospheric methane and global change, Earth-Sci. Rev., 57(3–4), 177–210, 2002.

Wunch, D., Toon, G. C., Blavier, J.-F. L., Washenfelder, R. A., Notholt, J., Connor, B. J., Griffith, D. W. T., Sherlock, V. and Wennberg, P. O.: The Total Carbon Column Observing Network, Philos. Trans. R. Soc. A, 369(1943), doi:10.1098/rsta.2010.0240, 2011.

Wunch, D., Toon, G. C., Hedelius, J. K., Vizenor, N., Roehl, C. M., Saad, K. M., Blavier, J.-F. L., Blake, D. R. and Wennberg, P. O.: Quantifying the loss of processed natural gas within California's South Coast Air Basin using long-term measurements of ethane and methane, Atmospheric Chem. Phys., 16(22), 14091–14105, doi:10.5194/acp-16-

14091-2016, 2016.

Wunch, D., Jones, D. B. A., Toon, G. C., Deutscher, N. M., Hase, F., Notholt, J., Sussmann, R., Warneke, T., Kuenen, J., Denier van der Gon, H., Fisher, J. A. and Maasakkers, J. D.: Emissions of methane in Europe inferred by total column measurements, Atmos Chem Phys, 19(6), 3963–3980, doi:10.5194/acp-19-3963-2019, 2019.

Xiao, K., F. Beulig, H. Røy, B. B. Jørgensen, and N. Risgaard-Petersen: Methylotrophic methanogenesis fuels cryptic methane cycling in marine surface sediment. Limnol. Oceanogr. **63**: 1519–1527. doi:10.1002/lno.10788, 2018

Xu, X. F., Tian, H. Q., Zhang, C., Liu, M. L., Ren, W., Chen, G. S., Lu, C. Q. and Bruhwiler, L.: Attribution of spatial and temporal variations in terrestrial methane flux over North America, Biogeosciences, 7(11), 3637–3655, doi:10.5194/bg-7-3637-2010, 2010.

Xu, X., P Sharma, S Shu, TZ Lin, P Ciais, F Tubiello, P Smith, N Campbell and AK Jain (2021), Global Greenhouse Gas Emissions from Plant- and Animal-Based Food, Nature Food, https://doi.org/10.1038/s43016-021-00358-x, 2021

Yacovitch, T. I. ,C. Daube, S. C. Herndon, and J. B. McManus: Isotopes on a Boat: Real-Time Spectroscopic Measurement of Methane Isotopologues from Offshore Oil and Gas Emissions, OSA Optical Sensors and Sensing Congress 2021 (AIS, FTS, HISE, SENSORS, ES), S. Buckley, F. Vanier, S. Shi, K. Walker, I. Coddington, S. Paine, K. Lok Chan, W. Moses, S. Qian, P. Pellegrino, F. Vollmer, G. , J. Jágerská, R. Menzies, L. Emmenegger, and J. Westberg, eds., OSA Technical Digest (Optica Publishing Group, 2021), paper EW5D.3, 2021

Yan, X., Akiyama, H., Yagi, K. and Akimoto, H.: Global estimations of the inventory and mitigation potential of methane emissions from rice cultivation conducted using the 2006 Intergovernmental Panel on Climate Change Guidelines, Glob. Biogeochem. Cycles, 23(2), doi:10.1029/2008gb003299, 2009.

Yang, P., D. Y. F. Lai, H. Yang, and others: Large increase in CH4 emission following conversion of coastal marsh to aquaculture ponds caused by changing gas transport pathways. Water Res. **222**: 118882. doi:10.1016/j.watres.2022.118882, 2022

Yin, Y., Chevallier, F., Ciais, P., Broquet, G., Fortems-Cheiney, A., Pison, I. and Saunois, M.: Decadal trends in global CO emissions as seen by MOPITT, Atmospheric Chem. Phys., 15(23), 13433–13451, doi:10.5194/acp-15-13433-2015, 2015.

Yoshida, Y., Kikuchi, N., Morino, I., Uchino, O., Oshchepkov, S., Bril, A., Saeki, T., Schutgens, N., Toon, G. C., Wunch, D., Roehl, C. M., Wennberg, P. O., Griffith, D. W. T., Deutscher, N. M., Warneke, T., Notholt, J., Robinson, J., Sherlock, V., Connor, B., Rettinger, M., Sussmann, R., Ahonen, P., Heikkinen, P., Kyrö, E., Mendonca, J., Strong, K., Hase, F., Dohe, S. and Yokota, T.: Improvement of the retrieval algorithm for GOSAT SWIR XCO2 and XCH4 and their validation using TCCON data, Atmospheric Meas. Tech., 6(6), 1533–1547, doi:10.5194/amt-6-1533-2013, 2013.

Yu, X., Millet, D. B., Henze, D. K., Turner, A. J., Delgado, A. L., Bloom, A. A., and Sheng, J.: A high-resolution satellite-based map of global methane emissions reveals missing wetland, fossil fuel, and monsoon sources, Atmos. Chem. Phys., 23, 3325–3346, https://doi.org/10.5194/acp-23-3325-2023, 2023.

Yuan, J., J. Xiang, D. Liu, and others: Rapid growth in greenhouse gas emissions from the adoption of industrial-scale aquaculture. Nat. Clim. Chang. **9**: 318–322. doi:10.1038/s41558-019-0425-9, 2019

Yver Kwok, C. E., Müller, D., Caldow, C., Lebègue, B., Mønster, J. G., Rella, C. W., Scheutz, C., Schmidt, M., Ramonet, M., Warneke, T., Broquet, G. and Ciais, P.: Methane emission estimates using chamber and tracer release experiments for a municipal waste water treatment plant, Atmospheric Meas. Tech., 8(7), 2853–2867, doi:10.5194/amt-8-2853-2015, 2015.

Zhang: Magnitude, spatio-temporal variability and environmental controls of methane emissions from global rice fields: Implications for water management and climate mitigation, Glob. Change Biol., 2016.

Zhang, B. and Chen, G. Q.: China's CH_4 and CO_2 Emissions: Bottom-Up Estimation and Comparative Analysis, Ecol. Indic., 47, 112–122, doi:10.1016/j.ecolind.2014.01.022, 2014.

Zhang, L., X. Xia, S. Liu, S. Zhang, S. Li, J. Wang, G. Wang, H. Gao, Z. Zhang, Q. Wang, W. Wen, R. Liu, Z. Yang, E.H. Stanley, and P.A. Raymond: Significant methane ebullition from alpine permafrost rivers on the East Qinghai–Tibet Plateau. Nature Geoscience, 13(5): p. 349-354, 2020

Zhang, L., H. Tian, H. Shi, S. Pan, J. Chang, S. R. S. Dangal, X. Qin, S. Wang, F. N. Tubiello, J. G. Canadell, R. B. Jackson: A 130-year global inventory of methane emissions from livestock: Trends, patterns, and drivers, Global Change Biology, 28 (17), 5142-5158. https://doi.org/10.1111/gcb.16280, 2022

Zhang, P., Zhang, Y., Liang, R., Chen, W., and Xie, X. : Evaluation of the stratospheric contribution to the inter-annual variabilities of tropospheric methane growth rates, Geophysical Research Letters, 50, e2023GL103350, https://doi.org/10.1029/2023GL103350, 2023.

Zhang, Y., Xiao, X., Wu, X., Zhou, S., Zhang, G., Qin, Y., and Dong, J.: A global moderate resolution dataset of gross primary production of vegetation for 2000–2016, Sci. Data, 4, 1–13, https://doi.org/10.1038/sdata.2017.165, 2017.

Zhang, Y., Jacob, D. J., Maasakkers, J. D., Sulprizio, M. P., Sheng, J.-X., Gautam, R., and Worden, J.: Monitoring global tropospheric OH concentrations using satellite observations of atmospheric methane, Atmos. Chem. Phys., 18, 15959–15973, https://doi.org/10.5194/acp-18-15959-2018, 2018.

Zhang, Y., Gautam, R., Pandey, S., Omara, M., Maasakkers, J. D., Sadavarte, P., Lyon, D., Nesser, H., Sulprizio, M. P., Varon, D. J., Zhang, R., Houweling, S., Zavala-Araiza, D., Alvarez, R. A., Lorente, A., Hamburg, S. P., Aben, I., and Jacob, D. J.: Quantifying Methane Emissions from the Largest Oil-Producing Basin in the United States from Space, Sci. Adv., 6, eaaz5120, https://doi.org/10.1126/sciadv.aaz5120, 2020.

Zhang, Z., Zimmermann, N. E., Kaplan, J. O. and Poulter, B.: Modeling spatiotemporal dynamics of global wetlands: comprehensive evaluation of a new sub-grid TOPMODEL parameterization and uncertainties, Biogeosciences, 13(5), 1387–1408, doi:10.5194/bg-13-1387-2016, 2016.

4115 Zhang, Z., Fluet-Chouinard, E., Jensen, K., McDonald, K., Hugelius, G., Gumbricht, T., et al. Development of the global

4116   dataset of Wetland Area and Dynamics for Methane Modeling (WAD2M), Earth System Science Data, 13(5), 2001–

4117   2023. https://doi.org/10.5194/essd-13-2001-2021, 2021a.

4118 Zhang, Z., Poulter, B., Knox, S., Stavert, A., McNicol, G., Fluet-Chouinard, E., Feinberg, A., Zhao, Y., Bousquet, P.,

4119   Canadell, J. G., Ganesan, A., Hugelius, G., Hurtt, G., Jackson, R. B., Patra, P. K., Saunois, M., Höglund-Isaksson, L.,

4120   Huang, C., Chatterjee, A., and Li, X.: Anthropogenic emission is the main contributor to the rise of atmospheric

4121   methane during 1993-2017, National science review, 9(5), nwab200, doi:10.1093/nsr/nwab200, 2021b

4122 Zhang, Z., Poulter, B., Feldman, A.F., Ying, Q, Ciais, P., Peng, S. and Li, X.: Recent intensification of wetland methane

4123   feedback, Nat. Clim. Chang, 13, 430–433, https://doi.org/10.1038/s41558-023-01629-0, 2023

4124 Zhang, Z., Poulter, B., Melton, J. R., Riley, W. J., Allen, G. H., Beerling, D. J., Bousquet, P., Canadell, J. G., Fluet-

4125   Chouinard, E., Ciais, P., Gedney, N., Hopcroft, P. O., Ito, A., Jackson, R. B., Jain, A. K., Jensen, K., Joos, F., Kleinen,

4126   T., Knox, S., Li, T., Li, X., Liu, X., McDonald, K., McNicol, G., Miller, P. A., Müller, J., Patra, P. K., Peng, C., Peng,

4127   S., Qin, Z., Riggs, R. M., Saunois, M., Sun, Q., Tian, H., Xu, X., Yao, Y., Yi, X., Zhang, W., Zhu, Q., Zhu, Q., and

4128   Zhuang, Q.: Ensemble estimates of global wetland methane emissions over 2000–2020, EGUsphere [preprint],

4129   https://doi.org/10.5194/egusphere-2024-1584, 2024.

4130 Zhao, J., M. Zhang, W. Xiao, L. Jia, X. Zhang, J. Wang, Z. Zhang, Y. Xie, Y. Pu, S. Liu, Z. Feng, and X. Lee: Large

4131   methan   emission from freshwater aquaculture ponds revealed by long-term eddy covariance observation.

4132   Agricultural and Forest Meteorology, 308-309: p. 108600, 2021

4133 Zhao, Y., Saunois, M., Bousquet, P., Lin, X., Berchet, A., Hegglin, M. I., Canadell, J. G., Jackson, R. B., Hauglustaine,

4134   D. A., Szopa, S., Stavert, A. R., Abraham, N. L., Archibald, A. T., Bekki, S., Deushi, M., Jöckel, P., Josse, B., Kinnison,

4135   D., Kirner, O., Marécal, V., O'Connor, F. M., Plummer, D. A., Revell, L. E., Rozanov, E., Stenke, A., Strode, S.,

4136   Tilmes, S., Dlugokencky, E. J. and Zheng, B.: Inter-model comparison of global hydroxyl radical (OH) distributions

4137   and their impact on atmospheric methane over the 2000–2016 period, Atmospheric Chem. Phys., 19(21), 13701–

4138   13723, doi:10.5194/acp-19-13701-2019, 2019.

4139 Zhao, Y., Saunois, M., Bousquet, P., Lin, X., Berchet, A., Hegglin, M. I., Canadell, J. G., Jackson, R. B., Dlugokencky,

4140   E. J., Langenfelds, R. L., Ramonet, M., Worthy, D., and Zheng, B.: Influences of hydroxyl radicals (OH) on top-down

4141   estimates of the global and regional methane budgets, Atmos. Chem. Phys., 20, 9525–9546,

4142   https://doi.org/10.5194/acp-20-9525-2020, 2020a.

4143 Zhao, Y., Saunois, M., Bousquet, P., Lin, X., Berchet, A., Hegglin, M. I., Canadell, J. G., Jackson, R. B., Deushi, M.,

4144   Jöckel, P., Kinnison, D., Kirner, O., Strode, S., Tilmes, S., Dlugokencky, E. J., and Zheng, B.: On the role of trend and

4145   variability in the hydroxyl radical (OH) in the global methane budget, Atmos. Chem. Phys., 20, 13011–13022,

4146   https://doi.org/10.5194/acp-20-13011-2020, 2020b.

4147 Zhao, Y., Saunois, M., Bousquet, P., Lin, X., Hegglin, M. I., Canadell, J. G., Jackson, R. B., and Zheng, B.: Reconciling

the bottom-up and top-down estimates of the methane chemical sink using multiple observations, Atmos. Chem. Phys., 23, 789–807, https://doi.org/10.5194/acp-23-789-2023, 2023.

Zheng, B., Chevallier, F., Ciais, P., Yin, Y. and Wang, Y.: On the Role of the Flaming to Smoldering Transition in the Seasonal Cycle of African Fire Emissions, Geophys. Res. Lett., 45(21), 11,998-12,007, doi:10.1029/2018GL079092, 2018a.

Zheng, B., Chevallier, F., Ciais, P., Yin, Y., Deeter, M. N., Worden, H. M., Wang, Y., Zhang, Q. and He, K.: Rapid decline in carbon monoxide emissions and export from East Asia between years 2005 and 2016, Environ. Res. Lett., 13(4), 044007, doi:10.1088/1748-9326/aab2b3, 2018b.

Zheng, B., Chevallier, F., Yin, Y., Ciais, P., Fortems-Cheiney, A., Deeter, M. N., Parker, R. J., Wang, Y., Worden, H. M., and Zhao, Y.: Global atmospheric carbon monoxide budget 2000–2017 inferred from multi-species atmospheric inversions, Earth Syst. Sci. Data, 11, 1411–1436, doi: 10.5194/essd-11-1411-2019, 2019.

Zheng, B., Ciais, P., Chevallier, F., Yang, H., Canadell, J. G., Chen, Y., van der Velde, I. R., Aben, I., Chuvieco, E., Davis, S. J., Deeter, M., Hong, C., Kong, Y., Li, H., Li, H., Lin, X., He, K., and Zhang, Q.: Record-high CO2 emissions from boreal fires in 2021, Science, 379, 912-917,doi: 10.1126/science.ade0805, 2023.

Zhu, Q., Liu, J., Peng, C., Chen, H., Fang, X., Jiang, H., Yang, G., Zhu, D., Wang, W. and Zhou, X.: Modelling methane emissions from natural wetlands by development and application of the TRIPLEX-GHG model, Geosci. Model Dev., 7(3), 981–999, doi:10.5194/gmd-7-981-2014, 2014.

Zhu, Q., Peng, C., Chen, H., Fang, X., Liu, J., Jiang, H., Yang, Y. and Yang, G.: Estimating global natural wetland methane emissions using process modelling: spatio-temporal patterns and contributions to atmospheric methane fluctuations, Glob. Ecol. Biogeogr., 24, 959–972, 2015.

Zhu, Q., Laughner, J.L., Cohen, R.C.: Combining Machine Learning and Satellite Observations to Predict Spatial and Temporal Variation of near Surface OH in North American Cities, Environ. Sci. Technol., 56, 11, doi:10.1021/acs.est.1c05636, 2022

Zhu, Y., K.J. Purdy, Ö. Eyice, L. Shen, S.F. Harpenslager, G. Yvon-Durocher, A.J. Dumbrell, and M. Trimmer: Disproportionate increase in freshwater methane emissions induced by experimental warming. Nature Climate Change, 10(7): p. 685-690., 2020

Zhuang, Q., Melillo, J. M., Kicklighter, D. W., Prinn, R. G., McGuire, A. D., Steudler, P. A., Felzer, B. S. and Hu, S.: Methane fluxes between terrestrial ecosystems and the atmosphere at northern high latitudes during the past century: A retrospective analysis with a process-based biogeochemistry model, Glob. Biogeochem Cycles, 18(3), GB3010, doi:10.1029/2004gb002239, 2004.

Zhuang, Q., Chen, M., Xu, K., Tang, J., Saikawa, E., Lu, Y., Melillo, J. M., Prinn, R. G. and McGuire, A. D.: Response of global soil consumption of atmospheric methane to changes in atmospheric climate and nitrogen deposition, Glob. Biogeochem. Cycles, 27(3), 650–663, doi:10.1002/gbc.20057, 2013.

4181   Zhuang, Q., M. Guo, J.M. Melack, X. Lan, Z. Tan, Y. Oh, and L.R. Leung: Current and Future Global Lake Methane
4182   Emissions: A Process-Based Modeling Analysis. Journal of Geophysical Research: Biogeosciences, 128(3): p.
4183   e2022JG007137, 2023

Table 1: Bottom-up (BU) models and inventories for anthropogenic and biomass burning used in this study. *Due to its limited sectoral breakdown this dataset was not used in Table 3.

B-U models and inventories	Contribution	Time period (resolution)	Gridded	References
CEDS (country based)	Fossil fuels, Agriculture and waste, Biofuel	1970-2019 (yearly)	no	Hoesly et al. (2018)
CEDS (gridded)*	Fossil fuels, Agriculture and waste, Biofuel	1970-2020 (monthly)	0.5x0.5°	Hoesly et al. (2018) O'Rourke et al (2021)
EDGARv6	Fossil fuels, Agriculture and waste, Biofuel	1990-2018^ (yearly, monthly for some sectors)	0.1x0.1°	Oreggioni et al. (2021), Crippa et al. (2021)
EDGARv7	Fossil fuels, Agriculture and waste, Biofuel	1990-2021 (yearly)	0.1x0.1°	Crippa et al. (2023)
IIASA GAINS v4.0	Fossil fuels, Agriculture and waste, Biofuel	1990-2020 (yearly)	0.5x0.5°	Höglund-Isaksson et al., (2020)
USEPA	Fossil fuels, Agriculture and waste, Biofuel, Biomass Burning	1990-2030 (10-yr interval, interpolated to yearly)	no	USEPA (2019)
FAO-CH4	Agriculture, Biomass Burning	1961-2020 1990-2020 (Yearly)	no	Federici et al. (2015) ; Tubiello et al. (2013); Tubiello (2019)
FINNv2.5	Biomass burning	2002-2020 (daily)	1km resolution	Wiedinmyer et al. (2023)
GFASv1.3	Biomass burning	2003-2020 (daily)	0.1x0.1°	Kaiser et al. (2012)
GFEDv4.1s	Biomass burning	1997-2020 (monthly)	0.25x0.25°	Giglio et al. (2013); van der Werf et al (2017)
QFEDv2.5	Biomass burning	2000-2020 (daily)	0.1x0.1°	Darmenov and da Silva (2015)

Table 2: Biogeochemical models that computed wetland emissions used in this study. Model runs were performed with two climate inputs, CRU and GSWP3-W5E5. Models were run with prognostic (using their own calculation of wetland areas) and/or diagnostic (using WAD2M (Zhang et al., 2021b)) wetland surface areas (see Sect 3.2.1).

Model	Institution	Prognostic		Diagnostic		References
		CRU	GSWP3-W5E5	CRU	GSWP3-W5E5	
CH4MOD$_{wetland}$	Institute of Atmospheric Physics, CAS	n	n	**y**	**y**	Li et al. (2010)
CLASSIC	Environment and Climate Change Canada	y	y*	y	y*	Arora et al. (2018); Melton and Arora (2016)
DLEM	Boston College	y	y	y	y	Tian et al. (2015, 2023)
ELM-ECA	Lawrence Berkeley National Laboratory	y	y	y	y	Riley et al. (2011)
ISAM	University of Illinois, Urbana-Champaign	y	y	y	y	Shu et al. (2020) Xu et al. (2021)
JSBACH	MPI	y	y	y	y	Kleinen et al. (2020, 2021, 2023)
JULES	UKMO	y	y	y	y	Gedney et al. (2019)
LPJ-GUESS	Lund University	n	n	y	y	McGuire et al. (2012)
LPJ-MPI	MPI	y	y	y	y	Kleinen et al. (2012)
LPJ-WSL	NASA GSFC	y	y	y	y	Zhang et al. (2016)
LPX-Bern	University of Bern	y	y	y	y	Spahni et al. (2011), Stocker et al. (2014)
ORCHIDEE	LSCE	y	y	y	y	Ringeval et al. (2011)

SDGVM	University of Birmingham/ University of Sheffield	y	y	y	y	Beerling & Woodward (2001), Hopcroft et al. (2011, 2020)
TEM-MDM	Purdue University	n	n	y	y	Zhuang et al. (2004)
TRIPLEX-GHG	UQAM	n	n	y	y	Zhu et al. (2014, 2015)
VISIT	NIES	y	y	y	y	Ito and Inatomi (2012)

01   ***CLASSIC uses GSWP3-W5E version 2 that covers the time period till 2016. All other models use GSWP-W5E5 version 3.**

Table 3: Global methane emissions by source type in Tg CH$_4$ yr^{-1} from Saunois et al. (2020) (left column pair) and from this work using bottom-up and top-down approaches. Because top-down models cannot fully separate individual processes, only five categories of emissions are provided (see text). Uncertainties are reported as [min-max] range of reported studies. The mean, minimum and maximum values are calculated while discarding outliers, for each category of source and sink. As a result, discrepancies may occur when comparing the sum of categories and their corresponding total due to differences in outlier detections. Differences of 1 Tg CH$_4$ yr^{-1} in the totals can also occur due to rounding errors. Compared to Saunois et al. (2020), emissions are split between "direct anthropogenic" emissions and "natural and indirect anthropogenic" sources. We also propose an estimate of the double-counting between bottom-up wetland and inland freshwater ecosystems emissions.

	Saunois et al. (2020)		This work					
Period of time	**2000-2009**		**2000-2009**		**2010-2019**		**2020**	
Approaches	bottom-up	top-down	bottom-up	top-down	bottom-up	top-down	bottom-up	top-down
NATURAL & indirect anthropogenic SOURCES								
Combined wetlands and inland freshwaters	**306** [229-391]	**180** [153-196]	**242** [156-355]	**158** [145-172]	**248** [159-369]	**165** [145-214]	**251** [171-364]	**175** [151-229]
Wetlands	**147** [102-179]	**180** [153-196]	**153** [116-189] (***)	**158** [145-172]	**159** [119-203] (***)	**165** [145-214]	**161** [131-198] (***)	**175** [151-229]
Inland freshwaters [a]	**159** [117-212]		**112** [49-202]		**112** [49-202]		**112** [49-202]	
Double counting [b]	NA		**-23** [-9 - -36]		**-23** [-9 - -36]		**-23** [-9 - -36]	
Other natural sources	**63** [26-94]	**35** [21-47]	**63** [24-93]	**44** [40-46]	**63** [24-93]	**43** [40-46]	**63** [24-93]	**44** [40-47]
Land sources Geological (onshore)	**50** [17-72] 38 [13-53]		**51** [18-73] 38 [13-53]					
Wild animals	2 [1-3]		2 [1-3]					
Termites	9 [3-15]		10 [4-16]					
Wildfires	(**)		(**)					
Permafrost soils (direct)	1 [0-1]		1 [0-1]					
Vegetation	(*)		(*)					
Coastal and Oceanic sources [c]	**13** [9-22]		**12** [6-20]					
Biogenic	6 [4-10]		5 [3-10]					
Geological (offshore)	7 [5-12]		7 [5-12]					
TOTAL NATURAL & INDIRECT SOURCES	**369** [245-485]	**215** [176-243]	**305** [180-448]	**204** [189-223]	**311** [183-462]	**206** [188-225]	**314** [195-457]	**216** [193-241]
DIRECT ANTHROPOGENIC SOURCES								
Agriculture and waste	**192** [178-206]	**202** [198-219]	**194** [181-208]	**210** [197-223]	**211** [195-231]	**228** [213-242]	**211** [204-216]	**245** [232-259]
Agriculture	**132 [NA]**		**134** [125-142]		**143** [132-155]		**147** [143-149]	
Enteric ferm. & manure	104 [93-109]		104 [100 -110]		112 [107 -118]		117 [114 -124]	
Rice cultivation	28 [23-34]		30 [24-34]		32 [25-37]		32 [29-37]	
Landfills and waste	**60** [55-63]		**61** [52-71]		**69** [56-80]		**71** [60-84]	
Fossil fuels	**110** [94-129]	**101** [71-151]	**105** [97-123]	**105** [88-115]	**120** [117-125]	**115** [100-124]	**128** [120-133]	**122** [101-133]
Coal mining	32 [24-42]		(****)		(****)		(****)	

	Saunois et al. (2020)		This work				
Period of time	**2000-2009**		**2000-2009**		**2010-2019**		**2020**
Oil & Gas	73 [60-85]		30 [26-32]		40 [37-44]		41 [38-43]
Industry	2 [0-6]		65 [63-71]		67 [57-74]		74 [67-80]
Transport	4 [1-11]		4 [1-8]		5 [1-9]		5 [1-8]
			3 [1-8]		2 [1-3]		2 [1-3]
Biomass & biof. burn.	**31** [26-46]	**29** [23-35]	**30** [22-44]	**26** [22-29]	**28** [21-39]	**27** [26-27]	**27** [20-41] / **26** [22-27]
Biomass burning	19 [15-32]		19 [14-29]		17 [12-24]		17 [13-27]
Biofuel burning	12 [9-14]		11 [8-14]		11 [8-14]		10 [7-14]
TOTAL DIRECT ANTHROPOGENIC SOURCES	**334**[d] [321-358]	**332** [312-347]	**333**[d] [305-365]	**341** [319-355]	**358**[d] [329-387]	**369** [350-391]	**372**[d] [345-409] / **392** [368-409]
SINKS							
Total chemical loss	**595** [489-749]	**505** [459-516]	**585** [481-716]	**504**[e] [496-511]	**602** [496-747]	**521**[e] [485-532]	**602** [496-747] / **538**[e] [503-554]
Tropospheric OH	553 [476-677]		546 [446-663]		563 [462-663]		563 [462-663]
Stratospheric loss	31 [12-37]		37 [27-51]		37 [28-43]		37 [28-43]
Tropospheric Cl	11 [1-35]		6 [1-13]		6 [1-13]		6 [1-13]
Soil uptake	**30** [11-49]	**34** [27-41]	**30** [11-49]	**34** [34-34]	**31** [11-49]	**35** [35-35]	**31** [11-49] / **36** [35-36]
TOTAL SINKS	**625** [500-798]	**540** [486-556]	**615** [492-765]	**538** [530-545]e	**633** [507-796]	**554** [520-567]e	**633** [507-796] / **575** [566-589]e
SOURCES – SINKS IMBALANCE							
TOTAL SOURCES	**703** [566-842]	**547** [524-560]	**638** [485-813]	**543** [526-558]	**669** [512-849]	**575** [553-586]	**685** [540-865] / **608** [581-627]
TOTAL SINKS	**625** [500-798]	**540** [486-556]	**615** [492-765]	**538** [530-545]e	**633** [507-796]	**554** [550-567]e	**633** [507-796] / **575** [566-589]e
IMBALANCE	**78**	**3** [-10-38]	**23**	**5** [-4-13]e	**36**	**21** [19-33]e	**52** / **32** [15-38]e
ATMOSPHERIC GROWTH [f]		5.8 [4.9-6.6][f]		6.1 [5.2-6.9][f]		20.9 [20.1-21.7][f]	41.8 [40.7-42.9][f]

(*) uncertain but likely small for upland forest and aerobic emissions, potentially large for forested wetland, but likely included elsewhere

(**) We stop reporting this value to avoid potential double counting with satellite-based products of biomass burning (see Sect. 3.1.5)

(***) Here the numbers are from prognostic runs. To ensure a fair comparison with previous budgets (Saunois et al., 2020), the numbers are 163[117-195] for 2000-2009 from diagnostic runs with CRU/CRU-JRA-55 climate inputs (see Sect. 3.2.1).

(****) Up to 8 Tg of additional emissions could account for ultra emitters (Lauvaux et al., 2022), as in Tibrewal et al. (2024), that are fully or partly missed in regular anthropogenic inventories

a: Freshwater includes lakes, ponds, reservoirs, streams and rivers, part of it is due to anthropogenic disturbances estimated in Sect.3.2.2

b: The double counting estimate is discussed in Sect. 3.2.2

c: includes flux from hydrates considered at 0 for this study, includes estuaries

d: Total anthropogenic emissions are based on estimates of full anthropogenic inventory and not on the sum of "Agriculture and Waste", "Fossil fuels" and "Biofuel and biomass burning" categories (see Sect. 3.1.2)

e: Some inversions did not provide the chemical sink. These values are derived from a subset of the inversion ensemble.

f: Atmospheric growth rates are given in the same unit Tg CH_4 yr^{-1}, based on the conversion factor of 2.75 Tg CH_4 ppb^{-1} given by Prather et al. (2012) and the atmospheric growth rates provided in the text in ppb yr^{-1}.

Table 4: Top-down studies used here with their contribution to the decadal and yearly estimates noted. For decadal means, top down studies must provide at least 8 years of data over the decade to contribute to the estimate. Details on each inverse system and inversions are provided in Table S8 to S11 in the Supplementary Material.

Model	Institution	Observation used	Time period	Number of inversions	2000-2009	2010-2019	2020	References
Carbon Tracker-Europe CH_4	FMI	Surface stations	2000-2020	4	y	y	y	Tsuruta et al. (2017)
LMDz-CIF	LSCE/CEA	Surface stations	2000-2020	4	y	y	y	Thanwerdas et al. (2022a)
LMDz-PYVAR	LSCE/CEA/THU	GOSAT Leicester v9.0	2010-2020	4	n	y	y	Zheng et al. (2018a, 2018b, 2019)
MIROC4-ACTM	JAMSTEC	Surface stations	2000-2020	5	y	y	y	Patra et al. (2018); Chandra et al. (2021)
NISMON-CH_4	NIES/MRI	Surface stations	2000-2020	2	y	y	y	Niwa et al. (2022; 2024)
NIES-TM-FLEXPART (NTFVAR)	NIES	Surface stations	2000-2020	2	y	y	y	Maksyutov et al. (2020); Wang et al. (2019a)
NIES-TM-FLEXPART (NTFVAR)	NIES	GOSAT NIES L2 v02.95	2010-2020	1	n	y	y	Maksyutov et al. (2020); Wang et al. (2019a)
TM5-CAMS	TNO/VU	Surface stations	2000-2020	1	y	y	y	Segers et al. (2022)
TM5-CAMS	TNO/VU	GOSAT ESA/CCI v2.3.8 (combined with surface observations)	2010-2020	1	n	y	y	Segers et al. (2022)
Total number of runs				24	18	24	24	

Table 5: Global and latitudinal total methane emissions in Tg CH$_4$ yr^{-1}, as decadal means (2000-2009 and 2010-2019) and for the year 2020 from this work using bottom-up and top-down approaches. Global and latitudinal emissions for 2000-2009 are also compared with Saunois et al. (2016, 2020) for top-down and bottom-up approaches when available. Uncertainties are reported as [min-max] range. The mean, minimum and maximum values are calculated while discarding outliers, for each category of source and sink. As a result, discrepancies may occur when comparing the sum of categories and their corresponding total due to differences in outlier detections. Differences of 1 Tg CH$_4$ yr^{-1} in the totals can also occur due to rounding errors. For the latitudinal breakdown, bottom-up anthropogenic estimates are based only on the gridded products (see Table 1). As a result, the total from the latitudinal breakdown (line called "This work (gridded BU products only") is slightly different from the values provided in Table 3 and recalled in the line "This work (all BU products)". BU stands for bottom-up.

Period	2000-2009		2010-2019		2020	
Approach	Bottom-up	Top-down	Bottom-up	Top-down	Bottom-up	Top-down
Global						
This work (all BU products)	638 [485-813]	543 [526-558]	669 [512-849]	575 [553-586]	685 [540-865]	608 [581-627]
This work (gridded BU products only)	642 [501-809]		676 [526-845]		691 [565-862]	
S2020	703 [566-842]	547 [524-560]	-	-	-	-
S2016	719[583-861]	552[535-566]	-	-	-	-
90°S-30°N						
This work	367 [254-487]	337 [311-361]	388 [275-503]	364 [337-390]	395 [292-521]	386 [353-425]
S2020	408 [322-532]	346 [320-379]	-	-	-	-
S2016	-	356 [334-381]	-	-	-	-
30°N-60°N						
This work	234 [169-335]	182 [162-197]	250 [184-345]	187 [160-204]	256 [186-356]	197 [170-215]
S2020	252 [202-342]	178 [159-199]	-	-	-	-
S2016	-	176[159-195]	-	-	-	-
60°N-90°N						
This work	42 [22-79]	26 [22-33]	38[17-73]	24 [18-29]	39 [17-74]	25 [20-32]
S2020	42 [28-70]	23 [17- 32]	-	-	-	-
S2016	-	20 [15-25]	-	-	-	-

38 **Table 6: Latitudinal methane emissions in Tg CH$_4$ yr^{-1} for the last decade 2010-2019, based on top-down and bottom-up approaches.**
39 **Uncertainties are reported as [min-max] range of reported studies. The mean, minimum, and maximum values are calculated while**
40 **discarding outliers, for each category of source and sink. As a result, discrepancies may occur when comparing the sum of categories**
41 **and their corresponding total due to differences in outlier detections. Differences of 1 Tg CH$_4$ yr^{-1} in the totals can also occur due to**
42 **rounding errors. For bottom-up approaches, natural and indirect anthropogenic sources are estimated based on available gridded**
43 **data sets (see text Sect 5.2). As some emissions are missing gridded products (wild animals, permafrost, and hydrates), discrepancies**
44 **may occur in terms of totals proposed in Table 3. Bottom-up direct anthropogenic estimates are based only on the gridded products**
45 **(see Table 1).**

Latitudinal band	90°S- 30°N		30°N-60°N		60°-90°N	
Approach	Bottom-up	Top-Down	Bottom-up	Top-Down	Bottom-up	Top-Down
Natural and indirect anthropogenic Sources	**178** [95-276]	**148** [133-164]	**100** [43-188]	**42** [36-50]	**28** [9-53]	**14** [10-21]
Combined wetland and Inland freshwaters	151 [85-234]	128 [112-155]	73 [32-147]	27 [20-42]	24 [9-53]	9 [7-17]
Other natural	27 [11-42]	22 [20-29]	27 [10-41]	19 [16-22]	4 [2-6]	3 [1-5]
Anthropogenic direct sources	**210** [180-227]	**215** [191-238]	**151** [142-157]	**144** [121-162]	**10** [6-14]	**10** [6-16]
Agriculture & Waste	140 [121-150]	150 [135-168]	81 [77-84]	77 [56-88]	1 [1-2]	2 [2-2]
Fossil Fuels	52 [44-65]	46 [36-62]	65 [61-71]	61 [50-69]	7 [4-10]	7 [3-13]
Biomass & biofuel burning	22 [18-30]	19 [16-21]	7 [4-10]	6 [2-7]	1 [0-1]	1 [1-2]
Sum of sources	**388** [275-503]	**364** [337-390]	**250** [184-345]	**187** [160-204]	**38** [7-73]	**24** [18- 29]

48

Table 7: Regional methane emissions (regions ranked by continent) in Tg CH$_4$ yr^{-1} for the last decade 2010-2019, based on top-down and bottom-up approaches. Uncertainties are reported as [min-max] range of reported studies. Differences of 1 Tg CH$_4$ yr^{-1} in the totals can occur due to rounding errors. For bottom-up approaches, natural and indirect anthropogenic sources are estimated based on available gridded data sets (see text Sect 5.2). As some emissions are missing gridded products (wild animals, permafrost, and hydrates), discrepancies may occur in terms of totals proposed in Table 3. Bottom-up direct anthropogenic estimates are based on all products (gridded and per country).

Region	Total emissions		Natural and indirect anthropogenic emissions		Direct anthropogenic emissions	
	Bottom-up	Top-down	Bottom-up	Top-down	Bottom-up	Top-down
USA	49 [27-77]	38 [32-46]	24 [7-43]	12 [7-22]	26 [19-34]	25 [16-31]
Canada	38 [14-71]	20 [17-24]	32 [11-63]	14 [11-22]	6 [3-8]	7[5-9]
Central America	18 [10-28]	17 [14-19]	8 [3-17]	5 [2-6]	10 [8-12]	12 [11-13]
Northern South America	19 [9-35]	16 [13-20]	10 [3-17]	9 [7-11]	9 [6-17]	7 [6-8]
Brazil	51 [26-79]	47 [41-58]	32 [11-57]	26 [22-36]	19 [16-22]	21 [17-26]
Southwest South America	34 [16-51]	38 [30-48]	21 [6-35]	24 [16-34]	13 [10-16]	14 [12-17]
Europe	42 [29-57]	31 [24-36]	17 [6-30]	7 [5-9]	25 [22-27]	24 [20-31]
Northern Africa	24 [18-33]	25 [23-29]	7 [2-13]	6 [6-8]	18 [16-20]	19 [17-21]
Equatorial Africa	47 [28-83]	47 [39-59]	23 [10-49]	24 [20-30]	24 [19-34]	23 [19-29]
Southern Africa	21 [5-43]	19 [16-24]	11 [2-29]	8 [7-10]	10 [3-14]	11 [10-12]
Russia	48 [24-83]	36 [27-45]	25 [9-47]	14 [11-18]	23 [15-36]	21 [14-29]
Central Asia	15 [6-29]	10 [8-13]	8 [2-19]	1 [0-2]	8 [4-10]	9 [7-11]
Middle East	35 [21-47]	31 [24-39]	9 [3-15]	4 [1-6]	26 [18-31]	28 [20-34]
China	71 [55-99]	57 [37-72]	15 [4-33]	4 [3-7]	57 [51-66]	53 [34-66]
Korean-Japan	6 [4-12]	5 [4-6]	3 [1-7]	1 [1-1]	4 [3-5]	4 [3-5]
South Asia	58 [49-72]	52 [43-60]	13 [5-25]	6 [5-6]	45 [44-47]	45[37-49]
Southeast Asia	64 [42-93]	63 [52-71]	32 [19-54]	27 [20-34]	32 [23-39]	35 [31-46]
Australasia	16 [9-26]	13 [10-17]	10 [4-19]	6 [4-7]	7 [6-7]	7 [6-7]
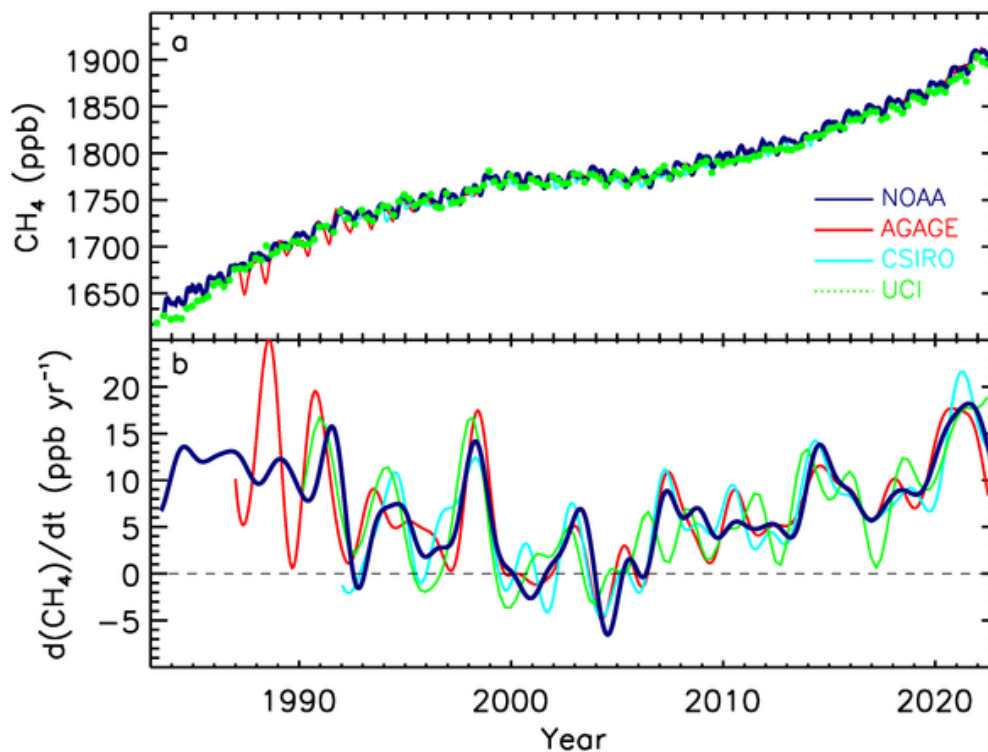
60 **Figure 1: Globally averaged atmospheric CH$_4$ concentrations (ppb) (a) and annual growth rates G$_{ATM}$ (ppb yr^{-1}) (b) between 1983**
61 **and 2022, from four measurement programs, National Oceanic and Atmospheric Administration (NOAA), Advanced Global**
62 **Atmospheric Gases Experiment (AGAGE), Commonwealth Scientific and Industrial Research Organisation (CSIRO), and**
63 **University of California, Irvine (UCI). Detailed descriptions of methods are given in the supplementary material of Kirschke et al.**
64 **(2013).**
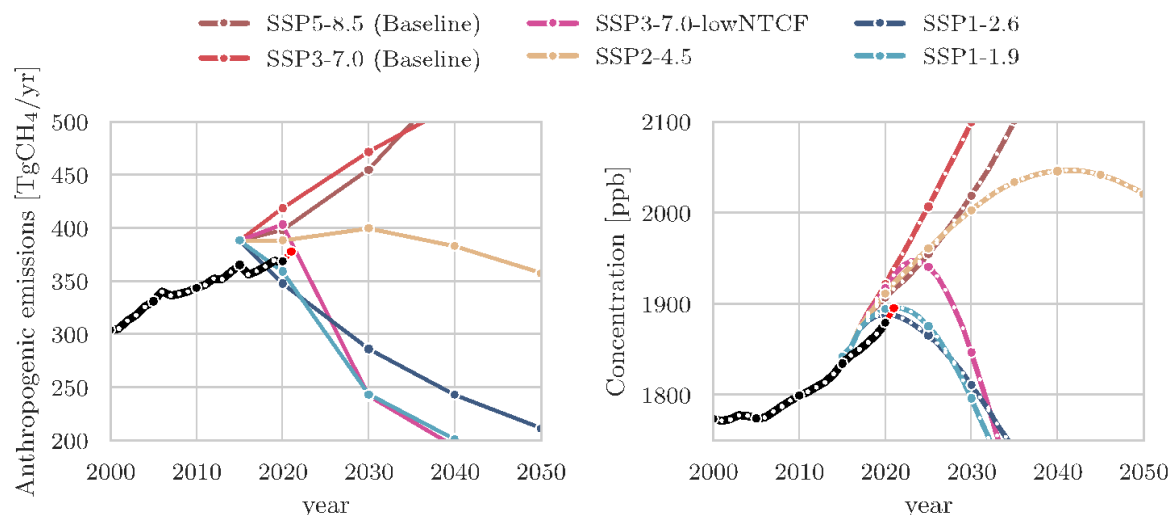
Figure 2: Left: Global anthropogenic methane emissions (including biomass burning) over 2000-2050 from historical inventories (black line and grey shaded area) and future projections (colored lines) (in Tg CH$_4$ yr^{-1}) from selected scenarios harmonized with historical emissions (CEDS) for CMIP6 activities (Gidden et al., 2019). Historical mean emissions correspond to the average of anthropogenic inventories listed in Table 1 added to the GFEDv4.1s (van der Werf et al., 2017) biomass burning historical emissions. Right: Global atmospheric methane concentrations for NOAA surface site observations (black) and projections based on SSPs (Riahi et al., 2017) with concentrations estimated using MAGICC (Meinshausen et al., 2017, 2020). Red dots show the last year available (2022 for observations).
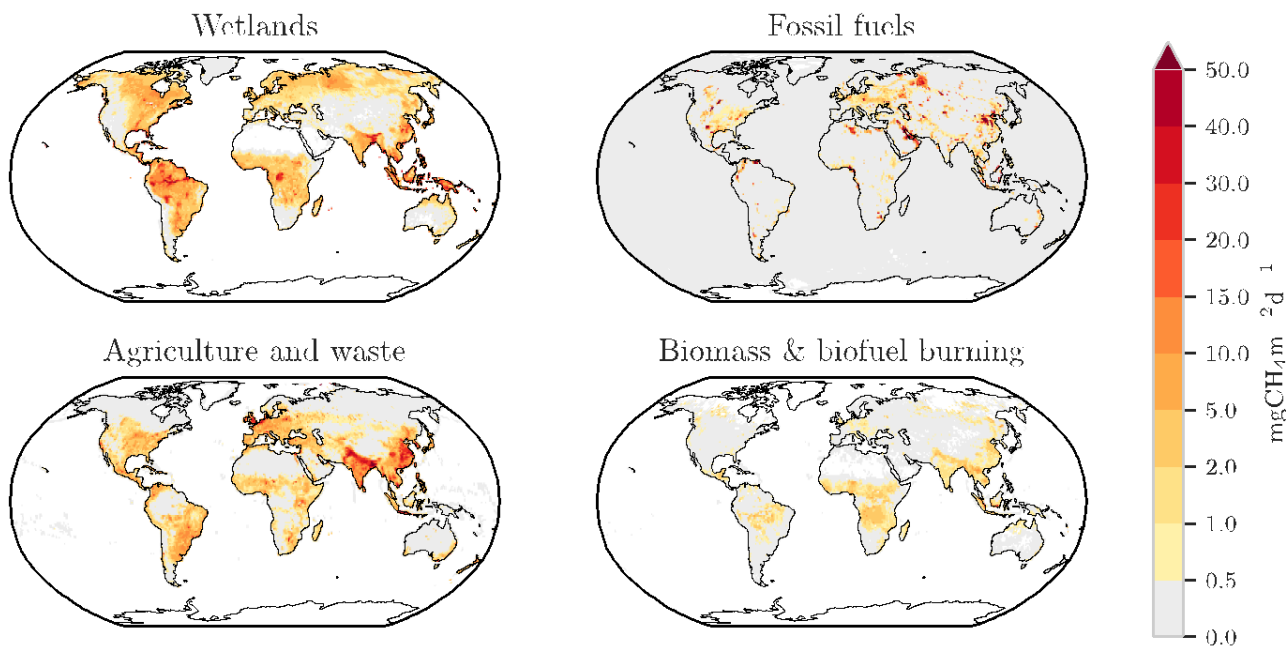
Figure 3: Methane emissions from four source categories: natural wetlands (excluding lakes, ponds, and rivers), biomass and biofuel burning, agriculture and waste, and fossil fuels for the 2010-2019 decade in mg CH_4 m^{-2} day^{-1}. The wetland emission map represents the mean daily emission average over the 16 biogeochemical models listed in Table 2 and over the 2010-2019 decade. Fossil fuel and Agriculture and Waste emission maps are derived from the mean estimates of gridded CEDS, EGDARv6, EDGARv7 and GAINS models. The biomass and biofuel burning map results from the mean of the biomass burning inventories listed in Table 1 added to the mean of the biofuel estimate from CEDS (O'Rourke et al., 2021), EDGARv6 (Crippa et al., 2021), EDGARv7 (Crippa et al., 2023) and GAINS (Höglund-Isaksson et al., (2020)) models.
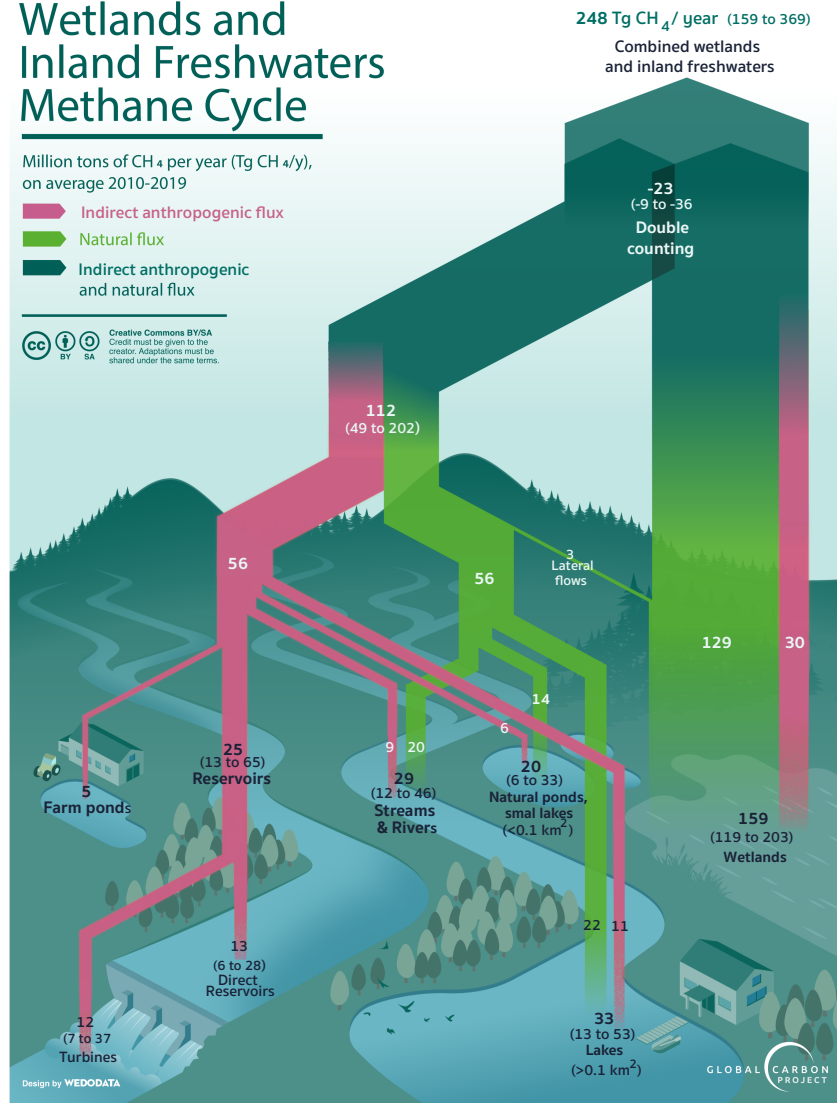
**Figure 4: Estimation of wetland and inland freshwater emissions over the 2010-2019 decade in Tg CH$_4$ yr^{-1}. The
fluxes related to voluntary (such as through reservoirs or farm ponds) or involuntary (land use or eutrophication-
related) perturbations of the methane cycle are shown here in pink. They are accounted for into the "natural and
indirect anthropogenic" sources in the Table 3 budget and depicted as "natural and indirect anthropogenic" sources
(darker green and pink hatches) in Fig. 7.**
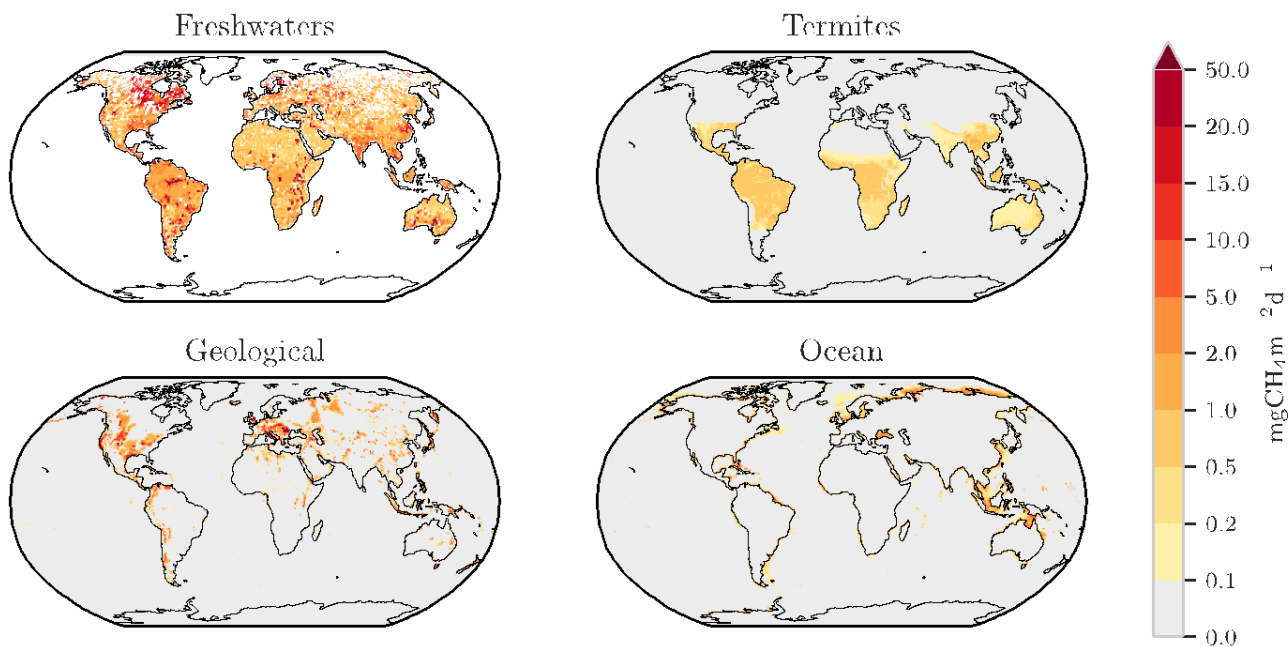
Figure 5: Methane emissions (mg CH$_4$ m^{-2} day^{-1}) from four natural and indirect anthropogenic sources: inland freshwaters (includes lakes, ponds (Johnson et al., 2022,), reservoirs (Johnson et al., 2021) and stream and rivers (Rocher-Ros et al., 2023) with a global total scaled to 89 Tg yr^{-1}), geological (Etiope et al., 2019), termites (this study) and oceans (Weber et al., 2019).
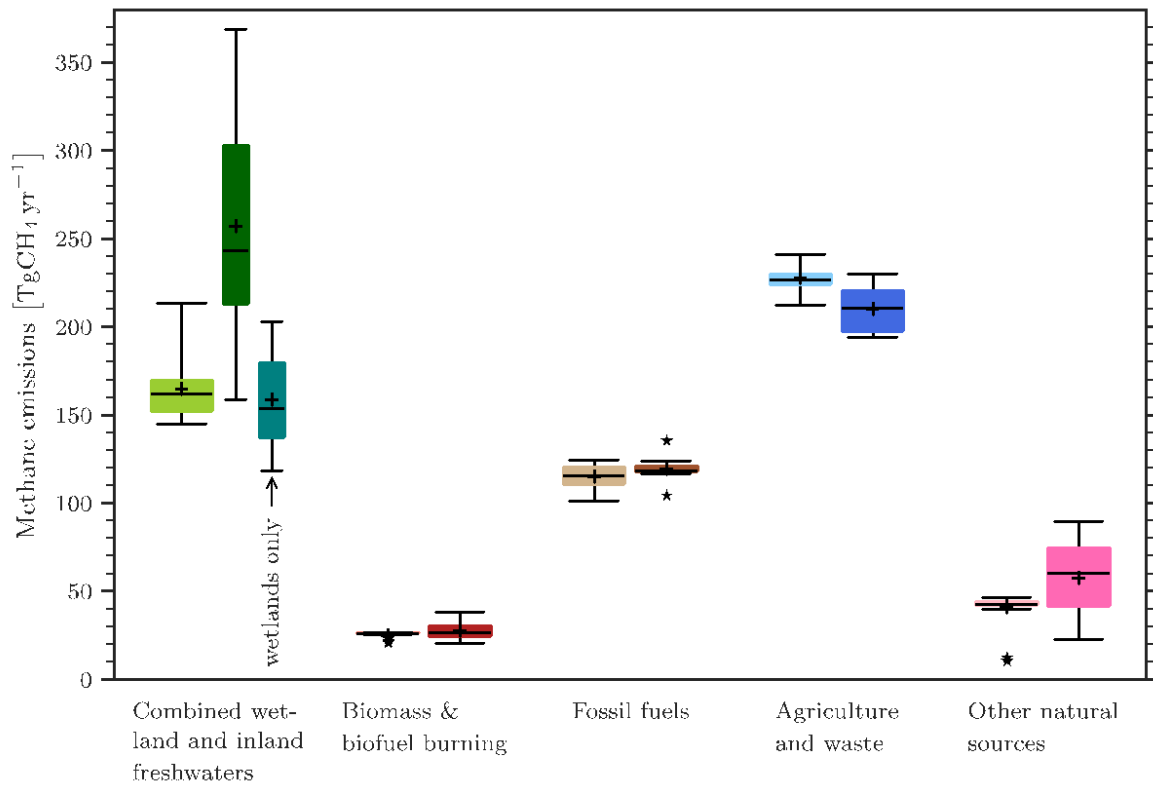
Figure 6: Methane global emissions from five broad categories (see Sect. 2.3) for the 2010-2019 decade for top-down inversion models (left light coloured boxplots) in Tg CH$_4$ yr^{-1} and for bottom-up models and inventories (right dark coloured boxplots). For combined wetland and inland freshwaters three estimates are given: left = top-down estimates, middle = bottom-up estimates, right = bottom-up estimates for wetlands only. Median value, first and third quartiles are presented in the boxes. The whiskers represent the minimum and maximum values when suspected outliers are removed (see Sect. 2.2). Suspected outliers are marked with stars. Bottom-up quartiles are not available for bottom-up estimates, except for wetland emissions. Mean values are represented with "+" symbols, these are the values reported in Table 3.

09
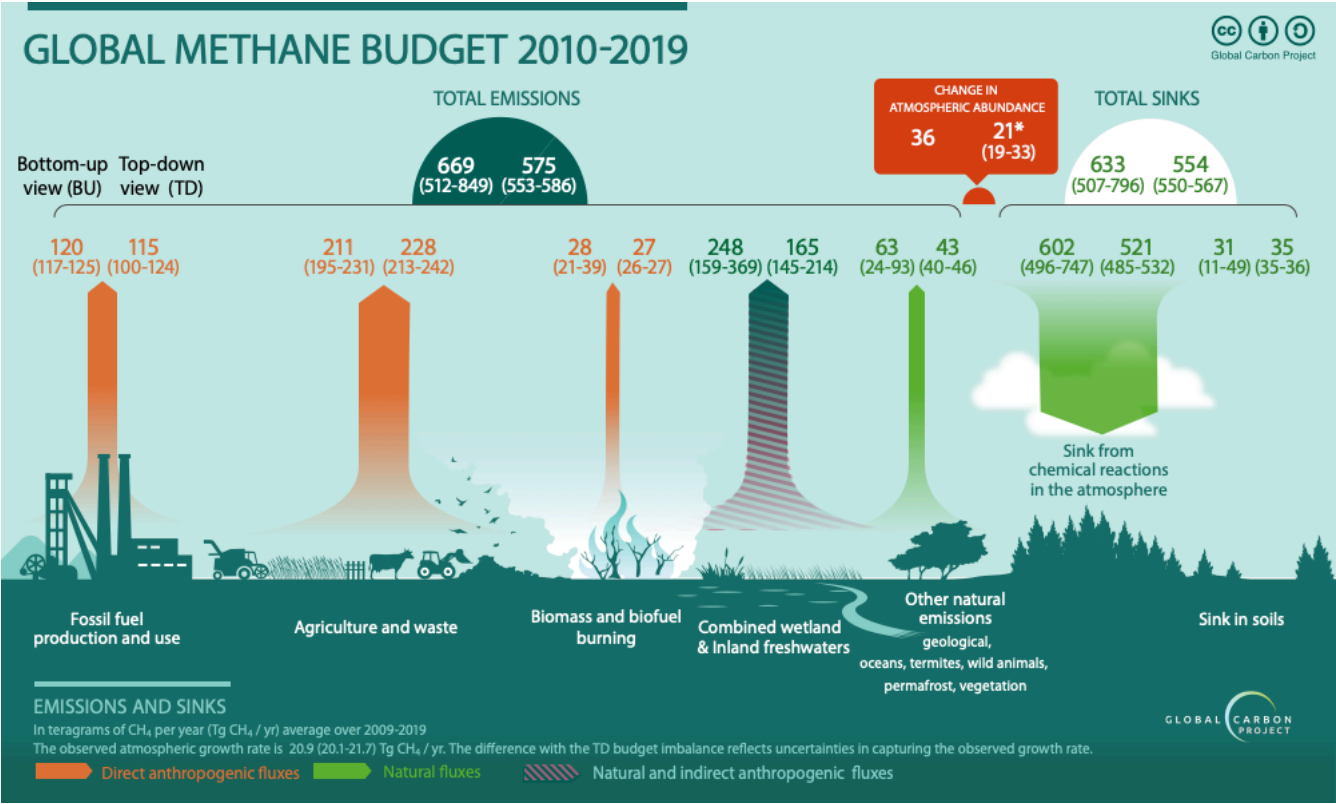
12 **Figure 7: Global Methane Budget for the 2010-2019 decade. Both bottom-up (left) and top-down (right) estimates are provided for**
13 **each emission and sink category in Tg CH_4 yr^{-1}, as well as for total emissions and total sinks. Combined wetland and inland**
14 **freshwaters are depicted as natural and indirect anthropogenic sources (darker green and pink hatches) to recall Figure 4 (Sect.**
15 **3.2.2   ).**
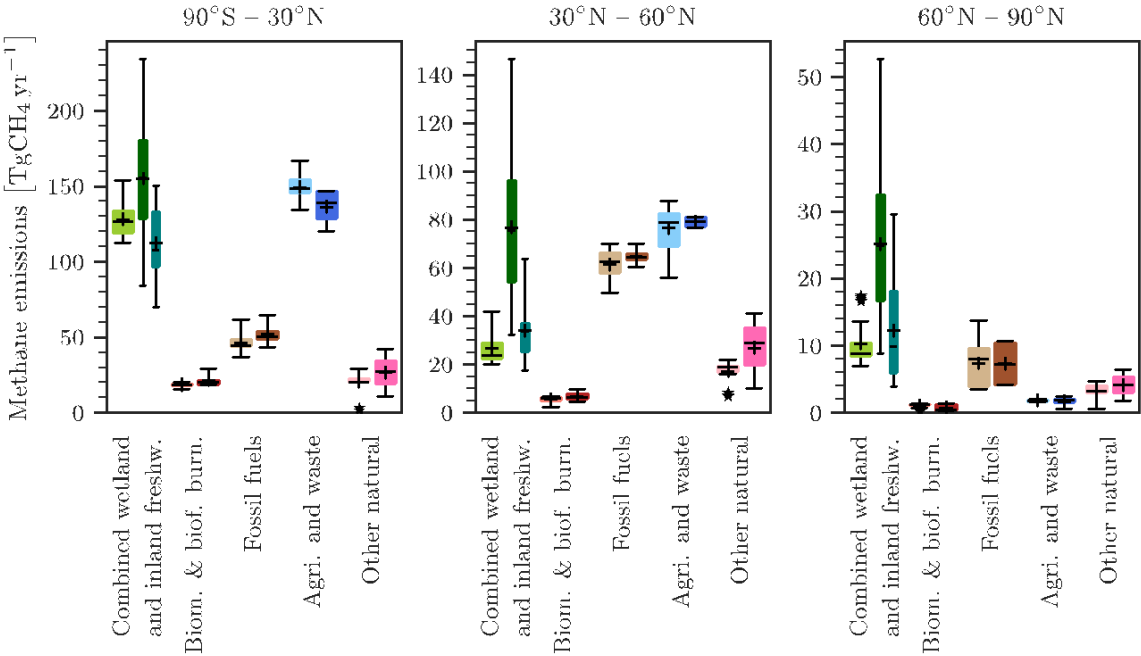
Figure 8: Methane latitudinal emissions from five broad categories (see Sect. 2.3) for the 2010-2019 decade for top-down inversion models (left light coloured boxplots) in Tg CH₄ yr⁻¹ and for bottom-up models and inventories (right dark coloured boxplots). For combined wetland and inland freshwaters three estimates are given: left = top-down estimates, middle = bottom-up estimates, right = bottom-up estimates for wetlands only. Median value, first and third quartiles are presented in the boxes. The whiskers represent the minimum and maximum values when suspected outliers are removed (see Sect. 2.2). Suspected outliers are marked with stars. Bottom-up quartiles are not available for bottom-up estimates, except wetland emissions. Mean values are represented with "+" symbols, these are the values reported in Table 6.
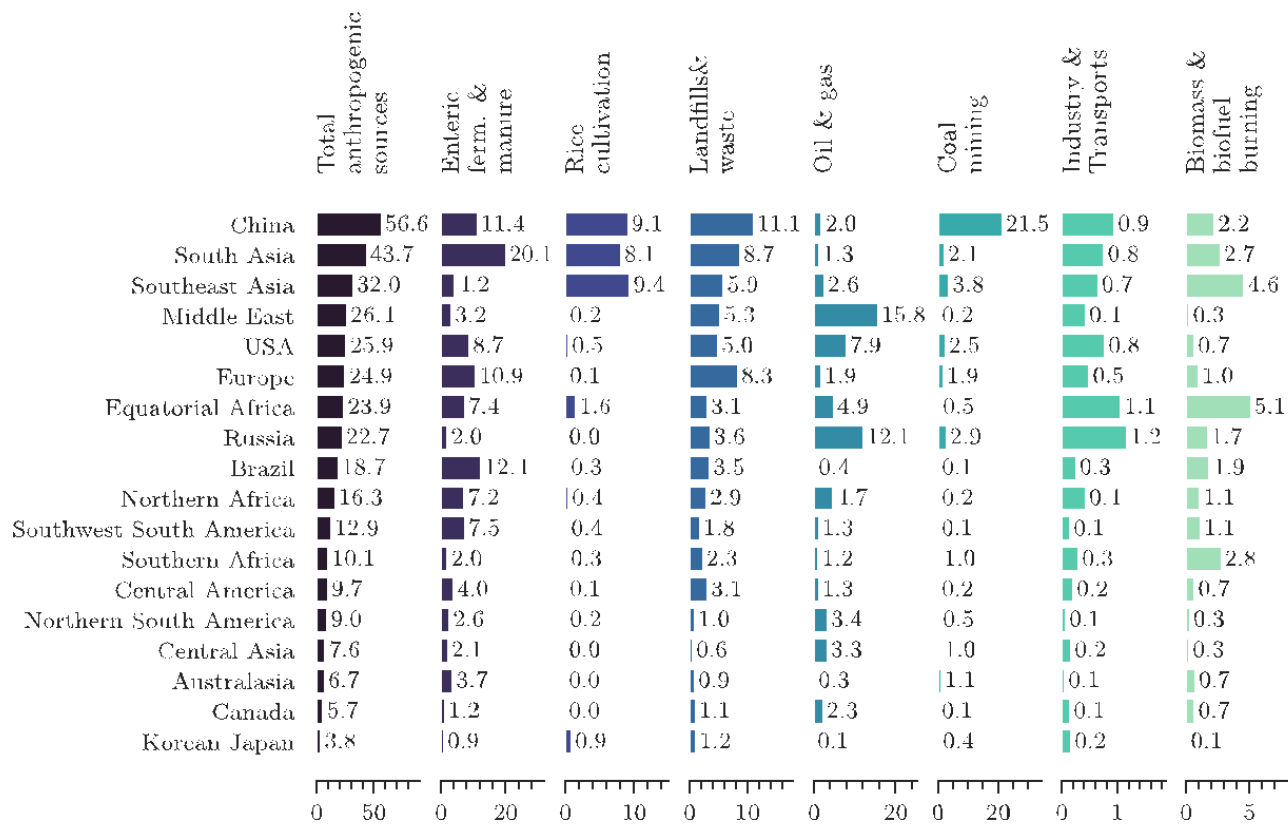
Figure 9: Regional anthropogenic emissions for the 2010-2019 decade from bottom-up estimates in Tg CH$_4$ yr^{-1}. Regions are ranked by their total anthropogenic emissions. Note that each category has its own emission scale.
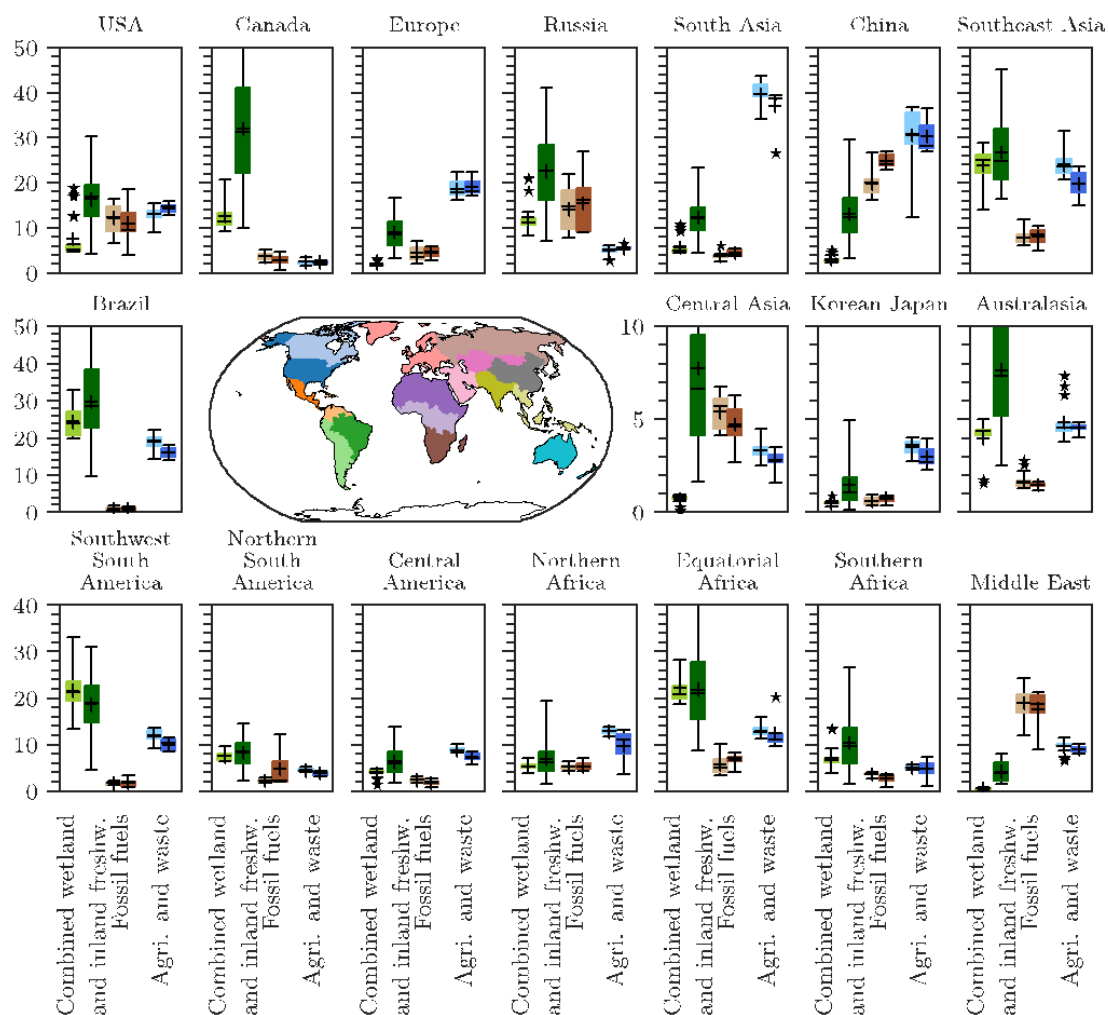
Figure 10: Regional emissions in Tg CH$_4$ yr^{-1} for three broad main emissions categories for the 2010-2019 decade: Combined wetland and inland freshwaters, fossil fuel and agriculture & waste from top-down estimates (left box-plots- and bottom-up estimates (right boxplots). The inner map shows the region's distribution (see also Supplementary material, Table S1 and Fig. S3). More categories are presented in the Supplementary Material in Figure S6.

36 **Table A1.** Comparison of terminologies used in this study and previous reports for methane sources.

GCP terminology (This study)		IPCC AR6 (Canadell et al., 2021)	National GHG inventories (used by UNFCCC according to IPCC (2006) and IPCC (2019))	IPCC (2006, 2019) Source sector numbering
Anthropogenic Sources				
Fossil fuels	Coal Mining	Coal Mining	Fugitive emissions from Fuels / Solid fuels	1B1
	Oil and gas	Oil and gas	Fugitive emissions from Fuels / Oil and natural gas	1B2
	Transport	Transport	Transport	1A3
	Industry	Industry	Mineral, chemical, metal industry and others	2A, 2B, 2C, 2D, 2E
			Energy/fuel Combustion activities	1A except 1A3 + 1B3
Agriculture	Enteric fermentation and manure management	Enteric fermentation and manure management	Livestock	3A
	Rice cultivation	Rice cultivation	Rice cultivation	3C7
Waste	Landfills and waste	Landfills and waste	Waste	4
Biofuel and biomass burning	Biofuel burning	Biofuel burning	Biofuel burning	1A4b
	Biomass burning	Biomass burning	Biomass burning	3C1
Natural and indirect sources				
Wetlands	Wetlands	Wetlands	– –	– –
Inland freshwaters	Reservoirs	included in Inland freshwaters	Land (incl Reservoirs)	in 3B
	Lakes, ponds, and rivers	incl in Inland freshwaters	only canal, ditches and ponds for human uses	in 3B
Other natural sources	Oceans	Oceans	– –	– –
	Termites	Termites	– –	– –

		Geological sources	Geological sources	– –	– –

Table A2. Summary of methodological changes since the previous budget (Saunois et al., 2020). No significant changes have been applied to the vegetation (Sect. 3.2.8), wild animal (Sect. 3.2.5) and terrestrial permafrost and hydrates (Sect 3.2.7) estimates, though litterature has been expanded and/or updated.

	Saunois et al. (2020)	This study
Regions definition (Table S1, Fig S3)	18 continental regions + ocean	same regions except the last region including only Australia and New-Zealand and called Australasia
Anthropogenic global inventories (See Table 1, Sect 3.1.1)	CEDS, EDGARv4.3.2, USEPA (2012), FAO and GAINS ECLIPSE v6	CEDS, EDGARv6 and v7, USEPA (2019), FAO, IIASA GAINS v4 Add estimate of ultra emitters from Lauvaux et al. (2022)
Biomass burning data sets	FINNv1.5, GFASv1.3, GFEDv4.1s, QFEDv2.5	FINNv2.5, GFASv1.3, GFEDv4.1s, QFEDv2.5
Estimate of wetland emissions (See Tables 2 and S3 and Section 3.2.1)	13 land surface models involved, runs with either prescribed areas or based on Hydrological scheme, single meteorological forcing	16 land surface models involved, runs with either prescribed areas or based on Hydrological scheme, two sets of meteorological forcings
Estimate of reservoirs emissions (Sect.3.2.2)	based on Deemer et al. (2016)	based on Johnson et al. (2021), Rosentreter et al. (2021) and Harrison et al. (2021)
Estimate of lakes and ponds emissions (Sect.3.2.2)	based on Bastviken et al. (2011), Wik et al. (2016b) and Tan and Zhuang (2015)	lakes > .1km2 : based on Rosentreter et al. (2021), Zhuang et al. (2023) and Johnson et al. (2022) lakes and ponds < 0.1 km2 : based on Rosentreter et al. (2021), and Johnson et al. (2022)
Estimates of stream and river emissions (Sect.3.2.2)	From Stanley et al. (2016)	based on Rosentreter et al. (2021) and Rocher-Ros et al. (2023)
Estimates of the anthropogenic perturbation component of inland freshwater emissions (Sect.3.2.2)	- -	based on several individual studies on the effect of eutrophication on emissions from lakes, and ponds (See text in Sect. 3.2.2)
Estimate of the double counting in the aquatic systems (Sect.3.2.2)	− −	due to the accounting of small lakes and ponds (<0.1km2) in the vegetated wetlands areas used in land surface models and to lateral transport from vegetated wetland to rivers.

Geological sources (Sect 3.2.3) - onshore and offshore	based on Etiope and Schwiezke et al. (2019)	same as in Saunois et al. (2020)
Termite emissions (Sect. 3.2.4)	GPP : Zhang et al. (2017) termite biomass: Jung et al. (2011) EF : Kirshke et al. (2013) and Fraser et al., 1986)	GPP: Wild et al. (2022) termite biomass: based on different studies depending on regions (see text) EF: Sugimoto et al. (1998) Applied a correction factor for mound from Nauer et al. (2018)
Oceanic sources (Sect 3.2.6)	modern biogenic: based on Wuebbles and Hayhoe (2002), Laruelle et al. (2013) and Rosentreter et al. (2018); geological: based on Etiope (2019)	modern biogenic: based on Rosentreter et al. (2021;2023) and Laruelle et al. (2025) geological: based on Etiope (2019)
Tropospheric OH oxidation (Sect 3.3.2) and stratospheric loss (Sect 3.3.3) (See Supplementary Table S4)	based on results from 11 models contributing to the Chemistry Climate Model Initiative (Morgenstern et al., 2017)	based on results from 11 models contributing to the Chemistry Climate Model Initiative 2022 (Plummer et al., 2021) and the CMIP6 simulations (Collins et al., 2017)
Tropospheric reaction with Cl	based on Hossaini et al. (2016), Wang et al. (2019b) and Gromov (2018)	based on Hossaini et al (2016), Sherwenn et al. (2016), Wang et al (2019b, 2021b) and Gromov (2018)
Soil uptake (See Table S6)	based on Tian et al. (2016)	based on VISIT, JSBACH en MeMo surface models.
Estimates through top-down approaches (See table S7 and S8 to S11)	9 inverse systems contributing, prior fluxes based on EDGARv4.2 or v4.3.2 for most inversions. Most inversion used constant OH.	7 inverse systems contributing, runs with constant and varying OH, prior fluxes based on either EDGARv6 or GAINS

45
46
Table A3. Funding supporting the production of the various components of the global methane budget in addition to the authors' supporting institutions (see also acknowledgements).

Funder and grant number (where relevant)	Authors/Simulations/Observations
Director, Office of Science, Office of Biological and Environmental Research of the US Department of Energy under Contract No. DE-AC02-05CH11231 to Lawrence Berkeley National Laboratory as part of the RUBISCO Scientific Focus Area.	WJR, QZ, E3SM/ELM simulations
Funded by NASA's Interdisciplinary Research in Earth Science (IDS) Program and the NASA Terrestrial Ecology and Tropospheric Composition Programs	MSJ; lake and reservoir bottom-up methane emission data sets
Funded by Agence National de la Recherche through the project Advanced Methane Budget through Multi-constraints and Multi-data streams Modelling (AMB-M^3) - (ANR-21-CE01-0030)	AM, MS
The Environment Research and Technology Development Fund (JPMEERF21S20800) of the Environmental Restoration and Conservation Agency provided by Ministry of the Environment of Japan	YN, NISMON-CH4
Funded by the German Federal Ministry of Education and Research (BMBF) via the "PalMod" project, grant No. 01LP1921A	TK; CH4 emission modelling with JSBACH and LPJ-MPI
Funded by the Swedish Research Council VR (2020-05338) and Swedish National Space Agency (209/19)	WZ; LPJ-GUESS simulations
Funded by BELSPO (project FedTwin ReCAP), EU Horizon 2020 project ESM2025 (nr. 101003536) and FRNS PDR project CH4-lake (T.0191.23)	PR; inland water, coastal and oceanic CH4 emission synthesis
EU H2020 (725546 ERC METLAKE and 101015825 TRIAGE) , Swedish Research Councils VR (2022-03841) and Formas (2018-01794)	DB; inland waters - data and bottom up estimation.
Supported by the Newton Fund through the Met Office Climate Science for Service Partnership Brazil (CSSP Brazil)	NG; JULES simulations
Funded by United Nations Environment Programme, Stanford University DTIE21-EN3143	RBJ; inversions and general budget support
the Joint Fund for Regional Innovation and Development of the National Natural Science Foundation (Grant No. U22A20570); the Natural Sciences and Engineering Research Council of Canada (NSERC, #371706)	Changhui Peng/TRIPLEX-GHG
Computing Resources	
LSCE computing resources	Marielle Saunois, Philippe Bousquet, Joël Thanwerdas and Adrien Martinez
NASA High-End Computing (HEC) Program through the NASA Advanced Supercomputing (NAS) Division at NASA Ames Research Center	Matthew S. Johnson (MSJ)
Deutsches Klimarechenzentrum (DKRZ), Hamburg, Germany	Thomas Kleinen (TK)

ALICE High Performance Computing Facility at the University of Leicester	GOSAT retrievals
FUJITSU PRIMERGY CX2550M5 at MRI and NEC SX-Aurora TSUBASA at NIES	Yosuke Niwa (YN)

Support for atmospheric observations

Australian Antarctic Division	CSIRO flask network
Australian Institute of Marine Science	CSIRO flask network
Bureau of Meteorology (Australia)	Kennaook/Cape Grim AGAGE, CSIRO flask network
Commonwealth Scientific and Industrial Research Organisation (CSIRO, Australia)	Kennaook/Cape Grim AGAGE, CSIRO flask network
Department of Climate Change, Energy, the Environment and Water (DCCEEW, Australia)	Kennaook/Cape Grim AGAGE
Meteorological Service of Canada	CSIRO flask network
NASA: grants NAG5-12669, NNX07AE89G, NNX11AF17G, NNX16AC98G and 80NSSC21K1369 to MIT with subawards to the University of Bristol (for Barbados and Mace Head) and CSIRO (for Kennaook/Cape Grim); grants NAG5-4023, NNX07AE87G, NNX07AF09G, NNX11AF15G, NNX11AF16G, NNX16AC96G, NNX16AC97G, 80NSSC21K1210 and 80NSSC21K1201 to SIO.	AGAGE calibrations and measurements at SIO, La Jolla and AGAGE station operations at Trinidad Head, Mace Head, Barbados, American Samoa, and Kennaook/Cape Grim
National Oceanic and Atmospheric Administration (NOAA, USA) contract RA133R15CN0008 to the University of Bristol	Barbados
NOAA USA	CSIRO flask network
Refrigerant Reclaim Australia	Kennaook/Cape Grim AGAGE
UK Department for Business, Energy & Industrial Strategy (BEIS) contract TRN1537/06/2018 and TRN 5488/11/2021 to the University of Bristol	Mace Head
National Oceanic and Atmospheric Administration (NOAA, USA)	Cape Matatula
Japanese Ministry of Environment	GOSAT data, Robert Parker
Japanese Aerospace Exploration Agency, National Institute for Environmental Studies	GOSAT data, Robert Parker
UKRI UK: grants NE/W004895/1, NE/R016518/1, NE/X019071/1 and MR/X033139/1	GOSAT data, Robert Parker
The Swedish Research Council VR (2022-04839), European Space Agency projects AMPAC-Net and CCI+ permafrost, European Union's Horizon 2020 Research and Innovation Programme to the Nunataryuk project (no. 773421)	Permafrost region, Gustaf Hugelius